

**THERMAL HYDRAULIC ANALYSIS OF A REDUCED SCALE
HIGH TEMPERATURE GAS-COOLED REACTOR TEST
FACILITY AND ITS PROTOTYPE WITH MELCOR**

A Thesis

by

BRADLEY AARON BEENY

Submitted to the Office of Graduate Studies of
Texas A&M University
in partial fulfillment of the requirements for the degree of

MASTER OF SCIENCE

Approved by:

Chair of Committee, Karen Vierow
Committee Members, Pavel Tsvetkov
Devesh Ranjan
Head of Department, Yassin Hassan

December 2012

Major Subject: Nuclear Engineering

Copyright 2012 Bradley Aaron Beeny

ABSTRACT

Pursuant to the energy policy act of 2005, the High Temperature Gas-Cooled Reactor (HTGR) has been selected as the Very High Temperature Reactor (VHTR) that will become the Next Generation Nuclear Plant (NGNP). Although plans to build a demonstration plant at Idaho National Laboratories (INL) are currently on hold, a cooperative agreement on HTGR research between the U.S. Nuclear Regulatory Commission (NRC) and several academic investigators remains in place.

One component of this agreement relates to validation of systems-level computer code modeling capabilities in anticipation of the eventual need to perform HTGR licensing analyses. Because the NRC has used MELCOR for LWR licensing in the past and because MELCOR was recently updated to include gas-cooled reactor physics models, MELCOR is among the system codes of interest in the cooperative agreement. The impetus for this thesis was a code-to-experiment validation study wherein MELCOR computer code predictions were to be benchmarked against experimental data from a reduced-scale HTGR testing apparatus called the High Temperature Test Facility (HTTF). For various reasons, HTTF data is not yet available from facility designers at Oregon State University, and hence the scope of this thesis was narrowed to include only computational studies of the HTTF and its prototype, General Atomics' Modular High Temperature Gas-Cooled Reactor (MHTGR). Using the most complete literature references available for MHTGR design and using preliminary design information on the HTTF, MELCOR input decks for both systems were developed. Normal and off-normal

system operating conditions were modeled via implementation of appropriate boundary and initial conditions. MELCOR Predictions of system response for steady-state, pressurized conduction cool-down (PCC), and depressurized conduction cool-down (DCC) conditions were checked against nominal design parameters, physical intuition, and some computational results available from previous RELAP5-3D analyses at INL.

All MELCOR input decks were successfully built and all scenarios were successfully modeled under certain assumptions. Given that the HTTF input deck is preliminary and was based on dated references, the results were altogether imperfect but encouraging since no indications of as yet unknown deficiencies in MELCOR modeling capability were observed. Researchers at TAMU are in a good position to revise the MELCOR models upon receipt of new information and to move forward with MELCOR-to-HTTF benchmarking when and if test data becomes available.

To my grandfathers, Billy Dye and Richard Beeny, who blessed my life by living theirs
as men of faith with a steadfast commitment to family

ACKNOWLEDGMENTS

I would like to thank Dr. Karen Vierow for her guidance and support as my employer, instructor, and faculty advisor ever since I began my time at TAMU in the fall of 2006. Her confidence in me and expectations of me have served as useful motivation during my undergraduate and graduate years. My association with her and the Nuclear Heat Transfer Systems Labs has enriched my technical education and has lead to several other professional relationships and developmental opportunities.

I would also like to thank the members of my thesis advisory committee: Dr. Karen Vierow, Dr. Pavel Tsvetkov, and Dr. Devesh Ranjan. I very much appreciate their time and technical advice. I have taken classes from each of them and know firsthand their quality as educators and researchers.

Since my first technical internship at Sandia National Laboratories during the summer of 2008, I have received much technical support from members of the reactor modeling and analysis division with whom I worked. I would especially like to thank Randy Gauntt and Larry Humphries for their several letters of recommendation in recent years. I would also like to thank Mike Young and John Reynolds for their help.

Lastly, I wish to thank my family for the support they have never ceased to give and for their unconditional love which I will never have to earn.

NOMENCLATURE

ANS	American Nuclear Society
BISO	Bi-Isotropic
CF	Control Function
CL	Cladding Component
COR	Core Package
CV	Control Volume
CVH	Control Volume Hydrodynamics Package
DCC	Depressurized Conduction Cool-Down
DCH	Decay Heat Package
DLOFC	Depressurized Loss of Forced Circulation
DOE	Department of Energy
EXEC	Executive Package
FL	Flow Path / Flow Path Package
FU	Fuel Component
GCR	Gas-Cooled Reactor
GTMHR	Gas Turbine Modular Helium Reactor
H2TS	Hierarchical Two-Tiered Scaling
HS	Heat Structure/ Heat Structure Package
HTGR	High Temperature Gas-Cooled Reactor

HTR-10	High Temperature Reactor - 10
HTS	Heat Transport System
HTTF	High Temperature Test Facility
HTTR	High Temperature Test Reactor
INL	Idaho National Laboratories
LEU	Low Enriched Uranium
LWR	Light Water Reactor
MHTGR	Modular High Temperature Gas-Cooled Reactor
MP	Material Properties Package
NCG	Noncondensable Gas Package
NGNP	Next Generation Nuclear Plant
NRC	Nuclear Regulatory Commission
NS	Non-Supporting Structure Component
Nu	Nusselt Number
OSU	Oregon State University
PBMR	Pebble Bed Modular Reactor
PCC	Pressurized Conduction Cool-Down
PIRT	Phenomena Identification and Ranking Tables
PLOFC	Pressurized Loss of Forced Circulation
PMR	Prismatic Modular Reactor
Pr	Prandtl Number
PSER	Pre-Application Safety Evaluation Report

PSID	Preliminary Safety Information Document
Ra	Rayleigh Number
RCCS	Reactor Cavity Cooling System
Re	Reynolds Number
RF	Reflector Component
SCS	Shutdown Cooling System
SNL	Sandia National Laboratories
SS	Support Structure Component
TAMU	Texas A&M University
TF	Tabular Function/ Tabular Functions Package
TRISO	Tri-Isotropic
VHTR	Very High Temperature Reactor

TABLE OF CONTENTS

	Page
1. INTRODUCTION.....	1
1.1 Thesis Objectives	2
1.2 Significance of Work	2
1.3 Technical Approach	3
1.4 Thesis Overview.....	4
2. MHTGR overview.....	5
2.1 Brief History.....	5
2.2 Objectives.....	6
2.3 General Design Description	8
2.3.1 Fuel Design	8
2.3.2 Core Element Design	9
2.3.3 Reactor Pressure Vessel, MHTGR Module, and Coolant Flow.....	12
2.3.4 Reactivity Control Systems.....	13
2.3.5 Fuel Loading and Power Distribution	14
2.3.6 Shutdown Cooling System and Reactor Cavity Cooling System ...	15
3. HTTF OVERVIEW.....	19
3.1 Brief History.....	19
3.2 Objectives.....	20
3.3 General Design Description	21
3.3.1 Core and Vessel Design	22
3.3.1.1 Typical Core Block Design.....	23
3.3.1.2 Reflector Design.....	24
3.3.2 Reactor Cavity Cooling System Design.....	25
4. MELCOR OVERVIEW	26
4.1 Background	26
4.2 Code Mechanics	27
4.3 Modeling Concepts	31
4.3.1 Control Volumes	31
4.3.2 Flow Paths.....	35
4.3.3 Heat Structures	36

	Page
4.3.4 Core Structures	38
4.4 Gas-Cooled Reactor Physics	42
4.4.1 Axial Conduction	43
4.4.2 Radial Conduction	44
4.4.2.1 General Inter-cell Conduction	44
4.4.2.2 Tanaka-Chisaka Effective Conductivity	45
4.4.2.3 Intra-Cell Conduction and “Thick Cladding”	46
4.4.2.4 Boundary Conduction	50
4.4.2.5 Convection	51
5. MELCOR MODELING APPROACH AND INPUT DEVELOPMENT	55
5.1 General MELCOR Modeling Approach	55
5.2 Specific MELCOR Modeling Approach	58
5.2.1 System Design Information	59
5.2.2 Core Nodalization	59
5.2.3 Core Characterization	64
5.2.4 In-Core Input	69
5.2.5 Ex-Core Input	71
5.2.6 Ancillary Input	73
5.2.7 Steady-State and Transient Control Logic	75
5.2.8 Decay Heat	77
6. RESULTS AND DISCUSSION	78
6.1 Rationale for Test Case Selection	78
6.2 MELCOR Predictions	79
6.2.1 MHTGR at 350 MW _{th}	79
6.2.1.1 Steady-State	79
6.2.1.2 Pressurized Conduction Cool-Down	84
6.2.1.3 Depressurized Conduction Cool-Down	88
6.2.2 MHTGR at 35 MW _{th}	93
6.2.2.1 Steady-State	93
6.2.2.2 Pressurized Conduction Cool-Down	97
6.2.2.3 Depressurized Conduction Cool-Down	100
6.2.3 HTTF at 2.2 MW _{th}	103
6.2.3.1 Steady-State	103
6.2.3.2 Depressurized Conduction Cool-Down	108
6.3 Prototype-to-Model Comparison with MELCOR Results	111
6.4 General Assessment of MELCOR/RELAP Agreement	113
7. CONCLUSIONS AND RECOMMENDATIONS	118

	Page
REFERENCES	120
APPENDIX A: MHTGR INPUT/CALCULATION NOTEBOOK	122
APPENDIX B: HTTF INPUT/CALCULATION NOTEBOOK	165

LIST OF TABLES

TABLE		Page
5.1	Ceramic material properties for the MHTGR	74
5.2	Ceramic material properties for the HTTF	75
6.1	Steady-state parameters for the 350 MW _{th} MHTGR.....	80
6.2	Steady-state core structural temperature map for Figure 6.1	81
6.3	Steady-state helium temperature map, 350 MW _{th} MHTGR	84
6.4	Steady-state parameters for the 35 MW _{th} MHTGR.....	93
6.5	Steady-state core structural temperature map for Figure 6.8	95
6.6	Steady-state helium temperature map, 35 MW _{th} MHTGR	97
6.7	Steady-state parameters for the 2.2 MW _{th} HTTF.....	104
6.8	Steady-state core structural temperature map for Figure 6.3	105
6.9	Steady-state helium temperature map, HTTF	107
A.1	Environmental variables input for MHTGR model	122
A.2	EXEC MELGEN input for MHTGR model.....	123
A.3	NCG input for MHTGR model	123
A.4	CVH input for MHTGR model	124
A.4.1	CV_NCG for MHTGR model.....	125
A.4.2	CV_VAT for MHTGR model	127
A.5	FL input for MHTGR model	133

TABLE	Page
A.5.1 FL_FT for MHTGR model.....	134
A.5.2 FL geometric parameters for MHTGR model.....	136
A.6 HS input for MHTGR model.....	138
A.6.1 HS geometric parameters for MHTGR model	139
A.6.2 HS LHS boundary conditions for MHTGR model	141
A.6.3 HS RHS boundary conditions for MHTGR model	142
A.7 COR input for MHTGR model	143
A.7.1 COR_ZP for MHTGR model	147
A.7.2 COR_RP for MHTGR model.....	147
A.7.3 COR_RBV for MHTGR model	148
A.7.4 COR_SS for MHTGR model	149
A.7.5 COR_KFU for MHTGR model.....	149
A.7.6 COR_KCL for MHTGR model.....	149
A.7.7 COR_KSS for MHTGR model	150
A.7.8 COR_KRF for MHTGR model.....	151
A.7.9 COR_EDR for MHTGR model.....	152
A.7.10 COR_RFD for MHTGR model.....	152
A.7.11 COR_RFG for MHTGR model.....	153
A.7.12 COR_BFA for MHTGR model.....	154
A.7.13 COR_SA for MHTGR model.....	156
A.7.14 COR_RFA for MHTGR model.....	157

TABLE	Page
A.8	MP input for MHTGR model 158
A.8.1	MP properties input for MHTGR model 159
A.9	TF input for MHTGR model 160
A.9.1	TF tabular input for MHTGR model 160
A.10	CF input for MHTGR model 163
A.10.1	CF arguments for MHTGR model 163
A.11	EXEC MELCOR input for MHTGR model 164
B.1	Environmental variables input for HTTF model 165
B.2	EXEC MELGEN input for HTTF model 166
B.3	NCG input for HTTF model 166
B.4	CVH input for HTTF model 167
B.4.1	CV_NCG for HTTF model 168
B.4.2	CV_VAT for HTTF model 171
B.5	FL input for HTTF model 177
B.5.1	FL_FT for HTTF model 178
B.5.2	FL geometric parameters for HTTF model 180
B.6	HS input for HTTF model 182
B.6.1	HS geometric parameters for HTTF model 183
B.6.2	HS LHS boundary conditions for HTTF model 186
B.6.3	HS RHS boundary conditions for HTTF model 187
B.7	COR input for HTTF model 189

TABLE	Page
B.7.1 COR_SS for HTTF model.....	193
B.7.2 COR_ZP for HTTF model.....	193
B.7.3 COR_RP for HTTF model	194
B.7.4 COR_RBV for HTTF model	194
B.7.5 COR_KFU for HTTF model	196
B.7.6 COR_KCL for HTTF model	197
B.7.7 COR_KSS for HTTF model	197
B.7.8 COR_KRF for HTTF model.....	198
B.7.9 COR_RFD for HTTF model.....	199
B.7.10 COR_RFG for HTTF model.....	199
B.7.11 COR_BFA for HTTF model.....	200
B.7.12 COR_SA for HTTF model	202
B.7.13 COR_RFA for HTTF model.....	204
B.8 MP input for HTTF model.....	205
B.8.1 MP properties input for HTTF model.....	205
B.9 TF input for HTTF model.....	206
B.9.1 TF tabular data for HTTF model	206
B.10 CF input for HTTF model	207
B.10.1 CF arguments for HTTF model	208
B. 11 EXEC MELCOR input for HTTF model	210

LIST OF FIGURES

FIGURE		Page
2.1.	TRISO fuel kernels, compacts, and elements	9
2.2.	Cross-sectional view of the MHTGR core	11
2.3.	MHTGR reactor vessel, cross duct, and secondary vessel	13
2.4.	Shutdown cooling system loop	15
2.5.	Reactor cavity cooling system diagram	16
2.6.	RCCS configuration, top view	17
4.1.	MELCOR execution flow diagram	27
4.2.	Volume/altitude concept for control volumes	33
4.3.	Generalized COR nodalization.....	39
4.4.	COR package DT/DZ cell-wise energy balance concept	54
5.1.	MELCOR input development flow diagram.....	56
5.2.	Geometric transformation of an HTGR core.....	60
5.3.	COR nodalization of the MHTGR	61
5.4.	COR nodalization of the HTTF.....	62
5.5.	Channel and bypass flow area for an HTGR fuel element.....	66
5.6.	Determination of an "effective clad radius" in an HTGR	68
5.7.	Representative CVH nodalization for MHTGR/HTTF.....	72
5.8.	DCH package decay heat curve based on ANS standard.....	77

FIGURE	Page
6.1	Steady-state core structural temperature distribution 82
6.2	Mass-averaged (by ring) core graphite temperatures during PCC 85
6.3	Mass-averaged (by level) core graphite temperatures during PCC..... 86
6.4	Area-averaged outer RPV wall temperature during PCC 88
6.5	Mass-averaged (by ring) core graphite temperatures during DCC 89
6.6	Mass-averaged (by level) core graphite temperatures during DCC 91
6.7	Area-averaged outer RPV wall temperature during DCC..... 92
6.8	Steady-state core structural temperature distribution 96
6.9	Mass-averaged (by ring) core graphite temperatures during PCC 98
6.10	Mass-averaged (by level) core graphite temperatures during PCC..... 99
6.11	Area-averaged outer RPV wall temperature for PCC 100
6.12	Mass-averaged (by ring) core graphite temperatures during DCC 101
6.13	Mass-averaged (by level) core graphite temperatures during DCC 102
6.14	Area-averaged outer RPV wall temperature for DCC..... 103
6.15	Steady-state core structural temperature distribution 106
6.16	Mass-averaged (by ring) core graphite temperatures during DCC 108
6.17	Mass-averaged (by level) core graphite temperatures during DCC 109
6.18	Area-averaged RPV outer wall temperature for DCC..... 110
6.19	Ratio of structural temperatures in active core MHTGR-to-HTTF 112
6.20	Hot-ring, mass-averaged FU temperature during PCC and DCC 114
6.21	Peak fuel temperature as reported by RELAP during PCC and DCC [4].. 115

FIGURE		Page
6.22	Area-averaged RPV outer wall temperature during PCC and DCC	116
6.23	RPV temperature as reported by RELAP during PCC and DCC.....	117

1. INTRODUCTION

The Department of Energy (DOE) has selected the high temperature gas-cooled reactor (HTGR) as the Very High Temperature Reactor (VHTR) that will become the Next Generation Nuclear Plant (NGNP) and will partially satisfy nuclear initiatives calling for increased safety and reliability. Prior to the economic downturn of 2008, plans were in place to build an NGNP demonstration plant at Idaho National Laboratories (INL) as per the Energy Policy Act of 2005. Realization of this goal is unlikely under present circumstances, but a cooperative agreement on HTGR research remains in place between several academic institutions and the Nuclear Regulatory Commission (NRC). The overall goal of the cooperative agreement is to expand the HTGR knowledge base through integral facility experiments, separate effects tests, and various computational studies. Texas A&M University (TAMU), as a party to this agreement, was appointed several tasks related to HTGR analysis. The studies detailed in this thesis follow from cooperative agreement research directives involving systems-level HTGR predictive simulations and a code-to-experiment benchmark.

MELCOR is a systems-level thermal hydraulics and severe accident computer code developed by Sandia National Laboratories (SNL) for the NRC. It has been used as a safety analysis tool to license light water reactors (LWRs) but was recently modified for application to HTGRs. Validation of its predictive capabilities is necessary to qualify MELCOR as a reliable NRC licensing tool for future HTGR installations. Hence, the need for a code-to-experiment benchmark study involving MELCOR is evident and was to be addressed through construction of a High Temperature Test Facility (HTTF) at Oregon State University (OSU). The HTTF is a reduced-scale model of General

Atomics' Modular High Temperature Gas-Cooled Reactor (MHTGR), which was the prototypical HTGR for the HTTF. Despite recent delays in construction and in commencement of shake-down testing, the need may still arise in the near future for validation of TAMU MELCOR models against the HTTF test matrix. The MELCOR models explained in this thesis would facilitate a future MELCOR-to-HTTF benchmark exercise, but only limited MELCOR validation activity is currently possible.

1.1 Thesis Objectives

The objectives of this thesis are as follows:

- To develop MELCOR input decks for the reduced-scale High Temperature Test Facility and its prototype, the Modular High Temperature Gas-Cooled Reactor using the latest references
- To apply and to test newly-implemented Gas-Cooled Reactor (GCR) MELCOR models as they pertain to HTGR thermal hydraulics
- To assess MELCOR capabilities for modeling normal (steady-state) and off-normal (pressurized/depressurized conduction cool-downs) HTGR operating scenarios by comparison with nominal design parameters and previously published results of other computer codes
- To make recommendations for improvements to MELCOR based on findings
- To prepare for future HTTF code-to-experiment benchmark studies

1.2 Significance of Work

Recent concern about materials temperature limits has caused downward revisions to the NGNP target outlet temperature. “High Temperature” or “Very High Temperature” as in HTGR/VHTR generally refers to core outlet temperatures

approaching 1000 °C. This outlet temperature is attractive from a thermodynamic perspective (increased thermal efficiency, less waste heat rejection) but also enables energy/hydrogen co-generation (via high-temperature electrolysis) and lends itself to any of several other industrial applications. The theoretically achievable outlet temperature of an HTGR makes it an attractive alternative to an LWR, but the appeal lessens at lower HTGR target outlet temperature. NGNP outlet temperature revisions have dropped the target from 1000 °C to less than 700 °C. As a direct result, both the NGNP program (supported by the DOE) and the cooperative agreement on HTGR research (supported by the NRC) have received less support recently. However, one may still anticipate a future need for HTGR licensing tool validation and it is in this sense that the work of this thesis bears relevance to the nuclear industry and to its regulators.

1.3 Technical Approach

Pursuant to aforementioned thesis objectives, MELCOR input decks were built for the MHTGR and the HTTF using the latest system design documents and the most recent GCR physics modeling features of MELCOR. For the MHTGR, the primary source of design information was a decades-old Preliminary Safety Information Document (PSID) submitted to the NRC and designated as HTGR-86-024. For the HTTF, the primary source of design information was the most recent set of design drawings obtained through direct communication with facility designers at OSU. To a lesser extent, the OSU report on HTTF scaling analysis also served as a useful reference. After extensive debugging, the basic input decks were fine-tuned and control logic was built in to allow for modeling of steady-state, pressurized conduction cool-down (PCC), and depressurized conduction cool-down (DCC) scenarios. Several assumptions were

made at this stage of the process because there is considerable uncertainty associated with off-normal HTGR operations. After gathering results, an attempt was made to partially validate MELCOR predictions of core thermal hydraulic response by comparison with nominal MHTGR/HTTF design parameters and published RELAP code results from INL.

1.4 Thesis Overview

Chapters 2 and 3 present overviews of the MHTGR and the HTTF, respectively, and include brief discussions of history, programmatic objectives, and design for each system. Chapter 4 gives insight in to the MELCOR code by introducing general code mechanics and modeling concepts before describing several relevant GCR physics models. Chapter 5 outlines the MELCOR modeling approach taken for both the MHTGR and the HTTF and goes on to describe the implementation of steady-state and conduction cool-down cases via control logic and boundary conditions. Chapter 6 presents results for the various analyses from which the useful conclusions and recommendations of chapter 7 are drawn. In the appendices, representative MELCOR input decks in tabular form are included for reference.

2. MHTGR OVERVIEW

2.1 Brief History

In the mid-1980's, the DOE submitted to the NRC the PSID for the MHTGR. The nuclear power system described therein was meant to be a simple, safe, economic, competitive alternative to LWRs for the nuclear power industry. In anticipation of the eventual need for licensing, the NRC responded to the MHTGR PSID with a Pre-application Safety Evaluation Report (PSER) designated as NUREG-1338 [5]. Various other DOE reports regarding different special topics were also submitted to the NRC for review around the same time. The nuclear system described by the DOE's PSID of 1986 and the NRC's NUREG-1338 of 1995 is the HTGR to which the HTTF is scaled.

Several countries have accrued substantial operating experience with gas cooled reactors since the European (U.K. and France) Magnox reactors of the 1950's. Germany, Japan, and China have had operational GCRs (experimental and/or power producing). With respect to HTGRs in the U.S., two facilities are of note for their similarities to the MHTGR: Fort St. Vrain in Colorado and Peach Bottom-1 in Pennsylvania. Unit 1 of the 40 MW_e Peach Bottom Atomic Power Station operated from the late 1960's to the early 1970's. It had a prismatic core, BISO-coated fuel particles, helium coolant, and a prismatic core design. The 330 MW_e Fort St. Vrain generating station operated from 1976 to 1989 and used TRISO-coated fuel particles with a prismatic core design. Lessons learned from the combined twenty years of HTGR operating experience in the U.S. may be leveraged for licensing purposes. For example, observations of fission product retention capability (at Fort St. Vrain) could help the

NRC to decide whether low-leakage LWR-style containment is a necessity for a TRISO-fueled HTGR.

NRC documents summarizing domestic operational experience have been published (e.g. NUREG-CR-6839 regarding Fort St. Vrain). A myriad of technical documents and research reports on GCR phenomenology are also available for review. Taken together, research efforts and operational experience world-wide have contributed to a fairly robust GCR knowledge base. Still, HTGR operational experience is limited as only Chinese and Japanese test reactors (HTR-10 and HTTR, respectively) are currently or were recently online. Of those two facilities, only the HTTR bears any similarity to the MHTGR. The state of the art of HTGR design has therefore had little chance to evolve in response to lessons learned from operational experience (compared to the state of the art in LWR design). Nevertheless, HTGRs have been proven viable and safe through limited industrial activity.

2.2 Objectives

The MHTGR was designed to be a passively safe and economic alternative to gen. II-III LWRs and was among the industry's first answers to congress' 1984 request for a simpler, safer fission power system. By reducing reliance on both operator action and active equipment, two factors often contributory to accident initiation/progression are minimized in potential impact. If operator intervention is not required to mitigate an accident, there is no chance that human error could exacerbate an event in progress. If fewer mechanically-active components comprise a given system, there is a smaller chance that mechanical failure may render it inoperable. Compared to an LWR, the MHTGR reduces reliance on operator action during off-normal conditions and can

inherently mitigate/manage accidents via its passive safety features and design characteristics. This “walk-away safety” of the MHTGR is its most attractive attribute.

High core material melting points, a low power density, and a high core/reflector heat capacity generally lead to sluggish MHTGR thermal transients. Core overheating is unlikely and could only occur if all cooling (including passive conduction/radiation) is lost for an extended time. Aforementioned attributes of the MHTGR contribute in part to satisfying the foremost objective of any nuclear power system, which is the preservation of public/environmental health and safety. To that end, the MHTGR design gives due consideration to siting criteria and standards for radiation protection as outlined in the various codes of federal regulations.

The MHTGR, unlike the higher temperature Gas Turbine Modular Helium Reactor (GTMHR), employs a Rankine power cycle for electricity production. The target core outlet temperature (690°C) is likely too low to be of use for electricity/hydrogen co-generation via electrolysis. However, there exists a wide array of potential industrial applications for MHTGR process heat or reduced pressure steam. Of course, such possibilities give rise to certain licensing issues that do not exist for LWRs. One might also imagine alternative MHTGR fuel cycles tailored for specific purposes (e.g. transmuting reprocessed LWR transuranics in TRISO fuel), but such applications were not among the HTGR primary programmatic objectives in the 1980's.

More recently, generation IV initiatives have called for HTGR designs that can both enhance proliferation resistance and reduce the domestic LWR spent fuel inventory. The GTMHR more completely addresses gen. IV objectives than does the MHTGR and offers more latitude in the way of process heat or co-generation applications. Because of

comparatively higher temperatures and coupled gas turbo-machinery (Brayton power cycle), GTMHR thermal efficiency is higher than that of the MHTGR and allows for reduced thermal pollution. Overall, the GTMHR satisfies all design objectives of the MHTGR while simultaneously reducing environmental impact and heavy metal wastes (relative to LWRs). Most research done at the MHTGR-based HTTF will bear some relevance to the GTMHR because of the resemblance in core design.

2.3 General Design Description

The MHTGR is similar to other previously licensed HTGR facilities such as Fort St. Vrain and Peach Bottom-1. However, DOE's programmatic objectives for the MHTGR necessitate certain safety and high-temperature design characteristics that distinguish it from previous systems. Safety characteristics include a low power density, a large and negative core Doppler coefficient of reactivity, a high heat capacity, a chemically and neutronically inert single phase coolant, and passive decay heat removal. These features prevent and mitigate (two pillars of defense-in-depth) potential accidents.

2.3.1 Fuel Design

The MHTGR is a thermal-spectrum reactor that uses tri-isotropic (TRISO) coated fissile (uranium) and fertile (thorium) fuel kernels suspended in carbonaceous cylindrical compacts (12.45 mm diameter, 49.3 mm long) that are stacked in hexagonal graphite blocks (fuel elements). A cut-away view of a typical TRISO particle is included in Figure 2.1 as are pictures of fuel compacts and elements.

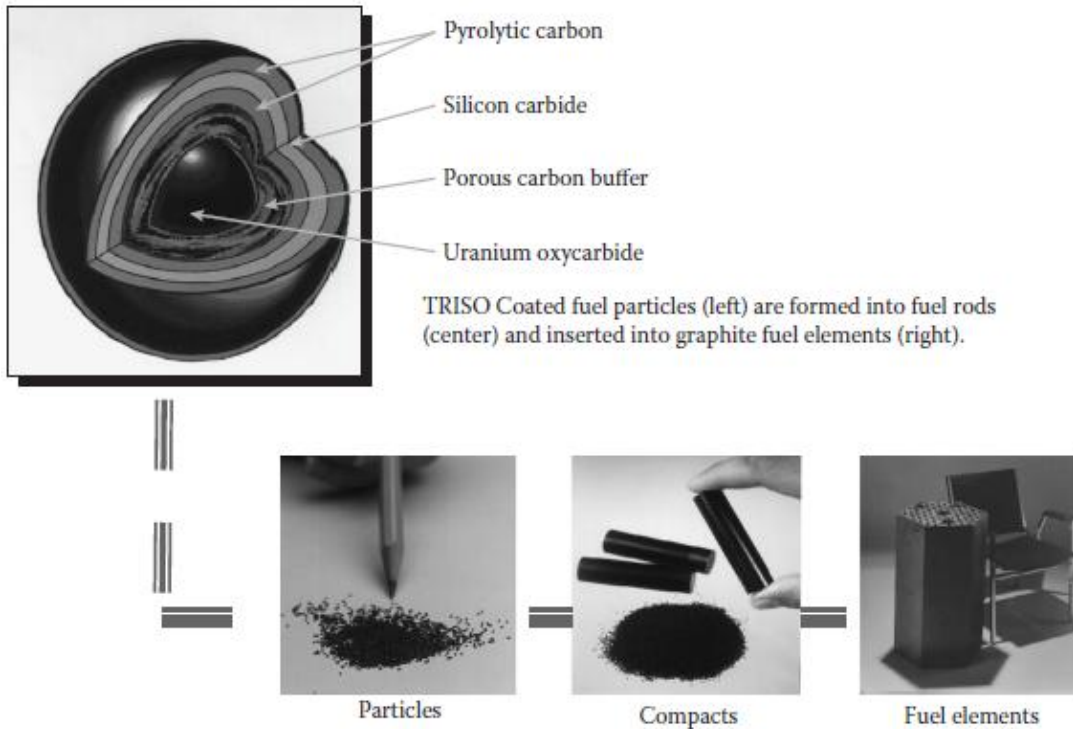


Figure 2.1. TRISO fuel kernels, compacts, and elements [6]

Uranium-bearing fuel kernels are 19.9% enriched (by weight), just under the 20% LEU limit. The various layers of kernel coating ensure structural integrity and fission product retention of each TRISO particle. The porous carbon buffer traps gaseous fission products and absorbs recoil energy while the silicon carbide layer provides structural stability against thermal and mechanical stresses. The outermost pyrolytic carbon layer acts as yet another barrier to fission products. The cylindrical graphite compacts maximize fuel conductivity and hinder fission product escape.

2.3.2 Core Element Design

The fuel elements are right hexagonal prisms (0.793m tall, 0.36m across flats) stacked ten high in an annular arrangement around a central reflector region and inside a

peripheral reflector. Each has coolant and fuel holes and a few have reserve shutdown control rod holes. Graphite regions are present above and below the active core for additional neutron reflection. Ceramic structures above the flow distribution block in the lower reflector are made of nuclear grade H451 graphite. Coolant channels and control material holes are present as necessary in the upper reflector, the outer portion of the central reflector, the inner portion of the side reflector, and the lower reflector. The innermost elements of the central reflector and the outermost regions of the side reflector are solid. MHTGR core layout is shown in Figure 2.2.

Hex blocks comprising the upper and lower reflectors are not all identical in height. The top reflector consists of two layers: a top layer of full height (0.793m) and a bottom layer of half height. The lower reflector consists of a three-quarters height layer atop a half height layer that acts to distribute coolant flow to the lower plenum. For purposes of construction, shuffling, and replacement, all blocks have handling holes at their geometric centers. Sockets are carved out of each block to accommodate graphite dowels that hold stacked structures together.

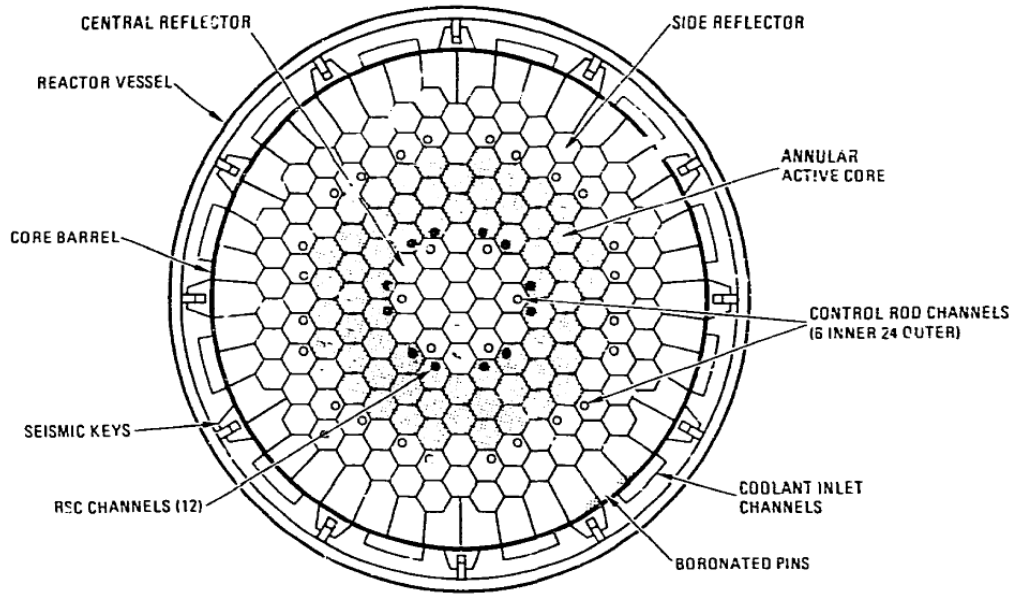


Figure 2.2. Cross-sectional view of the MHTGR core [6]

Several metallic components (Alloy 800H) designed for various purposes are present around the graphite core. Lateral restraints and the metallic support structure help to hold graphite in place. The upper plenum thermal protection structure shields the metallic vessel from thermal loads and provides a sealed upper plenum region that facilitates coolant flow. The metallic core barrel, up-comer ducts, and vessel wall all play important roles in core cooling (under both normal and accident conditions) as does the metallic cross duct leading to and from the reactor vessel. Also, metallic plenum elements (alloy 800H) resting atop the upper reflector serve to limit core bypass flow and provide neutron shielding for the rest of the upper plenum. Plenum elements differ in form and function depending on their radial location above the upper reflector. Elements on top of the active core region have all requisite coolant channels and reserve

shutdown control rod holes. Elements above the central or side reflector may or may not have coolant holes. Plenum blocks contain borated graphite pellets for neutron shielding.

2.3.3 Reactor Pressure Vessel, MHTGR Module, and Coolant Flow

The MHTGR steam cycle plant module is pictured in Figure 2.3, with the reactor vessel on the left and the steam generator vessel on the right. The nuclear island contains four 350 MW_{th} modules, each housed in an underground concrete silo that acts as a vented containment. Nominally, the core power density is 5.9 MW_{th}/m³ and the primary loop is pressurized to about 6.4 MPa.

The two vessels in each module are connected by a concentric cross duct through which hot helium exits the reactor vessel (through the inner channel) and cold helium enters the reactor vessel (through the outer channel). From the cross duct, cold helium is sent to up-comer ducts that lead to the upper plenum. Helium is then turned back downwards to flow through the core before being collected and mixed in the lower plenum. At core inlet conditions, the helium temperature is about 260 °C and is flowing at 157 kg/s. It is estimated that about 11% of the coolant flow bypasses the active core and is channeled through central reflector coolant holes, small control rod coolant passages, and intervening gaps between graphite blocks. Helium passing through core coolant channels sees no change in flow geometry across the core, leading to negligible form losses and a relatively small friction pressure drop. Coolant experiences a transition in channel geometry at the lower reflector flow distribution block just before it reaches the lower plenum. On average, the coolant exit temperature is 690 °C, but localized “hot streaks” could be significantly hotter.

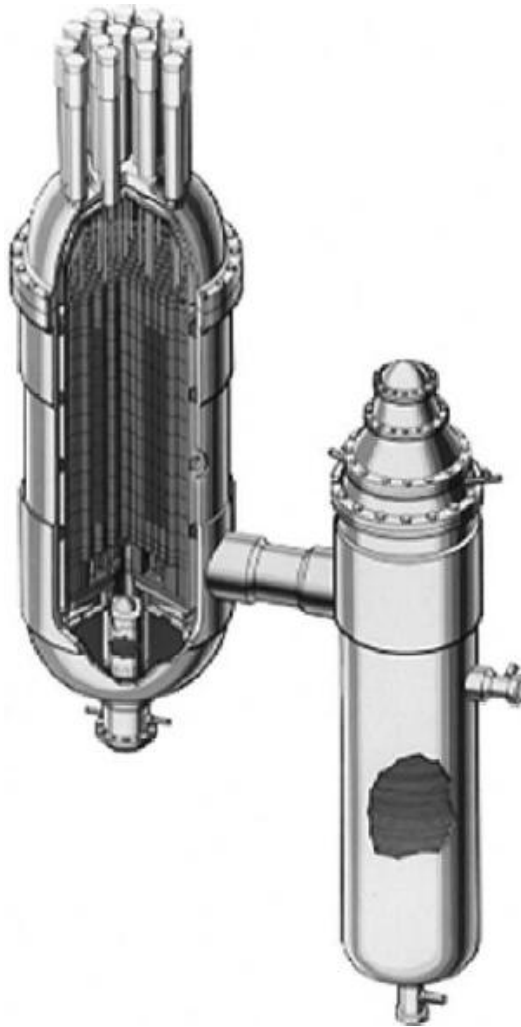


Figure 2.3. MHTGR reactor vessel, cross duct, and secondary vessel [6]

2.3.4 Reactivity Control Systems

Burnable poisons, standard control rods, and reserve shutdown control rods comprise the reactivity control strategy. Burnable poison (borated graphite pins) is included at the hexagonal corners of each fuel element to cope with excess reactivity over the course of core lifetime. Standard control rods reside in the central and side reflectors and consist of 40 weight percent enriched boron carbide granules dispersed in graphite rods that are canned in alloy 800H. Reserve shutdown control “pellets”

containing boron carbide are available for emergency insertion to reserve shutdown fuel elements. Thus, there is no control material other than burnable poison in the active core region under normal operating conditions. This design differs considerably from that of LWR's and is explained by the greater relative reactivity worth of control rods located in regions of peak thermal neutron flux (reflectors) vs. control rods dispersed throughout the active core.

Overall, reactivity temperature/power feedback is inherently negative under conceivable operating conditions. Major contributing effects include prompt fuel Doppler feedback, graphite moderator temperature feedback, and reflector temperature feedback. The first two feedback effects are negative, while the last one is small and positive for reasons related to control rod worth in reflectors subsequent to heat-up. By design, the helium coolant is neutronically transparent regardless of temperature. The delayed neutron fraction is approximately 0.0065 near the beginning of core life but evolves as a function of the fissile nuclide inventory thereafter.

2.3.5 Fuel Loading and Power Distribution

The metal inventory of a fresh MHTGR core consists of approximately 2.346 metric tons of thorium and 1.726 metric tons of uranium, which allows for an initial cycle length of just less than 2 years. The next three "transition reload" cycles call for replacement of half the core every 1.5 years. The Equilibrium burn-up cycle is then reached, where half the core is replaced every 1.65 years. Enrichment zoning is not part of the axial or radial power shaping strategy, but zoning by average fissile/fertile material concentration is employed to shift power radially outward. Axially, the profile is top-peaked so that incoming coolant first encounters regions of highest power.

2.3.6 Shutdown Cooling System and Reactor Cavity Cooling System

The shutdown cooling system (SCS), pictured in Figure 2.4, is a non-safety related backup to the normal operating heat transport system (HTS). It sits below the reactor vessel and allows helium heat rejection to a secondary shutdown water loop via a cross counter-flow tube and shell heat exchanger. Helium from the lower plenum is channeled to a central duct and then flows around helical cooling tubes before reversing direction and going back to the upper plenum. A single shutdown water loop services all four modules, but there is one SCS heat exchanger and helium circulator per module. Ultimately, a tertiary service water loop removes thermal energy from SCS water.

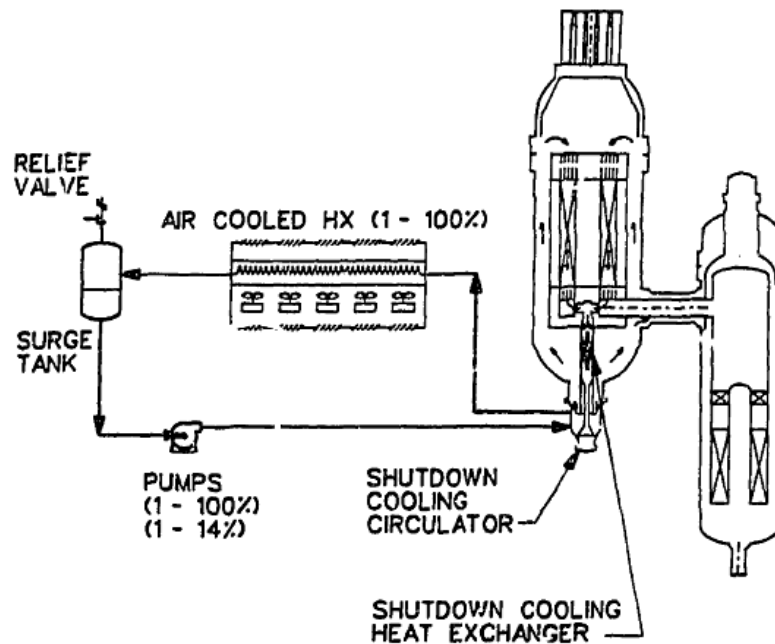


Figure 2.4. Shutdown cooling system loop [1]

The reactor cavity cooling system (RCCS) pictured in Figure 2.5 is the passive safety-grade core cooling system that makes the MHTGR “walk-away safe”. It involves no active components but instead relies on naturally-occurring phenomena to remove residual heat from the reactor vessel to the environment. In the event the normal HTS or SCS is unavailable, the RCCS automatically intervenes (without reliance on operators or actuation signals of any kind) to cool the metal vessel wall. As designed, the RCCS is air-cooled, but water-cooled alternatives have been proposed.

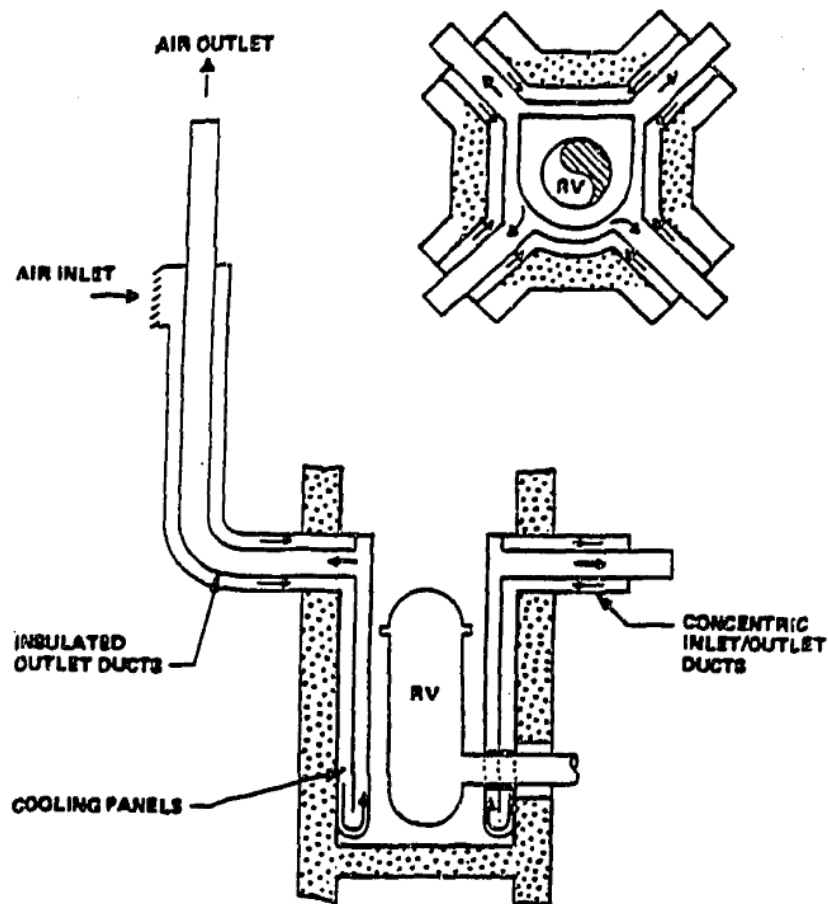


Figure 2.5. Reactor cavity cooling system diagram [1]

The RCCS consists of a cooling panel array that encloses the bare steel reactor vessel wall. Cold down-comer passages and insulated hot riser ducts facilitate natural draft air cooling. Across the intervening reactor cavity air space, the steel vessel surface radiates thermal energy to the steel RCCS panels so that natural circulation can carry this energy outside the system. Figure 2.6 below shows a top view of the pressure vessel wall, reactor cavity, and RCCS panels.

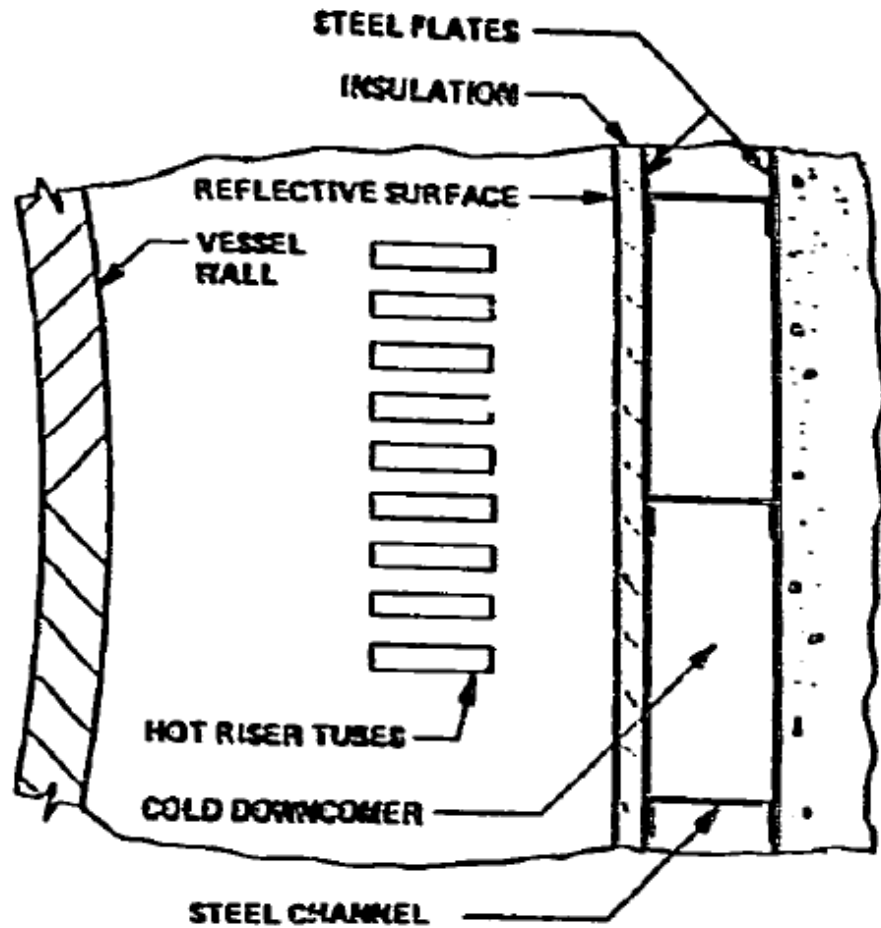


Figure 2.6. RCCS configuration, top view [1]

It is expected that radiation accounts for roughly 90% of the vessel heat removal, with the balance removed by cavity air circulation. Sufficient redundancy is built in to each module's RCCS, as there are hundreds of independent panels (hot ducts) and four separate inlets/outlets to communicate with the environment. Provided the core conduction pathway is not degraded, the RCCS can maintain core material temperatures below damage limits and thereby preclude a significant radioactivity release.

3. HTTF OVERVIEW

3.1 Brief History

As part of a recent cooperative agreement on HTGR research between the NRC and several academic researchers, Oregon State University was tasked with the design and construction of an integral test facility for study of HTGR thermal hydraulic phenomena. As the first of its kind in the U.S., it is envisioned that the HTTF will furnish valuable thermal hydraulics data that better characterizes some potential challenges of prismatic-type HTGR operation. Special attention will be afforded to “high priority and low knowledge” issues identified in a recent DOE Phenomena Identification and Ranking Table (PIRT) study (part of the NGNP project, 2008) [7]. For normal operating conditions, these issues include helium hot streaking, bypass flow, and other matters related to coolant flow distribution. For off-normal conditions, coolant behavior and overall system response during pressurized and/or depressurized conduction cool-down (P/DCC) is of great concern.

With the DCC event in mind, OSU performed a scaling analysis in accordance with NRC severe accident scaling methodology as described in appendix D of NUREG/CR-5809 [8]. Application of this Hierarchical Two-Tiered Scaling (H2TS) method resulted in a conceptual HTTF design and helped to quantify scaling distortions where similitude between prototype and model could not be preserved. It should be noted that the scaling analysis was performed for HTGRs of both prismatic or pebble-bed type. The MHTGR and/or the GTMHR are obvious references for prismatic-type HTGRs, but no specific consideration was given to either design in the scaling analysis.

3.2 Objectives

Integral HTTF experiments will address several deficiencies in the present knowledge base and will hopefully advance the state of the art of HTGR design. A judicious instrumentation plan and a well-designed test matrix will enable code-to-experiment benchmark studies with MELCOR (and other codes) to advance the state of the art of reactor thermal hydraulic analysis. Expansion of the knowledge base and code validation are of paramount importance to the NRC insofar as licensing, especially if the existing NRC code suite (of which MELCOR is a part) will be utilized for HTGR design basis and licensing calculations.

The NGNP PIRT [7] identified poorly understood physical phenomena associated with pressurized/depressurized losses of forced circulation (P/DLOFC). These events are also called pressurized/depressurized conduction cool-downs because after a loss of forced circulation, the main core cooling modes are radial conduction and radiation to the passive reactor cavity cooling system (RCCS) panels. In a pressurized conduction cool-down, there is no break in the pressure boundary and reactor vessel depressurization does not occur. The coolant will stagnate before eventual establishment of natural circulation. In a depressurized conduction cool-down, helium coolant crosses the pressure boundary and a vessel depressurization occurs (the timing of which depends on break characteristics). Natural circulation cooling patterns (air/helium mixture) will set up eventually, preceded by air ingress from the reactor cavity depending on breach location. The mode of air ingress and air/graphite interaction is crucial to the DCC event. Lock-exchange (counter-current air/helium flow) and molecular diffusion are expected to be the most important air ingress phenomena. The HTTF is scaled to accurately

reproduce the DCC with little distortion of core thermal hydraulic response. Certain attributes of other accidents (e.g. PLOFC) could be examined if inherent scaling distortions are properly quantified and if the HTTF is designed to reach necessary power and pressure levels.

While simulating accidents, the HTTF will give phenomenological insight in to certain MHTGR/GTMHR design features including the RCCS, the reactor cavity, and the ceramic core/reflector blocks. RCCS operation under degraded conditions (fouled panels, disabled panels, etc.) must be better understood. Effects of natural circulation in and radiation across the reactor cavity (an air space intervening between the vessel wall and RCCS panels) will be examined. Also, residual heat removal via radial conduction through the core and peripheral reflector must be better characterized. Such studies could help to tune predictive physics models or to create entirely new ones.

3.3 General Design Description

Similarity criteria following from the scaling analysis determined dimensions and operating/boundary conditions for the reduced-scale HTTF. Similarity criteria were formulated in terms of prototype-to-model scaling ratios involving geometric, fluid, and material properties. These ratios followed from non-dimensional forms of mass, momentum, and energy equations written for certain processes (e.g. depressurization stage of a DCC event). Of course, complete prototype-to-model similitude for any and all processes was impossible to achieve for a multitude of reasons. Only for the most important processes was similitude pursued. To obtain needed scaling ratios, designers adjusted certain free parameters like material properties and model dimensions. HTTF designers chose to preserve kinematic and friction/form loss similarity (according to the

DCC scaling analysis) between the prototype and model. Materials, geometry, and power scaling choices were made to facilitate a design that is full scale (i.e. completely similar) in temperature. Also, large distortions in time scaling were avoided so that all stages of important events may be studied. Core and vessel heat transport, air ingress by lock-exchange and diffusion, and single phase natural circulation are reproducible HTGR phenomena in the scaled HTTF. Therefore, DCC phenomenology may be studied in excellent detail, and higher-pressure PCC experiments could be possible too.

The reactor cavity cooling system plays a vital role in thermal hydraulic transient response and was given due consideration in the scaling analysis. Radiative heat transfer area, duct flow area, and duct flow kinematics were characterized by similarity ratios that were then used to make RCCS design decisions. Parameters such as exposed vessel steel area, vessel steel emissivity, and vessel-to-panel view factors are also subject to operator adjustment.

3.3.1 Core and Vessel Design

The test facility is 1:4 scale in height and radius (with respect to MHTGR dimensions), full scale in temperature, and approximately 1:8 scale in pressure (with respect to MHTGR normal operating conditions). Cross-sectional coolant flow area is roughly 1:16 scale. Ceramic core materials with varying heat transport characteristics (thermal conductivity, heat capacity, etc.) are used in the core block, reflectors, and lower plenum. These so-called “designer ceramics” specially tailored to HTTF scaling needs will be used where necessary to adjust overall core thermal resistance and facilitate temperature similitude. Fluid property similitude is preserved well enough (at least for a DCC event) by using helium as the HTTF working fluid.

For the aforementioned geometric scaling, the expected HTTF vessel height is approximately 4 m with an outer radius of roughly 1.93 m. The core region consists of a stack of hexagonal graphite blocks (perforated by coolant, fuel, “control rod” holes where necessary) with a solid central region, a coolant/fuel hole region, and a solid side reflector region. Atop the “active core” region where electric heater rods reside is an upper reflector region. Lower reflector and flow distribution regions exist below the active core and above the lower plenum structures. Ceramic structure surrounds the lower plenum gas space and allows coolant flow to exit through a concentric metal duct (as occurs in the MHTGR). More solid ceramic material sits outside the upper reflector, core, and lower reflector regions and is meant to represent the permanent side reflector of a prismatic-type HTGR. This permanent side reflector region is wrapped in a steel barrel around which rectangular up-comer ducts are situated circumferentially. The steel vessel surrounds the up-comer region and connects to steel, hemispherical upper and lower head structures at the top and bottom, respectively. An air cavity intervenes between the vessel surface and the surrounding steel RCCS panels.

3.3.1.1 Typical Core Block Design

Ten stacked core blocks constitute the active core region of the HTTF. Each core block is identical in terms of size and hole pattern. The core blocks resemble regular hexagons with distance across the flats of approximately 1.2 m, but have jagged edges designed to lock in with the permanent side reflector. The height of each block is 0.198 m so that the overall active core height is 1.98 m. In each block there are 270 electric heater rod holes, 384 coolant channels, and a total of 42 “control rod” holes consisting of 30 ordinary control rod holes and 12 reserve shutdown control rod holes. Control rod

holes are essentially adjustable coolant channels that allow for variable bypass flow and, to an extent, adjustable pressure drop across the core. Heater rods are 0.0191 m (3/4") in diameter, coolant channels are 0.0168 m (2/3") in diameter, ordinary control rod holes are 0.0238 m (0.938") in diameter, and reserve shutdown control rod holes are 0.0168 m (2/3") in diameter.

3.3.1.2 Reflector Design

Upper reflector blocks are regular hexagonal in shape and are almost identical in cross-section to the previously described core blocks. There is a top upper reflector block and a bottom upper reflector block (both 0.102 m thick) that are separated by a space meant to house heater rod electrical components. Thin graphite sleeves convey the coolant inventory from the upper plenum gas space through the entire upper reflector region. Therefore, the helium sees no flow channel geometry change between the upper reflector and active core regions. The top upper reflector block has the typical core coolant hole and control rod hole layout without any heater rod holes. The bottom upper reflector (below the space containing heater rod electrical connections) has typical core coolant, control, and heater holes.

The lower reflector block is regular hexagonal in shape and is similar to previously described components in that it retains the typical core coolant and control rod hole layout. A transition in coolant flow geometry occurs in the next-lowest block called the flow distribution block. Coolant enters the distribution block in the typical core flow pattern and transitions to a lower plenum flow pattern consisting of approximately 128 0.0254 m (1.0") coolant holes. This transition occurs about halfway down the distribution block and flow continues to the lower plenum from that point. It

should be noted that the MHTGR design features a similar flow transition between the active core and the lower plenum.

3.3.2 Reactor Cavity Cooling System Design

A circular array of swiveling steel panels will act as the passive reactor cavity cooling system for the HTTF. Recent RCCS design proposals call for a system of water-cooled panel arrays that “view” un-insulated segments of the outer vessel steel wall. The choice of water as opposed to air for cooling purposes has obvious implications insofar as applicability to the air-cooled MHTGR RCCS. The inclusion of rotating RCCS panels may allow investigation of degraded RCCS performance via view factor variations. Treating vessel-to-panel view factors parametrically would allow experimenters to put upper and lower bounds on the RCCS heat removal capability. Other factors including material surface emissivity and radiative vessel surface area give operators greater latitude for investigating RCCS performance.

4. MELCOR OVERVIEW

4.1 Background

Created by Sandia National Laboratories for the NRC, MELCOR was originally conceived as a flexible, fast-running probabilistic risk assessment tool that has since evolved in to a best-estimate, systems-level severe accident analysis code for light water reactors. MELCOR development began in 1982- a few years after the events at TMI unit 2- and has continued to the present day. MELCOR is capable of tracking severe accident progression up to source term generation. It can be employed in alternate capacities to study various thermal hydraulic, heat transfer, and aerosol transport phenomena. This is due in large part to MELCOR's lumped parameter control volume/flow path modeling approach that is quite general and adaptable. MELCOR is under active development and maintenance by the reactor modeling and analysis division at SNL. Good documentation is readily available to licensed users, as is a robust error reporting system that allows direct communication with code developers.

The recent release of code version 2.1 saw a shift towards "object oriented" programming and input construction, whereby MELCOR was made more user-friendly. MELCOR 2.1 is as capable as its predecessor, MELCOR 1.8.6, but enjoys added versatility due to a multitude of new input formatting options. Incorporation of gas cooled reactor physics and point kinetics models extends modeling capabilities beyond the realm of LWRs to include HTGRs. As part of a larger code suite, MELCOR will be used by the NRC for HTGR design basis calculations in the near future [9]. The immediate need for validation of MELCOR HTGR models is, in part, the impetus for the HTTF project.

4.2 Code Mechanics

MELCOR is comprised of a suite of packages that each fit in to one of three categories: basic physical phenomena, reactor-specific phenomena, or support functions [10]. Program execution involves two steps, MELGEN and MELCOR, as shown in Figure 4.1. All code packages used for a given problem communicate with one another as directed by an overseeing executive package. User input is processed by MELGEN, checked against code requirements, initialized, and used to write a restart file before running MELCOR. Calculation advancement through a specified problem time is performed by MELCOR. Text output and plot data are constantly written to certain output files as MELCOR runs. A Microsoft Excel macro, PTFREAD, allows data plotting from a MELCOR plot file.

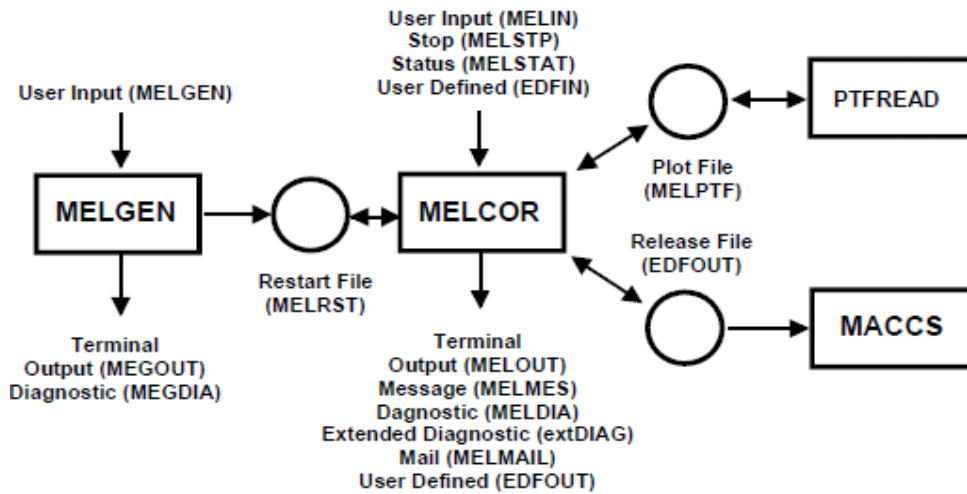


Figure 4.1. MELCOR execution flow diagram [11]

Of the approximately twenty packages, ten were used for purposes of this study. These were the executive (EXEC), control volume hydrodynamics (CVH), flow path (FL), heat structure (HS), core (COR), material properties (MP), noncondensable gas (NCG), decay heat (DCH), control functions (CF), and tabular functions (TF) packages.

The EXEC package is a support functions module responsible for overall execution control when running MELGEN or MELCOR. It essentially coordinates processing tasks for all other packages. It performs file handling functions, input and output processing, sensitivity coefficient modifications, time-step selection, problem time advancement, and calculation termination. [11]

The CVH package is a basic physical phenomena module. It models, in part, the thermal-hydraulic behavior of all hydrodynamic materials that are assigned to control volumes in a calculation. Control volume altitudes (relative to some chosen reference) as well as material volumes are specified by CVH input. The initial thermodynamic states of all control volumes are defined by CVH input as are any energy or material sources/sinks.

The FL package is a basic physical phenomena module that works in tandem with the CVH package to predict thermal-hydraulic response. The FL input defines all characteristics of the control volume connections through which hydrodynamic material can relocate. However, no material can physically reside within a flow path in any given time-step. Instead, the FL package is concerned with momentum and heat transport of single or two phase material as it moves from one control volume to another. Friction losses (e.g. to pipe walls), form losses, flow blockages, valves, and momentum sources (e.g. pumps) are defined through the FL package.

The HS package is another basic physical phenomena module that calculates one-dimensional heat conduction within any so-called heat structures. The structures are intact, solid, and comprised of some material with some definite geometry. The HS package also models energy transfer at a heat structure surface. This might include convection heat transfer to hydrodynamic material of an adjacent control volume or radiation heat transfer to separate heat structures.

The COR package is a reactor-specific phenomena module because the physics models employed generally depend on reactor type. It predicts the thermal response of the core and lower plenum. It frequently communicates with CVH, FL, and HS as fission thermal power is ultimately conveyed to hydrodynamic material or heat structures.

The MP package is a support functions module that acts as a repository for material properties data. Apart from the NCG package that treats noncondensable gases, the MP package is the sole reference for all thermo-physical data of materials. There are built-in properties for certain materials (most of which are common to LWR's), but the user may optionally overwrite those defaults or create new materials entirely. Density, thermal conductivity, specific heat capacity, and enthalpy/melt point can be defined as functions of material temperature.

The NCG package is a basic physical phenomena module in that it predicts noncondensable gas properties via the ideal gas law. Similar to the MP package, it acts in a support functions capacity because it passes requisite materials data to other physics packages for use. In the NCG package, a gas is characterized by its molecular weight, energy of formation, and specific heat capacity at constant volume which is assumed to be an analytic function of the gas temperature [11]. There are over a dozen built-in

noncondensable gases. As with the MP package, the user may overwrite any default properties or create entirely new materials.

The DCH package is a basic physical phenomena module. For purposes of this study, DCH is deployed in “whole-core” mode so that the power at all times subsequent to reactor scram is computed using a version of the ANS standard decay curve.

The CF package is a support functions module. It can be leveraged to create real or logical functions for use by the physics packages. Real-valued control functions return a real value (i.e. floating point value), while logical control functions return one of two integer values that are interpreted as either “true” or “false”. Most mathematical and logical functions available in FORTRAN are available for use in the CF package. A real-valued control function might be used to compute the density of some user-defined material via a user-defined function of material temperature. A logical-valued control function might be used to signal the start of a reactor scram or to close a user-defined valve in some flow path. Physics packages often reference control functions for required information. Control functions can also be helpful when a user is interested in calculating or plotting some variable that MELCOR does not compute by default.

The TF package is a support functions module. Tabular functions are utilized when definition of some dependent variable (e.g. decay heat) is required as a tabular function of some independent variable (usually time or temperature). As an example, the MP package often references tabular functions to retrieve material property values as a function of temperature. The user retains the option to define many input variables as either tabular or control functions. There are situations wherein a tabular function is more appropriate (e.g. material property data is known only at certain values of

temperature), and there are cases in which a control function is more useful (e.g. material property data is approximated by an analytic function of temperature).

4.3 Modeling Concepts

As previously stated, MELCOR is a control volume (CV) and flow path (FL) code with a prevailing theme of lumped-parameter variable treatment. This is to say that, within a given CV containing a single phase fluid, there is one temperature and pressure at which the hydrodynamic material exists. Similarly, for core cells (described in greater detail later) containing one or more core components, there is one temperature for any component within any cell. Generally, there are no field variable (temperature or pressure) gradients within the smallest building blocks of any MELCOR model. Bearing this fact in mind, it is the user's responsibility to appropriately nodalize all in-core and ex-core regions of the system so as to capture any relevant physical phenomena. Guided by knowledge of best practices, the user must work within the code constraints to translate a real-world system into a MELCOR model.

4.3.1 Control Volumes

The MELCOR CV/FL approach to model building is abstract and flexible relative to methods of other thermal-hydraulics codes. There are no pre-defined reactor components or structures. The user has the latitude to create pipes, vessels, ducts, core coolant channels, etc. using control volumes, flow paths, and heat structures in whatever manner deemed appropriate. Control volumes contain hydrodynamic material mass and associated energy consisting of internal energy and flow work (or just enthalpy, by definition). These materials can be liquids, vapors, and noncondensable gases so that in general all control volumes contain a "pool" of liquid and an "atmosphere" of vapor or

gas. For purposes of HTGR modeling, control volumes contain only noncondensable gases under normal operating conditions. If no liquid is present in a control volume, there is no pool and the atmosphere exists at a single temperature and pressure construed as the control volume average (at the geometric center of the control volume).

Control volume geometry specification is required, as the user must give an altitude and describe, indirectly, a control volume shape by specifying the available hydrodynamic volume between control volume elevations. A control volume altitude is measured with respect to some zero elevation chosen by the user (a natural choice might be the bottom of active fuel or bottom of the reactor vessel). Once fixed, this zero elevation is the reference for the entire problem. There is a top and bottom elevation to each control volume (both referenced to the zero elevation). It is sometimes necessary to give intermediate (between top and bottom) elevations within a control volume. MELCOR uses volume/altitude tables to fully specify the geometry of each control volume. For every given elevation of a control volume (top, bottom, or intermediate), there is a corresponding number interpreted as either the hydrodynamic volume between that elevation and the next lowest elevation or as the hydrodynamic volume between that elevation and the lowest elevation of the control volume.

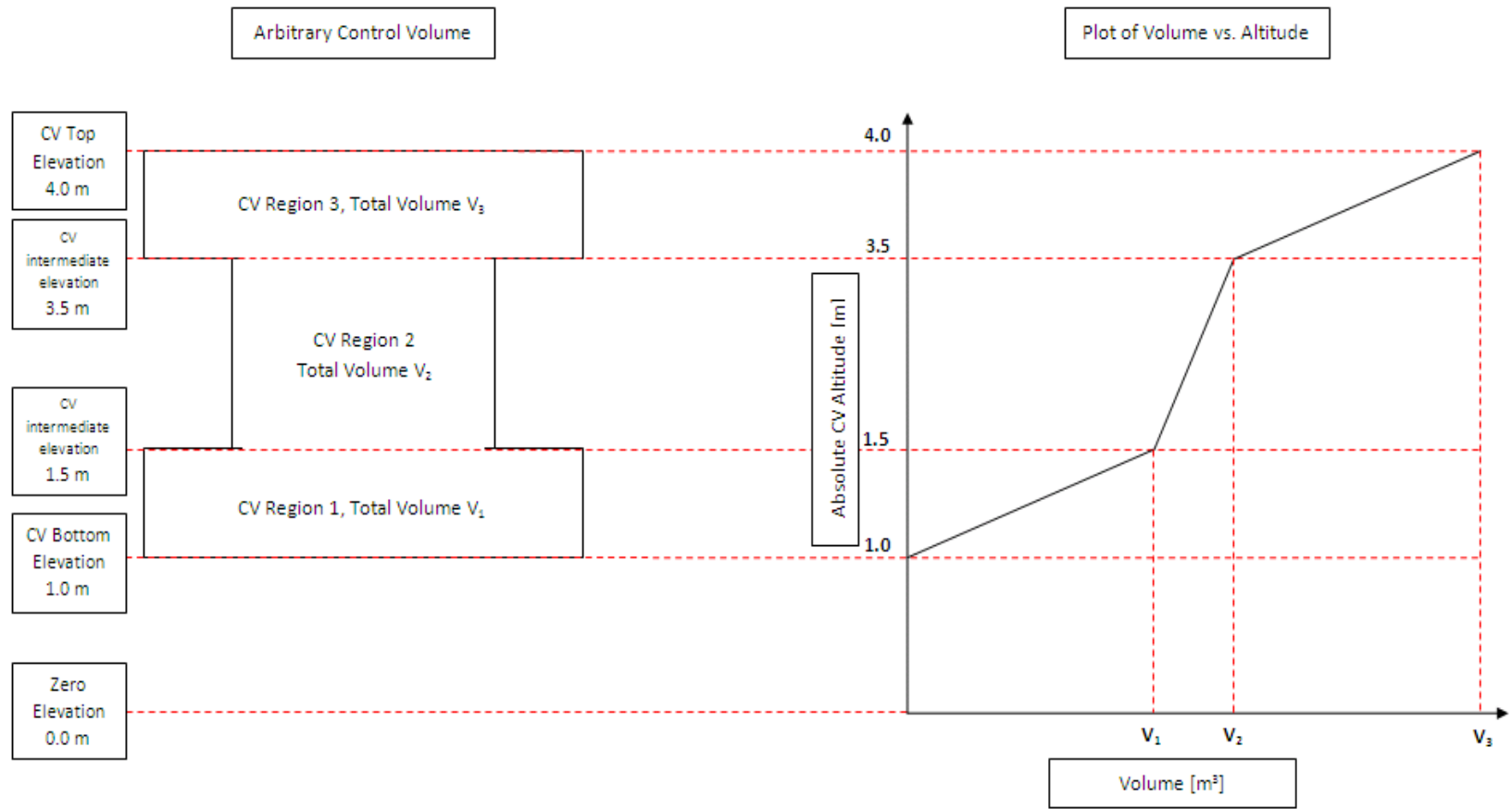


Figure 4.2. Volume/altitude concept for control volumes [11]

For clarity, Figure 4.2 above shows an arbitrarily-shaped control volume and includes a sketch of how hydrodynamic volume might vary with altitude. Note that the volumes V_1 , V_2 , and V_3 denote the volume values (positive in sign) that could appear in the CVH volume/altitude tables for elevations of 1.5 m, 3.5 m, and 4.0 m. Alternatively, the user could choose V_1 , V_2-V_1 , and V_3-V_2 as the volume values for the same elevations. In this case, the input volumes would be negative in sign to signify that they represent volume between the current and next-lowest elevation.

Thermodynamic conditions of the pool and atmosphere are initially set by the user and may evolve with time (subject to solution of the governing equations) or not. Thermodynamic states of active control volumes are advanced by solving linearized-implicit finite difference equations for mass, momentum, and energy [12]. Active control volumes are commonly used and usually account for the majority of control volumes in a calculation. Property-specified control volumes, wherein the temperature, pressure, gas fractions, etc. are set by the user and take values from control or tabular functions throughout the calculation, are often used as time-invariant source/sink control volumes. Initially, thermodynamic states are fixed by user-input. For control volumes with atmospheres but without pools, only initial temperatures and pressures are needed. Noncondensable gas fractions in the atmosphere must also be specified.

Any system component can be modeled as simply or as intricately as the user desires. Nodalizations should be fine enough to capture major physical phenomena but coarse enough that problem run times are not prohibitively long. Depending on the problem scenario, there may be other circumstances that influence a control volume

nodalization such as instrumentation layout or core cell nodalization. For sound comparison between an experiment and a MELCOR calculation, the spatial location of a pressure tap, for example, should be at or near the center of a MELCOR control volume. In this way, the average control volume pressure reported by MELCOR would correspond to roughly the same measurement recorded by the pressure tap. As for the control volume nodalization in the core region, it tends to follow directly from how the COR package models are implemented. Concerning ex-core components (e.g. pipes or ducts), two or more control volumes are adequate. For ex-core buildings and spaces (e.g. containment or reactor-adjacent rooms), single control volumes are often used.

4.3.2 Flow Paths

Flow paths are code constructs that model the flow and momentum transport of hydrodynamic material between control volumes. As mentioned before, hydrodynamic material has no residence time in a flow path across any time-step. The tacit assumption is that any amount of hydrodynamic material that would occupy the physical volume of the flow path connection is negligibly small compared to hydrodynamic volume of the connected control volumes [12]. The flow path package does account for friction losses, form losses, and inter-phase momentum/heat transport that would be associated with actual flow between connected volumes. Any single flow path connects only two control volumes, but there are no restrictions on the number of flow paths attached to any given control volume. Flow paths may be vertical or horizontal with several versions of each (e.g. atmosphere-first, pool-first, etc.)

The user must designate a “from”, or “donor”, control volume and a “to”, or “acceptor”, control volume, as well as several geometric parameters like from/to elevations, junction opening heights, flow path area, flow path length, and open fraction. Junction heights and from/to elevations have implications for any gravitational head terms appearing in the flow equations. The flow path length is related to the distance over which inter-phase momentum transport occurs. The importance is diminished in cases of single phase flow, and normally this length is assumed to be the center-to-center distance between connected control volumes. Flow paths may be fully open, partially open, or completely closed.

Regarding momentum transport, all dissipative pressure drops related to wall friction and form losses are accounted for in FL package input. The user must specify any and all form loss coefficients directly, as there are no predictive models for these values. Conversely, wall friction is handled by treating the flow path as one or more segments (in series along the flow direction), calculating an appropriate mixture Reynolds number based on a segment velocity, and deriving a Fanning friction factor that is used to compute a pressure drop in each segment [12]. All that is needed from the user are segment geometric parameters such as area, length, and hydraulic diameter.

4.3.3 Heat Structures

Heat structures treat one-dimensional conduction in some allowable geometry. These structures could represent pressure vessel walls, containment walls, pipe walls, or other structures associated with a reactor. One-dimensional mesh intervals marked by the presence of temperature nodes are used in a finite-difference technique to predict

heat structure temperature distributions. On the heat structure interior, a finite-difference form of the time-dependent heat diffusion equation is solved with or without an internal volumetric power source. On the mesh exteriors, one of many available boundary conditions is applied in finite-difference form to solve for surface node temperatures. Allowable geometries include rectangular, cylindrical, spherical, and hemispherical.

The user must specify structure geometry, elevation, and orientation. It falls to the user to decide the number of temperature nodes spaced across the heat structure. The gap between two neighboring nodes is called a mesh interval, and each may contain a different material. Node spacing and material allocation are user responsibilities.

Heat structure boundary conditions are needed from user input. There are essentially five kinds of conditions: adiabatic/symmetry, convective, specified heat transfer coefficient, specified heat flux, and specified temperature. Some conditions require that the heat structure be connected to neighboring control volumes while others do not. Convective conditions (without a specified heat transfer coefficient) signal to MELCOR that it must calculate its own convection heat transfer coefficient using internal models and information from surface-adjacent control volumes. In this case, MELCOR calculates Rayleigh and Reynolds numbers to characterize convection at heat structure surfaces. According to that characterization, heat transfer correlations are applied to arrive at a heat transfer coefficient. On occasion, the user must specify heat structure surface areas and characteristic lengths at the left and right faces. Surface power sources and volumetric power sources are available to the user through optional input records.

The structure-to-structure radiation model is available to predict radiation heat transfer with user-defined view factors between pairs of heat structure surfaces. The user may also assign surface emissivity values for use in the radiation equations. There are no models internal to MELCOR for calculating view factors, so the user must know these values beforehand or treat them parametrically.

4.3.4 Core Structures

The COR package predicts the thermal response of the reactor core and lower plenum. Built-in conduction, convection, radiation, oxidation, and thermal/mechanical stress models simulate core behavior under normal operating conditions. Various failure and accident progression models are available to treat off-normal and accident conditions where core melt and relocation are possible. When constructing the core nodalization, the user must adhere to MELCOR's two-dimensional cylindrical core modeling concept. The core and its contents - apart from hydrodynamic material associated with the CVH package - is split in to a user-defined number of radial rings and axial levels so as to create a network of core cells. Each cell is azimuthally symmetric about the core centerline and represents the intersection of a ring with a level. As such, each cell in the innermost core ring assumes a disc shape, while cells in outer core rings assume an annular shape. Ring numbers monotonically increase from inside to outside, while level numbers monotonically increase from bottom to top. A cell number, 'xyz', of three integers 'x', 'y', and 'z' is obtained by letting 'x' equal the ring number and letting 'yz' equal the level number. Thus, a core cell in the first ring ('x'=1) and tenth level ('yz'=10) would be cell 110, while a cell in the third ring ('x'=3) and fourth

level ('yz'=04) would be cell 304. Figure 4.3 shows an axial slice of a quarter section of a representative HTGR core. The general ring/level nodalization approach is illustrated. Each rectangular cell on the right hand side of Figure 4.3 is revolved around the core centerline to make an annulus. The assumption of azimuthal symmetry implies that the same quarter-section view exists all around the core.

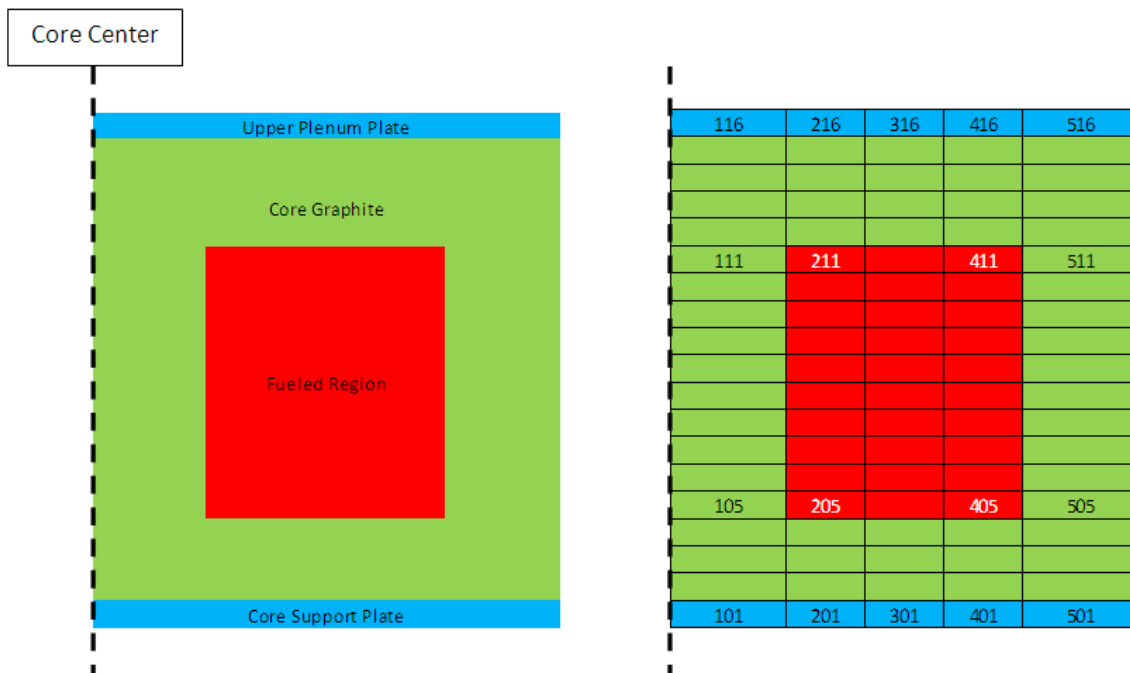


Figure 4.3. Generalized COR nodalization

Inside each core cell are one or more core components. There are designated components for fuel (FU), cladding (CL), supporting structure (SS), and non-supporting structure (NS) among others. Each component is normally comprised of one or two materials fully defined in the MP package input. Heat transfer occurs between core components or between core components and hydrodynamic material of the CVH

package. Effectively, fission power or decay heat causes the core cells to act as thermal power sources to core control volumes. The radial and axial power profiles are input by the user in the form of “relative power density”, or power per unit mass of fuel. Values are supplied for each fueled core cell and then normalized and multiplied by overall core power to determine cell power. The user must specify geometric parameters for all components including surface areas, equivalent diameters, flow areas, and cell boundary areas. This information affects calculations for convection, axial/radial conduction within the core, and axial/radial radiation within the core.

The core components that fill a given core cell should be assigned based on relative location within the core. For example, if the cell is within the “fueled region” of the HTGR core from Figure 4.3 above, it should contain fuel and cladding components to represent fuel compacts and surrounding graphite of the core block. If the cell is within the “core graphite” region, it might have reflector or supporting structure components that contain graphite material.

Core support logic should be given due consideration when assigning core components to axially adjacent cells. Components of stacked core cells within a given ring must be chosen so that the core is structurally sound. The core support logic considers the support characteristics of each core component and decides if the user-input configuration is allowable by MELCOR rules. Greater detail is available in the users’ guide, but some simple rules pertinent to HTGR modeling follow hereafter. Fuel (FU), cladding (CL), and reflector (RF) components in a cell can only support themselves and any FU/CL/RF material in cells above. FU can only support FU from

cells above, CL can only support CL from cells above, and RF can only support RF from cells above. This is to say that FU, CL, and RF are non-supporting in nature and must ultimately convey the load of their weight to a supporting structure. Looking again at Figure 4.3 above, the weight of all FU and CL that would lie within cells 205 to 211 would need to be supported by some SS in cell 204. Similarly, if RF was to exist in cells 213 to 215, there would need to be some SS in cell 212 between the RF and the FU/CL to support the load of the RF, as loads cannot be transmitted from RF to FU or CL. The SS component can support itself and anything in cells above (RF, FU, CL, etc.). Various failure models and support rules for the SS component exist in the COR package. The reader is referred to the users' guide for more information on these topics.

As built by the user, the core must be able to support itself. However, the user should refrain from filling the core with unnecessary SS merely to satisfy core support requirements. One must also consider that COR heat transfer models differ between components and that SS may not be the most appropriate component to model the true physics of the problem. Consider the "core graphite" region of Figure 4.3 as an example. In an HTGR, this region generally consists of center, top, bottom, or side reflectors made of solid graphite within which both radial and axial heat conduction occur. It is a better modeling strategy to use MELCOR's RF component (as opposed to SS) in this region as much as possible, as the RF was built with HTGR reflectors in mind. There should only be enough SS in the "core graphite" region to hold up the RF that sits above the active core and to hold up the FU/CL of the active core. In this way, all regions of the core are

adequately supported and the core heat transfer calculations are of highest achievable fidelity because the RF component is used as much as possible to model core reflectors.

Core package input requires specification of axial and radial boundary heat structures. Axial boundary heat structures might represent the outermost reflector region or the core barrel for an HTGR. Radial boundary heat structures might represent the hemispherical steel upper head or some other structure at the top of the reactor. For axial boundary structures, one HS is required per axial level in the core. For radial boundary structures, one HS may be used for all rings in the core. Boundary heat structures are recipients of thermal radiation from core components. For PMR-type reactors, the axial boundary structures are part of the thermal conduction pathway from the core interior to the periphery.

Though it is of little importance to the HTTF model, lower head and lower plenum geometry was necessarily specified. True to the actual design, hemispherical lower head geometry was applied to the lower head region. User input specifies the existence of lower head “segments” that coincide with the intersection of the lower head curvature with all axial level elevations and all ring radii. There are various parametric models to treat lower head failure and debris ejection to the reactor cavity, but these are of no consequence to study of the HTTF because no such events will occur.

4.4 Gas-Cooled Reactor Physics

The following overview of COR heat transfer treatments gives insight in to MELCOR predictions of core thermal response. Included in the discussion are axial,

radial, and boundary conduction as well as convection. Emphasis is placed on newly implemented prismatic reactor models used for the HTTF.

4.4.1 Axial Conduction

Component-wise axial conduction can occur between like components of axially-adjacent core cells. The conduction heat rate equation assumes the form [12]:

$$Q_{i,j} = K_{eff}(T_i - T_j) \quad (4.1)$$

$$K_{eff} = (K_i^{-1} + K_j^{-1})^{-1} \quad (4.2)$$

where

$$K_i = (k_i A_i)(\Delta x_i)^{-1} \quad (4.3)$$

$$A_i = V_{tot,i}(\Delta z_i)^{-1} \quad (4.4)$$

$$\Delta x_i = \frac{1}{2}(\Delta z_i) \quad (4.5)$$

An effective conductance, K_{eff} , is written as the parallel combination of conductance K_i for core cell i and conductance K_j for core cell j . The conductance of a cell, with units of power per temperature, is defined with respect to the actual component thermal conductivity (from MP package data for material(s) within the component), the “average horizontal cross-sectional area” of the component, and an axial conduction distance. Thus, the axial conduction heat rate between like components of two cells can be written with respect to the cell temperature difference and a parameter characterizing the power conducted per degree temperature difference between the two cells [12].

Drawing an analogy between electric current flow and heat conduction, one observes that the temperature difference is analogous to the driving force of a voltage potential while the conductance is analogous to the inverse of electrical resistance. MELCOR frequently uses this concept and formulates heat rate equations based on effective parameters (conductances or resistances) and a temperature difference. The equation(s) above apply to any core component. The only necessary condition for axial conduction is that there are two like components in the axially-adjacent cells i and j with some nonzero temperature difference between them.

4.4.2 Radial Conduction

Cases of inter-cell and intra-cell radial conduction will both be mentioned. The general, inter-cell formula for radial conduction is used for supporting structure. The same treatment with an augmented, effective conductivity from the Tanaka-Chisaka model is applied to radial conduction in a PMR core. The case of intra-cell conduction between fuel and cladding in prismatic-type reactors is also considered.

4.4.2.1 General Inter-cell Conduction

Equation 4.1 above for axial conduction is applied to the general case of radial conduction. The only differences are definitions of the conductance parameters [12]:

$$A_i = \left(\frac{V_{tot,i}}{V_{tot,j}} \right) (2\pi r_i \Delta z_{i,j}) \quad (4.6)$$

$$\Delta x_i = (V_{tot,i}) \left(2(2\pi r_i \Delta z_{i,j}) \right)^{-1} \quad (4.7)$$

The area used to define the radial conductance is that of the radial boundary between cells i and j multiplied by a cell volume fraction. The distance used to define the radial conductance is half the value of the ratio of cell i volume to radial boundary area.

4.4.2.2 Tanaka-Chisaka Effective Conductivity

In the case of PMR's, the core consists of solid graphite blocks perforated by coolant channels and fuel compact holes. The radial conductivity of the graphite blocks, modified to account for coolant and fuel effects, is obtained via the Tanaka-Chisaka expression [15]:

$$K_{eff} = k_s A + k_s (1 - A) \left(\frac{\ln \left(1 + 2B \left(\frac{k_{pore}}{k_s} - 1 \right) \right)}{2B \left(1 - \left(\frac{k_s}{k_{pore}} \right) \right)} \right) \quad (4.8)$$

where

$$A = 2(1 - \epsilon)(2 + \epsilon)^{-1} \quad (4.9)$$

$$B = (1 - \epsilon)(\epsilon)^{-1} \quad (4.10)$$

Under the assumption that the thermal conductivity of the fuel compacts approximately equals the thermal conductivity of the graphite block, k_s , the porosity is a simple function of material volumes [15]:

$$\epsilon = (V_{coolant\ channels})(V_{fuel\ compacts} + V_{graphite\ in\ block})^{-1} \quad (4.11)$$

The porosity is therefore the ratio of discontinuous volume (channel without solids) to continuous volume. The pore conductivity, k_{pore} , is a parallel combination of a “radiative conductivity”, k_{rad} , and helium thermal conductivity, k_{He} , as [15]:

$$k_{pore} = (k_{He}^{-1} + k_{rad}^{-1})^{-1} \quad (4.12)$$

$$k_{rad} = 4\varepsilon_r\sigma T^3 D \quad (4.13)$$

where

$$\varepsilon_r = \text{Ceramic emissivity} ; \sigma = \text{Stefan – Boltzmann constant}$$

Thus, the radial block conductivity is characterized only by the porosity, ϵ , the thermal conductivity of the solid graphite, k_s , and the effective pore conductivity k_{pore} . To get to the effective radial block conductivity, one must account for all gaps that exist between the many hexagonal blocks comprising a prismatic core. This amounts to adding a parallel resistance term for the gaps. In the HTTF, there is but one large, hexagonal block with no radial gaps. The radial block conductivity of the Tanaka-Chisaka expression should therefore need no correction for gaps. The Tanaka-Chisaka radial block conductivity is used in the previously presented radial conduction equation for radially-adjacent cells in the core of a prismatic reactor.

4.4.2.3 Intra-Cell Conduction “Thick Cladding”

Compared to the zircaloy cladding of an LWR, the PMR graphite regions that surround each fuel compact hole are much thicker. Whereas the assumption of a linear temperature profile in the cladding is allowable for an LWR, it is incorrect for a PMR.

The graphite “cladding” of the PMR is treated by MELCOR as “thick” by assumption of a logarithmic temperature profile. This result follows from the general solution to the heat diffusion equation for 1D radial conduction in cylindrical coordinates. Thus, there is actually a temperature distribution in the CL component of a PMR. However, in keeping with its lumped parameter philosophy, MELCOR derives an average CL temperature from the assumed temperature profile. It is instructive and worthwhile to outline the process of arriving at the average CL temperature from initial assumptions because it is mostly omitted from the users’ guide.

The steady-state heat diffusion equation reduces to the Laplace equation if no volumetric power sources exist. Given specified-temperature boundary conditions, the complete problem is:

$$\nabla^2 T(r) = \frac{1}{r} \frac{d}{dr} \left(r \frac{dT(r)}{dr} \right) = 0 ; T(r = R_0) = T_0 ; T(r = R_1) = T_1 \quad (4.14)$$

The radius R_0 is known from user input and is the inner radius of the cladding (the outer radius of the fuel compact plus any gap thickness). The radius R_1 is an effective cladding radius computed by transforming a hexagonal unit cell to a circular unit cell via preservation of total cell area. Solution of this equation subject to the given boundary conditions results in a radial temperature profile of the form:

$$T(r) = T_0 + (T_1 - T_0) \left(\ln \left(\frac{r}{R_0} \right) \right) \left(\ln \left(\frac{R_1}{R_0} \right) \right)^{-1} \quad (4.15)$$

Averaging T r with annular, cross-sectional cladding area as a weight function (i.e. taking an area average), one recovers:

$$\begin{aligned} \overline{T}_{CL} &= \frac{\int_0^{2\pi} \int_{R_0}^{R_1} T(r) r dr d\theta}{\int_0^{2\pi} \int_{R_0}^{R_1} r dr d\theta} = \left(\frac{2\pi}{\pi(R_1^2 - R_0^2)} \right) \int_{R_0}^{R_1} \left(T_0 + (T_1 - T_0) \left(\frac{\ln\left(\frac{r}{R_0}\right)}{\ln\left(\frac{R_1}{R_0}\right)} \right) \right) r dr = \\ & T_0 + (T_1 - T_0) \left(\frac{2R_1^2 \ln\left(\frac{R_1}{R_0}\right) - (R_1^2 - R_0^2)}{2 \ln\left(\frac{R_1}{R_0}\right) (R_1^2 - R_0^2)} \right) \end{aligned} \quad (4.16)$$

MELCOR defines a weighting factor (f) between the inner and outer surface temperatures [15]:

$$f = \left(2R_1^2 \ln\left(\frac{R_1}{R_0}\right) - (R_1^2 - R_0^2) \right) \left(2 \ln\left(\frac{R_1}{R_0}\right) (R_1^2 - R_0^2) \right)^{-1} \quad (4.17)$$

This weighting factor can be thought of as the fractional location of the average temperature in the wall [15]. If the wall is very thin so that R_1 is only slightly greater than R_0 , the weighting factor approaches 0.5. If the wall is very thick so that R_1 is much larger than R_0 , the weighting factor approaches unity. The location of the average temperature in the cylindrical wall moves towards R_1 from the midpoint between R_0 and R_1 as the wall thickens. The quantity f is used by MELCOR as a weighting factor for conductive resistance in the thick, cylindrical PMR cladding. As will be shown, f factors in to the definition of an effective conductance between the FU and CL

components. This conductance is then used to determine the heat transfer rate between the FU and CL components. MELCOR can therefore model the effects of the thick PMR cladding and still use just one CL average temperature and one extra conductance term in the FU to CL heat rate equation.

Similar to the axial conduction heat rate formula, the fuel-to-cladding heat rate equation uses an “effective total gap conductance” to account for all the factors affecting heat transfer between fuel and cladding. The gap conductance includes terms for conduction through the fuel, conduction across any existing gas gap, radiation between fuel and cladding across the gap, and conduction through the cladding (in the case of PMR’s with thick cladding). The fuel-to-cladding heat rate equation is [12]:

$$Q_{FU\ to\ CL} = h_{gap} A_f (T_{FU} - T_{CL}) \quad (4.18)$$

where

$$A_f = \pi D_{FU} H_{FU} \quad (4.19)$$

$$h_{gap}^{-1} = h_f^{-1} + z_0^{-1} + \left((h_{gas}^{-1} + h_{CF}^{-1})^{-1} + h_{rad} \right)^{-1} \quad (4.20)$$

and

$$h_f = 4 \left(\frac{k_{FU}}{R_{FU}} \right) \quad (4.21)$$

$$z_0 = (k_{CL}) \left(R_0 f \ln \left(\frac{R_i}{R_o} \right) \right)^{-1} \quad (4.22)$$

$$h_{gas} = (k_{gas}) (\Delta r_{gap})^{-1} \quad (4.23)$$

$$h_{rad} = \left(4\sigma \left(\frac{T_{FU} + T_{CL}}{2} \right)^3 \right) \left((\varepsilon_{FU})^{-1} + (\varepsilon_{CL})^{-1} - 1 \right)^{-1} \quad (4.24)$$

The area A_f is the fuel outer surface area obtained by multiplying the fuel circumference, πD_{FU} , by the user-defined fuel rod height (i.e. core cell height) H_{FU} . The conductance term h_{CF} is added so that the user can optionally include any other gas gap effects besides conduction and radiation. The z_0 term accounts for the conductance of the thick cladding in PMR's, so it includes the clad material conductivity k_{CL} as well as parameters f , R_0 , and R_1 that were used previously. The gas gap "radiative conductivity" assumes a form comparable to that used in the Tanaka-Chisaka model with the difference being that temperatures and emissivity values of both fuel and cladding (T_{FU} , T_{CL} , ε_{FU} , ε_{CL}) are encapsulated in h_{rad} .

4.4.2.4 Boundary Conduction

By design, prismatic-type reactors conduct heat to the core boundaries for purposes of cooling under accident scenarios. Heat conduction occurs within and across the core to peripheral reflector regions and through the core barrel on the way to the pressure vessel surface. Therefore, MELCOR must be able to model conduction at the boundary of the core region, where the core graphite treated by the COR package meets reflector graphite or barrel steel treated by the HS package. Axial boundary heat structures can receive thermal energy via conduction from designated components in the outermost radial ring of the core nodalization. The heat rate equation treats boundary conduction as a thermal circuit with resistance characterized by properties of any gas gap between the core component and heat structure:

$$Q_{C-HS} = (T_C - T_{HS})(R)^{-1} = (T_C - T_{HS}) \left((\Delta r_{gap}) (k_{gas})^{-1} + \sqrt{\frac{\pi \Delta t}{(k \rho C_p)_{HS}}} \right)^{-1} \quad (4.25)$$

The first term in the resistance R characterizes the resistance of conduction across a gap of thickness Δr_{gap} filled with a gas of thermal conductivity k_{gas} . The second term is included for numerical stability and is called the thermal diffusive resistance. It is a function of only material properties and the time-step length Δt . The temperature T_C is the single, average temperature of some general core component C . The temperature T_{HS} is that of the innermost node for the boundary heat structure in question. Conduction heat transfer at the core boundary is treated as occurring for 1D slab geometry and not cylindrical geometry. This is apparent from the definition of the gas gap resistance because it assumes the familiar form of a plane wall conduction resistance.

4.4.2.5 Convection

Convection heat transfer calculations in the core package occur for every component that has a user-specified, non-zero surface area. As is always the case with convection heat transfer, the problem reduces to computing a suitable heat transfer coefficient for the given flow conditions. The core package proceeds by first computing four Nusselt (Nu) numbers using various correlations for different possible flow conditions. This is to say that, regardless of the details of coolant flow, Nu is computed for cases of forced and free convection in both the laminar and turbulent regimes. Generally, Nu is correlated in terms of the Reynolds (Re), Prandtl (Pr), and/or Rayleigh (Ra) numbers. For laminar forced convection, Nu is formulated in terms of a developing

flow factor that accounts for entrance effects to the coolant channel. For turbulent forced convection, the familiar Dittus-Boelter correlation is applied. For both laminar and turbulent free convection, Nu is written in terms of Ra, the ratio of channel length to hydraulic diameter, and some empirical constant. There are a few special cases (e.g. pebble bed convection, boiling, and horizontal surfaces) where only one predetermined Nu correlation is applied, but these do not factor in to HTGR studies. Thus, two Nu values are obtained for forced convection and two for free convection. The numerically largest Nu values for both forced and free convection are identified and taken as representative of the core flow conditions. The heat transfer coefficient can then be computed, relaxed by an averaging technique to mitigate potential numerical instability, and used to compute a convection heat rate between coolant and core components:

$$Q_{conv} = h_{mix} A_s (T_s - T_f) \quad (4.26)$$

The surface area value A_s is that for the component in question (specified in COR input). The temperature T_s is the single, average value for the core component in question. The temperature T_f is related to the coolant temperature of the control volume interfacing with the core cell that contains the core component. However, because it is common practice to connect multiple axially-adjacent core cells to a single control volume (which has just one average temperature), the core package uses its “DT/DZ” model in an attempt to predict an axial temperature gradient within the control volume. The value of

T_f results from the DT/DZ model and is a more accurate prediction of local coolant temperature than the single control volume value.

The DT/DZ model is illustrated in Figure 4.4 for the case of three arbitrarily numbered core cells coupled to a single representative control volume. An inlet temperature to the control volume is determined and an energy balance is applied to each core cell. The balance consists of terms accounting for core cell energy storage across a time-step, enthalpy flow through the cell, and cell energy sources/sinks (e.g. from convection cooling of the cell or decay heat generation in the cell). The balance equations are solved for each cell to construct a rough axial temperature gradient within the control volume. Evident from Figure 4.4 is the fact that the coolant temperature calculated for cell 10(X-1) comes from the energy balance equation of cell 10X. Thus the coolant temperature in any arbitrary cell generally depends on the energy balance of the cell directly upstream of it (with reference to CVH data for definition of upstream and downstream). The reader is referred to the MELCOR reference manual for further information on each of the terms in the balance equation.

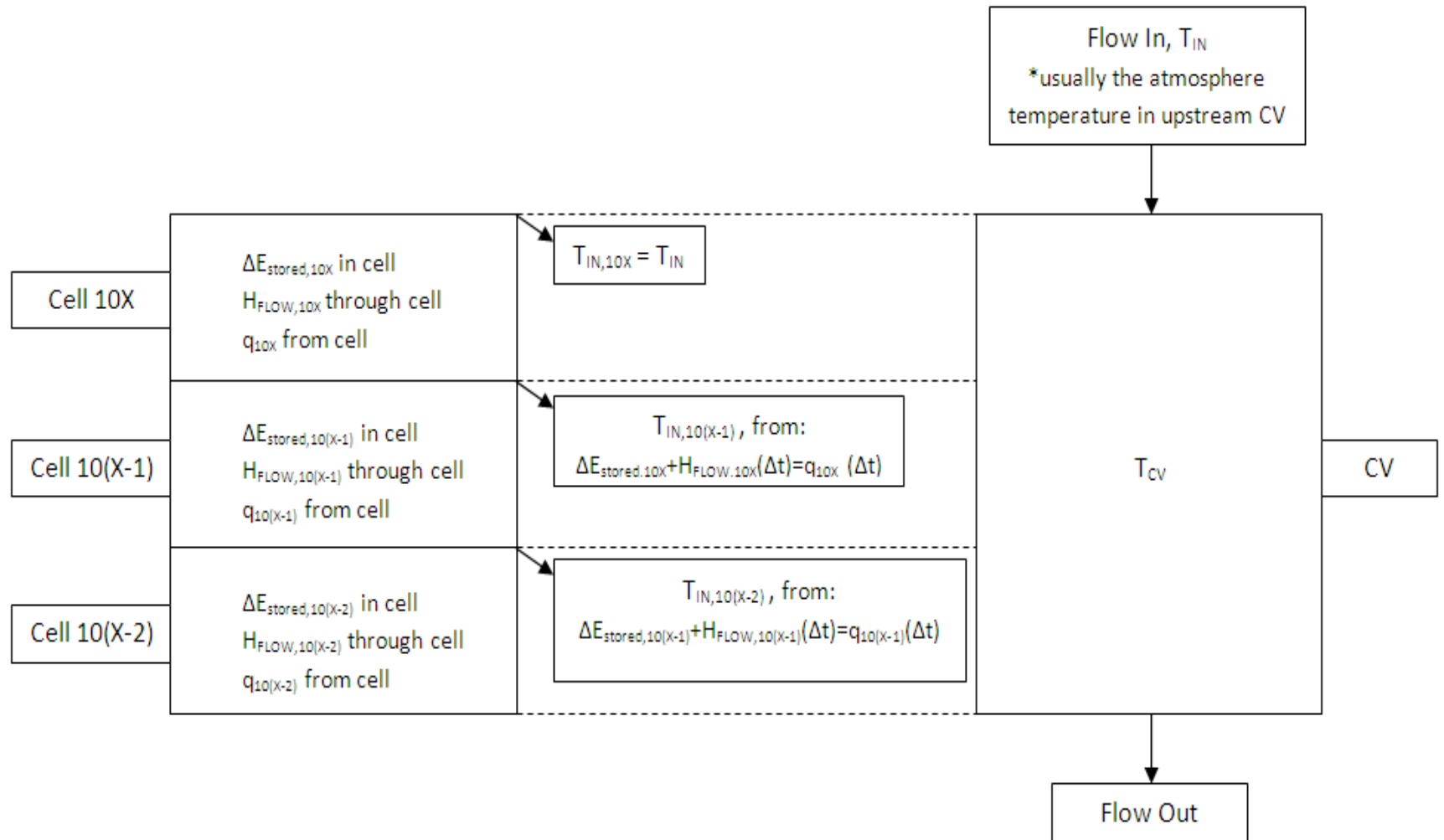


Figure 4.4. COR package DT/DZ cell-wise energy balance concept [12]

5. MELCOR MODELING APPROACH AND INPUT DEVELOPMENT

5.1 General MELCOR Modeling Approach

A MELCOR model of any general nuclear power system adheres to certain code requirements that largely dictate modeling approach. The user must appropriately translate a geometrically complex reactor core into a simplified 2D cylindrical representation. The near cylindrical geometry of LWRs lends readily to this transformation, but the hexagonal/triangular geometry typical of HTGRs does not.

In-core control volume and flow path nodalization follows naturally from the chosen reactor core nodalization scheme, while ex-core control volumes and flow paths are often built with other system components in mind (e.g. plenum structures, up-comer and down-comer regions, steam generator tubes, etc.). The MHTGR and HTTF MELCOR models are intended only to represent the reactor/facility vessel and communicating components. Therefore only the active core region, reflector regions, metallic vessel structures, plenum spaces, inlet/outlet flow ducts, and reactor cavity cooling system (at least as a boundary condition) are represented in both models. Appropriate boundary conditions are applied where necessary as a stand-in for omitted parts of the primary and/or secondary loop. The intent of this section is to explain model layout and important MHTGR/HTTF input parameters as well as the physical reasoning behind their definitions. The MHTGR and HTTF input development strategies were similar, but noteworthy differences will be mentioned when necessary.

In general terms, MELCOR model development proceeded as shown in Figure 5.1. An accurate representation of a nuclear system in MELCOR requires access to a fairly complete design description. This reference could be one or more publications resembling a design control document wherein the system geometry is described in sufficient detail. The user must identify system components such as the reactor core and upper/lower plenum that are important to modeling. Inconsequential system components should be omitted if possible to avoid undue computational burden.

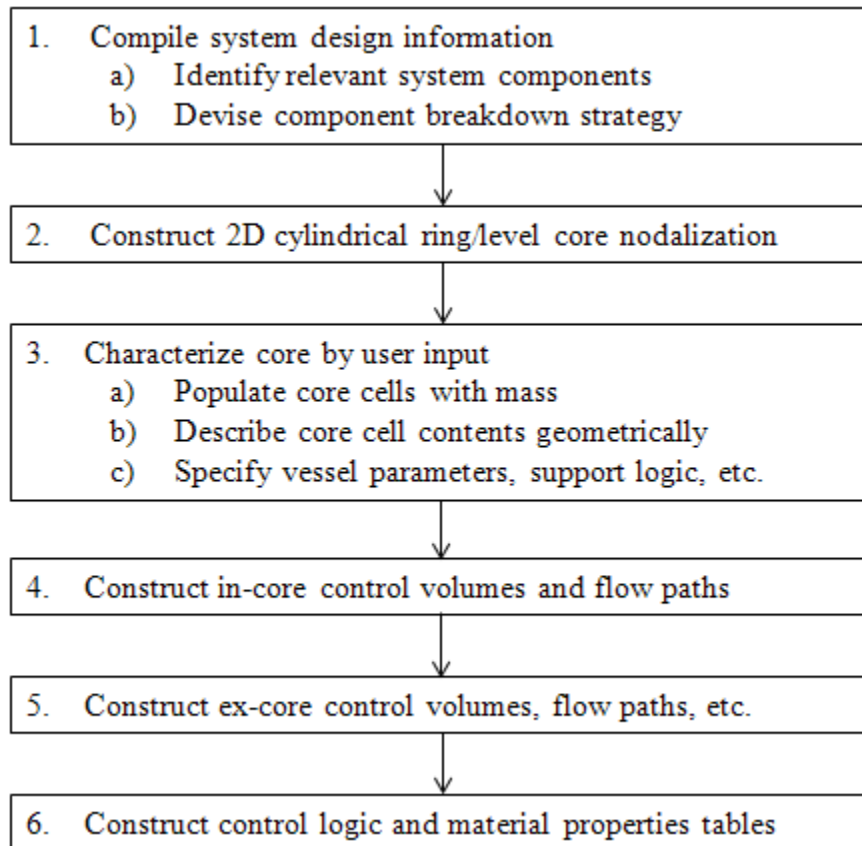


Figure 5.1. MELCOR input development flow diagram

Important system components may or may not need to be broken down to smaller constituents. Ultimately, such modeling decisions are driven by problem geometry, problem phenomenology, or other considerations. As an example, the core will likely be split to axial levels along natural geometric divisions (e.g. the physically separate, stacked core blocks in the MHTGR) and grouped in radial rings by region (e.g. the solid center reflector, the active core, the replaceable and permanent side reflector). As further example, a plenum region could consist of one large control volume or several connected control volumes if plenum flow modeling is important. The desire to create consistency between an instrumented test facility and its MELCOR model may also be an influential factor at this stage.

Once the user has decided which components to include and how best to nodalize the problem based on modeling goals, the 2D core nodalization can be built. It is at this stage that geometry transformations occur via conservation of certain geometric characteristics like cross-sectional area. In this way, hexagonally shaped regions of an HTGR may be transformed to equivalent circular regions. Each MELCOR core cell (representing the intersection of a radial ring with an axial level) must be assigned core components (fuel, cladding, reflector, support structure, etc.) and geometrically described through specification of cell boundary area, cell cross-sectional flow area, component equivalent diameters, and component surface areas. Also, each component with nonzero surface area in each cell must be assigned some material mass. There are various other required input parameters that relate to core support logic, vessel geometry, and the fuel/cladding dimensions.

After core package input requirements are met, in-core and ex-core control volumes, flow paths, and heat structures should be added. Because MELCOR performs hydrodynamic volume consistency checks between core cells and coupled control volumes, the user must carefully consider the specifications for in-core control volumes. Also, the in-core flow paths should be geometrically consistent with core flow parameters. Core axial and radial boundary heat structures should be configured and, in the case of HTGRs, coupled to the core periphery so as to enable radial heat conduction. Ex-core control volumes, flow paths, and heat structures should be utilized as necessary to represent coolant inlets and outlets, upper and lower plena, and time-invariant coolant sources and sinks (i.e. problem boundary conditions).

After the core, control volumes, flow paths, and heat structures are created, remaining support functions should be addressed. Any required control logic for transients must be implemented. Additionally, material properties tables that alter MELCOR defaults or that characterize entirely new materials must be defined. The user has enough latitude to incorporate HTGR materials via substitution and redefinition. As an example, the MELCOR default material properties of zircaloy (one of two possible materials for the cladding component) might be redefined to match H-451 graphite so that this material can be used for HTGR modeling.

5.2 Specific MELCOR Modeling Approach

This section deals with specifics of MHTGR and HTTF input development following the general procedure outlined in Figure 5.1. Because they are similar in many respects, the approach to modeling was comparable for both systems. Where appropriate, differences between the two models will be noted.

5.2.1 System Design Information

The primary reference for HTTF design details was the most recent collection of drawings released by OSU [2]. It furnished enough information to create the MELCOR model and to estimate important quantities like coolant flow area, material mass, etc. Supplementary sources gave other vital information like anticipated operational conditions and designer ceramic properties. These sources included a draft copy of the facility scaling analysis report [3], previous presentations from national conferences or program review meetings, and direct communications with OSU [2,13].

The MHTGR PSID [1] was the primary reference for MHTGR design details. Chapters 4 and 5 describing the reactor, the vessel, and the heat transport systems were frequently referenced for geometric details, normal operating conditions, and other important information. The component and system drawings were not as complete as those of the HTTF, so some assumptions about problem geometry were made.

5.2.2 Core Nodalization

The cores of both the MHTGR and HTTF were divided along axial and radial boundaries to fit within a 2D cylindrical geometry and thus meet MELCOR requirements. The MHTGR is considerably larger in physical dimensions than the HTTF, so the two core nodalization schemes are similar but not identical. In both nodalizations, the axial levels generally correspond to physical elevations where stacked core elements meet. To satisfy input requirements related to core support logic, the lower-most level of the upper reflector and the upper-most level of the lower reflector required special treatment (see section 4.3.4). Radially, a region-wise grouping strategy was adopted for both systems.

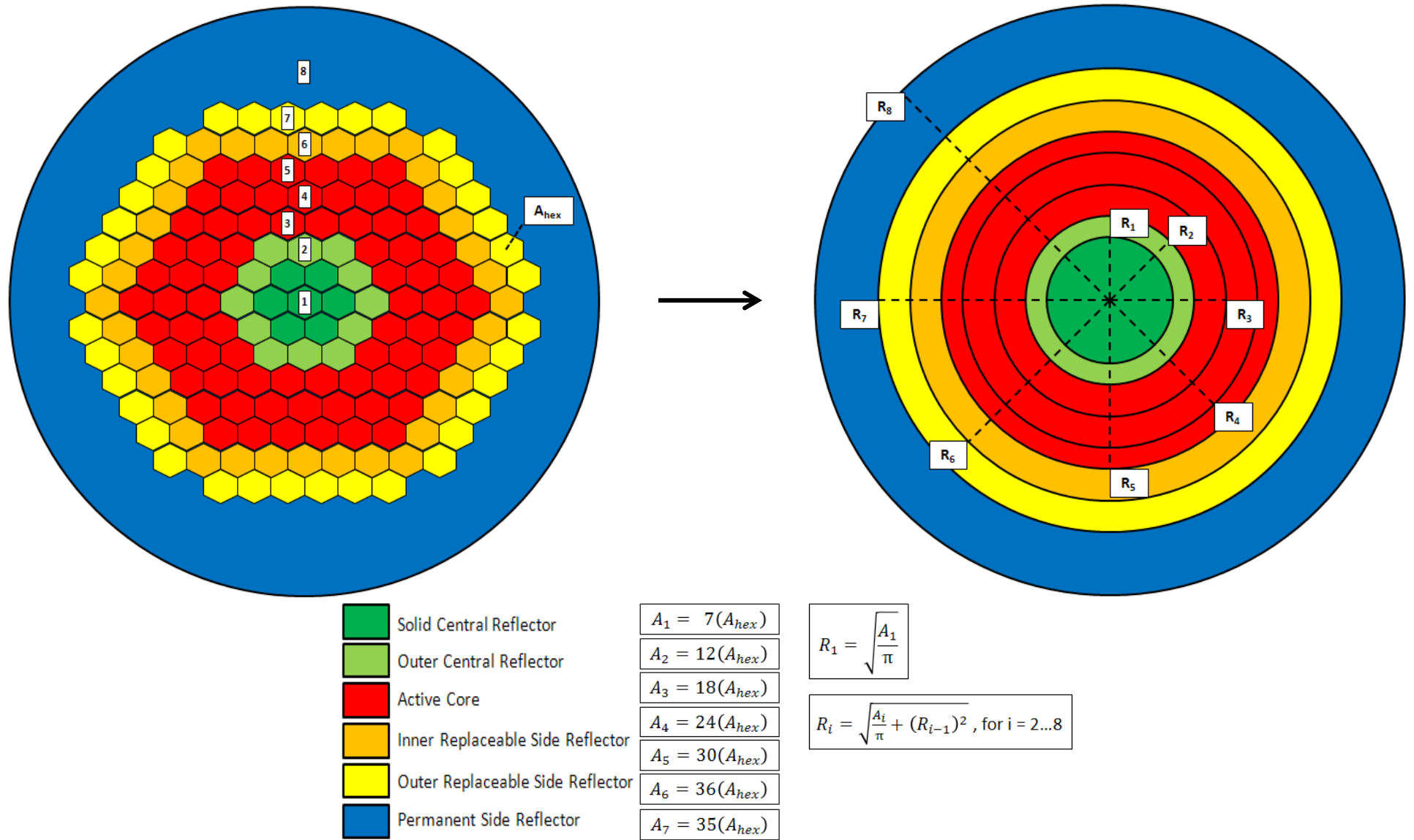


Figure 5.2. Geometric transformation of an HTGR core

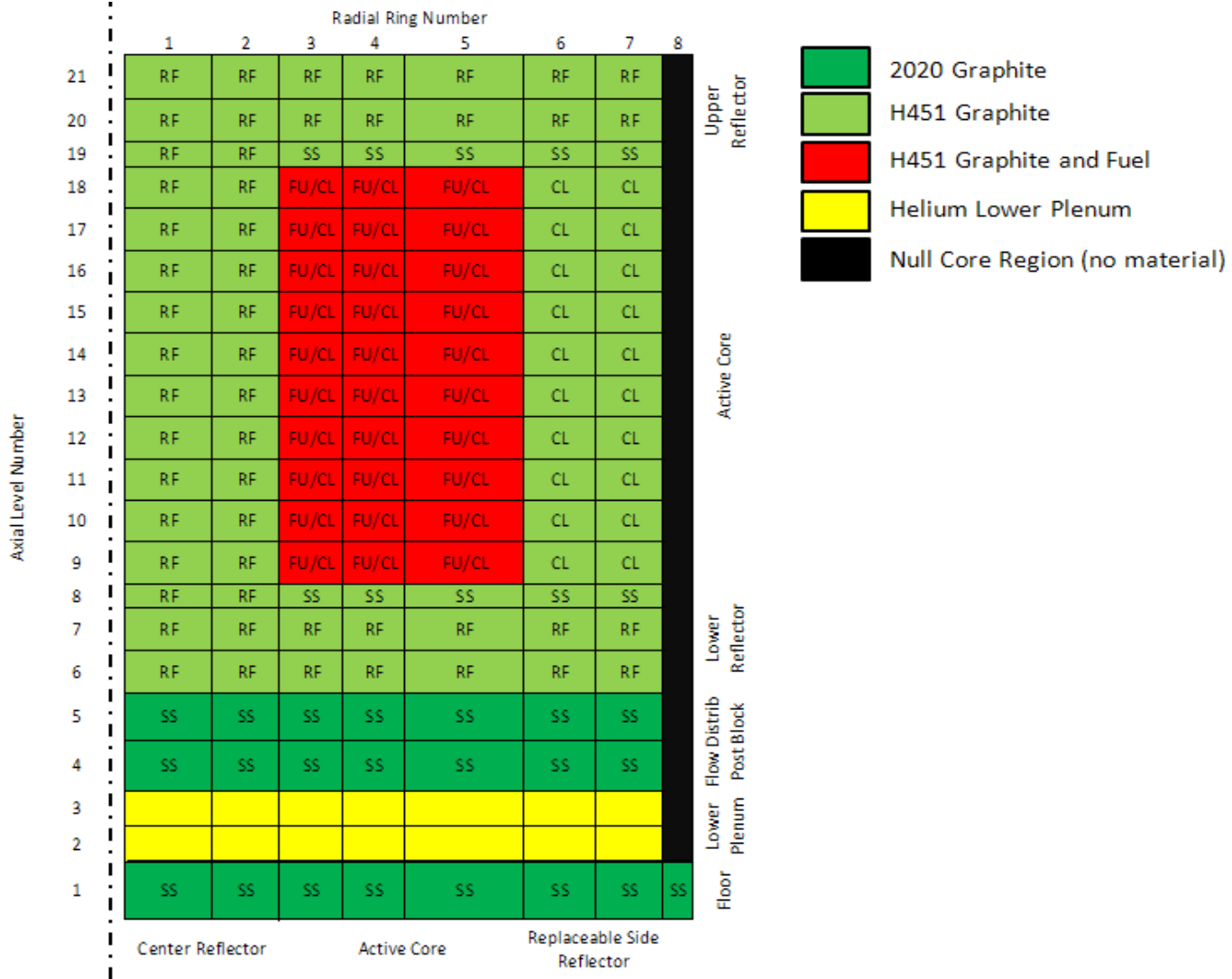


Figure 5.3. COR nodalization of the MHTGR

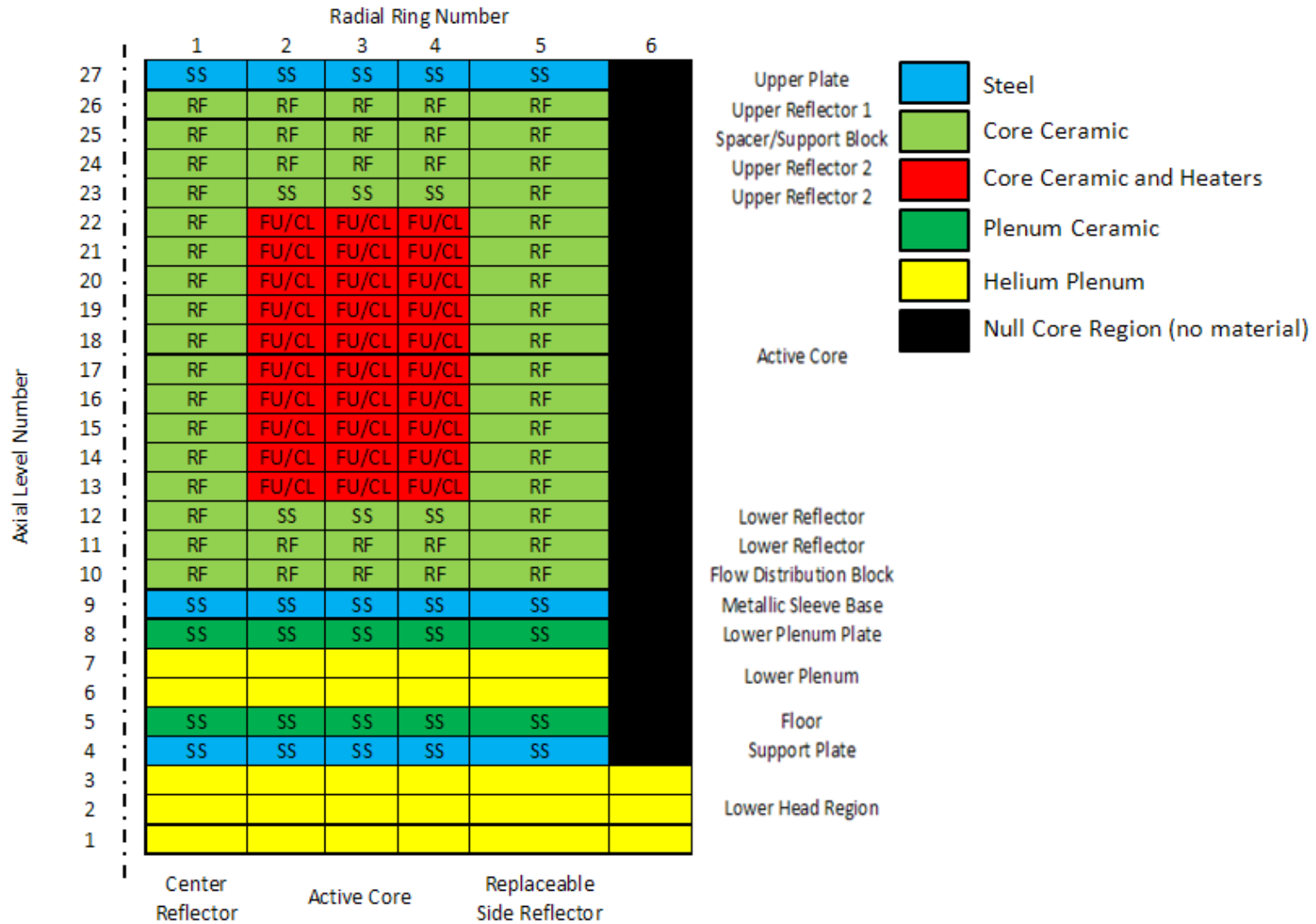


Figure 5.4. COR nodalization of the HTTF

Each core ring was associated with a region such as the solid central reflector, the periphery of the central reflector, a portion of the active core, the inner replaceable side reflector, the solid side reflector, or the solid/perforated regions of the upper and lower reflectors. The aforementioned regions are hexagonal as opposed to circular in the real-world systems, so each was transformed to a circular/annular shape based on preservation of cross sectional area (which includes structural and flow area). The number of hexagonal elements within a given region was totaled and multiplied by the hexagonal area of a single element cross section. The resulting total area was used to sequentially solve simple equations for ring radii and thereby derive a radial ring nodalization. This process is illustrated in Figure 5.2 for a general HTGR core.

The MHTGR and HTTF core nodalization diagrams are included in Figures 5.3 and 5.4, respectively. Each diagram represents a vertical half-section view of the azimuthally symmetric core region. The axial level and radial ring numbers are noted, as are the core components associated with each core cell. The “null” black regions contain no COR package materials, but boundary heat structures representing permanent side reflector graphite actually occupy this physical volume. As is evident from the materials legend, the MHTGR uses two kinds of graphite in its core and similarly the HTTF uses two different ceramics in its core. For reasons more fully explained in the facility scaling analysis report, the HTTF core ceramics are designer materials with customized heat transport properties that facilitate model-to-prototype similitude.

Each model has one or more central reflector rings (rings 1 and 2 in MHTGR, ring 1 in HTTF), three active core rings (rings 3-5 in MHTGR, rings 2-4 in HTTF), and one or more replaceable side reflector rings (rings 6-7 in MHTGR, ring 5 in HTTF). Within a given ring, there are several axial regions. Short descriptions of axial and radial regions are included in both nodalization diagrams for clarity. The MHTGR has two rings dedicated to each of the central and replaceable side reflectors, whereas the HTTF has only one ring dedicated to each of these regions. This is partly because the MHTGR contains so much more material mass than does the HTTF, but it also facilitates bypass flow modeling in the MHTGR.

5.2.3 Core Characterization

After devising the core nodalization and defining its geometric boundaries, all constituent cells must be more completely characterized. Every cell, regardless of its contents, is described by an outer radius, a bottom elevation, an axial thickness, a boundary area, and channel/bypass flow areas. Channel and bypass flow areas are nonzero only if coolant and bypass flow channels are physically present in the cell. Each cell is optionally assigned one or more core components that each contain one or more materials. The core components used for MHTGR and HTTF modeling were fuel (FU), cladding (CL), reflector (RF), and support structure (SS). Each component is described by an equivalent diameter (i.e. hydraulic diameter), a surface area, and some amount of material mass. Special components such as RF may require additional information. Any materials assigned to components have either default or user-specified transport properties depending on MP package input.

Each cell has radial boundaries (inner and outer) and an axial thickness so that cross-sectional area and boundary area are computed simply as:

$$A_{cross-section} = \pi(R_{o,j}^2 - R_{i,j}^2) \quad (5.1)$$

$$A_{boundary} = 2\pi R_o(\Delta Z_j) \quad (5.2)$$

These are equations for the annular and cylindrical areas defining a cell. These parameters help to define not only the nodalization geometry, but also the cell-to-cell contact areas used to predict conduction and radiation heat transfer between like components in adjacent cells. Cell flow area is specified by two numbers representing aggregate channel and bypass flow area. Based on the nodalization, the user should determine the number of coolant channels in a given core cell and compute the cross-sectional flow area of one channel. Those two values should be multiplied together to arrive at the channel flow area of the given core cell. Bypass flow may have several interpretations depending on the system. In an HTGR, helium may enter gaps between hexagonal elements or small passages in/around control rod canning to bypass the core. To estimate bypass flow area, inter-element gap geometry must be examined.

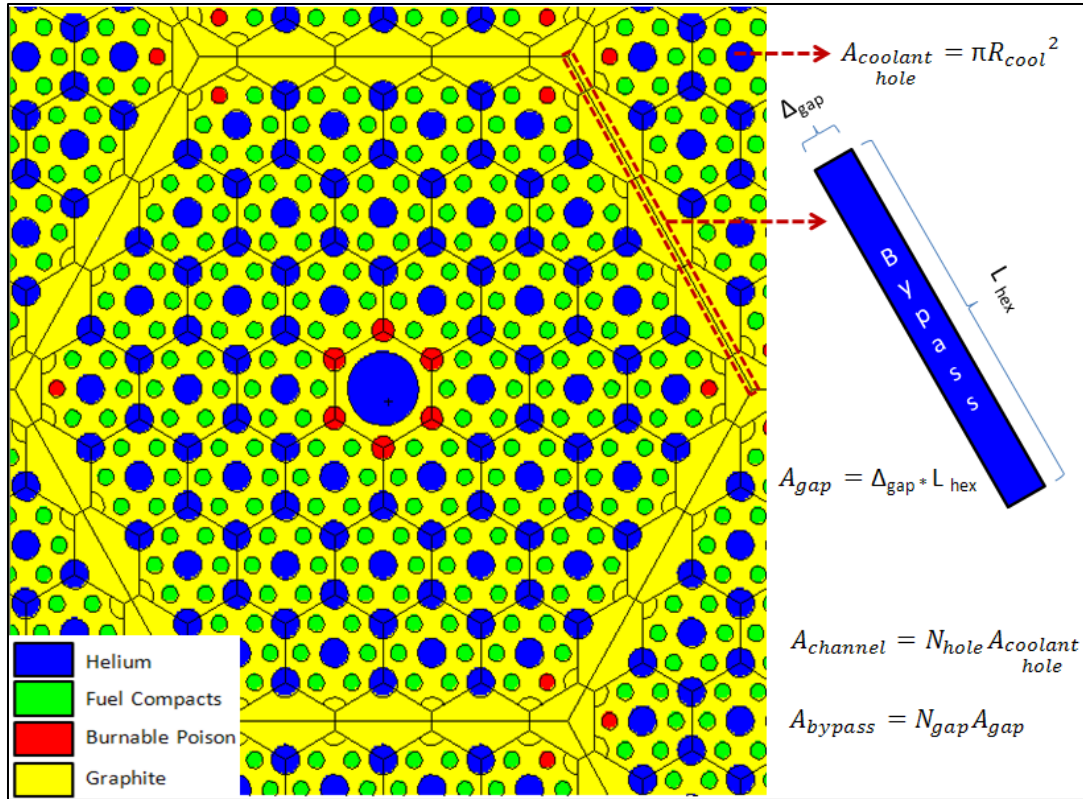


Figure 5.5. Channel and bypass flow area for an HTGR fuel element

Multiplying gap flow area by the number of gaps in a core cell yields an approximate bypass flow area. A simple illustration of bypass and channel flow area in a general HTGR fuel element is included in Figure 5.5. Because each ring generally consists of multiple elements (only one of which is pictured in Figure 5.5), a given cell is assigned flow areas representing sums over several elements. The user should take care to properly apportion flow area and to avoid double-counting of bypass flow area since adjacent elements share bypass gaps. The hydrodynamic volume within a core cell is implied by the channel/bypass flow area and cell height. The product of these two quantities must at least match the hydrodynamic volume imparted to interfacing control volumes. It should be noted that convection calculations using bypass flow only occur if

two-sided core components (e.g. RF) exist in a core cell, so it is pointless to specify a bypass flow area for a core cell containing only single-sided components (e.g. CL).

MELCOR characterizes core contents by assigning materials (e.g. zircaloy, UO_2) to components (e.g. clad, fuel). Each core component has a specific purpose and is handled differently by the core physics models. To apply its heat transfer correlations and predict energy transfer between components, MELCOR requires a geometric description of each component in each core cell. The “equivalent diameter” assumes the conventional definition of a hydraulic diameter (four times the flow area, divided by the wetted perimeter) and is used to calculate convective heat transfer coefficients. The component surface area represents that area which would be exposed to coolant and would be available for convection heat transfer and oxidation. Subject to nodalization boundaries, the user must specify component mass in each cell.

The interpretation of core components in MELCOR varies with reactor type. For a PMR-type reactor in MELCOR, the “cladding” actually represents the fuel element graphite “webbing” in and around the fuel compacts and coolant channels. The equivalent diameter of “cladding” is simply the coolant channel diameter, while the surface area in a cell is the total inside area of the coolant channels associated with that cell. The user must also come up with a “cladding radius”, which is a well-defined design characteristic in LWRs but is a derived quantity for HTGRs. The graphite “webbing” should be transformed to an annular region with some effective “cladding radius” as shown in Figure 5.6.

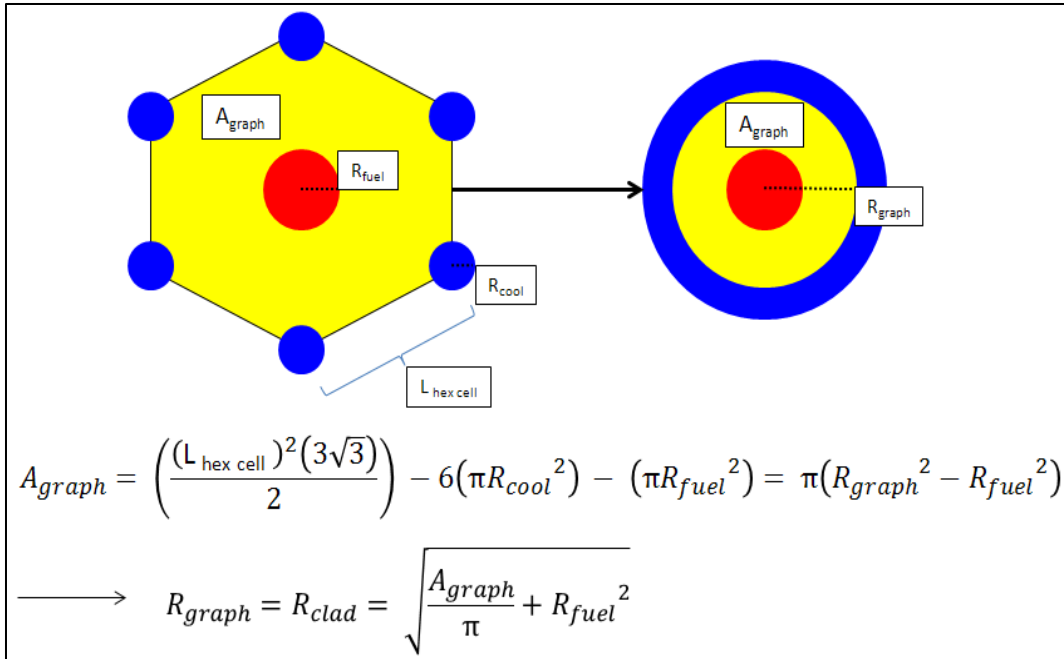


Figure 5.6. Determination of an "effective clad radius" in an HTGR

The reflector component actually replaces the two-sided (channel and bypass) canister component when a PMR-type reactor is modeled. As with other components, it requires equivalent diameters and surface areas. However, it requires a pair of values for each parameter, one for the channel side and one for the bypass side. Also, extra information specifying reflector geometry (flat plate or cylindrical), thickness, and orientation (which distinguishes the channel side from the bypass side) is required.

Several miscellaneous parameters describing reactor vessel dimensions and lower head geometry are required. The vessel input is self-explanatory and the lower head input, while not arbitrary, is irrelevant to the calculations because lower head failure is not modeled. A special set of input parameters for prismatic core conduction heat transfer are more fully described hereafter for clarity. As mentioned in section 4.4.2.2, the Tanaka-Chisaka model is used to compute effective radial core conductivity

based on block porosity. The user must compute this porosity from a ratio of discontinuous volume (helium channels, or “pores”) to continuous (fuel and graphite) volume. The user must also characterize hexagonal graphite elements by a single dimension termed the “effective size”, which follows from a simple geometry transformation. If multiple hexagonal elements comprise the core, a nonzero element-to-element gap thickness should be specified. MELCOR uses this value to compute an extra gap conduction resistance term. The MHTGR has several hexagonal elements in the core, but the HTTF does not. Because of this dissimilarity, there are distinct differences in radial block conductivity input for the MHTGR and HTTF.

5.2.4 In-Core Input

Within the core, control volumes are coupled to core cells and connected by flow paths to transport hydrodynamic material. The control volume volume-altitude tables and flow path geometry should be consistent with core cell input. At the core periphery, boundary heat structures should be configured for conduction heat transfer.

To establish a link between core structure and hydrodynamic materials, each core cell must be coupled to a control volume. It is not necessary and is often impractical to pair a unique control volume with each core cell. Often, the user will choose to assign several axial levels within a given ring to a single control volume. Thus, the in-core control volume nodalization usually resembles the core nodalization but is coarser in the axial direction. The volume-altitude tables of each in-core control volume must still reflect the axial core nodalization in full detail. Accordingly, there must be an altitude/volume data pair for each bottom elevation of each core cell interfaced to a control volume. The discussion of the DT/DZ model in section 4.4.2.5 clarifies the

details of convection calculations under this cell-to-volume coupling. MELCOR performs consistency checks between the hydrodynamic volume specified in volume-altitude tables and the hydrodynamic volume implied by core package input.

The flow paths connecting in-core control volumes are fully defined by junction elevations, junction opening heights, flow path area and open fraction, and segmentation parameters. The “from” and “to” flow path elevations refer to meeting points of connected control volumes. The flow path length is taken as equal to the center-to-center distance between interconnected control volumes. The flow path areas should be consistent with channel or bypass flow areas specified in core package input. If the information is available, channel surface roughness and forward/reverse loss coefficients may be specified. In both the HTTF and MHTGR models, only axial flow within coolant channels or bypass gaps is considered because lateral flow is disallowed by geometry.

Boundary conduction between the outermost core ring and its adjoining heat structures should be enabled to model conduction from the core. As per MELCOR requirements, there must be a one-to-one relationship between boundary heat structures and interfacing core cells so that thermal energy conducted radially within an axial level is conveyed to a unique heat structure across the core boundary. In the HTTF and MHTGR models, the outermost core ring consists of replaceable side reflector graphite while the boundary heat structures consist of permanent side reflector graphite. To calculate a helium gas gap resistance, a gap thickness between these reflectors was assumed. Permanent reflector graphite properties were used to compute the thermal diffusion constant appearing in the boundary conduction equation of section 4.4.2.4.

5.2.5 Ex-Core Input

Parts of the system external to the core are created with control volumes, flow paths, and heat structures. Both the MHTGR and HTTF have upper and lower plena, a set of up-comer ducts, an outlet duct, an air cavity, and steel structures like the core barrel, pressure vessel wall, and RCCS panels. Each of these features is discussed below. Remaining portions of the primary and secondary loops are short-circuited with time-independent helium source and sink control volumes.

For both models, the upper plenum is treated with three large control volumes that accept coolant from the up-comer and send coolant to one of many flow paths leading to the core region. Without several inter-connected control volumes, upper plenum circulation cannot be modeled in good detail. This is acceptable for purposes of modeling normal operation or a depressurized conduction cool-down scenario. The upper plenum appears in Figure 5.7 showing the MHTGR/HTTF ex-core nodalization.

The lower plenum in both models consists of a single, large control volume as shown in Figure 5.7. Flow exits the core from one of several flow paths and enters the large plenum to mix/equilibrate before moving to the outlet duct. A finer plenum nodalization was judged as impractical for purposes of this study because MELCOR currently does not model air/graphite oxidation reactions. Hence, air ingress and air circulation in the lower plenum are of no significance and a fine lower plenum nodalization would only slow the calculation. Furthermore, the effects of graphite support structures or coolant hot streaks on plenum mixing likely cannot be ascertained by MELCOR. The plenum dimensions were surmised from design drawings, but plenum support posts and other miscellaneous structures were not considered.

The outlet duct in both models is represented by a single control volume. If air ingress after a duct break was of concern, a two-volume approach would have been taken so as to capture counter-current helium/air flow (as occurs during lock-exchange air ingress). No heat structure surfaces are included as duct walls, though this could be changed if necessary.

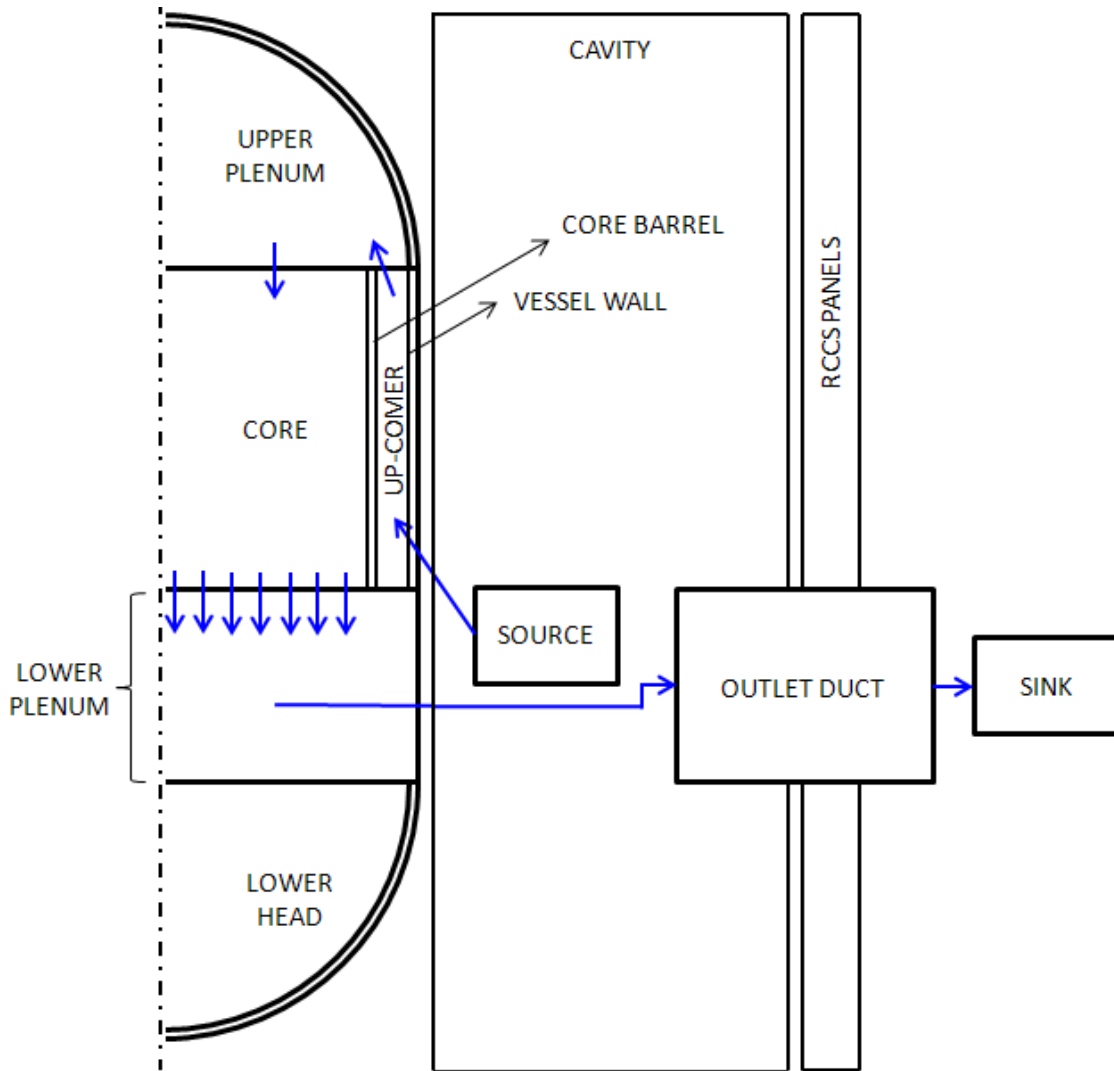


Figure 5.7. Representative CVH nodalization for MHTGR/HTTF

An air cavity surrounds the vessel in both models and separates the reactor vessel wall from the RCCS panels. Radiation occurs across the cavity and it is expected that some natural air circulation occurs within the cavity. Currently, the cavity is not built to capture circulation effects since radiation is the dominant vessel heat removal mechanism. In the event of an outlet duct break, air ingress from the cavity would commence by molecular diffusion or lock-exchange. The cavity dimensions were somewhat ambiguous in the literature, so assumptions about geometry were made as necessary. If a single, large control volume is used, the only important characteristics are cavity thickness and overall volume.

Steel structures are included in both models. Each system has a core barrel and/or metallic sleeve structure between the permanent side reflector and the up-comer region. Up-comer duct metal is not modeled, but the neighboring vessel wall is included and is “visible” to the core barrel so as to permit radiation heat transfer. The barrel and vessel walls are modeled with heat structures and are either stainless steel or carbon steel. The RCCS consists of little more than a set of steel heat structures with a constant-temperature boundary condition at the outside surface. This is because there is much uncertainty as to the exact RCCS configuration in the HTTF. As is, the vessel-to-RCCS view factors or material emissivity values can be varied parametrically.

5.2.6 Ancillary Input

Material substitutions and redefinitions are used extensively in the models. In the HTTF, core ceramics are specialized to allow for prototype-to-model similitude and must be completely user-specified. In both models, certain LWR core materials like zircaloy must be replaced with nuclear grade graphite or a custom ceramic. Also, UO₂

must be modified to more closely match HTGR fuel compacts or HTTF heater rods. If necessary, this can be accomplished by assigning multiple materials to the FU components (e.g. UO_2 and porous fuel compact graphite both present in FU).

The HTTF designers at OSU furnished all HTTF materials information, whereas a previously published graphite materials handbook [14] from General Atomics was referenced for H451 graphite and 2020 graphite. MELCOR defaults for metallic materials (carbon steel, stainless steel) were kept unchanged.

Table 5.1
Ceramic material properties for the MHTGR [14]

H451 Graphite				2020 Graphite			
T [K]	k [W/m*K]	T [K]	C_p [J/kg*K]	T [K]	k [W/m*K]	T [K]	C_p [J/kg*K]
500.0	115.01	300.0	712.76	295.0	62.40	300.0	712.76
600.0	106.13	400.0	990.36	473.0	67.20	400.0	990.36
700.0	97.91	500.0	1217.63	673.0	57.20	500.0	1217.63
800.0	90.34	600.0	1389.86	873.0	49.80	600.0	1389.86
900.0	83.43	700.0	1519.84	1073.0	43.90	700.0	1519.84
1000.0	77.18	800.0	1619.44			800.0	1619.44
1100.0	71.58	900.0	1697.26			900.0	1697.26
1200.0	66.64	1000.0	1759.23			1000.0	1759.23
1300.0	62.36	1100.0	1809.43			1100.0	1809.43
1400.0	58.74	1200.0	1850.73			1200.0	1850.73
1500.0	55.77	1300.0	1885.16			1300.0	1885.16
1600.0	53.45	1400.0	1914.21			1400.0	1914.21
1700.0	51.80	1500.0	1938.97			1500.0	1938.97
1800.0	50.80	1600.0	1960.27			1600.0	1960.27
		1700.0	1978.74			1700.0	1978.74
		1800.0	1994.87			1800.0	1994.87
		1900.0	2009.05			1900.0	2009.05
		2000.0	2021.58			2000.0	2021.58
		2100.0	2032.72			2100.0	2032.72
		2200.0	2042.65			2200.0	2042.65
		2300.0	2051.56			2300.0	2051.56
		2400.0	2059.57			2400.0	2059.57
		2500.0	2066.79			2500.0	2066.79
		2600.0	2073.33			2600.0	2073.33
		2700.0	2079.26			2700.0	2079.26
		2800.0	2084.66			2800.0	2084.66
		2900.0	2089.58			2900.0	2089.58
		3000.0	2094.07			3000.0	2094.07

Table 5. 2
Ceramic material properties for the HTTF (preliminary data) [13]

Core-Type Ceramic				Plenum-Type Ceramic			
T [K]	k [W/m*K]	T [K]	C _p [J/kg*K]	T [K]	k [W/m*K]	T [K]	C _p [J/kg*K]
25	4.1	25	428	25	1.9	25	451
400	3.9	400	849	370	1.8	370	876
985	3.4	985	1078	925	1.6	925	1113
1315	5	1315	1131	1130	2.1	1130	1149
1800	6.5	1800	1173	1320	3.6	1320	1175

The material properties and tabular functions packages were used to specify thermal conductivity, specific heat capacity, etc. as functions of temperature. Selected materials data is included in Tables 5.1 and 5.2. MELCOR uses linear interpolation to deduce material property values when temperature falls between tabular function data points. Published density values for H-451 and 2020 graphite were not given as functions of material temperature, so this data was treated as temperature-independent. H-451 graphite density was taken to be 1740.0 kg/m³, whereas 2020 graphite density was 1780.0 kg/m³. The temperature-independent density values for HTTF ceramics are 2971.63 kg/m³ for core-type ceramic and 2954.63 kg/m³ for plenum-type ceramic.

5.2.7 Steady-State and Transient Control Logic

Steady-state boundary conditions consist of source and sink control volumes connected to the rest of the system with valves and flow paths. The source control volume is connected with a time-independent flow path so that the incoming coolant mass flow rate may be user-specified. The thermodynamic conditions of the source control volume match nominal core inlet conditions, while those of the sink control volume match expected outlet conditions. Time-independent flow paths were used between the up-comer and upper plenum control volumes so that bypass flow could be

split off from coolant channel flow as desired. MELCOR eventually brings the system to a steady state wherein structure and coolant temperatures no longer change over time.

To model pressurized and depressurized conduction cool-downs in both the MHTGR and HTTF, some event-initiating control logic was required. For both cases, a loss of forced circulation must occur at some user-appointed problem time subsequent to establishment of a steady state. In practice, the LOFC is achieved by changing steady-state boundary conditions so as to immediately eliminate or quickly coast down the coolant flow rate from the time-independent source. This LOFC induces a transient state and sets in motion a PCC or DCC accident sequence. In a PCC, the stagnating coolant remains in the system at pressure and is able to develop natural circulation patterns. Thus, for a PCC the source control volume mass flow rate must be immediately forced to zero or forced to coast down at the time of LOFC. The sink control volume may remain connected to the system at operating pressure to preclude a depressurization. Control functions and flow path “valves” may be used to program the PCC. In a DCC, the system must blow down (i.e. depressurize) through a duct break to the reactor cavity. Thus, the source and sink control volumes must be isolated and, simultaneously, a flow path must be opened to the reactor cavity. The depressurization timing may be dictated by the user (e.g with a CF-controlled linear vessel depressurization) or may be left for MELCOR to determine. Similar to the PCC, all that is required to implement a DCC are control functions and flow paths. PCC and DCC control logic is similar for the MHTGR and HTTF.

5.2.8 Decay Heat

For both accident scenarios, intervention of the reactor protection system at the point of LOFC is assumed. Accordingly, a reactor scram occurs and the core thermal power immediately transitions to decay heat. As recommended in the OSU scaling analysis and in accordance with other HTGR computational studies, an ANS standard decay curve (in MELCOR's DCH package) was used to calculate decay heat. MHTGR decay heat is based on a steady-state power level of 350 MW. Because the HTTF heater rods can achieve an integral power of 2200 kW, a full-scale decay heat profile is available for experimental purposes. The whole-core decay heat calculation assumes a long irradiation time before shutdown (584 days) and a certain distribution of fission power (before shutdown) between three nuclides: ^{235}U , ^{239}Pu , and ^{238}U . The MHTGR decay heat as predicted from the DCH package is plotted in Figure 5.8 below.

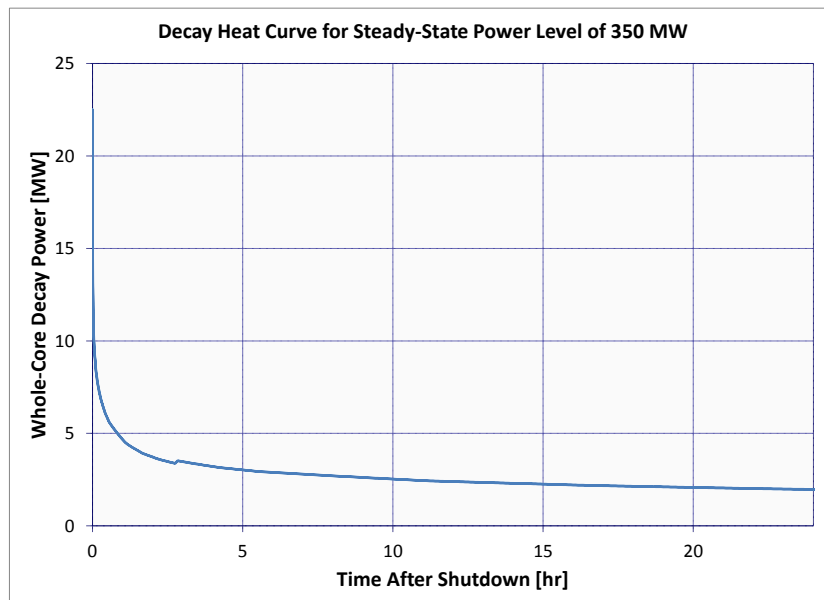


Figure 5.8. DCH package decay heat curve based on ANS standard

6. RESULTS AND DISCUSSION

Two different systems, the MHTGR and the HTTF, were used to create three separate test case sets each consisting of three operating scenarios. The MHTGR was modeled at full power (350 MW_{th}) and at 10% power (35 MW_{th}) with decay heat calculated by MELCOR accordingly. The HTTF was modeled at its full power level of 2200 kW_{th} with a decay heat curve matching that of the reduced-power MHTGR. Three operating scenarios were considered for MHTGR models: steady-state, pressurized conduction cool-down, and depressurized conduction cool-down. Two operating scenarios were considered for the HTTF model: steady-state and depressurized conduction cool-down. A more thorough explanation of modeling decisions follows in the first section of this chapter. The second section presents results of the various MELCOR calculations, itemized by operating scenario. The third section draws comparisons of transient response between the reduced-power MHTGR and the HTTF. The fourth section discusses MELCOR results as they compare to those of RELAP.

6.1 Rationale for Test Case Selection

The choice of modeling a full-power MHTGR, a reduced-power MHTGR, and the reduced-scale HTTF facilitates comparison of MELCOR predictions to available RELAP results previously published by INL. Since no HTTF experimental data is available for a MELCOR-to-experiment benchmark, a RELAP-to-MELCOR comparison is pursued as the only validation activity currently possible. In accordance with the methodology of INL, the reduced-power MHTGR model was constructed so that it featured a one-to-one correspondence to the HTTF in terms of decay power and temperature. If the general transient response of the full-scale MHTGR resembles that of

the reduced-power MHTGR and if, in turn, the general transient response of the reduced-power MHTGR matches that of the HTTF, one may reasonably conclude that the HTTF can reproduce full-scale MHTGR phenomena with fair fidelity. Furthermore, one may gain some measure of confidence in MELCOR modeling capabilities if good agreement between MELCOR and RELAP is observed.

6.2 MELCOR Predictions

The MELCOR results presented in subsequent sections cover several operating scenarios for each of the three systems modeled. For the steady-state scenario of each system, core structure and coolant temperature distributions are included. For the PCC and DCC scenarios, the predicted time evolution of certain derived quantities (mass-averaged thermal hydraulics parameters) is presented. For PCC and DCCs in all systems, instantaneous LOFC is assumed.

6.2.1 MHTGR at 350 MW_{th}

This section presents MELCOR predictions for the full-scale, full-power MHTGR at steady state and under certain transient/accident conditions. Maps and plots detailing core structure or coolant temperature distributions comprise the bulk of the MELCOR results. Certain other noteworthy parameters are mentioned as well.

6.2.1.1 Steady-State

Table 6.1 summarizes some important steady-state characteristics. User-defined boundary conditions set the specified inlet mass flow rate, temperature, and pressure.

Table 6.1
Steady-state parameters for the 350 MW_{th} MHTGR

Parameter	Value
Power	350 MW _{th}
Coolant Temperature (In Out)	259.0 °C 685.8 °C
Coolant flow rate (total channel)	174.44 kg/s 157.0 kg/s
Bypass flow rate	17.44 kg/s (10%)
Inlet Pressure	6.4 MPa






The desired outlet temperature was achieved if 157.0 kg/s of helium cooled the active core (rings 3, 4, and 5). For this “channel-side” mass flow rate and for an estimated 10% bypass flow [1], a total (channel plus bypass) coolant mass flow rate of 174.44 kg/s must come from the time-independent source control volume.

Table 6.2 is a color-coded core structural temperature map that tabulates the data plotted in Figure 6.1. Axial levels and radial rings are noted in Table 6.2 (IA/IR), as are the geometric locations of axial level mid-heights (*Z*) and radial ring centers (*R*). The pressure vessel temperatures are omitted from Figure 6.1. The cladding temperatures of Table 6.2 (green boxes within the thick black boundaries of the active core) were used to produce Figure 6.1 as opposed to the fuel temperatures. Note that Figure 6.1d is basically a color-coded replica of Table 6.2 so that the hotter and cooler regions are more readily identifiable.

Table 6.2
Steady-state core structural temperature map for Figure 6.1 (all temperatures given in °C)

		CR		ACTIVE CORE					RSR		PSR		CB		RPV	
IA/IR		1	2	3	4	5	6	7	N1	N2	N3	N4	N5	N6		
	Z/R [m]	0.25	0.66	0.99	1.31	1.64	1.97	2.27	2.41	2.69	2.96	3.04	3.27	3.40		
UR	21	8.72	265.85	263.19	259.56	259.15	259.15	258.93	258.56	249.16	241.97	235.15	232.30	130.16 120.21		
	20	8.13	282.03	275.19	260.51	259.15	259.15	258.86	258.36	249.45	241.81	234.61	231.62			
	19	7.94	294.55	289.64	259.46	259.17	259.17	258.85	258.38	250.96	242.51	234.73	231.55			
ACTIVE CORE	18	7.53	320.96	319.94	314.31	301.55	311.70	298.92	312.86	300.07	322.04	326.18	288.30	283.92	277.47	274.29
	17	6.74	381.21	381.49	426.35	389.31	418.77	381.69	420.88	383.81	376.87	369.01	299.94	292.71	284.56	280.95
	16	5.95	451.90	454.23	541.56	483.96	528.71	471.04	531.93	474.26	444.14	423.82	318.06	306.18	295.29	291.00
	15	5.16	529.06	534.04	649.68	577.33	631.70	559.22	635.94	563.48	510.48	477.37	337.26	320.19	306.29	301.25
	14	4.36	603.91	611.45	741.13	661.26	718.56	638.51	723.61	643.59	568.13	522.62	354.16	332.21	315.57	309.86
	13	3.57	663.68	671.98	799.08	719.48	773.74	693.94	779.13	699.36	609.73	555.21	365.76	339.78	320.82	314.54
	12	2.78	706.94	716.25	835.72	764.22	807.99	736.19	813.55	741.81	639.03	577.38	374.66	345.94	325.47	318.85
	11	1.98	724.54	734.11	838.48	781.80	809.72	752.80	815.09	758.21	650.45	586.04	378.19	348.35	327.29	320.52
	10	1.19	713.62	721.68	801.84	765.33	773.94	737.32	778.76	742.17	641.92	580.69	376.42	347.35	326.78	320.15
	9	0.40	691.94	696.37	740.87	728.26	714.82	702.17	718.88	706.24	623.76	570.00	371.90	344.17	324.34	317.89
LR	8	-0.01	695.90	698.71	706.51	681.19	684.49	622.39	575.46	493.36	473.80	447.41	435.23	309.68 269.41		
	7	-0.30	698.75	700.48	702.81	677.77	682.61	536.11	528.58	493.29	470.69	445.40	434.39			
	6	-0.79	697.40	699.43	702.44	677.78	682.50	554.76	543.43	502.55	475.96	448.16	436.45			
LP	5	-1.19	691.26	693.95	696.60	678.18	679.66	602.01	570.72	487.66	469.47	445.56	434.52	312.89 272.19		
	4	-1.69	685.24	689.61	695.11	678.20	680.21	624.96	591.95	496.06	475.66	450.59	439.28			

CR Central Reflector
 RSR Replaceable Side Reflector
 PSR Permanent Side Reflector
 CB Core Barrell
 RPV Reactor Pressure Vessel

 Fuel
 Core Ceramic
 SR/LP Ceramic
 Core Barrel
 Vessel Wall

UR Upper Reflector
 LR Lower Reflector
 LP Lower Plenum

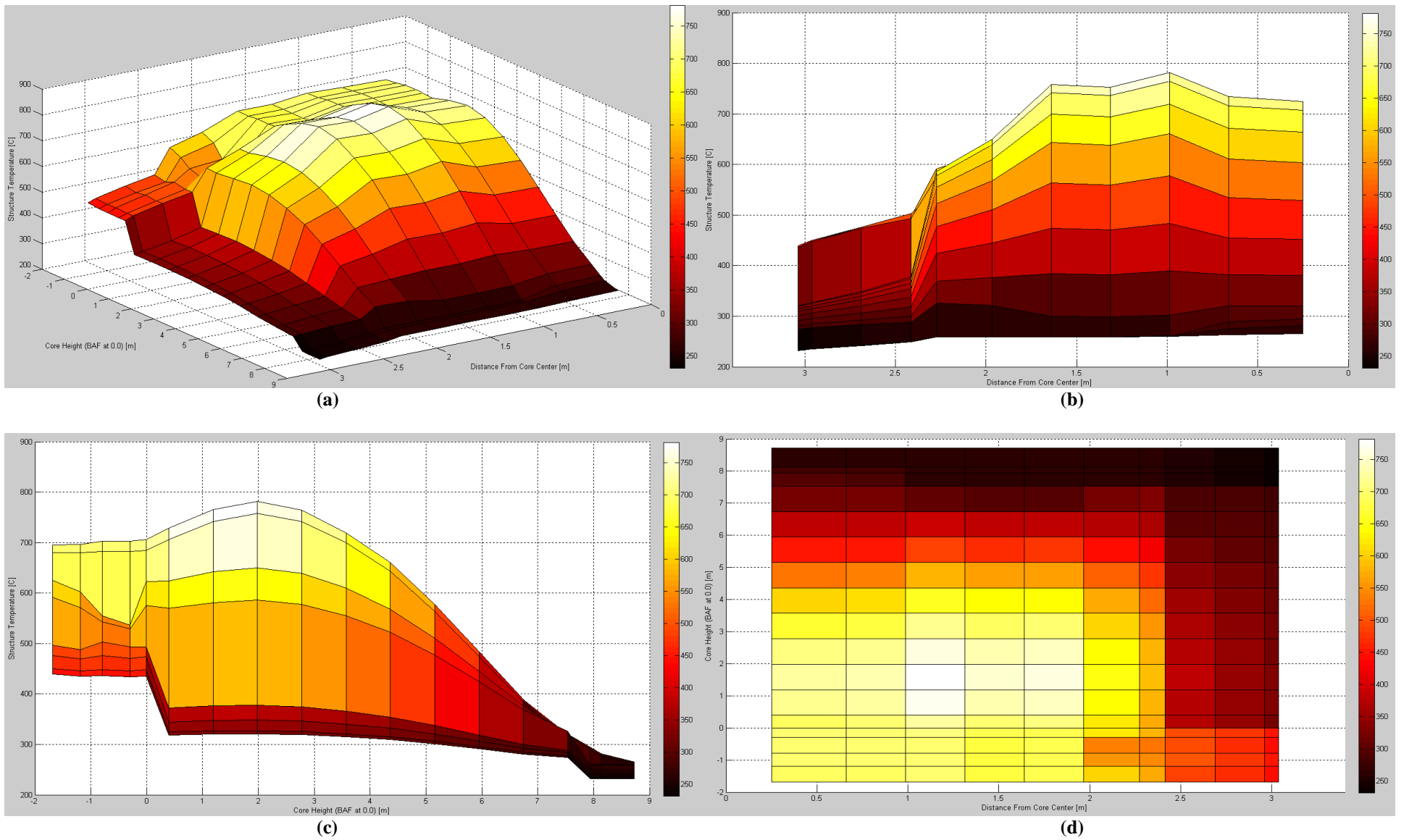


Figure 6.1 Steady-state core structural temperature distribution

The axial temperature distribution (Figure 6.1c) is relatively flat in the upper and lower reflector regions and is consistent with the chopped cosine power profile in the active core region. Also, the active core distribution is somewhat bottom-peaked with the hottest reported temperature (excluding fuel) being 781.8 °C. In the radial direction (Figure 6.1b), the central reflector temperature distribution is relatively flat but indicates the reflector is warmer in the region nearest the active core. This suggests that upon LOFC, heat conduction to the center of the central reflector will proceed. In the active core, the innermost region is hotter than the outermost region, which in turn is hotter than the central region. The replaceable side reflector exhibits a relatively steep radial temperature gradient, while the permanent side reflector is characterized by a more gradual temperature gradient. Thus, conduction heat transfer may occur “downhill” along temperature gradients from the active core to both the central and side reflector.

Table 6.3 shows the steady-state coolant temperatures from the CVH package as they correspond to core axial levels and radial rings. The coolant enters the upper reflector at a uniform 259.15 °C before entering the core channel/bypass CVs. The active core uses three CVs per ring (rings 3 to 5) between levels 9 and 18, while the bypass regions (rings 1, 2, 6, and 7) use only one CV for this same axial level range. All helium emerges from the core and mixes in the large lower plenum CV so that a coolant temperature roughly equaling the MHTGR target is achieved.

Table 6.3Steady-state helium temperature map, 350 MW_{th} MHTGR (all temperatures given in °C)

		CR		ACTIVE CORE			RSR		
IA/IR		1	2	3	4	5	6	7	
ACTIVE CORE	UR	19-21	259.15	259.15	259.22	259.15	259.15	259.15	
		14-18			481.63	468.38	471.75		
		11-13	298.85	327.00	661.08	637.67	642.79	385.25	314.95
		9-10			703.17	677.75	682.61		
		6-8			703.16	677.77	682.62		
LR	4-5	692.69	695.44	703.07	677.82	682.26	581.99	560.06	
LP		3							
		2			685.77				

6.2.1.2 Pressurized Conduction Cool-Down

At the time of LOFC, an immediate stoppage in coolant flow was imposed by boundary conditions and the system was opened to a time-independent CV at normal operating pressure (no breach in the pressure boundary). Also, the core power transitioned from steady-state to decay heat as would occur after actuation of the reactor protection system. In the ensuing PCC transient, natural coolant circulation patterns lead to axial core temperature redistribution from the initial steady state. Also, radial conduction to the central reflector and core boundary removed residual heat from the active core region. The transient was run out to a problem time of seven days as this was enough time for core temperatures to rise, peak, turn over, and begin to decrease. MELCOR results in this section are presented as mass or area averaged transient temperature traces for core rings, core levels, and the RPV outer wall. The physical phenomena encapsulated in each plot are discussed as necessary.

To observe central reflector heat-up and subsequent radial conduction to the core periphery, Figure 6.2 showing mass-averaged (by core ring) core graphite temperatures was created from MELCOR data. The time-to-peak temperature and peak temperature for each average core ring may be readily obtained from Figure 6.2

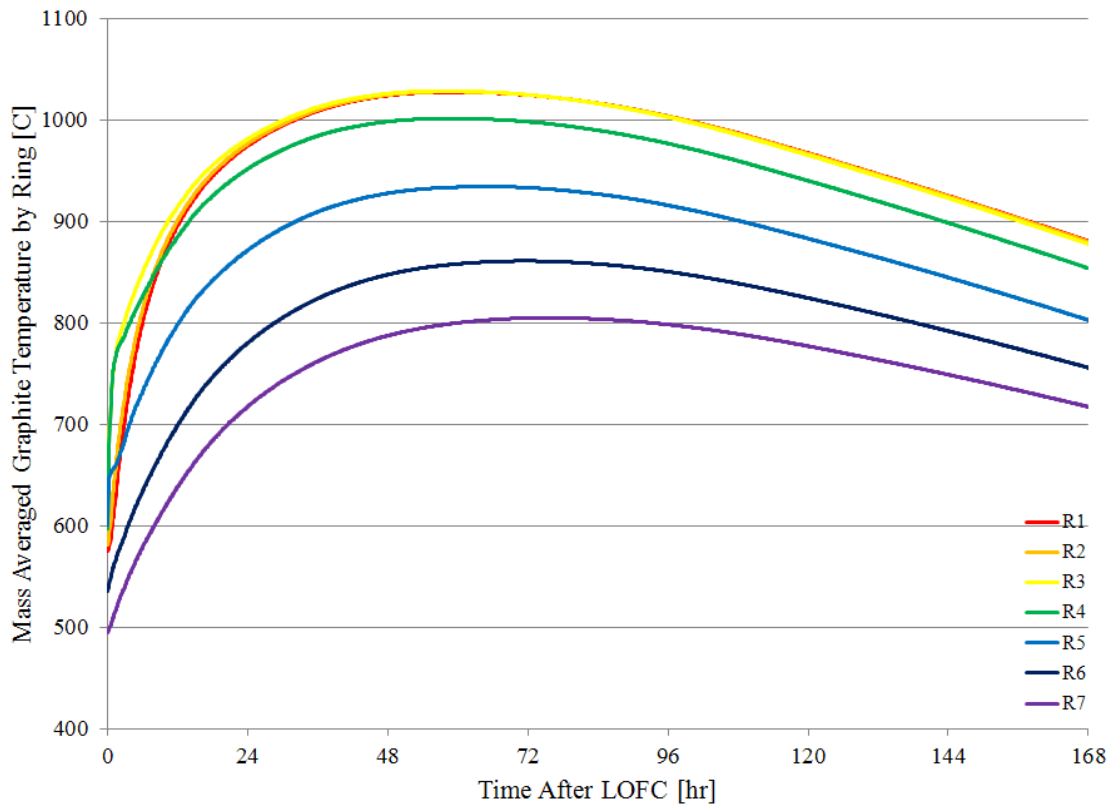


Figure 6.2 Mass-averaged (by ring) core graphite temperatures during PCC

The rate of central reflector (R1 and R2) heat-up exceeds that of other rings, and at about 57.2 hr post-LOFC, rings R1 through R3 reach a maximum temperature of approximately 1028 °C. This behavior is consistent with expectations, as the large inventory of graphite in the central reflector is designed to act as a heat sink for the core

under accident conditions. The outer rings R4 through R7 subsequently reach their respective peak temperatures of 1001 °C, 934 °C, 861 °C, and 805 °C at times of 59.5 hr, 65.3 hr, 71.5 hr, and 75.5 hr. Radial conduction from the active core to both the central and side reflector act to remove residual heat before any damage limits (beginning around 1650 °C) are reached.

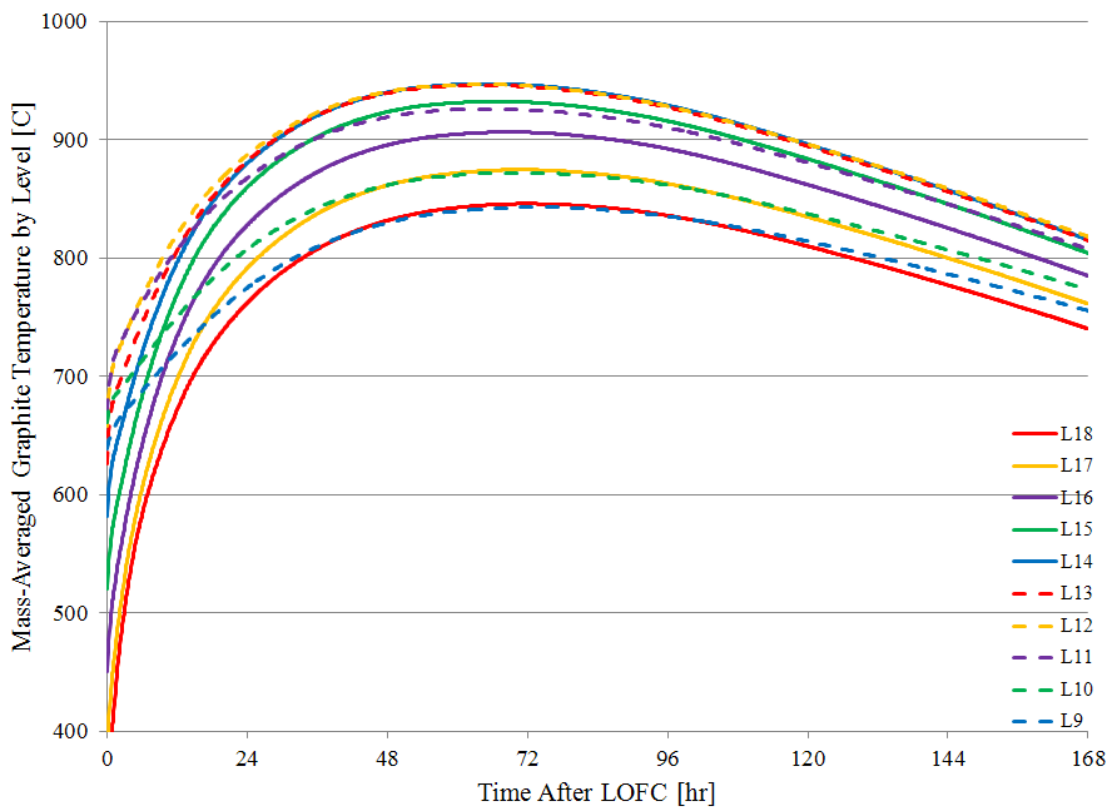


Figure 6.3 Mass-averaged (by level) core graphite temperatures during PCC

The effects of natural, density gradient driven helium circulation on axial core temperature redistribution during a PCC event are noticeable in Figure 6.3. The lower core structures (L9 through L13) are much warmer than the upper core structures (L14

through L18) at the point of LOFC. When forced convection stops, the lower structures will heat stagnant coolant and cause it to rise towards the cooler upper structures. Thus, heat is removed from the lower core structures and is effectively relocated by convection to the upper core structures. All core structures will heat up, but the upper core graphite will do so at a comparatively greater rate so that the axial core temperature distribution flattens out from its bottom-peaked steady-state shape. This behavior is evident from Figure 6.3, as the high rate of temperature increase in L14-L18 and the lower rate of temperature increase in L9-L13 allows L18 to catch up with L9, L17 to catch up with L10, etc. The peak temperatures of Figure 6.3 do not coincide with those of Figure 6.2 because level averages were used instead of ring averages to ascertain natural circulation effects on the axial temperature profile.

As an indirect indicator of passive heat removal from the metallic pressure vessel, an area average of the RPV outer wall temperature was computed from MELCOR data. Figure 6.4 shows the result and suggests that radial conduction causes RPV heat-up and, in turn, increases radiation heat transfer to the RCCS. The RPV outer wall reaches a maximum temperature of about 291 °C at 95.5 hr post-LOFC. It makes physical sense that the RPV is the last structure to reach its peak temperature because all thermal energy from inner structures must conduct through and radiate from the RPV to be removed from the system.

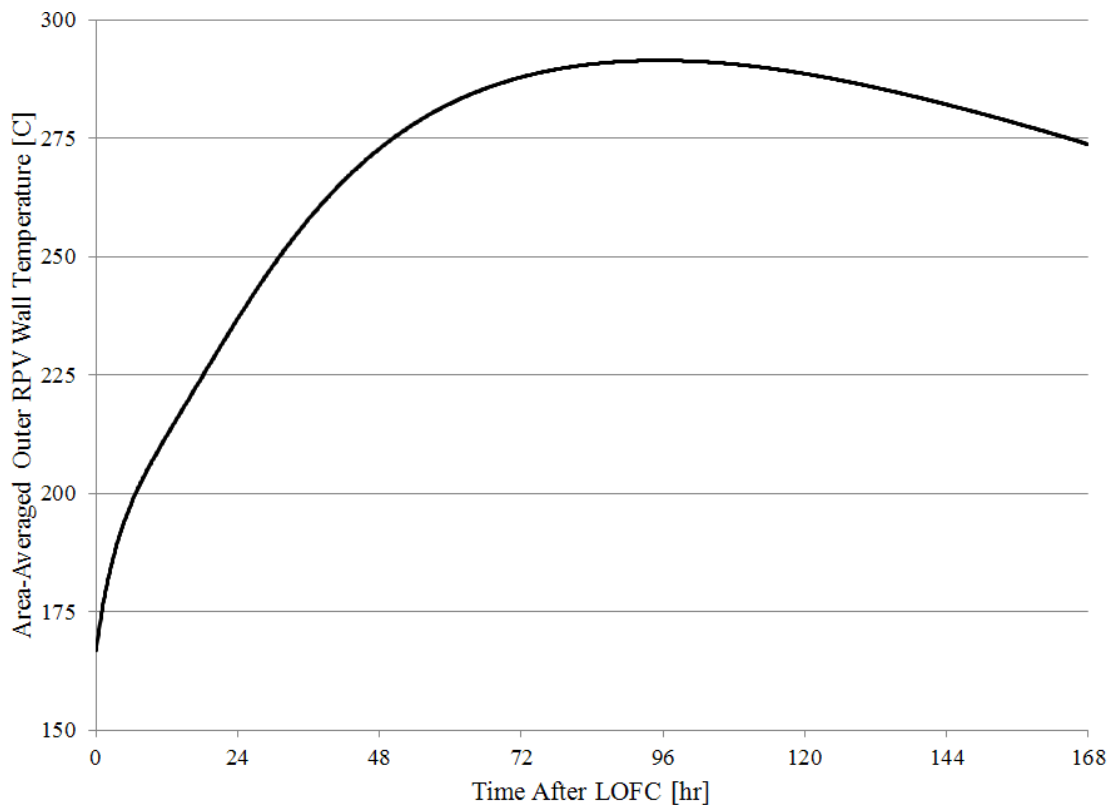


Figure 6.4 Area-averaged outer RPV wall temperature during PCC

6.2.1.3 Depressurized Conduction Cool-Down

At the time of LOFC, an immediate stoppage in coolant flow along with a linear, 10 second system depressurization was enforced by system boundary conditions. Also, the core power transitioned from steady-state to decay heat as would occur after actuation of the reactor protection system. Subsequently, the system was connected to time-independent CVs at atmospheric pressure and temperature. In the ensuing DCC transient, core cooling through the sole mechanism of radial conduction was observed. The transient was run out to a problem time of seven days as this was enough time for core temperatures to rise, peak, turn over, and begin to decrease. MELCOR results in

this section are presented as mass or area averaged transient temperature traces for core rings, core levels, and the RPV outer wall. The physical phenomena encapsulated in each plot are discussed as necessary.

Figure 6.5 shows mass-averaged (by ring) core graphite temperatures during the DCC in much the same way as Figure 6.2 during the PCC.

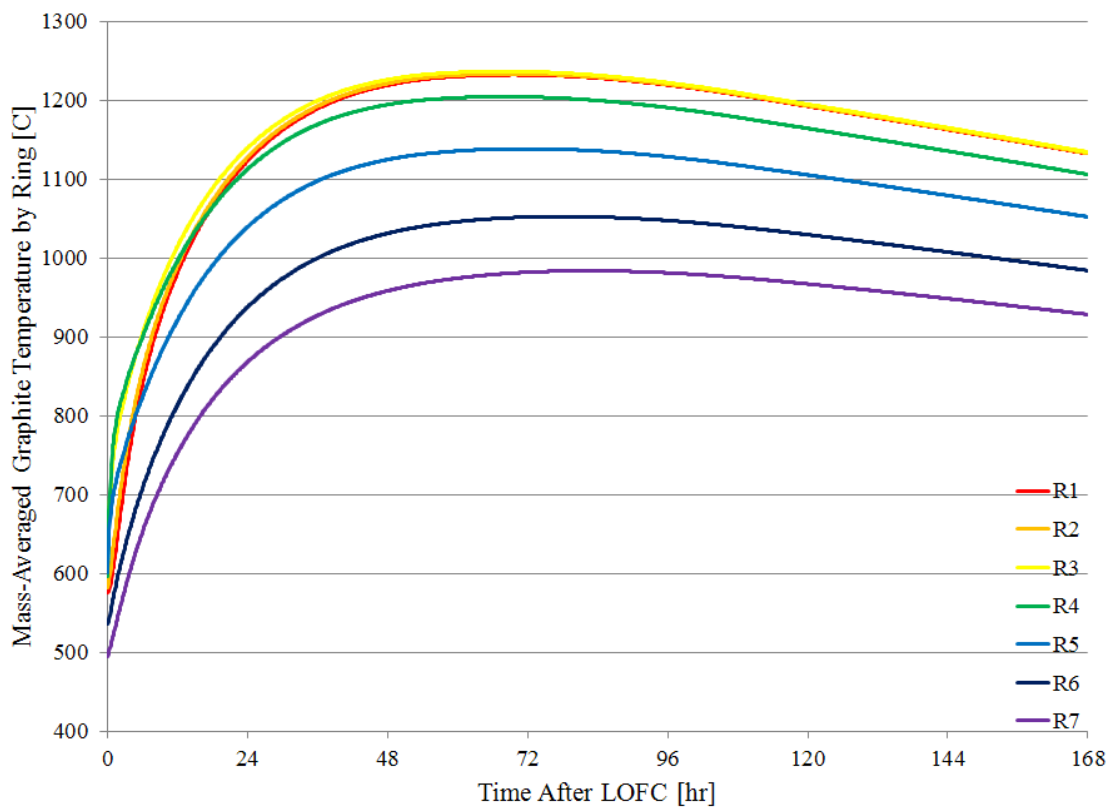


Figure 6.5 Mass-averaged (by ring) core graphite temperatures during DCC

The temperature response in Figure 6.5 for the DCC resembles that of the PCC shown previously because radial conduction remains the most important heat removal mechanism. For a DCC vs. a PCC, peak temperatures on a ring-to-ring basis tend to be

larger by about 200 degrees on average. Additionally, more time is required for core structural temperatures to peak before leveling off. This difference may be explained by the absence of circulation effects during the DCC. Because natural circulation cannot act to remove or redistribute core heat, more thermal energy must be stored in structures as radial conduction acts to convey thermal energy to the RPV. Hence, more time is required for conduction heat removal to first catch up with thermal energy storage and then begin to cool the structures. Rings R1 to R3 reach a peak temperature of 1232 °C, while rings R4 through R7 achieve maximums at 1204 °C, 1138 °C, 1052 °C, and 983 °C, respectively. Rings R1 to R3 require roughly 69.7 hr to reach maximum temperature, while rings R4 to R7 need 70.0 hr, 71.4 hr, 77.9 hr, and 82.25 hr, respectively.

Figure 6.6 shows mass-averaged (by level) core structural temperatures during the DCC. There is no axial temperature profile redistribution due to natural circulation as occurred in the PCC, so some differences are discernible between Figures 6.6 and 6.3. In Figure 6.6, the lower levels L9-L13 heat up at a greater rate than in Figure 6.3 because energy is being stored instead of being removed via natural convection. Because the lower structures begin at higher temperatures than the upper structures and because convection does not redistribute thermal energy from the lower core to the upper core, there is a greater lag in time-to-peak between the upper and lower core. One may then conclude that the lower core conducts more energy and stores less energy early on in the DCC transient. This suggests an interesting axial asymmetry with regard to radial core conduction, as the lower core may be cooling down while the upper core is heating up.

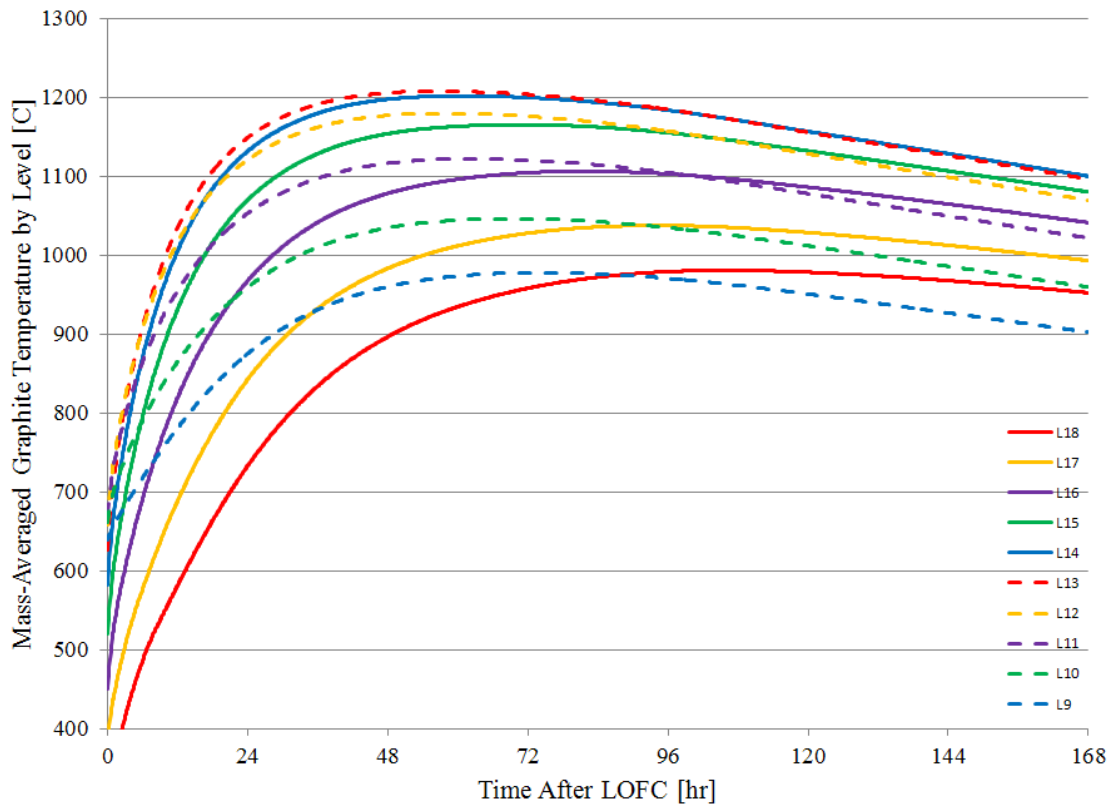


Figure 6.6 Mass-averaged (by level) core graphite temperatures during DCC

As an indirect indicator of passive heat removal from the metallic pressure vessel, an area average of the RPV outer wall temperature was computed from MELCOR data. Figure 6.6 shows the result and suggests that radial conduction causes RPV heat-up and, in turn, increases radiation heat transfer to the RCCS. A peak temperature of 301 °C was reached after about 102 hr. Comparing to Figure 6.4, one notices that the curve in Figure 6.6 exhibits a slight “nose” within 24 hr after the LOFC. This is likely a consequence of the area-averaging method use to derive the RPV wall temperature. The upper RPV heat structures have a larger surface area in the MELCOR

model. Also, for a DCC the upper core structures store more energy than they conduct early on in the transient, meaning the upper core periphery stays cooler for a longer time after LOFC. Hence, the large upper RPV heat structures have cooler temperatures early on in a DCC, and this causes the area-averaged RPV wall temperature to be cooler. However, this effect is not purely an artifact of area averaging because it indicates different axial core temperature distributions in a PCC vs. a DCC shortly after LOFC.

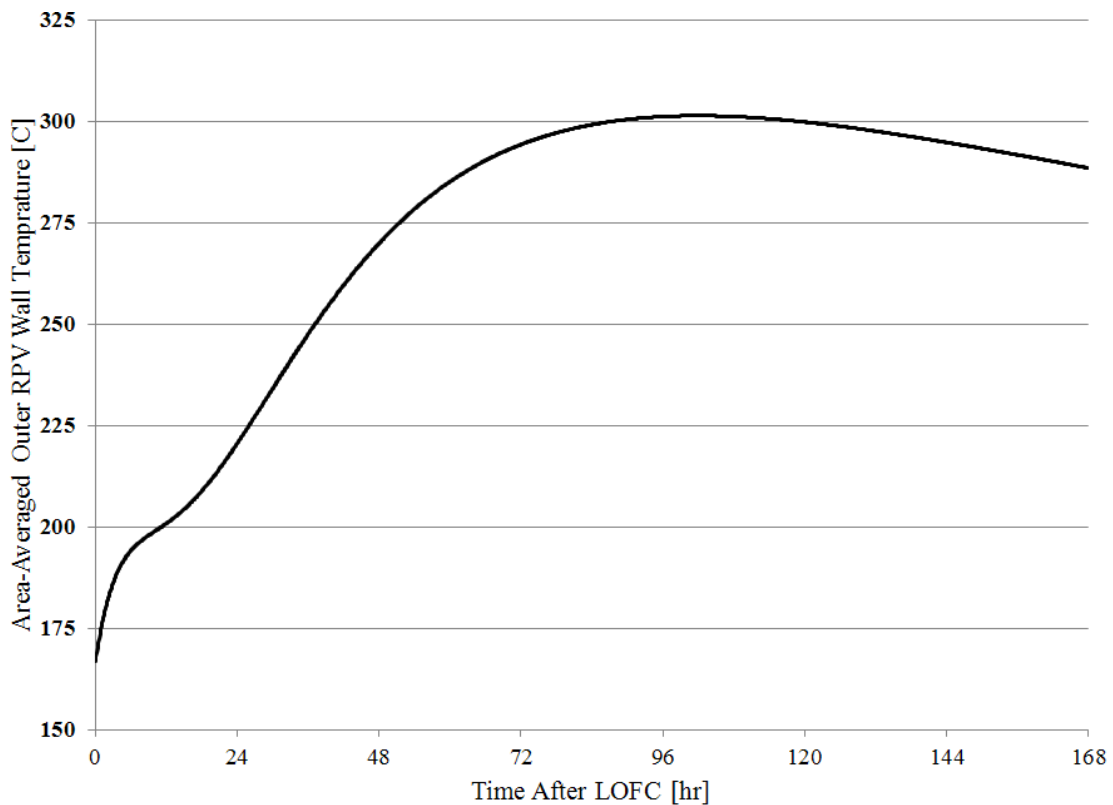


Figure 6.7 Area-averaged outer RPV wall temperature during DCC

6.2.2 MHTGR at 35 MW_{th}

This section presents MELCOR predictions for the full-scale, reduced (10%) power MHTGR at steady state and under certain transient/accident conditions. Maps and plots detailing core structure or coolant temperature distributions comprise the bulk of the MELCOR results. Certain other noteworthy parameters are mentioned as well.

6.2.2.1 Steady-State

Table 6.4 summarizes some important steady-state characteristics. User-defined boundary conditions set the specified inlet mass flow rate, temperature, and pressure. Because the power was scaled down to 10%, the coolant flow rate was reduced accordingly to preserve full-scale inlet/outlet coolant temperatures and pressures.

Table 6.4
Steady-state parameters for the 35 MW_{th} MHTGR

Parameter	Value
Power	35 MW _{th}
Coolant Temperature (In Out)	259.15 °C 687.79 °C
Coolant flow rate (total channel)	16.85 kg/s 15.17 kg/s
Bypass flow rate	1.685 kg/s (10%)
Inlet Pressure	6.4 MPa

The total (channel plus bypass) coolant mass flow rate was reduced by 90.3 % from full scale in response to the 90% reduction in core power. A 10% bypass flow fraction was imposed by boundary conditions in keeping with the full-power MHTGR case.






Table 6.5 is a color-coded core structural temperature map that tabulates the data plotted in Figure 6.2. Axial levels and radial rings are noted in Table 6.5 (IA/IR), as are

the geometric locations of axial level mid-heights (Z) and radial ring centers (R). The pressure vessel temperatures are omitted from Figure 6.8. The cladding temperatures of Table 6.5 (green boxes within the thick black boundaries of the active core) were used to produce Figure 6.8 as opposed to the fuel temperatures. Note that Figure 6.8d is a color-coded replica of Table 6.5 so that hotter and cooler regions are more readily identifiable.

The axial temperature distribution (Figure 6.8c) is relatively flat in the upper and lower reflector regions and is consistent with the chopped cosine power profile in the active core region. As was the case at a 350 MW_{th} power, the active core distribution at 35 MW_{th} is somewhat bottom-peaked with the hottest reported temperature (excluding fuel) being 743.8 °C. In the radial direction (Figure 6.8b), the central reflector temperature distribution is relatively flat but indicates the reflector is warmer in the region nearest the active core. Generally, structural temperatures on a cell-by-cell basis are tens of degrees cooler for a 35 MW_{th} power level despite the fact that coolant flow was adjusted to preserve inlet/outlet helium temperatures. Presumably, this difference occurs because less thermal energy is stored in the graphite core and reflectors at a lower steady-state power level. According to Figure 6.8d, the core hot spots remain in essentially the same geometric locations despite the lowered power level.

Table 6.5
Steady-state core structural temperature map for Figure 6.8 (all temperatures given in °C)

		CR		ACTIVE CORE					RSR		PSR		CB		RPV			
IA/IR		1	2	3	4	5	6	7	N1	N2	N3	N4	N5	N6				
	Z/R [m]	0.25	0.662	0.987	1.313	1.639	1.966	2.271	2.413	2.687	2.961	3.037	3.267	3.4				
UR	21	8.723	267.19	264.22	260.18	259.15	259.15	258.69	258.35	250.60	247.55	241.80	238.67	118.42 107.78				
	20	8.133	283.69	276.60	261.83	259.15	259.15	258.58	258.14	252.00	248.68	242.53	239.18					
ACTIVE CORE	19	7.935	296.53	291.34	260.29	259.18	259.17	258.58	258.16	251.84	248.02	241.49	237.99					
	18	7.534	323.03	321.59	299.50	298.45	296.78	295.73	299.97	298.91	322.75	328.31	296.68			292.10	284.09	280.02
	17	6.741	375.98	375.31	374.08	371.07	368.14	365.11	369.64	366.62	367.54	363.34	304.23			297.33	288.06	283.72
	16	5.948	433.74	434.78	458.22	453.55	449.00	444.30	448.49	443.80	424.43	409.30	316.02			305.24	293.94	289.18
	15	5.155	496.40	500.20	543.98	537.88	531.92	525.79	528.75	522.64	481.91	455.04	329.08			313.79	300.17	294.95
	14	4.362	557.14	564.25	622.35	615.62	608.24	601.47	601.75	595.00	532.69	494.37	340.60			321.12	305.42	299.80
	13	3.569	606.52	614.82	672.27	665.55	657.39	650.64	647.91	641.18	567.13	520.97	347.79			325.07	307.46	301.31
	12	2.776	650.12	660.69	722.31	716.28	706.86	700.79	693.37	687.32	596.47	542.11	354.22			328.97	310.17	303.80
	11	1.983	675.45	687.03	748.53	743.75	733.46	728.65	716.18	711.40	611.83	553.10	357.55	330.93	311.50	305.02		
	10	1.189	677.31	687.78	743.67	740.60	729.79	726.71	709.92	706.86	610.37	552.66	357.68	331.22	311.99	305.59		
LR	9	0.397	671.14	678.50	721.43	720.37	708.89	707.83	686.87	685.83	600.52	547.53	355.82	330.00	311.09	304.76		
	8	-0.005	680.91	687.67	712.78	699.40	675.62	599.90	553.01	509.91	491.31	461.77	447.73	307.52 265.16				
	7	-0.302	688.07	694.41	703.78	692.90	675.01	532.49	526.99	500.58	481.71	455.77	443.61					
	6	-0.793	682.41	690.23	701.80	692.59	674.25	547.95	538.90	506.27	483.79	455.93	443.33					
	5	-1.189	661.13	671.80	685.76	687.76	662.58	589.02	562.02	500.92	485.16	459.27	446.68					
	4	-1.685	640.61	655.44	676.14	686.04	663.46	607.71	578.47	506.29	488.78	462.38	449.77			312.10	268.76	

CR	Central Reflector		Fuel	UR	Upper Reflector
RSR	Replaceable Side Reflector		Core Ceramic	LR	Lower Reflector
PSR	Permanent Side Reflector		SR/LP Ceramic	LP	Lower Plenum
CB	Core Barrel		Core Barrel		
RPV	Reactor Pressure Vessel		Vessel Wall		

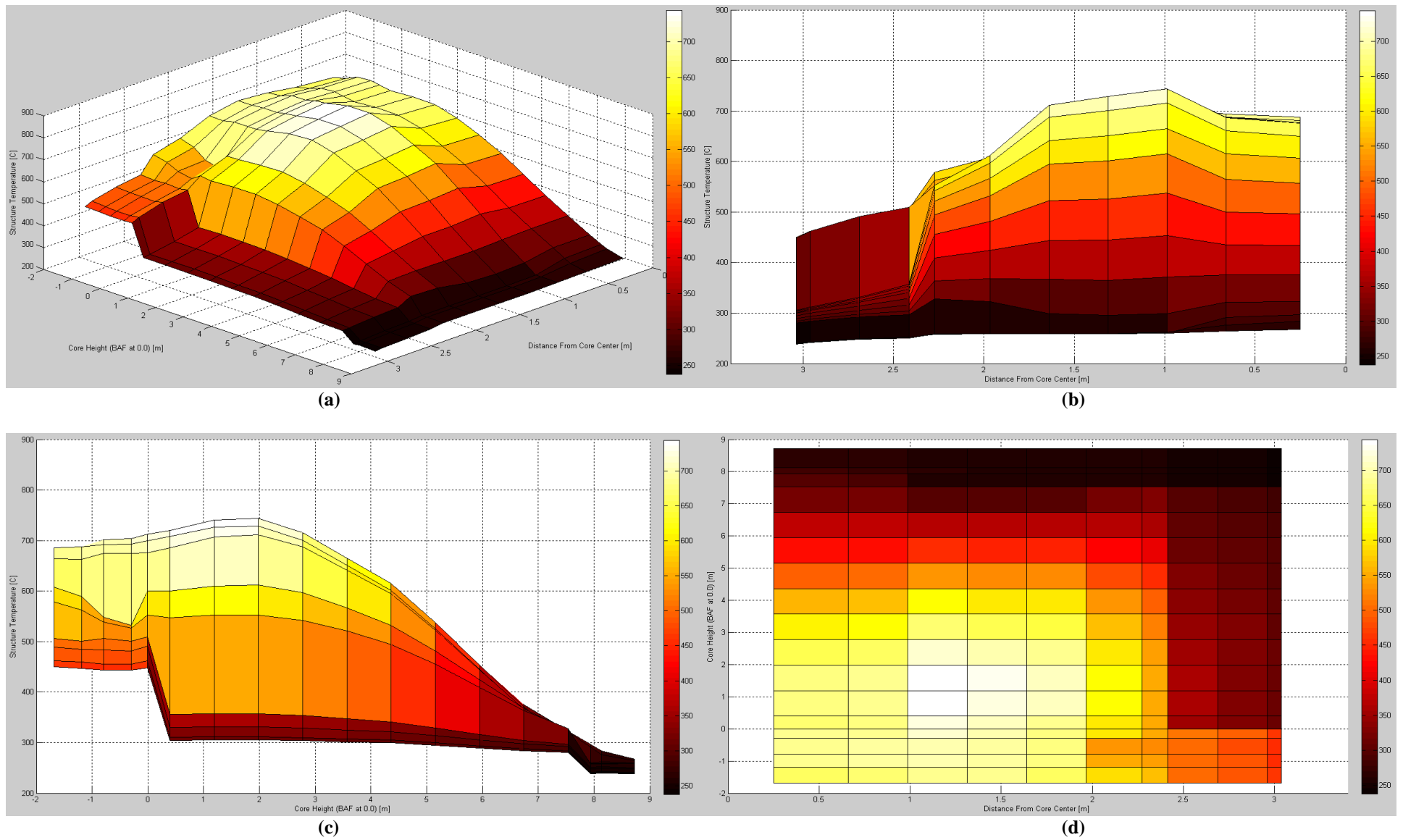


Figure 6.8 Steady-state core structural temperature distribution

Table 6.6 shows the steady-state coolant temperatures from the CVH package as they correspond to core axial levels and radial rings. The coolant enters the upper reflector at about 259 °C before entering the core channel/bypass CVs. The active core uses three CVs per ring (rings 3 to 5) between levels 9 and 18, while the bypass regions (rings 1, 2, 6, and 7) use only one CV for this same axial level range. All helium emerges from the core and mixes in the large lower plenum CV so that a coolant temperature roughly equaling the MHTGR target is achieved. The active core coolant temperatures of Table 6.6 are equal to those of Table 6.3 within a few degrees.

Table 6.6
Steady-state helium temperature map, 35 MW_{th} MHTGR (all temperatures given in °C)

		CR		ACTIVE CORE			RSR		
IA/IR		1	2	3	4	5	6	7	
ACTIVE CORE	UR	19-21	259.15	259.15	259.96	259.15	259.15	259.15	259.15
		14-18			487.24	477.34	474.73		
		11-13	298.85	327.00	666.69	652.26	640.65	385.25	314.95
		9-10			706.51	692.83	675.06		
LR		6-8	666.65	676.59	705.33	692.86	674.94	571.26	552.58
		4-5			704.85	691.59	672.51		
LP		3							
		2				687.79			

6.2.2.2 Pressurized Conduction Cool-Down

The same methodology presented in section 6.2.1.2 was applied to the 35 MW_{th} MHTGR. The PCC transient for this case was similar to that of the 350 MW_{th} as no new physical phenomena came in to play. The same mass and area averaged quantities are

plotted in Figures 6.9 through 6.11, and their respective trajectories through the transient are seen to agree with Figures 6.2 through 6.4.

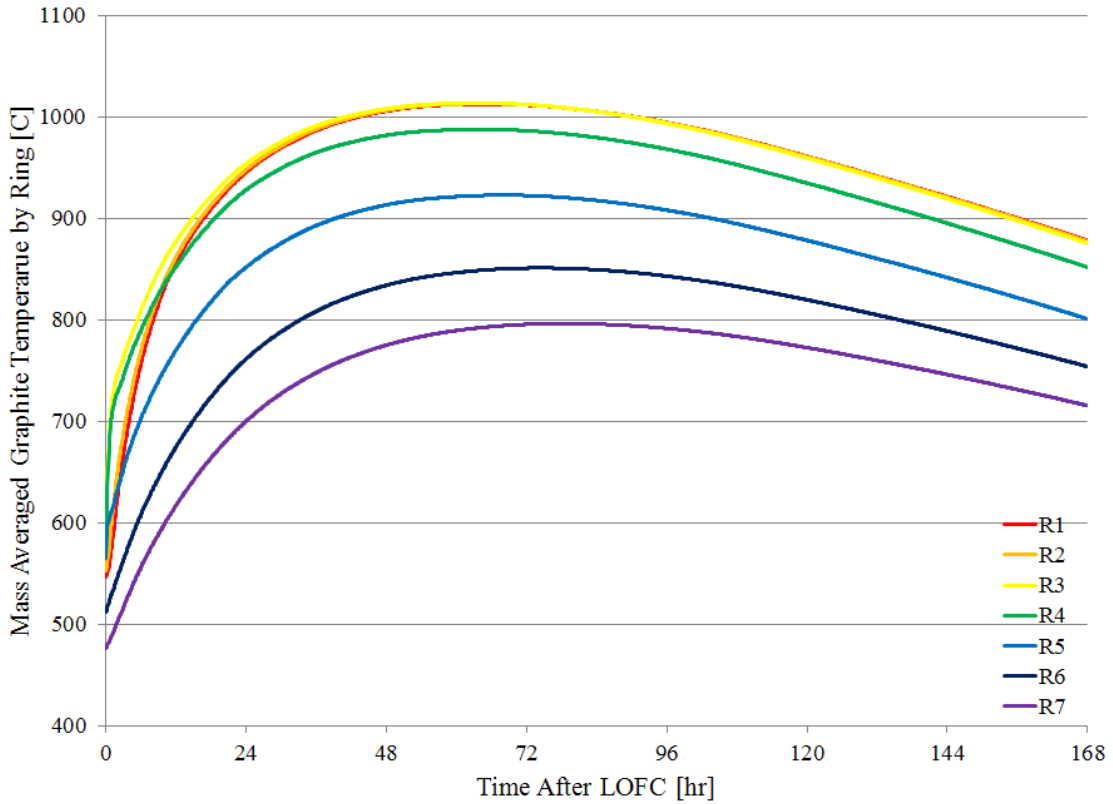


Figure 6.9 Mass-averaged (by ring) core graphite temperatures during PCC

The only observable differences in mass-averaged temperatures of Figures 6.9, 6.2, 6.10, and 6.3 are in peak values. They are lower for the decreased power level, as expected. The two area-averaged parameters of Figures 6.11 and 6.4 are also different, though very close, in terms of peak temperature.

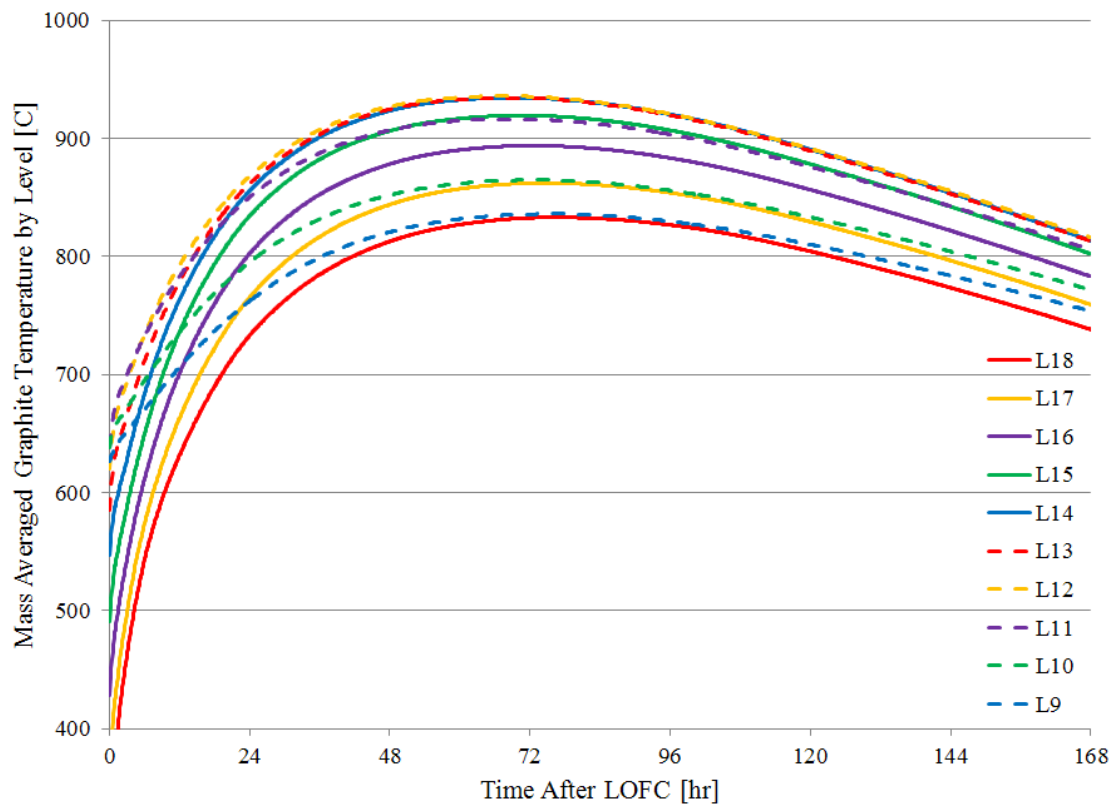


Figure 6.10 Mass-averaged (by level) core graphite temperatures during PCC

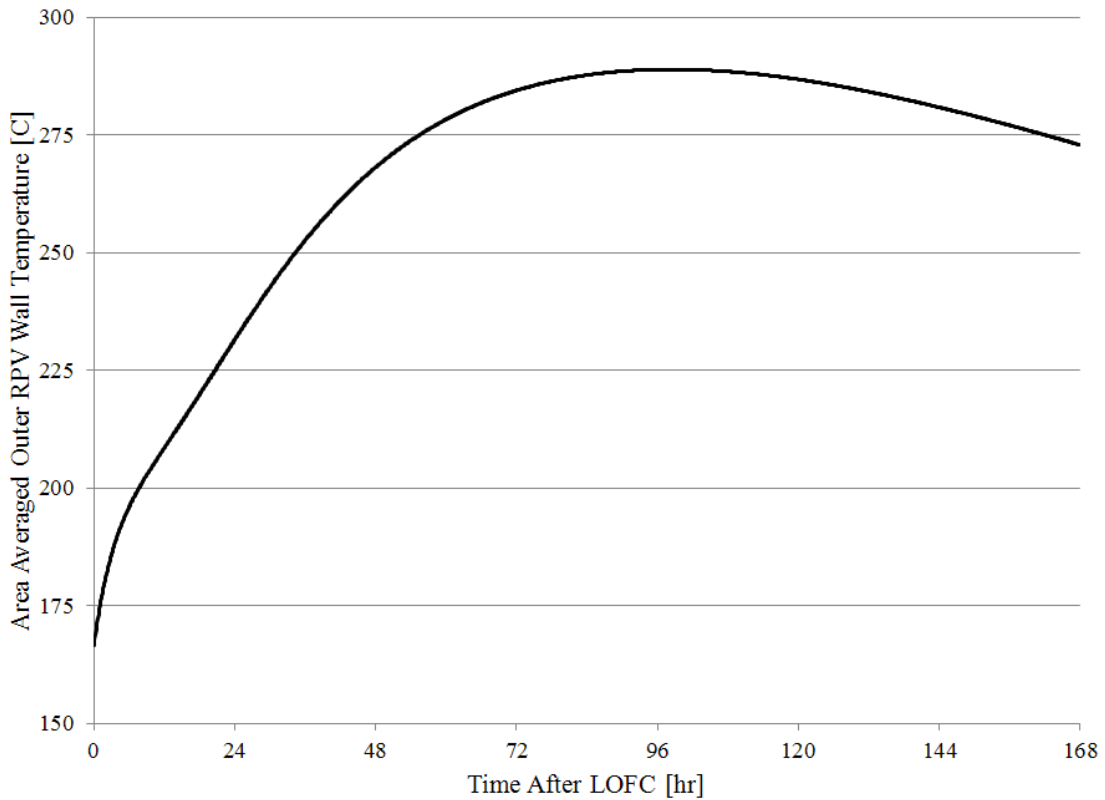


Figure 6.11 Area-averaged outer RPV wall temperature for PCC

6.2.2.3 Depressurized Conduction Cool-Down

The same methodology presented in section 6.2.1.3 was applied to the 35 MW_{th} MHTGR. The DCC transients at 350 MW_{th} and 35 MW_{th} evolved similarly in time, although peak temperatures were lower and were reached sooner due to the lower amount of stored energy in the 35 MW_{th} core. Figures 6.12 to 6.15 may be compared directly to Figures 6.5 to 6.7 to confirm these observations.

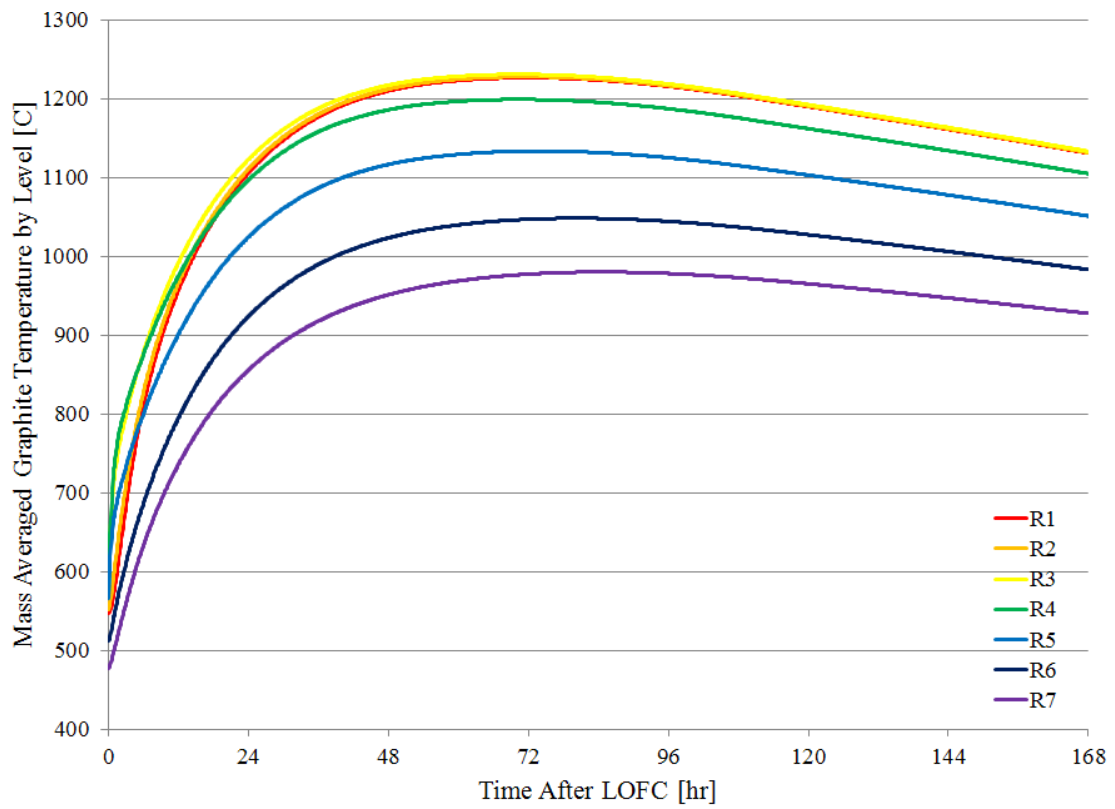


Figure 6.12 Mass-averaged (by ring) core graphite temperatures during DCC

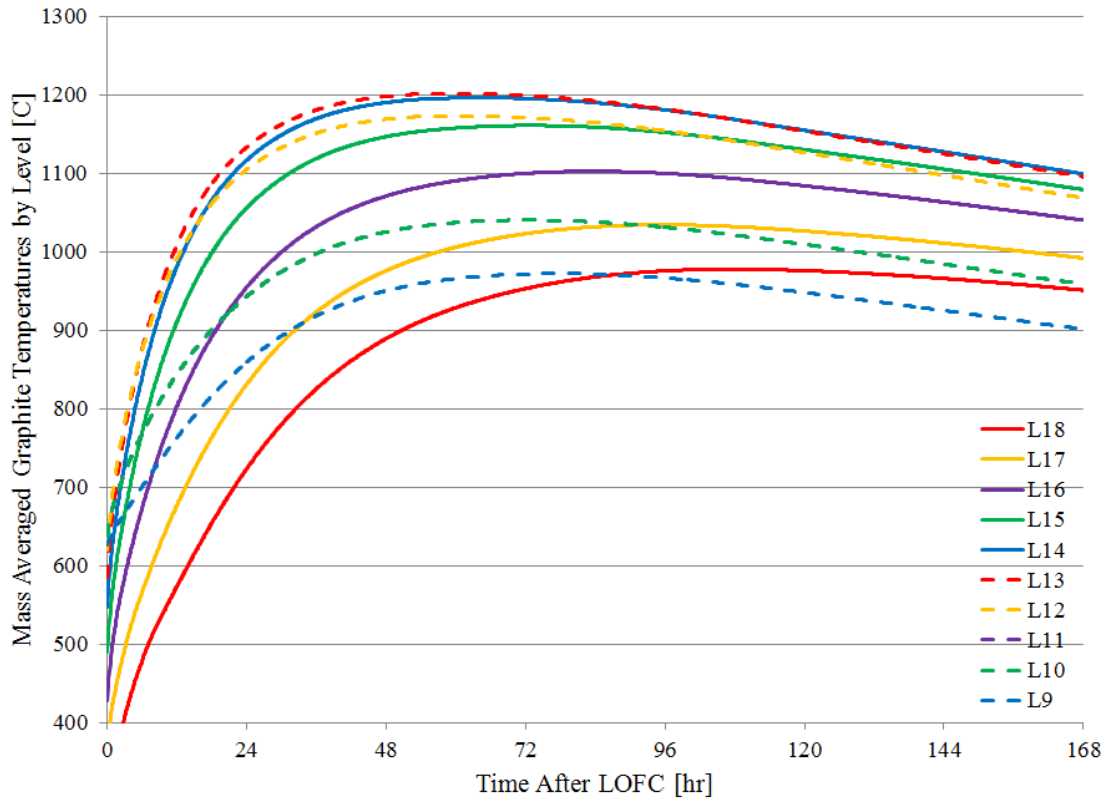


Figure 6.13 Mass-averaged (by level) core graphite temperatures during DCC

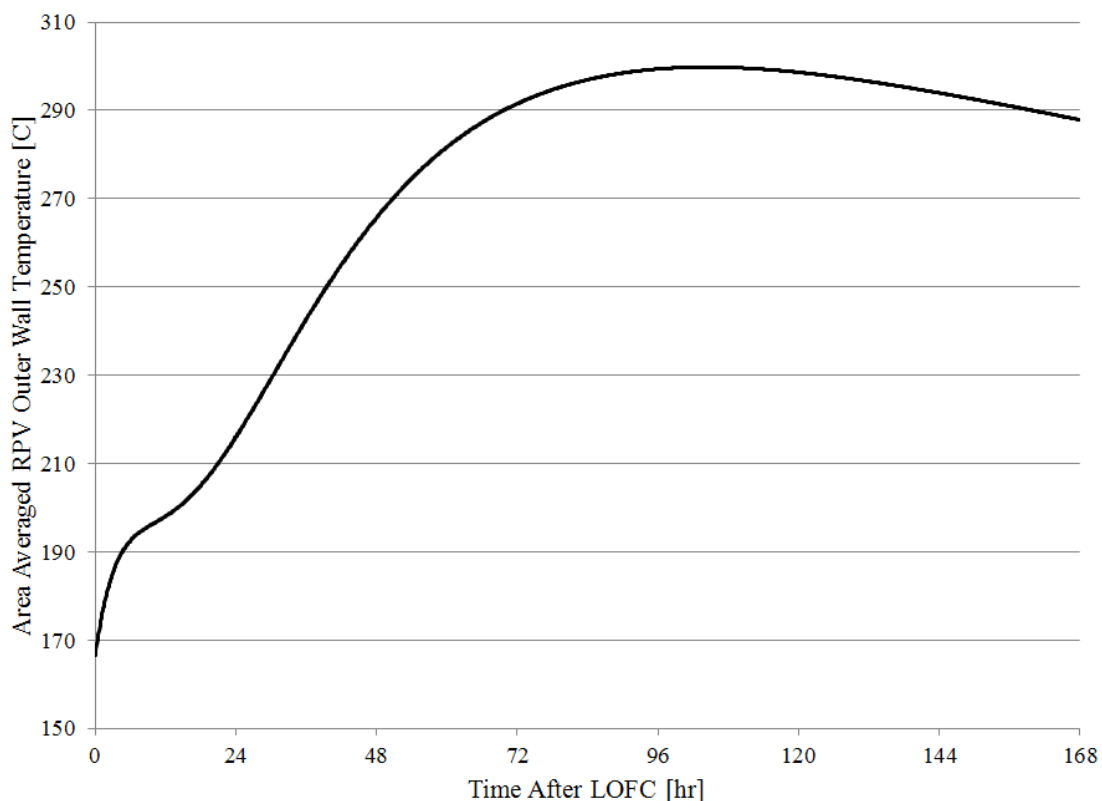


Figure 6.14 Area-averaged outer RPV wall temperature for DCC

6.2.3 HTTF at 2.2 MW_{th}

This section presents MELCOR predictions for the 2.2 MW_{th} HTTF at steady state and under DCC transient/accident conditions. Maps and plots detailing core structure or coolant temperature distributions comprise the bulk of the MELCOR results. Certain other noteworthy parameters are mentioned as well.

6.2.3.1 Steady-State

Table 6.7 presents some steady-state parameters for the HTTF. No nominal coolant mass flow rate was available from literature, but with some trial and error steady-state runs it was determined that 0.96 kg/s of helium was required to reach the

target outlet temperatures. Bypass flow was not considered in the HTTF model, but the actual facility will have control rod sleeve inlet orifices to allow for bypass flow.

Table 6.7
Steady-state parameters for the 2.2 MW_{th} HTTF

Parameter	Value
Power	2.2 MW _{th}
Coolant Temperature (In Out)	260.6 °C 685.1 °C
Coolant flow rate (total)	0.96 kg/s
Inlet Pressure	0.8 MPa

Table 6.8 and Figure 6.15 present core temperature maps and plots for the HTTF at steady-state. HTTF structural temperatures are significantly hotter than those of the MHTGR, so while full-scale coolant temperature is preserved, structural temperatures are generally not.

Table 6.8

Steady-state core structural temperature map for Figure 6.3 (all temperatures given in °C)

		CR	ACTIVE CORE						RSR	PSR		CB		RPV	
IA/IR		1	2	3	4	5	N1	N2	N3	N4	N5	N6			
	Z/R [m]	0.091	0.247	0.357	0.438	0.539	0.603	0.7	0.743	0.762	0.819	0.832			
UR	27	317.97	263.27	262.92	276.60	337.23	260.49	258.27	256.87	256.18					
	26	568.90	-	-	-	508.10	481.09	318.25	278.89	277.78	72.31	71.74			
	25	572.32	262.10	261.41	264.95	513.44	476.23	317.00	278.09	276.98					
	24	568.05	308.46	319.59	333.65	516.80	485.16	320.83	282.64	281.64	61.99	61.46			
	23	556.44	-	-	-	515.40	303.60	261.40	246.17	245.47					
ACTIVE CORE	22	518.12	365.05	340.40	369.04	344.38	396.07	371.29	524.30	329.44	280.71	264.47	263.77	71.72	71.21
	21	558.53	551.73	478.89	570.25	497.22	602.74	529.31	564.46	337.53	282.02	264.96	264.25		
	20	610.96	736.78	620.61	770.94	654.14	803.62	686.16	611.74	385.58	323.87	303.11	302.21	85.08	84.39
	19	662.02	883.67	738.81	920.34	781.08	942.51	806.27	654.20	395.66	325.36	303.63	302.71		
	18	706.75	974.34	825.73	1019.22	876.55	1035.30	894.54	690.94	449.75	375.25	348.59	347.43	103.54	102.60
	17	737.61	1023.32	881.10	1074.13	937.70	1082.90	947.36	713.09	455.63	376.05	348.85	347.68		
	16	745.92	1023.40	896.59	1076.56	954.93	1078.14	956.64	717.93	491.40	414.69	383.50	382.13	119.87	118.70
	15	732.37	979.87	877.80	1033.16	935.33	1027.05	928.76	703.81	487.21	414.08	383.30	381.92		
	14	696.29	885.25	816.43	935.33	869.40	922.21	855.56	672.86	492.49	428.01	396.30	394.85	126.53	125.26
	13	650.30	750.11	724.33	795.12	770.44	774.47	749.31	634.08	483.11	426.67	395.86	394.42		
LR/FDB	12	623.13	668.83	713.78	689.87	616.10	471.51	418.57	383.47	381.77					
	11	607.16	627.59	652.90	624.19	549.83	525.41	437.74	395.92	394.14					
	10	610.07	631.27	649.41	634.58	579.10	566.79	450.03	401.42	399.49	147.53	146.17			
	9	621.30	654.17	678.56	656.97	597.67	433.91	428.64	424.36	422.12					
	8	613.99	663.73	706.22	680.97	602.14	468.90	421.68	390.23	388.71					

CR Central Reflector
 RSR Replaceable Side Reflector
 PSR Permanent Side Reflector
 CB Core Barrel
 RPV Reactor Pressure Vessel

Fuel
 Core Ceramic
 SR/LP Ceramic
 Core Barrel
 Vessel Wall

UR Upper Reflector
 LR Lower Reflector
 LP Lower Plenum

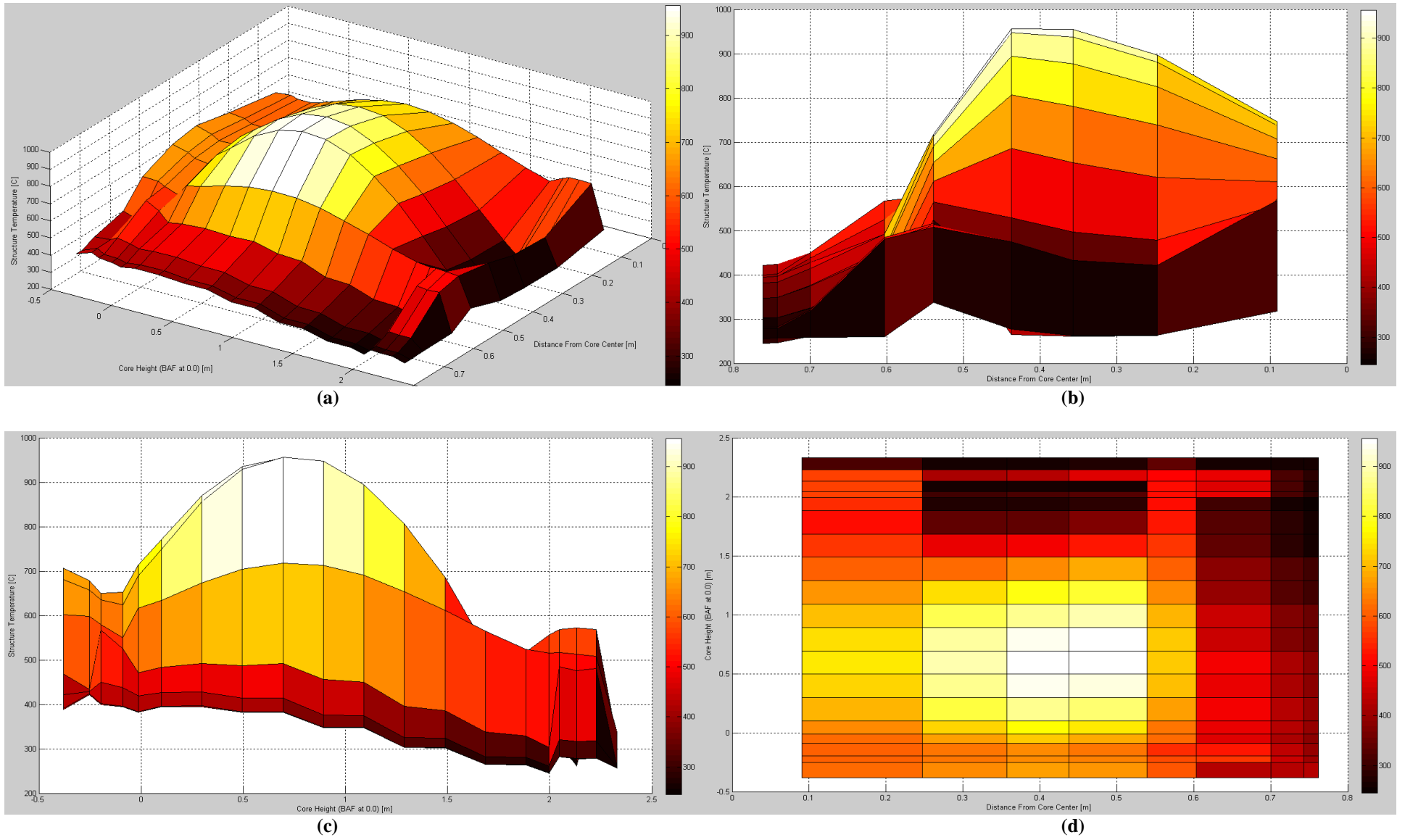


Figure 6.15 Steady-state core structural temperature distribution

The general disagreement between the HTTF and MHTGR in terms of structural temperatures is likely due to one or more distortions in the relevant scaling ratios defined by the scaling analysis report [3]. Most likely, the overall core thermal resistance to heat transfer is not appropriately scaled between the MHTGR and HTTF. This result was not unexpected, as HTTF heater rod and core ceramic material properties are uncertain. Thermal conductivity and specific heat capacity are vital components of core thermal resistance, so if values for these parameters are incorrect one cannot expect similarity.

The axial temperature distribution of Figure 6.15c is more severely peaked than that of the MHTGR but assumes the same general shape. The radial temperature distribution of Figure 6.15b appears shifted towards the outer core region. The HTTF hot spots remain in the lower structure (as in the MHTGR), but are nearer to the periphery.

Table 6.9
Steady-state helium temperature map, HTTF (all temperatures given in °C)

	IA/IR	CR		ACTIVE CORE		RSR	
		1	2	3	4	5	
UR	25-27	260.45	260.45	260.32	261.92	261.92	
	23-24	260.93	260.93	260.81	262.77	262.77	
ACTIVE CORE	21-22	300.89	300.89	305.30	308.93	308.93	
	19-20	401.54	401.54	419.01	416.87	416.87	
	17-18	525.06	525.06	557.98	545.67	545.67	
	15-16	624.68	624.68	669.00	647.51	647.51	
	13-14	663.25	663.25	710.66	685.60	685.60	
LR/FDB	11-12	663.29	663.29	710.52	685.58	685.58	
	10	663.24	663.24	710.43	685.43	685.43	
	8-9	663.17	663.17	709.08	684.04	684.04	
LP	6-7			685.07			

6.2.3.2 Depressurized Conduction Cool-Down

The only conduction cool-down transient considered for the HTTF was of the DCC variety, as the facility was not scaled with a PCC in mind. The results of the DCC include level and ring mass-averaged graphite temperature plots as well as an area-averaged RPV temperature plot.

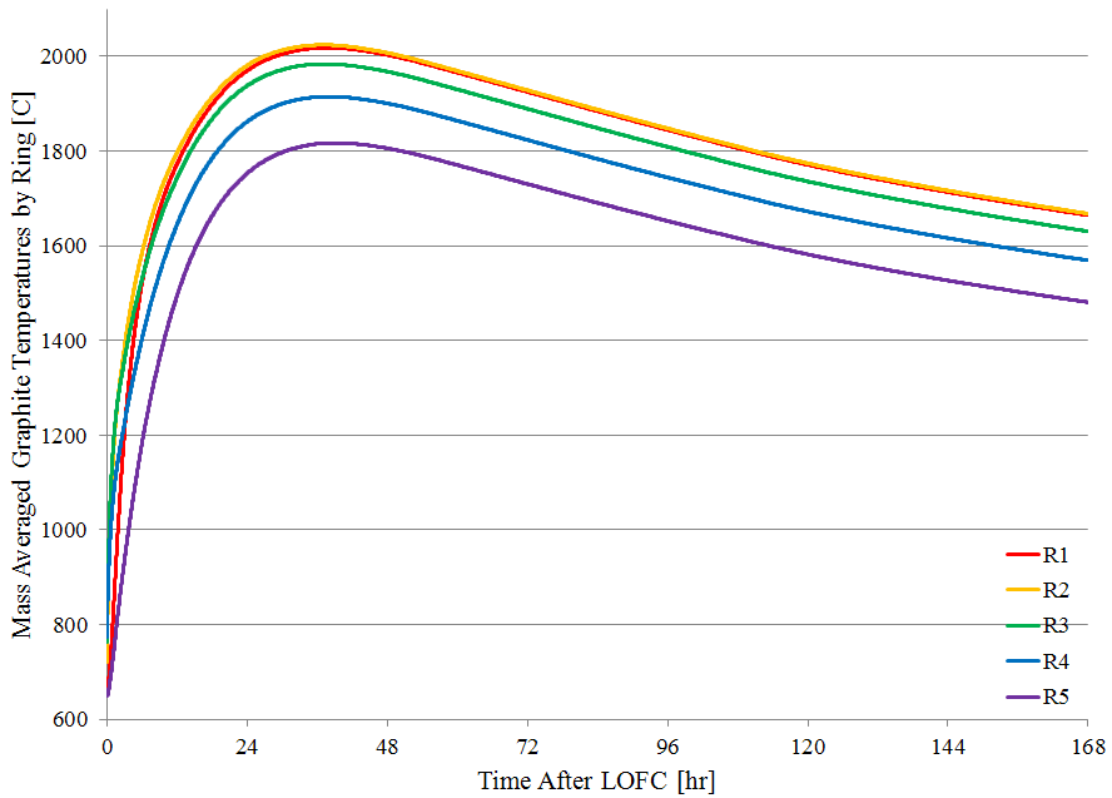


Figure 6.16 Mass-averaged (by ring) core graphite temperatures during DCC

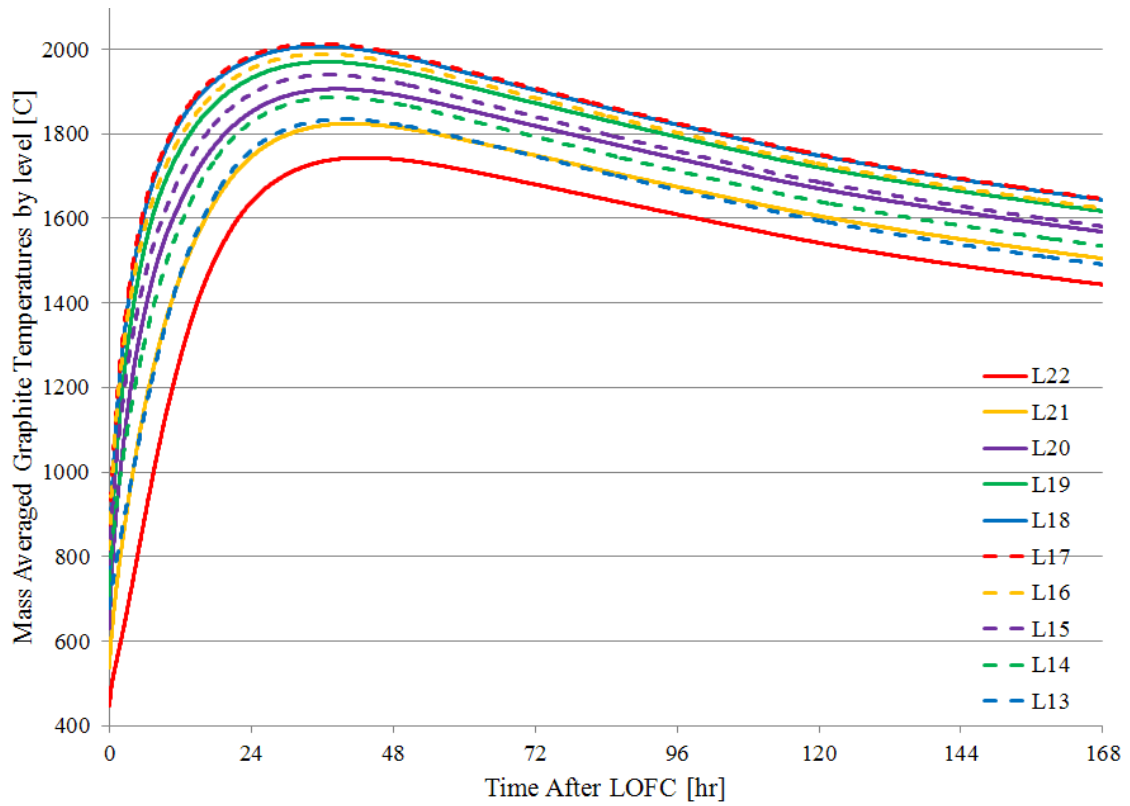


Figure 6.17 Mass-averaged (by level) core graphite temperatures during DCC

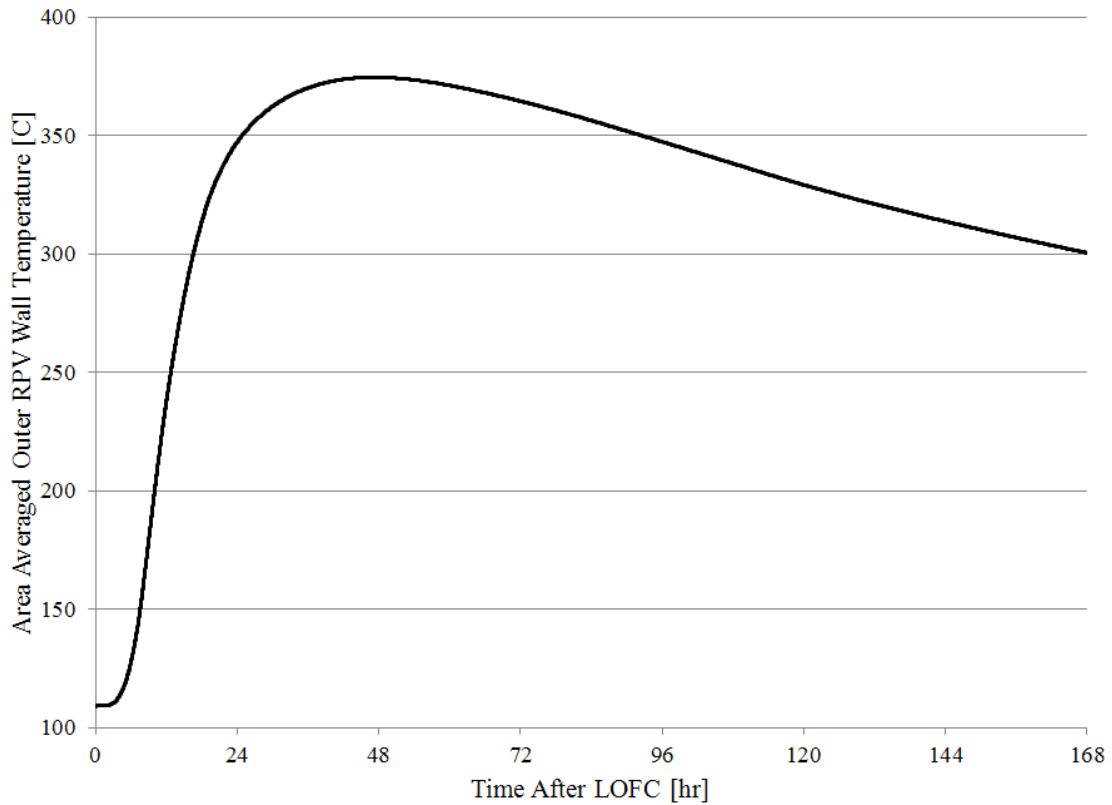


Figure 6.18 Area-averaged RPV outer wall temperature for DCC

Figure 6.16 and 6.17 look very comparable to one another in terms of timing and peak temperature. Hence, the ring and level averages do not differ significantly at any point in transient time. This suggests that the same kinds of effects attributable to the bottom-peaked axial temperature distribution in the MHTGR are not preserved in the HTTF under DCC conditions. In the HTTF, the upper and lower core structural temperatures seem to increase, level off, and cool down together without any significant region-wise time lag. This character is not in agreement with MHTGR system response during a DCC, regardless of power level. The general curve shapes in Figure 6.16 agree with those of Figure 6.5 apart from the more severe rates of structural heat-up predicted for the HTTF. This suggests that no new physical phenomena beyond core conduction

factor in to DCC event progression of the HTTF. Looking at the average RPV wall temperature in Figure 6.18, one observes that after about 48 hours the vessel steel begins to cool off from its peak temperature of 374 °C. Thus the RPV of the HTTF gets about 70 degrees hotter than that of the MHTGR but begins to cool off in only half the time.

6.3 Prototype-to-Model Comparison with MELCOR Results

To reiterate previous observations on MHTGR-to-HTTF scaling, poor agreement was observed under steady-state and DCC conditions, as ring and level mass-averaged temperature plots showed few similarities. The HTTF design iteration modeled in this study seems capable of reproducing full-scale MHTGR coolant temperatures, but there were significant over-predictions in structural temperature. The core temperature distribution from the MHTGR was not exactly preserved either, as a more center-peaked axial profile was seen instead of the MHTGR bottom-peaked profile. Because the two systems were so different at steady-state, DCC transients evolved from dissimilar starting points and any chance of observing good agreement was lost.

Despite the fact that the same physical phenomena are present in both systems (forced convection, radial conduction, radiation), a 2.2 MW_{th} HTTF model built with the latest design information does not scale well with a 350 MW_{th} or 35 MW_{th} MHTGR. There are simple explanations for this result, namely a lack of preservation in certain scaling ratios vital to GCR phenomenology. Scaling ratios, especially those related to conduction heat transfer and thermal energy storage, are strong functions of transport properties like thermal conductivity and specific heat capacity. If HTTF ceramic properties have changed from those communicated by OSU some time ago [13] or if

further design iterations have altered system characteristics, such revisions are not accounted for in this study.

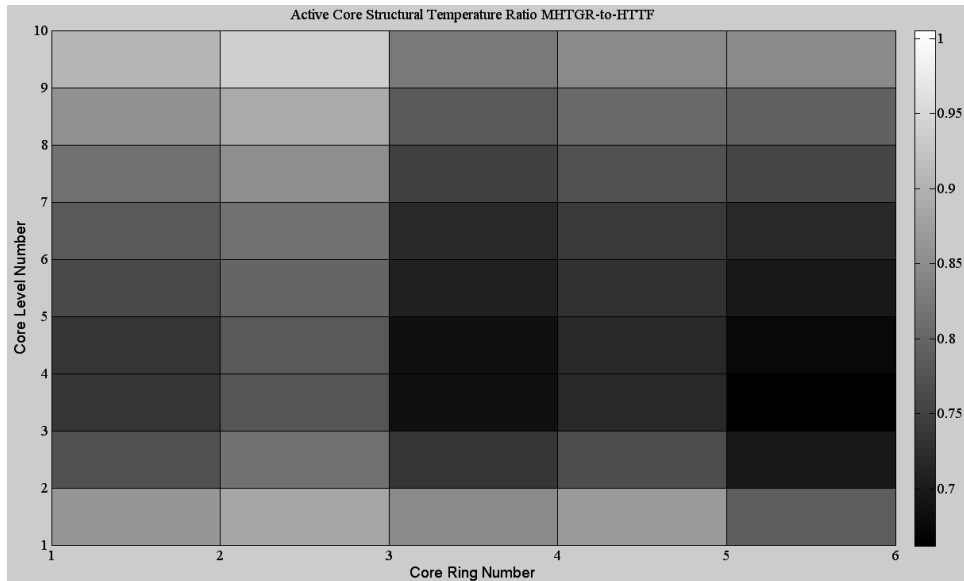


Figure 6.19 Ratio of structural temperatures in active core MHTGR-to-HTTF

Figure 6.19 is a map of the active core structural temperature ratios as listed in Tables 6.2 and 6.8. The temperatures of the MHTGR are divided by those of the HTTF on a cell-by-cell basis in the active core. Ideally, this ratio would be nearly equal to 1.0 in all cells so as to signify perfect similitude between the two systems. However, Figure 6.19 shows considerable disagreements in most places, especially the lower portions of the active core.

There were a few encouraging results to be gleaned from MELCOR predictions. The ring and level average core temperatures in the DCC behaved as expected under conduction cool-down conditions, as temperatures underwent an excursion to some maximum before decreasing in a reasonable amount of time. The character of the

excursion, turn-over, and drop-off was comparable between the MHTGR and HTTF. The ratio of time-to-peak temperature under DCC conditions (prototype-to-model) is roughly 1:2, which is consistent with targets set in the draft scaling analysis report [3]. Furthermore, there is nothing to suggest that MELCOR GCR models are invalid or that GCR transients cannot be modeled with judicious implementation of boundary conditions. While there are certain aspects of GCR operation currently beyond the scope of MELCOR analytical capabilities like plenum hot streaking, air ingress, and air/graphite oxidation, they can be addressed in the future with new MELCOR models or with separate effects testing.

6.4 General Assessment of MELCOR/RELAP Agreement

The INL report on analyses of full-scale MHTGR transients was used to draw a comparison between RELAP and MELCOR predictions of a DCC and PCC. MELCOR model boundary conditions for a PCC were necessarily adjusted to match those used in RELAP. A 60 second, linear forced flow coast-down after LOFC was therefore imposed on the MELCOR PCC. The RELAP analyses use “peak fuel temperature” and RPV outer wall temperature as metrics to judge response and to contrast the DCC and PCC. From MELCOR, a mass average of the core cell FU component temperatures in the hottest core ring was chosen to represent “peak fuel temperature”.

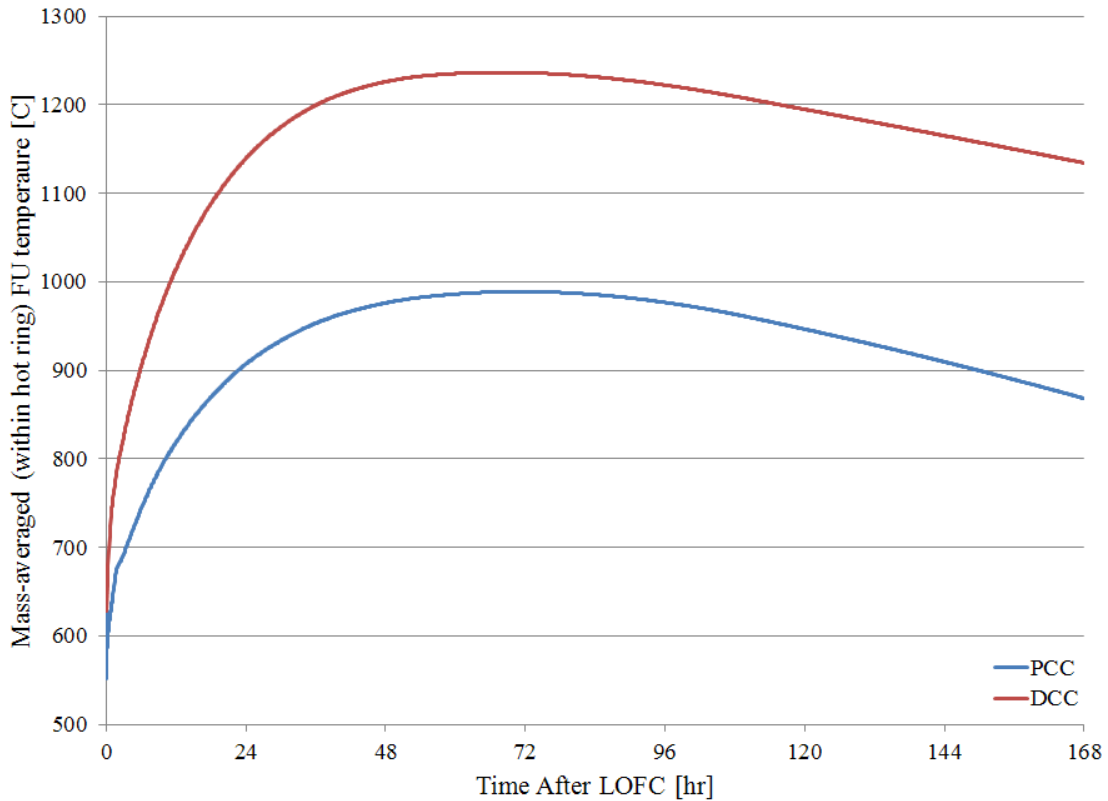


Figure 6.20 Hot-ring, mass-averaged FU temperature during PCC and DCC

Comparing Figure 6.20 to Figure 6.21 (reproduced from [4]), one deduces that MELCOR seems to predict higher “fuel” temperatures than RELAP. Furthermore, it seems as though the 60 second forced flow coast-down has different effects in RELAP than it does in MELCOR as far as fuel temperatures are concerned. A significantly larger dip in fuel temperatures occurs initially in RELAP, presumably because forced cooling coast down is slower than the transition from operating power to decay heat [4]. The same occurs in MELCOR, but a much shorter-term fuel cooling effect is observed and cannot be seen on the time scale of Figure 6.20. The time-to-peak is also different, but this may be partly due to the mass averaging of MELCOR data.

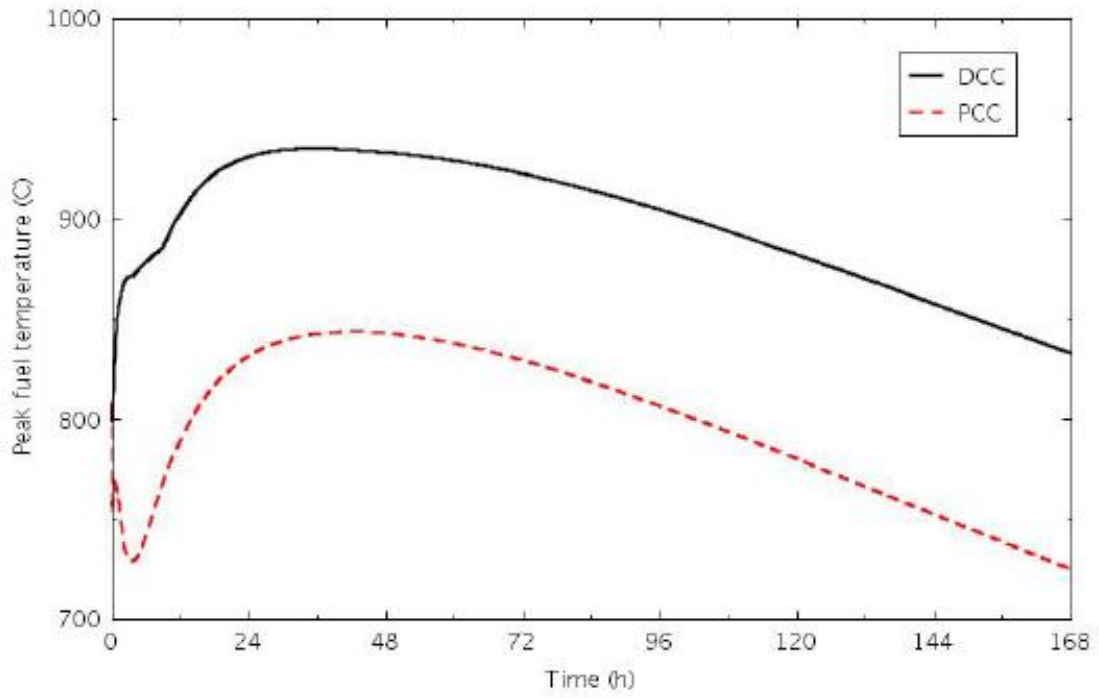


Figure 6.21 Peak fuel temperature as reported by RELAP during PCC and DCC [4]

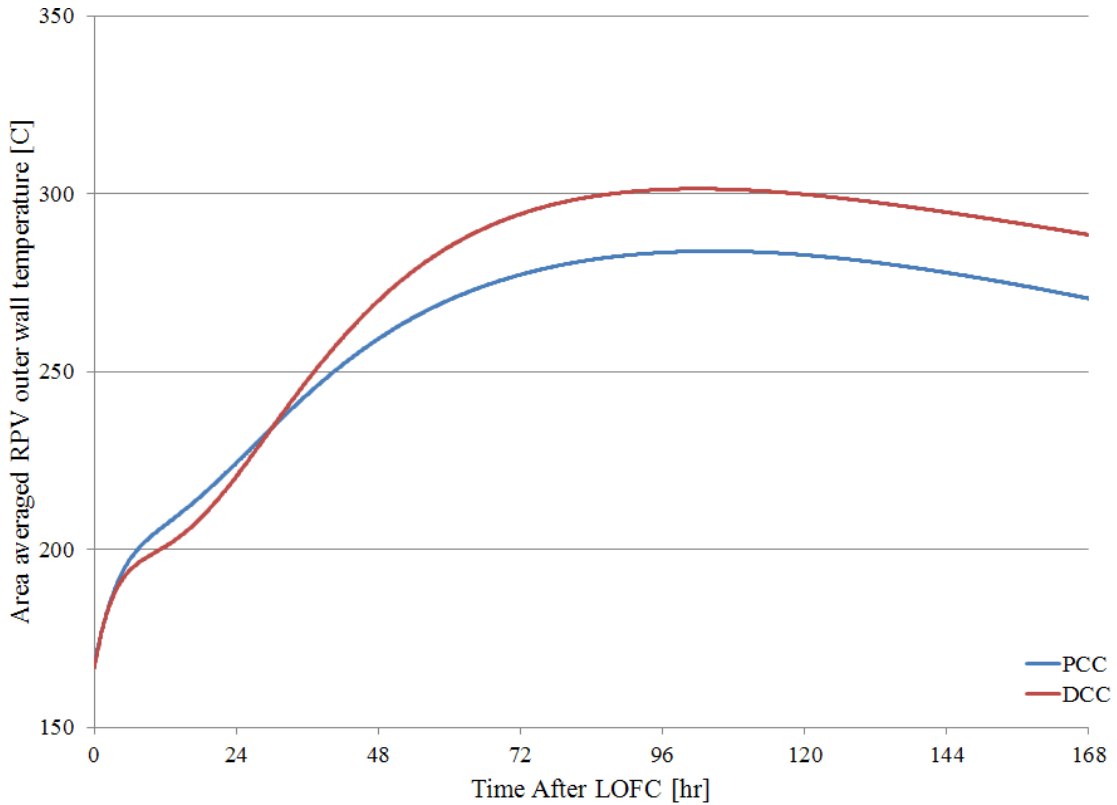


Figure 6.22 Area-averaged RPV outer wall temperature during PCC and DCC

An area-averaged RPV wall temperature shown in Figure 6.22 was chosen to compare with the RELAP RPV temperature in Figure 6.23. As was the case with the fuel temperature comparison, early stage cooling effects seen in RELAP results are not present or occur on a much shorter time scale in MELCOR results. The magnitudes of peak temperatures, while not in excellent agreement, are fairly close considering the MELCOR result is area-averaged over the entire RPV and the RELAP result is not.

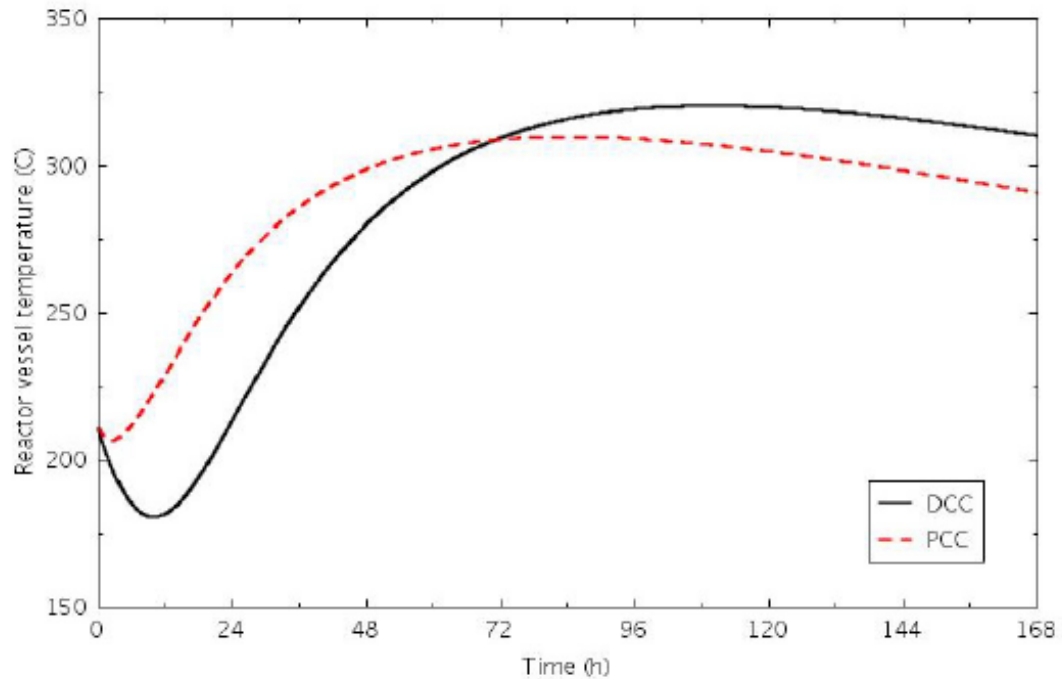


Figure 6.23 RPV temperature as reported by RELAP during PCC and DCC

Without a detailed study assessing MELCOR vs. RELAP models, it is difficult to judge whether differences in core heat transfer models are to blame for the several discrepancies in results. The RCCS in the MELCOR model was simply a constant-temperature boundary condition, whereas a more complete air-cooled RCCS may have been used in the RELAP analyses. Differences in core geometry likely do not contribute to observed disagreements because the MHTGR PSID was used in the development of both models. Also, due consideration should be given to material properties. It is unclear whether the time-dependent thermal conductivity and specific heat capacity values found in the graphite design handbook [14] are implemented in RELAP as in MELCOR.

7. CONCLUSIONS AND RECOMMENDATIONS

MELCOR input decks for both the HTTF and MHTGR were constructed according to the latest available design references. Using new GCR modeling capabilities of MELCOR, steady-state and transient cases for both systems were run so as to predict thermal-hydraulic response. Computational data and general observations of system behavior were compared to nominal design parameters and to expectations following from engineering judgment. No code-to-experiment benchmark was possible because experimental data is as yet unavailable. Several model-to-model and code-to-code comparisons lead to the conclusion that, while the current MELCOR models require further revision, MELCOR phenomenological models work as intended to predict GCR response under steady-state, PCC, and DCC conditions. Most observed disagreements in prototype-to-model (i.e. MHTGR-to-HTTF) scaling or in MELCOR-to-RELAP predictions may be explained by and are likely due to factors other than MELCOR phenomenological modeling. As further information - i.e. a facility instrumentation plan, a more detailed and complete set of facility drawings, a finalized set of material properties, etc. - becomes available, the HTTF input may be reconsidered.

There are several issues related to GCR modeling that MELCOR developers at SNL could work to resolve in the near future. Several improvements dealing with core support logic, core component material options, oxidation models, and PMR-type fuel modeling could be made to the COR package for PMR-type reactors. The fact that the RF component is only self-supporting tends to over-complicate core package input. Also, if more than two or three materials exist in the core as FU, CL, SS, and RF, the user is forced to make several materials substitutions and may not be able to

accommodate all materials. Air/graphite oxidation and graphite dust transport models are forthcoming from developers, and incorporation of these models would certainly enhance code capabilities. Also, an alternative model or method of predicting heat generation in PMR fuel compacts could increase the fidelity of MELCOR predictions. However, the developers must wait on such models (empirical or theoretical) to be created and validated.

When OSU begins testing, SNL might consider building its own models of the HTTF test matrix. Then, as was done with several other test facilities, the developers could incorporate this system into the MELCOR automated test suite. Recommendations for MELCOR users as to best GCR modeling practices would be helpful and could be developed concurrently. Also, users might benefit from an expanded plotting capability that includes new variables to indicate core conduction heat transfer and core-to-structure boundary conduction. At present, the user can only confirm indirectly that conduction is occurring in the core and at the boundary.

REFERENCES

- [1] Preliminary Safety Information Document for the Standard MHTGR. Technical Report, HTGR-86-024, Department of Energy, 1986.

- [2] S. Cadell, “HTTF Collection”. May 2010. Personal Communication.

- [3] B.G. Woods, R.B. Jackson, and B.L. Nelson. Scaling analysis for the very high temperature reactor test facility at Oregon State University. Technical Report DRAFT copy, OSU-VHTR-0001, Oregon State University, February 2009.

- [4] Studies related to the Oregon State University high temperature test facility: scaling, the validation matrix, and similarities to the modular high temperature gas-cooled reactor. Technical Report, INL/EXT-10-19803, Idaho National Laboratories, September 2010.

- [5] Pre-application safety evaluation report for the modular high temperature gas-cooled reactor (MHTGR). Technical Report, NUREG-1338, U.S. Nuclear Regulatory Commission, December 1995.

- [6] K. Kok. *Nuclear Engineering Handbook*. CRC Press. Boca Raton, FL. 2009.

- [7] S.J. Ball and S.E. Fisher. Next generation nuclear plant phenomena identification and ranking tables (PIRTs). Technical Report NUREG/CR-6944, Vol. 2: Accident and Thermal Fluids Analysis, U.S. Nuclear Regulatory Commission, March 2008.

- [8] N. Zuber. Appendix D: hierarchical, two-tiered scaling analysis. Technical Report, NUREG/CR-5809, 1991.

- [9] S. Basu. Status of the NRC HTGR R&D activities. In *Proceedings from the Cooperative Severe Accident Research Program*, Bethesda, MD, September 2009. US Nuclear Regulatory Commission, Rockville, MD.

- [10] MELCOR Workshop Presentation. In *Proceedings from the MELCOR Workshop, Bethesda, MD, September 2009*. U.S. Nuclear Regulatory Commission, Rockville, MD.
- [11] MELCOR computer code manuals vol. 1: Primer and users' guide, version 1.8.6. Technical Report NUREG/CR-6119, Sandia National Laboratories.
- [12] MELCOR computer code manuals vol. 2: Reference manual. Technical Report NUREG/CR-6119, Sandia National Laboratories, September 2008.
- [13] R.B. Jackson. "HTTF Properties". January 2011. Personal Communication.
- [14] Graphite design handbook. Technical Report, DOE-HTGR-88111, General Atomics, August 1991.
- [15] M. Young, "MELCOR equations". September 2012. Personal Communication.

APPENDIX A: MHTGR INPUT/CALCULATION NOTEBOOK

Appendix A contains a package-by-package breakdown of MHTGR MELCOR input. Tables outlining all input cards, words, and values are included. A brief explanation of each card is also included where appropriate. Hand calculations based on the system design description (the MHTGR PSID document) were used to compute many of the required input parameters. The input below is a representative example for the MHTGR and represents one of several input deck iterations.

Table A.1
Environmental variables input for MHTGR model

<i>CARD</i>	<i>WORD</i>	<i>VALUE</i>	<i>BASIS</i>
MEG_DIAGFILE	-	'mhtgrg.dia'	Name of MELGEN diagnostic file
MEL_DIAGFILE	-	'mhtgr.dia'	Name of MELCOR diagnostic file
MEG_OUTPUTFILE	-	'mhtgrg.out'	Name of MELGEN output file
MEL_OUTPUTFILE	-	'mhtgr.out'	Name of MELCOR output file
PLOTFILE	-	'mhtgr.ptf'	Name of plot file
MEG_RESTARTFILE	-	'mhtgr.rst'	Name of MELGEN restart file
MEL_RESTARTFILE	-	mhtgr.rst'	Name of MELCOR restart file
	CYCLE	NCYCLE	Restart based on cycle number
	NREST	-1	Use last available restart dump
MESSAGEFILE	-	'mhtgr.mes'	Name of message file
STATUSFILE	-	'MELSTT_v2-0'	Name of status file
STOPFILE	-	'MELSTP_v2-0'	Name of stop file
WRITENEWINP	-	'mhtgr.txt'	Name of re-written input file

Table A.2
EXEC MELGEN input for MHTGR model

<i>CARD</i>	<i>WORD</i>	<i>VALUE</i>	<i>BASIS</i>
EXEC_INPUT	-	-	Signal start of EXEC input
EXEC_TITLE	TITLE	'MHTGR'	Title of the calculation
EXEC_JOBID	JOBID	'mhtgr -'	Job identifier
EXEC_TSTART	TSTART	-1000	Time at which to start calculation
EXEC_SS		-1000	Accelerated steady state run at -1000 seconds
		0	Run the accelerated steady state case until time 0
		0.01	Take 0.01 s timesteps from -1000 s to 0 s

Table A.3
NCG input for MHTGR model

<i>CARD</i>	<i>WORD</i>	<i>VALUE</i>	<i>BASIS</i>
NCG_INPUT	-	-	Signal start of NCG input
NCG_ID	MNAME	'HE'	Activate helium
NCG_ID	MNAME	'H2'	Activate hydrogen
NCG_ID	MNAME	'CO'	Activate carbon monoxide
NCG_ID	MNAME	'O2'	Activate oxygen
NCG_ID	MNAME	'CO2'	Activate carbon dioxide
NCG_ID	MNAME	'CH4'	Activate CH4
NCG_ID	MNAME	'N2'	Activate nitrogen

Table A.4
CVH input for MHTGR model

CARD	WORD	VALUE	BASIS
CVH_INPUT	-	-	Signal start of CVH input
CV_ID	CVNAME	Table A.4.1	Unique CV name identifier
	ICVNUM		User-defined CV number
CV_THR	ICVTHR	NONEQUIL	Thermodynamics switch
	IPFSW	FOG	Fog/no fog switch
	ICVACT	ACTIVE	Active/inactive switch
CV_PAS	ITYPTH	SEPARATE	Type of thermodynamic input
	IPORA	ONLYATM	Pool/atmosphere/both switch
	VAPORSTATE	SUPERHEATED	Thermo. state of CV atmosphere
CV_PTD	PTDID	PVOL	Keyword for CV pressure
	PVOL	6.40E+06	Initial CV pressure
CV_AAD	ATMID	TATM	Keyword for CV atm. temperature
	TATM	763.15	Initial atmosphere temperature
CV_NCG	NMMAT		Number of NCG materials
	NCGID		Keyword Identifier, RHUM for all
	VALUE	Table A.4.1	Value from key, 0.0 = RHUM for all
	NUM		Table row index
	NAMGAS		NCG MELCOR name
	MLFR		Mole fraction of NCG in CV
CV_VAT	ICVVZP		Number of volume/altitude data pairs
	NCVZ	Table A.4.2	Table row index
	CVZ		Altitude of current data pair
	CVVOL		Volume of current data pair

Table A.4.1
CV_NCG for MHTGR model

CV_ID		CV_NCG					
CVNAME	ICVNUM	NMMAT	NCGID	VALUE	NUM	NAMGAS	MLFR
DUMMY_IA1	100	1	RHUM	0.0	1	HE	1.0
LH_CV	101	1	RHUM	0.0	1	HE	1.0
LP_1_2	102	1	RHUM	0.0	1	HE	1.0
LP_1_3	103	1	RHUM	0.0	1	HE	1.0
POST_FDB_1	104	1	RHUM	0.0	1	HE	1.0
LR_1	105	1	RHUM	0.0	1	HE	1.0
CORE_1_1	106	1	RHUM	0.0	1	HE	1.0
CORE_1_2	107	1	RHUM	0.0	1	HE	1.0
CORE_1_3	108	1	RHUM	0.0	1	HE	1.0
UR_1	109	1	RHUM	0.0	1	HE	1.0
LP_2_2	202	1	RHUM	0.0	1	HE	1.0
LP_2_3	203	1	RHUM	0.0	1	HE	1.0
POST_FDB_2	204	1	RHUM	0.0	1	HE	1.0
LR_2	205	1	RHUM	0.0	1	HE	1.0
CORE_2_1	206	1	RHUM	0.0	1	HE	1.0
CORE_2_2	207	1	RHUM	0.0	1	HE	1.0
CORE_2_3	208	1	RHUM	0.0	1	HE	1.0
UR_2	209	1	RHUM	0.0	1	HE	1.0
LP_3_2	302	1	RHUM	0.0	1	HE	1.0
LP_3_3	303	1	RHUM	0.0	1	HE	1.0
POST_FDB_3	304	1	RHUM	0.0	1	HE	1.0
LR_3	305	1	RHUM	0.0	1	HE	1.0
CORE_3_1	306	1	RHUM	0.0	1	HE	1.0
CORE_3_2	307	1	RHUM	0.0	1	HE	1.0
CORE_3_3	308	1	RHUM	0.0	1	HE	1.0
UR_3	309	1	RHUM	0.0	1	HE	1.0
LP_4_2	402	1	RHUM	0.0	1	HE	1.0
LP_4_3	403	1	RHUM	0.0	1	HE	1.0
POST_FDB_4	404	1	RHUM	0.0	1	HE	1.0
LR_4	405	1	RHUM	0.0	1	HE	1.0
CORE_4_1	406	1	RHUM	0.0	1	HE	1.0
CORE_4_2	407	1	RHUM	0.0	1	HE	1.0
CORE_4_3	408	1	RHUM	0.0	1	HE	1.0
UR_4	409	1	RHUM	0.0	1	HE	1.0
LP_5_2	502	1	RHUM	0.0	1	HE	1.0

LP_5_3	503	1	RHUM	0.0	1	HE	1.0
POST_FDB_5	504	1	RHUM	0.0	1	HE	1.0
LR_5	505	1	RHUM	0.0	1	HE	1.0
CORE_5_1	506	1	RHUM	0.0	1	HE	1.0
CORE_5_2	507	1	RHUM	0.0	1	HE	1.0
CORE_5_3	508	1	RHUM	0.0	1	HE	1.0
UR_5	509	1	RHUM	0.0	1	HE	1.0
LP_6_2	602	1	RHUM	0.0	1	HE	1.0
LP_6_3	603	1	RHUM	0.0	1	HE	1.0
POST_FDB_6	604	1	RHUM	0.0	1	HE	1.0
LR_6	605	1	RHUM	0.0	1	HE	1.0
CORE_6_1	606	1	RHUM	0.0	1	HE	1.0
CORE_6_2	607	1	RHUM	0.0	1	HE	1.0
CORE_6_3	608	1	RHUM	0.0	1	HE	1.0
UR_6	609	1	RHUM	0.0	1	HE	1.0
LP_7_2	702	1	RHUM	0.0	1	HE	1.0
LP_7_3	703	1	RHUM	0.0	1	HE	1.0
POST_FDB_7	704	1	RHUM	0.0	1	HE	1.0
LR_7	705	1	RHUM	0.0	1	HE	1.0
CORE_7_1	706	1	RHUM	0.0	1	HE	1.0
CORE_7_2	707	1	RHUM	0.0	1	HE	1.0
CORE_7_3	708	1	RHUM	0.0	1	HE	1.0
UR_7	709	1	RHUM	0.0	1	HE	1.0
UPPER_PLENUM	800	1	RHUM	0.0	1	HE	1.0
LOWER_DUCT	801	1	RHUM	0.0	1	HE	1.0
UPPER_DUCT	802	1	RHUM	0.0	1	HE	1.0
SINK	803	1	RHUM	0.0	1	HE	1.0
SOURCE	804	1	RHUM	0.0	1	HE	1.0
CAVITY_1	901	2	RHUM	0.0	2		
CAVITY_2	902	2	RHUM	0.0	2		
CAVITY_3	903	2	RHUM	0.0	2	N2	0.8
CAVITY_4	904	2	RHUM	0.0	2	O2	0.2
CAVITY_5	905	2	RHUM	0.0	2		
CAVITY_6	906	2	RHUM	0.0	2		

Table A.4.2
CV_VAT for MHTGR model

CV_ID		CV_VAT				
CVNAME	ICVNUM	ICVVZP	NCVZ	CVZ	CVVOL	BASIS
DUMMY_IA1	100	2	1	-6.28250	0.0	Bottom of Z1
			2	-2.88250	3.0395E+01	Top of Z1, nominal
LH_CV	101	2	1	-6.28250	0.0	Dummy for COR
			2	-2.88250	1.0000E+01	
LP_1_2	102	2	1	-2.88250	0.0	Bottom of Z2
			2	-2.43250	-3.5343E-01	IR 1, IA 2
LP_1_3	103	2	1	-2.43250	0.0	Bottom of Z3
			2	-1.98250	-3.5343E-01	IR 1, IA 3
POST_FDB_1	104	3	1	-1.98250	0.0	Bottom of Z4
			2	-1.38775	-1.4833E-04	IR 1, IA 4
			3	-0.99125	-9.8890E-05	IR 1, IA 5
LR_1	105	4	1	-0.99125	0.0	Bottom of Z6
			2	-0.59475	-9.8890E-05	IR 1, IA 6
			3	-0.01000	-1.4584E-04	IR 1, IA 7
			4	0.00000	-2.4940E-06	IR 1, IA 8
CORE_1_1	106	3	1	0.00000	0.0	Bottom of Z9
			2	0.79300	-1.9780E-04	IR 1, IA 9
			3	1.58600	-1.9780E-04	IR 1, IA 10
CORE_1_2	107	4	1	1.58600	0.0	Bottom of Z11
			2	2.37900	-1.9780E-04	IR 1, IA 11
			3	3.17200	-1.9780E-04	IR 1, IA 12
			4	3.96500	-1.9780E-04	IR 1, IA 13
CORE_1_3	108	6	1	3.96500	0.0	Bottom of Z14
			2	4.75800	1.9800E-04	IR 1, IA 14
			3	5.55100	1.9800E-04	IR 1, IA 15
			4	6.34400	1.9800E-04	IR 1, IA 16
			5	7.13700	1.9800E-04	IR 1, IA 17
			6	7.93000	1.9800E-04	IR 1, IA 18
UR_1	109	4	1	7.93000	0.0	Bottom of Z19
			2	7.94000	-2.4940E-06	IR 1, IA 19
			3	8.32650	-9.6393E-05	IR 1, IA 20
			4	9.11950	-1.9780E-04	IR 1, IA 21
LP_2_2	202	2	1	-2.88250	0.0	Bottom of Z2
			2	-2.43250	-6.0590E-01	IR 2, IA 2
LP_2_3	203	2	1	-2.43250	0.0	Bottom of Z3

POST_FDB_2	204	3	2	-1.98250	-6.0590E-01	IR 2, IA 3
			1	-1.98250	0.0	Bottom of Z4
			2	-1.38775	-3.7080E-04	IR 2, IA 4
LR_2	205	4	3	-0.99125	-2.4720E-04	IR 2, IA 5
			1	-0.99125	0.0	Bottom of Z6
			2	-0.59475	-2.4720E-04	IR 2, IA 6
CORE_2_1	206	3	3	-0.01000	-3.6453E-04	IR 2, IA 7
			4	0.00000	-6.2340E-06	IR 2, IA 8
			1	0.00000	0.0	Bottom of Z9
CORE_2_2	207	4	2	0.79300	-4.9440E-04	IR 2, IA 9
			3	1.58600	-4.9440E-04	IR 2, IA 10
			1	1.58600	0.0	Bottom of Z11
CORE_2_3	208	6	2	2.37900	-4.9440E-04	IR 2, IA 11
			3	3.17200	-4.9440E-04	IR 2, IA 12
			4	3.96500	-4.9440E-04	IR 2, IA 13
UR_2	209	4	1	3.96500	0.0	Bottom of Z14
			2	4.75800	-4.9440E-04	IR 2, IA 14
			3	5.55100	-4.9440E-04	IR 2, IA 15
LP_3_2	302	2	4	6.34400	-4.9440E-04	IR 2, IA 16
			5	7.13700	-4.9440E-04	IR 2, IA 17
			6	7.93000	-4.9440E-04	IR 2, IA 18
LP_3_3	303	2	1	7.93000	0.0	Bottom of Z19
			2	7.94000	-6.2300E-06	IR 2, IA 19
			3	8.32650	-2.4094E-04	IR 2, IA 20
POST_FDB_3	304	3	4	9.11950	-4.9440E-04	IR 2, IA 21
			1	-2.88250	0.0	Bottom of Z2
			2	-2.43250	-9.0882E-01	IR 3, IA 2
LR_3	305	4	1	-2.43250	0.0	Bottom of Z3
			2	-1.98250	-9.0882E-01	IR 3, IA 3
			1	-1.98250	0.0	Bottom of Z4
CORE_3_1	306	3	2	-1.38775	-1.5553E-01	IR 3, IA 4
			3	-0.99125	-1.0370E-01	IR 3, IA 5
			1	-0.99125	0.0	Bottom of Z6
			2	-0.59475	-1.3743E-01	IR 3, IA 6
			3	-0.01000	-2.0267E-01	IR 3, IA 7
			4	0.00000	-3.4660E-03	IR 3, IA 8
			1	0.00000	0.0	Bottom of Z9
			2	0.79300	-2.7490E-01	IR 3, IA 9
			3	1.58600	-2.7490E-01	IR 3, IA 10

CORE_3_2	307	4	1	1.58600	0.0	Bottom of Z11
			2	2.37900	-2.7490E-01	IR 3, IA 11
			3	3.17200	-2.7490E-01	IR 3, IA 12
			4	3.96500	-2.7490E-01	IR 3, IA 13
CORE_3_3	308	6	1	3.96500	0.0	Bottom of Z14
			2	4.75800	-2.7490E-01	IR 3, IA 14
			3	5.55100	-2.7490E-01	IR 3, IA 15
			4	6.34400	-2.7490E-01	IR 3, IA 16
			5	7.13700	-2.7490E-01	IR 3, IA 17
			6	7.93000	-2.7490E-01	IR 3, IA 18
UR_3	309	4	1	7.93000	0.0	Bottom of Z19
			2	7.94000	-3.4660E-03	IR 3, IA 19
			3	8.32650	-1.3396E-01	IR 3, IA 20
			4	9.11950	-2.7485E-01	IR 3, IA 21
LP_4_2	402	2	1	-2.88250	0.0	Bottom of Z2
			2	-2.43250	-1.2118E+00	IR 4, IA 2
LP_4_3	403	2	1	-2.43250	0.0	Bottom of Z3
			2	-1.98250	-1.2118E+00	IR 4, IA 3
POST_FDB_4	404	3	1	-1.98250	0.0	Bottom of Z4
			2	-1.38775	-3.1099E-01	IR 4, IA 4
			3	-0.99125	-2.0733E-01	IR 4, IA 5
LR_4	405	4	1	-0.99125	0.0	Bottom of Z6
			2	-0.59475	-1.9995E-01	IR 4, IA 6
			3	-0.01000	-2.4940E-01	IR 4, IA 7
			4	0.00000	5.0430E-03	IR 4, IA 8
CORE_4_1	406	3	1	0.00000	0.0	Bottom of Z9
			2	0.79300	-3.9991E-01	IR 4, IA 9
			3	1.58600	-3.9991E-01	IR 4, IA 10
CORE_4_2	407	4	1	1.58600	0.0	Bottom of Z11
			2	2.37900	-3.9991E-01	IR 4, IA 11
			3	3.17200	-3.9991E-01	IR 4, IA 12
			4	3.96500	-3.9991E-01	IR 4, IA 13
CORE_4_3	408	6	1	3.96500	0.0	Bottom of Z14
			2	4.75800	-3.9991E-01	IR 4, IA 14
			3	5.55100	-3.9991E-01	IR 4, IA 15
			4	6.34400	-3.9991E-01	IR 4, IA 16
			5	7.13700	-3.9991E-01	IR 4, IA 17
			6	7.93000	-3.9991E-01	IR 4, IA 18
UR_4	409	4	1	7.93000	0.0	Bottom of Z19

			2	7.94000	-5.0430E-03	IR 4, IA 19
			3	8.32650	-1.9491E-01	IR 4, IA 20
			4	9.11950	-3.9991E-01	IR 4, IA 21
LP_5_2	502	2	1	-2.88250	0.0	Bottom of Z2
			2	-2.43250	-1.5147E+00	IR 5, IA 2
LP_5_3	503	2	1	-2.43250	0.0	Bottom of Z3
			2	-1.98250	-1.5147E+00	IR 5, IA 3
POST_FDB_5	504	3	1	-1.98250	0.0	Bottom of Z4
			2	-1.38775	-3.1099E-01	IR 5, IA 4
			3	-0.99125	-2.0733E-01	IR 5, IA 5
LR_5	505	4	1	-0.99125	0.0	Bottom of Z6
			2	-0.59475	-1.9995E-01	IR 5, IA 6
			3	-0.01000	-2.9490E-01	IR 5, IA 7
			4	0.00000	-5.0430E-03	IR 5, IA 8
CORE_5_1	506	3	1	0.00000	0.0	Bottom of Z9
			2	0.79300	-3.9991E-01	IR 5, IA 9
			3	1.58600	-3.9991E-01	IR 5, IA 10
CORE_5_2	507	4	1	1.58600	0.0	Bottom of Z11
			2	2.37900	-3.9991E-01	IR 5, IA 11
			3	3.17200	-3.9991E-01	IR 5, IA 12
			4	3.96500	-3.9991E-01	IR 5, IA 13
CORE_5_3	508	6	1	3.96500	0.0	Bottom of Z14
			2	4.75800	-3.9991E-01	IR 5, IA 14
			3	5.55100	-3.9991E-01	IR 5, IA 15
			4	6.34400	-3.9991E-01	IR 5, IA 16
			5	7.13700	-3.9991E-01	IR 5, IA 17
			6	7.93000	-3.9991E-01	IR 5, IA 18
UR_5	509	4	1	7.93000	0.0	Bottom of Z19
			2	7.94000	-5.0430E-03	IR 5, IA 19
			3	8.32650	-1.9491E-01	IR 5, IA 20
			4	9.11950	-3.9991E-01	IR 5, IA 21
LP_6_2	602	2	1	-2.88250	0.0	Bottom of Z2
			2	-2.43250	-1.8176E+00	IR 6, IA 2
LP_6_3	603	2	1	-2.43250	0.0	Bottom of Z3
			2	-1.98250	-1.8176E+00	IR 6, IA 3
POST_FDB_6	604	3	1	-1.98250	0.0	Bottom of Z4
			2	-1.38775	-1.4213E-03	IR 6, IA 4
			3	-0.99125	-9.4752E-04	IR 6, IA 5
LR_6	605	4	1	-0.99125	0.0	Bottom of Z6

			2	-0.59475	-9.4752E-04	IR 6, IA 6
			3	-0.01000	-1.3974E-03	IR 6, IA 7
			4	0.00000	-2.3897E-05	IR 6, IA 8
CORE_6_1	606	3	1	0.00000	0.0	Bottom of Z9
			2	0.79300	-1.8950E-03	IR 6, IA 9
			3	1.58600	-1.8950E-03	IR 6, IA 10
CORE_6_2	607	4	1	1.58600	0.0	Bottom of Z11
			2	2.37900	-1.8950E-03	IR 6, IA 11
			3	3.17200	-1.8950E-03	IR 6, IA 12
			4	3.96500	-1.8950E-03	IR 6, IA 13
CORE_6_3	608	6	1	3.96500	0.0	Bottom of Z14
			2	4.75800	-1.8950E-03	IR 6, IA 14
			3	5.55100	-1.8950E-03	IR 6, IA 15
			4	6.34400	-1.8950E-03	IR 6, IA 16
			5	7.13700	-1.8950E-03	IR 6, IA 17
			6	7.93000	-1.8950E-03	IR 6, IA 18
UR_6	609	4	1	7.93000	0.0	Bottom of Z19
			2	7.94000	-2.3897E-05	IR 6, IA 19
			3	8.32650	-9.2362E-04	IR 6, IA 20
			4	9.11950	-1.8950E-03	IR 6, IA 21
LP_7_2	702	2	1	-2.88250	0.0	Bottom of Z2
			2	-2.43250	-1.8176E+00	IR 7, IA 2
LP_7_3	703	2	1	-2.43250	0.0	Bottom of Z3
			2	-1.98250	-1.8176E+00	IR 7, IA 3
POST_FDB_7	704	3	1	-1.98250	0.0	Bottom of Z4
			2	-1.38775	-1.4090E-03	IR 7, IA 4
			3	-0.99125	-9.3930E-04	IR 7, IA 5
LR_7	705	4	1	-0.99125	0.0	Bottom of Z6
			2	-0.59475	-9.3930E-04	IR 7, IA 6
			3	-0.01000	-1.3852E-03	IR 7, IA 7
			4	0.00000	-2.3690E-05	IR 7, IA 8
CORE_7_1	706	3	1	0.00000	0.0	Bottom of Z9
			2	0.79300	-1.8790E-03	IR 7, IA 9
			3	1.58600	-1.8790E-03	IR 7, IA 10
CORE_7_2	707	4	1	1.58600	0.0	Bottom of Z11
			2	2.37900	-1.8790E-03	IR 7, IA 11
			3	3.17200	-1.8790E-03	IR 7, IA 12
			4	3.96500	-1.8790E-03	IR 7, IA 13
CORE_7_3	708	6	1	3.96500	0.0	Bottom of Z14

			2	4.75800	-1.8790E-03	IR 7, IA 14
			3	5.55100	-1.8790E-03	IR 7, IA 15
			4	6.34400	-1.8790E-03	IR 7, IA 16
			5	7.13700	-1.8790E-03	IR 7, IA 17
			6	7.93000	-1.8790E-03	IR 7, IA 18
UR_7	709	4	1	7.93000	0.0	Bottom of Z19
			2	7.94000	-2.3689E-05	IR 7, IA 19
			3	8.32650	-9.1560E-04	IR 7, IA 20
			4	9.11950	-1.8790E-03	IR 7, IA 21
UPPER_PLENUM	800	2	1	9.11950	0.0000E+00	Top of UR
			2	12.15630	2.9419E+01	Half volume of sphere with RCOR
LOWER_DUCT	801	2	1	-2.88250	0.0000E+00	
			2	-2.28750	1.5350E+00	Half of horizontal cylinder hot duct
UPPER_DUCT	802	2	1	-2.28750	0.0000E+00	
			2	-1.69250	1.5350E+00	Half of horizontal cylinder hot duct
UPCOMER	805	2	1	-1.98250	0.0000E+00	
			2	11.53200	1.6269E+01	12 ducts, 6" by 26" = 0.152 m by 0.66 m
CAVITY_1	901	2	1	-1.98250	0.0000E+00	
			2	-0.99125	2.4290E+01	1 m thick cavity
CAVITY_2	902	2	1	-0.99125	0.0000E+00	
			2	0.00000	2.4290E+01	1 m thick cavity
CAVITY_3	903	2	1	0.00000	0.0000E+00	
			2	1.58600	3.8860E+01	1 m thick cavity
CAVITY_4	904	2	1	1.58600	0.0000E+00	
			2	3.96500	5.8290E+01	1 m thick cavity
CAVITY_5	905	2	1	3.96500	0.0000E+00	
			2	7.93000	9.7160E+01	1 m thick cavity
CAVITY_6	906	2	1	7.93000	0.0000E+00	
			2	9.11950	2.9150E+01	1 m thick cavity

Table A.5
FL input for MHTGR model

<i>CARD</i>	<i>WORD</i>	<i>VALUE</i>	<i>BASIS</i>
FL_INPUT	-	-	Signal start of FL input
FL_ID	FPNAME		FL name
	IFPNUM		User-defined FL number
FL_FT	KCVFM	Table A.5.1	Name of "from" control volume
	KCVTO		Name of "to" control volume
	ZFM		Altitude of "from" junction
	ZTO		Altitude of "to" junction
FL_GEO	FLARA		Flow path area
	FLEN		Flow path length
	FLOPO		Flow path open fraction
	FLHGTF		Junction opening height, "from"
	FLHGTT		Junction opening height, "to"
FL_JSW	KFLGFL	Table A.5.2	Flow path orientation (0 = vertical, 3 = horizontal)
FL_SEG	IPNSG		Number of segments
	NSEG		Table row index
	SAREA		Segment flow area
	SLEN		Segment flow length
	SHYD		Segment hydraulic diameter
FL_VTM	NVOFT	1	Number of time-dependent flow paths
	NFLT	1	Table row index
	FLNAME	SRC_to_UPCOMER	Name of time-dependent flow path
	NTFLAG	CF	Flag for CF or TF defining velocity vs. time
	NFUN	VELOCITY	Name of CF or TF

Table A.5.1
FL_FT for MHTGR model

FL_ID		FL_FT			
FPNAME	IFPNUM	KCVFM	KCVTO	ZFM	ZTO
UR_1_to_CORE_1_3	101	UR_1	CORE_1_3	7.930	7.930
CORE_1_3_to_1_2	102	CORE_1_3	CORE_1_2	3.965	3.965
CORE_1_2_to_1_1	103	CORE_1_2	CORE_1_1	1.586	1.586
CORE_1_1_to_LR_1	104	CORE_1_1	LR_1	0.000	0.000
LR_1_to_POST_FDB_1	105	LR_1	POST_FDB_1	-0.991	-0.991
UR_2_to_CORE_2_3	201	UR_2	CORE_2_3	7.930	7.930
CORE_2_3_to_2_2	202	CORE_2_3	CORE_2_2	3.965	3.965
CORE_2_2_to_2_1	203	CORE_2_2	CORE_2_1	1.586	1.586
CORE_2_1_to_LR_2	204	CORE_2_1	LR_2	0.000	0.000
LR_2_to_POST_FDB_2	205	LR_2	POST_FDB_2	-0.991	-0.991
UR_3_to_CORE_3_3	301	UR_3	CORE_3_3	7.930	7.930
CORE_3_3_to_3_2	302	CORE_3_3	CORE_3_2	3.965	3.965
CORE_3_2_to_3_1	303	CORE_3_2	CORE_3_1	1.586	1.586
CORE_3_1_to_LR_3	304	CORE_3_1	LR_3	0.000	0.000
LR_3_to_POST_FDB_3	305	LR_3	POST_FDB_3	-0.991	-0.991
UR_4_to_CORE_4_3	401	UR_4	CORE_4_3	7.930	7.930
CORE_4_3_to_4_2	402	CORE_4_3	CORE_4_2	3.965	3.965
CORE_4_2_to_4_1	403	CORE_4_2	CORE_4_1	1.586	1.586
CORE_4_1_to_LR_4	404	CORE_4_1	LR_4	0.000	0.000
LR_4_to_POST_FDB_4	405	LR_4	POST_FDB_4	-0.991	-0.991
UR_5_to_CORE_5_3	501	UR_5	CORE_5_3	7.930	7.930
CORE_5_3_to_5_2	502	CORE_5_3	CORE_5_2	3.965	3.965
CORE_5_2_to_5_1	503	CORE_5_2	CORE_5_1	1.586	1.586
CORE_5_1_to_LR_5	504	CORE_5_1	LR_5	0.000	0.000
LR_5_to_POST_FDB_5	505	LR_5	POST_FDB_5	-0.991	-0.991
UR_6_to_CORE_6_3	601	UR_6	CORE_6_3	7.930	7.930
CORE_6_3_to_6_2	602	CORE_6_3	CORE_6_2	3.965	3.965
CORE_6_2_to_6_1	603	CORE_6_2	CORE_6_1	1.586	1.586
CORE_6_1_to_LR_6	604	CORE_6_1	LR_6	0.000	0.000
LR_6_to_POST_FDB_6	605	LR_6	POST_FDB_6	-0.991	-0.991
UR_7_to_CORE_7_3	701	UR_7	CORE_7_3	7.930	7.930
CORE_7_3_to_7_2	702	CORE_7_3	CORE_7_2	3.965	3.965
CORE_7_2_to_7_1	703	CORE_7_2	CORE_7_1	1.586	1.586
CORE_7_1_to_LR_7	704	CORE_7_1	LR_7	0.000	0.000
LR_7_to_POST_FDB_7	705	LR_7	POST_FDB_7	-0.991	-0.991
POST_FDB_1_to_LP_1_3	106	POST_FDB_1	LP_1_3	-1.983	-1.983
LP_1_3_to_LP_1_2	107	LP_1_3	LP_1_2	-2.433	-2.433

POST_FDB_2_to_LP_2_3	206	POST_FDB_2	LP_2_3	-1.983	-1.983
LP_2_3_to_LP_2_2	207	LP_2_3	LP_2_2	-2.433	-2.433
POST_FDB_3_to_LP_3_3	306	POST_FDB_3	LP_3_3	-1.983	-1.983
LP_3_3_to_LP_3_2	307	LP_3_3	LP_3_2	-2.433	-2.433
POST_FDB_4_to_LP_4_3	406	POST_FDB_4	LP_4_3	-1.983	-1.983
LP_4_3_to_LP_4_2	407	LP_4_3	LP_4_2	-2.433	-2.433
POST_FDB_5_to_LP_5_3	506	POST_FDB_5	LP_5_3	-1.983	-1.983
LP_5_3_to_LP_5_2	507	LP_5_3	LP_5_2	-2.433	-2.433
POST_FDB_6_to_LP_6_3	606	POST_FDB_6	LP_6_3	-1.983	-1.983
LP_6_3_to_LP_6_2	607	LP_6_3	LP_6_2	-2.433	-2.433
POST_FDB_7_to_LP_7_3	706	POST_FDB_7	LP_7_3	-1.983	-1.983
LP_7_3_to_LP_7_2	707	LP_7_3	LP_7_2	-2.433	-2.433
LP_1_3_to_2_3	1001	LP_1_3	LP_2_3	-2.208	-2.208
LP_1_2_to_2_2	1002	LP_1_2	LP_2_2	-2.433	-2.433
LP_2_3_to_3_3	2001	LP_2_3	LP_3_3	-2.208	-2.208
LP_2_2_to_3_2	2002	LP_2_2	LP_3_2	-2.433	-2.433
LP_3_3_to_4_3	3001	LP_3_3	LP_4_3	-2.208	-2.208
LP_3_2_to_4_2	3002	LP_3_2	LP_4_2	-2.433	-2.433
LP_4_3_to_5_3	4001	LP_4_3	LP_5_3	-2.208	-2.208
LP_4_2_to_5_2	4002	LP_4_2	LP_5_2	-2.433	-2.433
LP_5_3_to_6_3	5001	LP_5_3	LP_6_3	-2.208	-2.208
LP_5_2_to_6_2	5002	LP_5_2	LP_6_2	-2.433	-2.433
LP_6_3_to_7_3	6001	LP_6_3	LP_7_3	-2.208	-2.208
LP_6_2_to_7_2	6002	LP_6_2	LP_7_2	-2.433	-2.433
to_up_duct	801	LP_7_3	UPPER_DUCT	-2.208	-2.208
to_lwr_duct	802	LP_7_2	LOWER_DUCT	-2.433	-2.433
up_duct_to_snk	803	UPPER_DUCT	SINK	-2.208	-2.208
lwr_duct_to_snk	804	LOWER_DUCT	SINK	-2.433	-2.433
UP_to_R1	111	UPPER_PLENUM	UR_1	9.120	9.120
UP_to_R2	112	UPPER_PLENUM	UR_2	9.120	9.120
UP_to_R3	113	UPPER_PLENUM	UR_3	9.120	9.120
UP_to_R4	114	UPPER_PLENUM	UR_4	9.120	9.120
UP_to_R5	115	UPPER_PLENUM	UR_5	9.120	9.120
UP_to_R6	116	UPPER_PLENUM	UR_6	9.120	9.120
UP_to_R7	117	UPPER_PLENUM	UR_7	9.120	9.120
SRC_to_UPCOMER	120	SOURCE	UPCOMER	0.000	0.000
UPCOMER_to_UP	121	UPCOMER	UPPER_PLENUM	10.32	10.32

Table A.5.2
FL geometric parameters for MHTGR model

FPNAME	FLARA	FLLEN	FLOPO	KFLGFL	SAREA	SLEN	SHYD
UR_1_to_CORE_1_3	2.4940E-04	2.577	1.0	0	2.4940E-04	2.577	1.9900E-05
CORE_1_3_to_1_2	2.4940E-04	3.172	1.0	0	2.4940E-04	3.172	1.9900E-05
CORE_1_2_to_1_1	2.4940E-04	1.983	1.0	0	2.4940E-04	1.983	1.9900E-05
CORE_1_1_to_LR_1	2.4940E-04	1.289	1.0	0	2.4940E-04	1.289	1.9900E-05
LR_1_to_POST_FDB_1	2.4940E-04	0.991	1.0	0	2.4940E-04	0.991	1.9900E-05
UR_2_to_CORE_2_3	6.2340E-04	2.577	1.0	0	6.2340E-04	2.577	1.9900E-05
CORE_2_3_to_2_2	6.2340E-04	3.172	1.0	0	6.2340E-04	3.172	1.9900E-05
CORE_2_2_to_2_1	6.2340E-04	1.983	1.0	0	6.2340E-04	1.983	1.9900E-05
CORE_2_1_to_LR_2	6.2340E-04	1.289	1.0	0	6.2340E-04	1.289	1.9900E-05
LR_2_to_POST_FDB_2	6.2340E-04	0.991	1.0	0	6.2340E-04	0.991	1.9900E-05
UR_3_to_CORE_3_3	3.4660E-01	2.577	1.0	0	3.4660E-01	2.577	1.5900E-02
CORE_3_3_to_3_2	3.4660E-01	3.172	1.0	0	3.4660E-01	3.172	1.5900E-02
CORE_3_2_to_3_1	3.4660E-01	1.983	1.0	0	3.4660E-01	1.983	1.5900E-02
CORE_3_1_to_LR_3	3.4660E-01	1.289	1.0	0	3.4660E-01	1.289	1.5900E-02
LR_3_to_POST_FDB_3	2.6150E-01	0.992	1.0	0	3.4660E-01	0.496	1.5900E-02
UR_4_to_CORE_4_3	5.0430E-01	2.577	1.0	0	5.0430E-01	2.577	1.5900E-02
CORE_4_3_to_4_2	5.0430E-01	3.172	1.0	0	5.0430E-01	3.172	1.5900E-02
CORE_4_2_to_4_1	5.0430E-01	1.983	1.0	0	5.0430E-01	1.983	1.5900E-02
CORE_4_1_to_LR_4	5.0430E-01	1.289	1.0	0	5.0430E-01	1.289	1.5900E-02
LR_4_to_POST_FDB_4	5.0430E-01	0.992	1.0	0	5.0430E-01	0.496	1.5900E-02
UR_5_to_CORE_5_3	5.0430E-01	2.577	1.0	0	5.0430E-01	2.577	1.5900E-02
CORE_5_3_to_5_2	5.0430E-01	3.172	1.0	0	5.0430E-01	3.172	1.5900E-02
CORE_5_2_to_5_1	5.0430E-01	1.983	1.0	0	5.0430E-01	1.983	1.5900E-02
CORE_5_1_to_LR_5	5.0430E-01	1.289	1.0	0	5.0430E-01	1.289	1.5900E-02
LR_5_to_POST_FDB_5	5.0430E-01	0.992	1.0	0	5.0430E-01	0.496	1.5900E-02
UR_6_to_CORE_6_3	2.3897E-03	2.577	1.0	0	2.3897E-03	2.577	1.9900E-05
CORE_6_3_to_6_2	2.3897E-03	3.172	1.0	0	2.3897E-03	3.172	1.9900E-05
CORE_6_2_to_6_1	2.3897E-03	1.983	1.0	0	2.3897E-03	1.983	1.9900E-05
CORE_6_1_to_LR_6	2.3897E-03	1.289	1.0	0	2.3897E-03	1.289	1.9900E-05
LR_6_to_POST_FDB_6	2.3897E-03	0.992	1.0	0	2.3897E-03	0.992	1.9900E-05
UR_7_to_CORE_7_3	2.3689E-03	2.577	1.0	0	2.3689E-03	2.577	1.9900E-05
CORE_7_3_to_7_2	2.3689E-03	3.172	1.0	0	2.3689E-03	3.172	1.9900E-05
CORE_7_2_to_7_1	2.3689E-03	1.983	1.0	0	2.3689E-03	1.983	1.9900E-05
CORE_7_1_to_LR_7	2.3689E-03	1.289	1.0	0	2.3689E-03	1.289	1.9900E-05
LR_7_to_POST_FDB_7	2.3689E-03	0.992	1.0	0	2.3689E-03	0.992	1.9900E-05
POST_FDB_1_to_LP_1_3	7.8540E-01	0.721	1.0	0	7.8540E-01	0.721	1.0000E+00
LP_1_3_to_LP_1_2	7.8540E-01	0.450	1.0	0	7.8540E-01	0.450	1.0000E+00
POST_FDB_2_to_LP_2_3	1.3464E+00	0.721	1.0	0	1.3464E+00	0.721	1.5280E+00

LP_2_3_to_LP_2_2	1.3464E+00	0.450	1.0	0	1.3464E+00	0.450	1.5280E+00
POST_FDB_3_to_LP_3_3	2.0196E+00	0.721	1.0	0	2.0196E+00	0.721	3.9460E+00
LP_3_3_to_LP_3_2	2.0196E+00	0.450	1.0	0	2.0196E+00	0.450	3.9460E+00
POST_FDB_4_to_LP_4_3	2.6928E+00	0.721	1.0	0	2.6928E+00	0.721	5.2510E+00
LP_4_3_to_LP_4_2	2.6928E+00	0.450	1.0	0	2.6928E+00	0.450	5.2510E+00
POST_FDB_5_to_LP_5_3	3.3660E+00	0.721	1.0	0	3.3660E+00	0.721	6.5570E+00
LP_5_3_to_LP_5_2	3.3660E+00	0.450	1.0	0	3.3660E+00	0.450	6.5570E+00
POST_FDB_6_to_LP_6_3	4.0392E+00	0.721	1.0	0	4.0392E+00	0.721	7.8660E+00
LP_6_3_to_LP_6_2	4.0392E+00	0.450	1.0	0	4.0392E+00	0.450	7.8660E+00
POST_FDB_7_to_LP_7_3	4.0392E+00	0.721	1.0	0	4.0392E+00	0.721	9.0860E+00
LP_7_3_to_LP_7_2	4.0392E+00	0.450	1.0	0	4.0392E+00	0.450	9.0860E+00
LP_1_3_to_2_3	1.4137E+00	0.412	1.0	3	1.4137E+00	0.412	9.0000E-01
LP_1_2_to_2_2	1.4137E+00	0.412	1.0	3	1.4137E+00	0.412	9.0000E-01
LP_2_3_to_3_3	2.3292E+00	0.488	1.0	3	2.3292E+00	0.488	9.0000E-01
LP_2_2_to_3_2	2.3292E+00	0.488	1.0	3	2.3292E+00	0.488	9.0000E-01
LP_3_3_to_4_3	3.2504E+00	0.327	1.0	3	3.2504E+00	0.327	9.0000E-01
LP_3_2_to_4_2	3.2504E+00	0.327	1.0	3	3.2504E+00	0.327	9.0000E-01
LP_4_3_to_5_3	4.1736E+00	0.327	1.0	3	4.1736E+00	0.327	9.0000E-01
LP_4_2_to_5_2	4.1736E+00	0.327	1.0	3	4.1736E+00	0.327	9.0000E-01
LP_5_3_to_6_3	5.0976E+00	1.118	1.0	3	5.0976E+00	1.118	9.0000E-01
LP_5_2_to_6_2	5.0976E+00	1.118	1.0	3	5.0976E+00	1.118	9.0000E-01
LP_6_3_to_7_3	6.0219E+00	0.635	1.0	3	6.0219E+00	0.635	9.0000E-01
LP_6_2_to_7_2	6.0219E+00	0.635	1.0	3	6.0219E+00	0.635	9.0000E-01
to_up_duct	5.5610E-01	2.000	1.0	3	5.5610E-01	2.000	2.9080E+00
to_lwr_duct	5.5610E-01	2.000	1.0	3	5.5610E-01	2.000	2.9080E+00
up_duct_to_snk	5.5610E-01	2.000	1.0	3	5.5610E-01	2.000	2.9080E+00
lwr_duct_to_snk	5.5610E-01	2.000	1.0	3	5.5610E-01	2.000	2.9080E+00
UP_to_R1	2.4940E-04	1.801	1.0	0	2.4940E-04	1.801	1.9900E-05
UP_to_R2	6.2340E-04	1.801	1.0	0	6.2340E-04	1.801	1.9900E-05
UP_to_R3	3.4660E-01	1.801	1.0	0	3.4660E-01	1.801	1.5900E-02
UP_to_R4	5.0430E-01	1.801	1.0	0	5.0430E-01	1.801	1.5900E-02
UP_to_R5	5.0430E-01	1.801	1.0	0	5.0430E-01	1.801	1.5900E-02
UP_to_R6	2.3897E-03	1.801	1.0	0	2.3897E-03	1.801	1.9900E-05
UP_to_R7	2.3689E-03	1.801	1.0	0	2.3689E-03	1.801	1.9900E-05
SRC_to_UPCOMER	1.2040E+00	1.000	1.0	0	1.2040E+00	1.000	2.9660E+00
UPCOMER_to_UP	1.2040E+00	1.000	1.0	3	1.2040E+00	1.000	2.9660E+00

Table A.6
HS input for MHTGR model

<i>CARD</i>	<i>WORD</i>	<i>VALUE</i>	<i>BASIS</i>
HS_INPUT	-	-	Signal start of HS input
HS_ID	HSNAME		HS name
	NUM		User-defined HS number
HS_GD	IGEOM	Table A.6.1	HS geometry
HS_EOD	HSALT		HS bottom elevation
	ALPHA		HS orientation
HS_SRC	ISRC	NO	Internal Power Source Flag
HS_ND	NP		Number of temperature nodes
	N	Table A.6.1	Node index
	XI		Spatial node location
	MATNAM		Material name associated with node N
HS_LB	IBCL	CALCCOEFHS	Boundary condition type
	IBVL	Table A.6.2	Boundary control volume name
	MTEVAL	NO	Switch to evaluate mass transfer at boundary
HS_LBP	IFLOWL	INT	Internal/external flow flag
	CPFPL	0.0	Critical pool fraction
	CPFAL	0.0	Critical pool fraction for atmosphere
HS_LBF	IOPTL		Fluid temperature options for LHS
	NUMAXL	Table A.6.2	Axial level of coupled core cell if necessary
	NUMRAD		Radial ring of coupled core cell if necessary
HS_LBS	ASURFL	1.0	LHS area, calculate internally for cylinders
	CLNL		LHS characteristic length, cylinder height
	BNDZL	Table A.6.2	Heat structure LHS boundary height, cylinder height
HS_LBR	EMISWL	0.8	Surface material emissivity (LHS)
	RMODL	EQUIV-BAND	Radiation model flag (LHS)
	PATHL	0.0508	Radiation path length (LHS)
HS_RB	for RHS , See HS_LB		Same as HS_LB, but for RHS
HS_RBR	for RHS , See HS_LBR	Table A.6.3	Same as HS_LBR, but for RHS
HS_RBP	for RHS , See HS_LBP		Same as HS_LBP, but for RHS
HS_RBS	for RHS , See HS_LBS	Table A.6.3	Same as HS_LBS, but for RHS
HS_FT	IFTNUM	OFF	Film tracking on/off switch

Table A.6.1
HS geometric parameters for MHTGR model

HSNAME	NUM	IGEOM	HSALT	ALPHA	NP	N	XI	MATNAM
LPbnd_2	102	CYLINDRICAL	-2.8825	1.0	3	1	2.4128	ALUMINUM
						2	2.9608	ALUMINUM
						3	3.0368	CARBSTEEL
LPbnd_3	103	CYLINDRICAL	-2.4325	1.0	3	1	2.4128	ALUMINUM
						2	2.9608	ALUMINUM
						3	3.0368	CARBSTEEL
PBbnd_4	104	CYLINDRICAL	-1.9825	1.0	3	1	2.4128	ALUMINUM
						2	2.9608	ALUMINUM
						3	3.0368	CARBSTEEL
FDBbnd_5	105	CYLINDRICAL	-1.3878	1.0	3	1	2.4128	ALUMINUM
						2	2.9608	ALUMINUM
						3	3.0368	CARBSTEEL
LRbnd_6	106	CYLINDRICAL	-0.9913	1.0	3	1	2.4128	ALUMINUM
						2	2.9608	ALUMINUM
						3	3.0368	CARBSTEEL
LRbnd_7	107	CYLINDRICAL	-0.5948	1.0	3	1	2.4128	ALUMINUM
						2	2.9608	ALUMINUM
						3	3.0368	CARBSTEEL
LRbnd_8	108	CYLINDRICAL	-0.0100	1.0	3	1	2.4128	ALUMINUM
						2	2.9608	ALUMINUM
						3	3.0368	CARBSTEEL
SRCB_9	109	CYLINDRICAL	0.0000	1.0	3	1	2.4128	ALUMINUM
						2	2.9608	ALUMINUM
						3	3.0368	CARBSTEEL
SRCB_10	110	CYLINDRICAL	0.7930	1.0	3	1	2.4128	ALUMINUM
						2	2.9608	ALUMINUM
						3	3.0368	CARBSTEEL
SRCB_11	111	CYLINDRICAL	1.5860	1.0	3	1	2.4128	ALUMINUM
						2	2.9608	ALUMINUM
						3	3.0368	CARBSTEEL
SRCB_12	112	CYLINDRICAL	2.3790	1.0	3	1	2.4128	ALUMINUM
						2	2.9608	ALUMINUM
						3	3.0368	CARBSTEEL
SRCB_13	113	CYLINDRICAL	3.1720	1.0	3	1	2.4128	ALUMINUM
						2	2.9608	ALUMINUM
						3	3.0368	CARBSTEEL
SRCB_14	114	CYLINDRICAL	3.9650	1.0	3	1	2.4128	ALUMINUM
						2	2.9608	ALUMINUM

						3	3.0368	CARBSTEEL
SRCB_15	115	CYLINDRICAL	4.7580	1.0	3	1	2.4128	ALUMINUM
						2	2.9608	ALUMINUM
						3	3.0368	CARBSTEEL
SRCB_16	116	CYLINDRICAL	5.5510	1.0	3	1	2.4128	ALUMINUM
						2	2.9608	ALUMINUM
						3	3.0368	CARBSTEEL
SRCB_17	117	CYLINDRICAL	6.3440	1.0	3	1	2.4128	ALUMINUM
						2	2.9608	ALUMINUM
						3	3.0368	CARBSTEEL
SRCB_18	118	CYLINDRICAL	7.1370	1.0	3	1	2.4128	ALUMINUM
						2	2.9608	ALUMINUM
						3	3.0368	CARBSTEEL
URbnd_19	119	CYLINDRICAL	7.9300	1.0	3	1	2.4128	ALUMINUM
						2	2.9608	ALUMINUM
						3	3.0368	CARBSTEEL
URbnd_20	120	CYLINDRICAL	7.9400	1.0	3	1	2.4128	ALUMINUM
						2	2.9608	ALUMINUM
						3	3.0368	CARBSTEEL
URbnd_21	121	CYLINDRICAL	8.3265	1.0	3	1	2.4128	ALUMINUM
						2	2.9608	ALUMINUM
						3	3.0368	CARBSTEEL
UP_TPS	122	HEMISPHERE	9.1195	1.0	2	1	2.9608	SS304
						2	3.0368	SS304
RPV_1	201	CYLINDRICAL	-1.9825	1.0	2	1	3.267	SS304
						2	3.4	SS304
RPV_2	202	CYLINDRICAL	-0.9913	1.0	2	1	3.267	SS304
						2	3.4	SS304
RPV_3	203	CYLINDRICAL	0.0000	1.0	2	1	3.267	SS304
						2	3.4	SS304
RPV_4	204	CYLINDRICAL	1.5860	1.0	2	1	3.267	SS304
						2	3.4	SS304
RPV_5	205	CYLINDRICAL	3.9650	1.0	2	1	3.267	SS304
						2	3.4	SS304
RPV_6	206	CYLINDRICAL	7.9300	1.0	2	1	3.267	SS304
						2	3.4	SS304

Table A.6.2
HS LHS boundary conditions for MHTGR model

HSNAME	IBVL	IOPTL	NUMAXL	NUMRAD	CLNL	BNDZL
LPbnd_2	LP_7_2	DTDZ	2	7	0.45000	0.45000
LPbnd_3	LP_7_3	DTDZ	3	7	0.45000	0.45000
PBbnd_4	POST_FDB_7	DTDZ	4	7	0.59475	0.59475
FDBbnd_5	POST_FDB_7	DTDZ	5	7	0.39650	0.39650
LRbnd_6	LR_7	DTDZ	6	7	0.39650	0.39650
LRbnd_7	LR_7	DTDZ	7	7	0.58475	0.58475
LRbnd_8	LR_7	DTDZ	8	7	0.01000	0.01000
SRCB_9	CORE_7_1	DTDZ	9	7	0.79300	0.79300
SRCB_10	CORE_7_1	DTDZ	10	7	0.79300	0.79300
SRCB_11	CORE_7_2	DTDZ	11	7	0.79300	0.79300
SRCB_12	CORE_7_2	DTDZ	12	7	0.79300	0.79300
SRCB_13	CORE_7_2	DTDZ	13	7	0.79300	0.79300
SRCB_14	CORE_7_3	DTDZ	14	7	0.79300	0.79300
SRCB_15	CORE_7_3	DTDZ	15	7	0.79300	0.79300
SRCB_16	CORE_7_3	DTDZ	16	7	0.79300	0.79300
SRCB_17	CORE_7_3	DTDZ	17	7	0.79300	0.79300
SRCB_18	CORE_7_3	DTDZ	18	7	0.79300	0.79300
URbnd_19	UR_7	DTDZ	19	7	0.01000	0.01000
URbnd_20	UR_7	DTDZ	20	7	0.38650	0.38650
URbnd_21	UR_7	DTDZ	21	7	0.79300	0.79300
UP_TPS	UPPER_PLENUM	-	-	-	1.00000	3.03680
RPV_1	UPCOMER	-	-	-	0.99125	0.99125
RPV_2	UPCOMER	-	-	-	0.99125	0.99125
RPV_3	UPCOMER	-	-	-	1.58600	1.58600
RPV_4	UPCOMER	-	-	-	2.37900	2.37900
RPV_5	UPCOMER	-	-	-	3.17200	3.17200
RPV_6	UPCOMER	-	-	-	1.18950	1.18950

Table A.6.3
HS RHS boundary conditions for MHTGR model

HSNAME	IBCR	IBVR	IFLOWR	CPFPL	CPFAL	CLNR	BNDZR
LPbnd_2	SYMMETRY	NO	INT	0.0	0.0	0.45000	0.45000
LPbnd_3	SYMMETRY	NO	INT	0.0	0.0	0.45000	0.45000
PBbnd_4	CALCCOEFHS	UPCOMER	INT	0.0	0.0	0.59475	0.59475
FDBbnd_5	CALCCOEFHS	UPCOMER	INT	0.0	0.0	0.39650	0.39650
LRbnd_6	CALCCOEFHS	UPCOMER	INT	0.0	0.0	0.39650	0.39650
LRbnd_7	CALCCOEFHS	UPCOMER	INT	0.0	0.0	0.58475	0.58475
LRbnd_8	CALCCOEFHS	UPCOMER	INT	0.0	0.0	0.01000	0.01000
SRCB_9	CALCCOEFHS	UPCOMER	INT	0.0	0.0	0.79300	0.79300
SRCB_10	CALCCOEFHS	UPCOMER	INT	0.0	0.0	0.79300	0.79300
SRCB_11	CALCCOEFHS	UPCOMER	INT	0.0	0.0	0.79300	0.79300
SRCB_12	CALCCOEFHS	UPCOMER	INT	0.0	0.0	0.79300	0.79300
SRCB_13	CALCCOEFHS	UPCOMER	INT	0.0	0.0	0.79300	0.79300
SRCB_14	CALCCOEFHS	UPCOMER	INT	0.0	0.0	0.79300	0.79300
SRCB_15	CALCCOEFHS	UPCOMER	INT	0.0	0.0	0.79300	0.79300
SRCB_16	CALCCOEFHS	UPCOMER	INT	0.0	0.0	0.79300	0.79300
SRCB_17	CALCCOEFHS	UPCOMER	INT	0.0	0.0	0.79300	0.79300
SRCB_18	CALCCOEFHS	UPCOMER	INT	0.0	0.0	0.79300	0.79300
URbnd_19	CALCCOEFHS	UPCOMER	INT	0.0	0.0	0.01000	0.01000
URbnd_20	CALCCOEFHS	UPCOMER	INT	0.0	0.0	0.38650	0.38650
URbnd_21	CALCCOEFHS	UPCOMER	INT	0.0	0.0	0.79300	0.79300
UP_TPS	SYMMETRY	NO	EXT	0.0	0.0	1.00000	3.03680
RPV_1	CALCCOEFHS	CAVITY_1	EXT	0.5	0.5	0.99125	0.99125
RPV_2	CALCCOEFHS	CAVITY_2	EXT	0.5	0.5	0.99125	0.99125
RPV_3	CALCCOEFHS	CAVITY_3	EXT	0.5	0.5	1.58600	1.58600
RPV_4	CALCCOEFHS	CAVITY_4	EXT	0.5	0.5	2.37900	2.37900
RPV_5	CALCCOEFHS	CAVITY_5	EXT	0.5	0.5	3.17200	3.17200
RPV_6	CALCCOEFHS	CAVITY_6	EXT	0.5	0.5	1.18950	1.18950

Table A.7
COR input for MHTGR model

COR_INPUT	-	-	Signal start of COR input
COR_RT	IRTYP	PMR	Reactor type flag
	MCRP	B4C	Poison material (insignificant for this calculation)
COR_GP	RFUEL	0.006225	Fuel rod (i.e. fuel compact) outer radius
	RCLAD	0.00863	Clad outer radius
	DRGAP	1.25E-04	Gap thickness between fuel/clad
	PITCH	0.0188	Fuel rod (i.e. fuel compact) center-to-center distance
COR_VP	RCOR	2.4128	Outer radius for active core region
	RVESS	3.4	Inner radius of vessel
	ILHTRN	RVESS	LH transition type (inconsequential in this calculation)
	DZRV	0.133	Vessel wall thickness
	DZLH	0.133	LH thickness (inconsequential in this calculation)
	ILHTYP	HEMISPHERE	LH geometry (inconsequential in this calculation)
	RVLH	3.4	For hemispherical lower head, radius of curvature
	COR_AVP	HLST	-2.8825
HCSP		-2.8825	Elevation of core support plate, > HLST
COR_TP	NTPCOR	NO	TP name for CAV/FDI (inconsequential)
	RNTPCOR	NO	TP name for radionuclides (inconsequential)
	ICFGAP	NO	FU/CL gap conductance CF name (inconsequential)
	ICFFIS	FISPOWALL	Fission power CF, FISPOWALL = whole-core power
	CFNAME	CORE-POWER	CF name giving fission power
COR_MS	IEUMOD	0	Materials interactions model switch (inconsequential)
	IHSDT	0	HS boundary switch, set to DT/DZ model
	IDTDZ	0	DT/DZ inlet specification option switch
	ICORCV	1	COR/CVH hydrodynamic volume consistency switch
COR_BCP	ICBCD	CB	Component Mnemonic for conducting core component
	MATBCD	HE	Gap material separating core and the heat structures
	DXBCD	1.00E-04	Gap thickness
	CDFBCD	1.58E-04	Thermal diffusion constant
COR_CLM	CLMAT	GRAPH	Identifier for cladding material
COR_RFM	RFMAT	GRAPH	Identifier for reflector material
COR_FUM	XFUMAT	INC	Identifier for fuel "extra", inconel is compact graphite
COR_LP	IAXSUP	2	Axial level containing support plate (inconsequential)
	HDBH2O	100	HTC from in-vessel falling debris to (inconsequential)
	PPFAIL	2.00E+07	Differential pressure for LH failure (inconsequential)
	VFALL	1	Falling debris velocity (inconsequential)
COR_TKE	TKETF	NO	Name of TF for effective conductivity, if used

	PORCHAN	0.2369	Eff. block porosity used in Tanaka-Chisaka model
	DBLK	0.378	Effective graphite block size for gap model
	BLKGAP	0.0001	Gap width between graphite blocks for gap model
COR_LH	NLH	2	Number of LH temperature nodes (inconsequential)
	NINSLH	0	Number of insulation mesh layers (inconsequential)
COR_EDV	ITEMP	1	Temperature edit flag
	IMASS	1	Mass edit flag
	IVOL	1	Volume edit flag
	IASUR	1	Surface area edit flag
	IPMV	1	Component masses plot flag
	IPOW	1	Decay heat/fission power edit flag
COR_ZP	IA		Axial Level number(s)
	Z		Bottom elevation of axial level
	DZ	Table A.7.1	Axial height of axial level
	PORDP		Particulate debris porosity
	IHSA		Axial boundary heat structure name
	FZPOW		Relative power density
COR_RP	IR		Radial Ring number(s)
	RINGR		Outer ring radius
	ASCELA		Total ring cross-sectional area
	IHSR	Table A.7.2	Radial boundary heat structure name
	UNUSED		Placeholder, use '-'
	ICFCHN		Name of CF to infer positive flow direction in channel
	ICFBYP		Name of CF to infer positive flow direction in bypass
	FRPOW		Relative power density
COR_RBV	IA		Axial level number(s)
	IR		Radial Ring number(s)
	IREF	Table A.7.3	Axial level number for reference cell if necessary
	JREF		Radial ring number for reference cell if necessary
	ICVHC		Channel-side control volume name
	ICVHB		Bypass-side control volume name
COR_SS	IA		Axial level number(s)
	IR		Radial Ring number(s)
	ISSMOD	Table A.7.4	Structural model option for SS component
	ISSFAI		Failure model flag
	TSSFAI		Failure temperature (used for ISSFAI = TSFAIL)
	SSMETAL		SS material name
COR_KFU	IA	Table A.7.5	Axial level number(s)
	IR		Radial Ring number(s)

	XMFUUO		Mass of UO ₂ in FU
	XMFUHT		Mass of electric heater rod material in FU
	XMFXM		Mass of user-defined extra material in FU
	XMFXO		Mass of user-defined extra material oxide in FU
COR_KCL	IA		Axial level number(s)
	IR		Radial Ring number(s)
	XMCLZR	Table A.7.6	Mass of zircaloy in CL
	XMCLZX		Mass of ZrO ₂ in CL
COR_KSS	XMCLIN		Mass of inconel in CL
	IA		Axial level number(s)
	IR		Radial Ring number(s)
	XMSSSS	Table A.7.7	Mass of steel in SS
COR_KRF	XMSSSX		Mass of steel oxide in SS
	XMSSZR		Mass of zircaloy in SS
	XMSSZX		Mass of zircaloy oxide in SS
	IA		Axial level number(s)
COR_KPD	IR	Table A.7.8	Radial Ring number(s)
	XMRF		Mass of graphite in RF
	IA	ALL	Axial level number(s)
COR_CIT	IR	ALL	Radial Ring number(s)
	XMPDZR	0.0	Mass of zircaloy in PD component
	XMPDZX	0.0	Mass of ZrO ₂ in PD component
	XMPDUO	0.0	Mass of UO ₂ in PD component
	XMPDSS	0.0	Mass of steel in PD component
	XMPDSX	0.0	Mass of Steel oxide in PD component
	XMPDCP	0.0	Mass of control poison in PD component
	XMPDIN	0.0	Mass of inconel in PD component
	TFU	763.15	Initial FU temperature
	TCL	763.15	Initial CL temperature
TCN	763.15	Initial CN temperature	
TCB	763.15	Initial CB temperature	
TPD	763.15	Initial PD temperature	
TSS	763.15	Initial SS temperature	
TNS	763.15	Initial NS temperature	
TPB	763.15	Initial PB temperature	
COR_EDR	IA		Axial level number(s)
	IR	Table A.7.9	Radial Ring number(s)

	DHYCL		CL equivalent diameter
	DHYPD		PD equivalent diameter
	DHYCNC		CNC equivalent diameter
	DHYCNB		CNB equivalent diameter
	DHYSS		SS equivalent diameter
	DHYNS		NS equivalent diameter
	DHYPB		PB equivalent diameter
COR_RFD	IA		Axial level number(s)
	IR	Table A.7.10	Radial Ring number(s)
	DHYRFC		RF channel side equivalent diameter
	DHYRFB		RF bypass side equivalent diameter
COR_RFG	IA		Axial level number(s)
	IR		Radial Ring number(s)
	RADI	Table A.7.11	Reflector channel-side radius
	THKRF		Reflector thickness
	IGEOMRF		Reflector geometry flag
	FACRF		Factor to split thermal conductances to inner/outer surfaces
COR_BFA	IA		Axial level number(s)
	IR		Radial Ring number(s)
	ASCELR	Table A.7.12	Area of outer radial cell boundary = $2\pi R(DZ)$
	AFLOWC		Channel flow area of cell
	AFLOWB		Bypass flow area of cell
COR_SA	IA		Axial level number(s)
	IR		Radial Ring number(s)
	ASFU		FU surface area
	ASCL	Table A.7.13	CL surface area
	ASCN		CN surface area
	ASSS		SS surface area
	ASNS		NS surface area
COR_RFA	IA		Axial level number(s)
	IR	Table A.7.14	Radial Ring number(s)
	ASRF		Channel-side reflector surface area
	ASRFB		Bypass-side reflector surface area

Table A.7.1
COR_ZP for MHTGR model

IA	Z	DZ	COR_ZP		
			PORDP	IHSA	FZPOW
1	-6.2825	3.40000	0.0	NO	0.00
2	-2.8825	0.45000	0.0	LPbnd_2	0.00
3	-2.4325	0.45000	0.0	LPbnd_3	0.00
4	-1.9825	0.59475	0.0	PBbnd_4	0.00
5	-1.3878	0.39650	0.0	FDBbnd_5	0.00
6	-0.9913	0.39650	0.0	LRbnd_6	0.00
7	-0.5948	0.58475	0.0	LRbnd_7	0.00
8	-0.0100	0.01000	0.0	LRbnd_8	0.00
9	0.0000	0.79300	0.0	SRCB_9	0.50
10	0.7930	0.79300	0.0	SRCB_10	0.50
11	1.5860	0.79300	0.0	SRCB_11	0.75
12	2.3790	0.79300	0.0	SRCB_12	0.75
13	3.1720	0.79300	0.0	SRCB_13	0.75
14	3.9650	0.79300	0.0	SRCB_14	1.35
15	4.7580	0.79300	0.0	SRCB_15	1.35
16	5.5510	0.79300	0.0	SRCB_16	1.35
17	6.3440	0.79300	0.0	SRCB_17	1.35
18	7.1370	0.79300	0.0	SRCB_18	1.35
19	7.9300	0.01000	0.0	URbnd_19	0.00
20	7.9400	0.38650	0.0	URbnd_20	0.00
21	8.3265	0.79300	0.0	URbnd_21	0.00

Table A.7.2
COR_RP for MHTGR model

IR	RINGR	ASCELA	IHSR	COR_RP			
				UNUSED	ICFCHN	ICFBYP	FRPOW
1	0.5000	0.7854	UP-TPS	-	NO	NO	0.00
2	0.8238	1.3464	UP-TPS	-	NO	NO	0.00
3	1.1496	2.0196	UP-TPS	-	NO	NO	0.87
4	1.4761	2.6928	UP-TPS	-	NO	NO	1.01
5	1.8029	3.3660	UP-TPS	-	NO	NO	1.08
6	2.1298	4.0392	UP-TPS	-	NO	NO	0.00
7	2.4128	4.0392	UP-TPS	-	NO	NO	0.00
8	3.4000	18.0270	UP-TPS	-	NO	NO	0.00

Table A.7.3
COR_RBV for MHTGR model

COR_RBV					
IA	IR	IREF	JREF	ICVHC	ICVHB
1	1	0	0	DUMMY_IA1	DUMMY_IA1
2	1	0	0	LP_1_2	LP_1_2
3	1	0	0	LP_1_3	LP_1_3
4-5	1	0	0	POST_FDB_1	POST_FDB_1
6-8	1	0	0	LR_1	LR_1
9-10	1	0	0	CORE_1_1	CORE_1_1
11-13	1	0	0	CORE_1_2	CORE_1_2
14-18	1	0	0	CORE_1_3	CORE_1_3
19-21	1	0	0	UR_1	UR_1
1	2	1	1	-	-
2	2	0	0	LP_2_2	LP_2_2
3	2	0	0	LP_2_3	LP_2_3
4-5	2	0	0	POST_FDB_2	POST_FDB_2
6-8	2	0	0	LR_2	LR_2
9-10	2	0	0	CORE_2_1	CORE_2_1
11-13	2	0	0	CORE_2_2	CORE_2_2
14-18	2	0	0	CORE_2_3	CORE_2_3
19-21	2	0	0	UR_2	UR_2
1	3	1	1	-	-
2	3	0	0	LP_3_2	LP_3_2
3	3	0	0	LP_3_3	LP_3_3
4-5	3	0	0	POST_FDB_3	POST_FDB_3
6-8	3	0	0	LR_3	LR_3
9-10	3	0	0	CORE_3_1	CORE_3_1
11-13	3	0	0	CORE_3_2	CORE_3_2
14-18	3	0	0	CORE_3_3	CORE_3_3
19-21	3	0	0	UR_3	UR_3

Table A.7.4
COR_SS for MHTGR model

COR_SS					
IA	IR	ISSMOD	ISSFAI	TSSFAI	SSMETA
1	1-8	PLATEG	TSFAIL	5000.0	STEEL
4	1-7	PLATEG	TSFAIL	5000.0	STEEL
5	1-7	PLATEG	TSFAIL	5000.0	STEEL
8	3-5	PLATEG	TSFAIL	5000.0	ZIRC
19	3-5	PLATEG	TSFAIL	5000.0	ZIRC

Table A.7.5
COR_KFU for MHTGR model

COR_KFU					
IA	IR	XMFUUO	XMFUHT	XMFOXM	XMFOXO
9-18	3	190.61	0.00	294.73	0.00
9-18	4-5	271.51	0.00	419.83	0.00

Table A.7.6
COR_KCL for MHTGR model

COR_KCL				
IA	IR	XMCLZR	XMCLZX	XMCLIN
9-18	3	1677.04	0.00	0.00
9-18	4	2124.35	0.00	0.00
9-18	5	2124.35	0.00	0.00

Table A.7.7
COR_KSS for MHTGR model

IA	IR	COR_KSS			
		XMSSSS	XMSSSX	XMSSZR	XMSSZX
4	1	829.10	0.00	0.00	0.00
5	1	552.73	0.00	0.00	0.00
4	2	1421.30	0.00	0.00	0.00
5	2	947.53	0.00	0.00	0.00
4	3	1716.68	0.00	0.00	0.00
5	3	1144.45	0.00	0.00	0.00
8	3	0.00	0.00	29.00	0.00
19	3	0.00	0.00	27.29	0.00
4	4	2288.91	0.00	0.00	0.00
5	4	1525.94	0.00	0.00	0.00
8	4	0.00	0.00	37.93	0.00
19	4	0.00	0.00	37.93	0.00
4	5	2288.91	0.00	0.00	0.00
5	5	1525.94	0.00	0.00	0.00
8	5	0.00	0.00	37.93	0.00
19	5	0.00	0.00	37.93	0.00
4	6	4974.55	0.00	0.00	0.00
5	6	3316.37	0.00	0.00	0.00
4	7	4263.90	0.00	0.00	0.00
5	7	2842.60	0.00	0.00	0.00
1	1	10.00	0.00	0.00	0.00
1	2	10.00	0.00	0.00	0.00
1	3	10.00	0.00	0.00	0.00
1	4	10.00	0.00	0.00	0.00
1	5	10.00	0.00	0.00	0.00
1	6	10.00	0.00	0.00	0.00
1	7	10.00	0.00	0.00	0.00

Table A.7.8
COR_KRF for MHTGR model

COR_KRF		
IA	IR	XMRF
6	1	540.34
7	1	796.88
8	1	13.63
9-18	1	1080.68
19	1	13.63
20	1	526.71
21	1	1080.68
6	2	926.24
7	2	1366.00
8	2	23.36
9-18	2	1785.49
19	2	23.36
20	2	870.23
21	2	1785.49
6	3	1149.69
7	3	1695.54
20	3	1054.76
21	3	2164.10
6	4	1516.39
7	4	2236.34
20	4	1478.15
21	4	3032.78
6	5	1516.39
7	5	2236.34
20	5	1478.15
21	5	3032.78
6	6	3241.84
1	8	10.00

Table A.7.9
COR_EDR for MHTGR model

COR_EDR								
IA	IR	DHYCL	DHYPD	DHVCNC	DHVCNB	DHYSS	DHYNS	DHYPB
1-3	1-7	0.1726	0.0159	0.0159	0.0159	0.0159	0.0159	0.0159
4-5	1-2	0.1726	0.0159	0.0159	0.0159	0.0002	0.0159	0.0159
4-5	3-5	0.0159	0.0159	0.0159	0.0159	0.0680	0.0159	0.0159
4-5	6-7	0.0159	0.0159	0.0159	0.0159	0.0002	0.0159	0.0159
6-7	1-7	0.0159	0.0159	0.0159	0.0159	0.0159	0.0159	0.0159
8	1-2	0.0159	0.0159	0.0159	0.0159	0.0002	0.0159	0.0159
8	3-5	0.0159	0.0159	0.0159	0.0159	0.1726	0.0159	0.0159
8	6-7	0.0159	0.0159	0.0159	0.0159	0.0002	0.0159	0.0159
9-18	1-7	0.1726	0.0159	0.0159	0.0159	0.0159	0.0159	0.0159
19	1-2	0.0159	0.0159	0.0159	0.0159	0.0002	0.0159	0.0159
19	3-5	0.0159	0.0159	0.0159	0.0159	0.0002	0.0159	0.0159
19	6-7	0.0159	0.0159	0.0159	0.0159	0.0159	0.0159	0.0159
20-21	1-7	0.1726	0.0159	0.0159	0.0159	0.0159	0.0159	0.0159
1	8	0.0159	0.0159	0.0159	0.0159	0.0159	0.0159	0.0159

Table A.7.10
COR_RFD for MHTGR model

COR_RFD			
IA	IR	DHYRFC	DHYRFB
6-21	1	1.00E-10	2.00E-04
6-21	2	0.0159	2.00E-04
20-21	3-5	0.0159	1.00E-10
6-7	3-5	0.0159	1.00E-10
6-21	6	0.0159	2.00E-04
6-21	7	1.00E-10	2.00E-04

Table A.7.11
COR_RFG for MHTGR model

COR_RFG				
IA	IR	RADI	THKRF	IGEOMRF
6-21	1	0.5	-0.50000	1
6-21	2	0.8238	-0.32380	1
20	3	1.1496	-0.38650	0
21	3	1.1496	-0.79300	0
20	4	1.4761	-0.38650	0
21	4	1.4761	-0.79300	0
20	5	1.8029	-0.38650	0
21	5	1.8029	-0.79300	0
6	3	1.1496	0.39650	0
7	3	1.1496	0.58475	0
6	4	1.4761	0.39650	0
7	4	1.4761	0.58475	0
6	5	1.8029	0.39650	0
7	5	1.8029	0.58475	0
6-21	6	2.1298	0.32690	1
6-21	7	2.4128	0.28300	1

Table A.7.12
COR_BFA for MHTGR model

COR_BFA				
IA	IR	ASCELR	AFLOWC	AFLOWB
1	1	3.1416	0.00263	0.00000
2-3	1	1.4137	0.78540	0.00000
4	1	1.8685	0.00000	2.49E-04
5	1	1.2456	0.00000	2.49E-04
6	1	1.2456	0.00000	2.49E-04
7	1	1.837	0.00000	2.49E-04
8	1	0.0314	0.00000	2.49E-04
9-18	1	2.4913	0.00000	2.49E-04
19	1	0.0314	0.00000	2.49E-04
20	1	1.2142	0.00000	2.49E-04
21	1	2.4913	0.00000	2.49E-04
1	2	5.1761	0.01113	0.00000
2-3	2	2.3292	1.34640	0.00000
4	2	3.0785	0.00000	0.00062
5	2	2.0523	0.00000	6.23E-04
6	2	2.0523	0.00000	6.23E-04
7	2	3.0267	0.00000	6.23E-04
8	2	0.0518	0.00000	6.23E-04
9-18	2	4.1046	0.00000	6.23E-04
19	2	0.0518	0.00000	6.23E-04
20	2	2.0006	0.00000	6.23E-04
21	2	4.1046	0.00000	6.23E-04
1	3	7.2231	0.02788	0.00000
2-3	3	3.2504	2.01960	0.00000
4	3	4.296	0.26150	0.00000
5	3	2.864	0.26150	0.00000
6	3	2.864	0.34660	0.00000
7	3	4.2237	0.34660	0.00000
8	3	0.0722	0.34660	0.00000
9-18	3	5.728	0.34660	0.00000
19	3	0.0722	0.34660	0.00000
20	3	2.7917	0.34660	0.00000
21	3	5.728	0.34660	0.00000
1	4	9.2746	0.05296	0.00000
2-3	4	4.1736	2.69280	0.00000
4	4	5.5161	0.52290	0.00000
5	4	3.6774	0.52290	0.00000

6	4	3.6774	0.50430	0.00000
7	4	5.4233	0.50430	0.00000
8	4	0.0927	0.50430	0.00000
9-18	4	7.3548	0.50430	0.00000
19	4	0.0927	0.50430	0.00000
20	4	3.5846	0.50430	0.00000
21	4	7.3548	0.50430	0.00000
1	5	11.3279	0.08848	0.00000
2-3	5	5.0976	3.36600	0.00000
4	5	6.7373	0.52290	0.00000
5	5	4.4915	0.52290	0.00000
6	5	4.4915	0.50430	0.00000
7	5	6.624	0.50430	0.00000
8	5	0.1133	0.50430	0.00000
9-18	5	8.9831	0.50430	0.00000
19	5	0.1133	0.50430	0.00000
20	5	4.3783	0.50430	0.00000
21	5	8.9831	0.50430	0.00000
1	6	13.3819	0.13829	0.00000
2-3	6	6.0219	4.03920	0.00000
4	6	7.9589	0.00000	2.39E-03
5	6	5.3059	0.00000	2.39E-03
6	6	5.3059	0.00000	2.39E-03
7	6	7.8251	0.00000	2.39E-03
8	6	0.1338	0.00000	2.39E-03
9-18	6	10.6119	0.00000	2.39E-03
19	6	0.1338	0.00000	2.39E-03
20	6	5.1721	0.00000	2.39E-03
21	6	10.6119	0.00000	2.39E-03
1	7	15.1601	0.15221	0.00000
2-3	7	6.822	4.03920	0.00000
4	7	9.0164	0.00000	2.37E-03
5	7	6.011	0.00000	2.37E-03
6	7	6.011	0.00000	2.37E-03
7	7	8.8648	0.00000	2.37E-03
8	7	0.1516	0.00000	2.37E-03
9-18	7	12.0219	0.00000	2.37E-03
19	7	0.1516	0.00000	2.37E-03

Table A.7. 13
COR_SA for MHTGR model

IA	IR	COR_SA				
		ASFU	ASCL	ASCN	ASSS	ASNS
1	1	0.00	0.00	0.00	1.00E-10	0.00
2-3	1	0.00	0.00	0.00	0.00	0.00
4	1	0.00	0.00	0.00	2.9679	0.00
5	1	0.00	0.00	0.00	1.9788	0.00
6-21	1	0.00	0.00	0.00	0.00	0.00
1	2	0.00	0.00	0.00	1.00E-10	0.00
2-3	2	0.00	0.00	0.00	0.00	0.00
4	2	0.00	0.00	0.00	7.4189	0.00
5	2	0.00	0.00	0.00	4.947	0.00
6-21	2	0.00	0.00	0.00	0.00	0.00
1	3	0.00	0.00	0.00	1.00E-10	0.00
2-3	3	0.00	0.00	0.00	0.00	0.00
4	3	0.00	0.00	0.00	0.7623	0.00
5	3	0.00	0.00	0.00	0.5082	0.00
6-7	3	0.00	0.00	0.00	0.00	0.00
8	3	0.00	0.00	0.00	0.8788	0.00
9-18	3	112.00	69.68	0.00	0.00	0.00
19	3	0.00	0.00	0.00	0.8788	0.00
20-21	3	0.00	0.00	0.00	0.00	0.00
1	4	0.00	0.00	0.00	1.00E-10	0.00
2-3	4	0.00	0.00	0.00	0.00	0.00
4	4	0.00	0.00	0.00	18.30	0.00
5	4	0.00	0.00	0.00	12.20	0.00
6-7	4	0.00	0.00	0.00	0.00	0.00
8	4	0.00	0.00	0.00	1.28	0.00
9-18	4	159.50	101.50	0.00	0.00	0.00
19	4	0.00	0.00	0.00	1.28	0.00
20-21	4	0.00	0.00	0.00	0.00	0.00
1	5	0.00	0.00	0.00	1.00E-10	0.00
2-3	5	0.00	0.00	0.00	0.00	0.00
4	5	0.00	0.00	0.00	18.30	0.00
5	5	0.00	0.00	0.00	12.20	0.00
6-7	5	0.00	0.00	0.00	0.00	0.00
8	5	0.00	0.00	0.00	1.28	0.00

9-18	5	159.5	101.50	0.00	0.00	0.00
19	5	0.00	0.00	0.00	1.28	0.00
20-21	5	0.00	0.00	0.00	0.00	0.00
1	6	0.00	0.00	0.00	1.00E-10	0.00
2-3	6	0.00	0.00	0.00	0.00	0.00
4	6	0.00	0.00	0.00	28.44	0.00
5	6	0.00	0.00	0.00	18.96	0.00
6-21	6	0.00	0.00	0.00	0.00	0.00
1	7	0.00	0.00	0.00	1.00E-10	0.00
2-3	7	0.00	0.00	0.00	0.00	0.00
4	7	0.00	0.00	0.00	28.19	0.00
5	7	0.00	0.00	0.00	18.80	0.00
6-21	7	0.00	0.00	0.00	0.00	0.00
1	8	0.00	0.00	0.00	1.00E-10	0.00

Table A.7. 14
COR_RFA for MHTGR model

COR_RFA			
IA	IR	ASRF	ASRFB
6	1	1.00E-10	1.9780
7	1	1.00E-10	2.9180
8	1	1.00E-10	0.0499
9-18	1	1.00E-10	3.9566
19	1	1.00E-10	0.0499
20	1	1.00E-10	1.9280
21	1	1.00E-10	3.9566
6	2	1.00E-10	4.9460
7	2	1.00E-10	7.2940
8	2	1.00E-10	0.1247
9-18	2	1.00E-10	9.8920
19	2	1.00E-10	0.1247
20	2	1.00E-10	4.8210
21	2	1.00E-10	9.8920
6	3	34.8400	1.00E-10
7	3	51.3800	1.00E-10
20	3	33.9600	1.00E-10
21	3	69.6800	1.00E-10
6	4	50.7600	1.00E-10

7	4	74.8600	1.00E-10
20	4	49.4800	1.00E-10
21	4	101.5000	1.00E-10
6	5	50.7600	1.00E-10
7	5	74.8600	1.00E-10
20	5	49.4800	1.00E-10
21	5	101.5000	1.00E-10
6	6	1.00E-10	18.9600
7	6	1.00E-10	27.9600
8	6	1.00E-10	0.4780
9-18	6	1.00E-10	37.9200
19	6	1.00E-10	0.4780
20	6	1.00E-10	18.4800
21	6	1.00E-10	37.9200
6	7	1.00E-10	18.7900
7	7	1.00E-10	27.7200
8	7	1.00E-10	0.4740
9-18	7	1.00E-10	37.5900
19	7	1.00E-10	0.4740
20	7	1.00E-10	18.3200
21	7	1.00E-10	37.5900

Table A.8
MP input for MHTGR model

MP_INPUT	-	-	Signal start of MP input
MP_ID	MATNAM		Material name
MP_PRTF	PROP		Property Mnemonic (ENH, CPS, THC, or RHO)
	ITBPRP		Name of TF for property
	CFKEY	Table A.8.1	CF/TF flag
MP_PRC	RHOM		Material density (constant property)
	TMLT		Material melt temperature (constant property)
	LHF		Material latent heat of fusion (constant property)

Table A.8.1
MP properties input for MHTGR model

MP_ID	MP_PRTF			MP_PRC		
MATNAM	PROP	ITBPRP	CFKEY	RHOM	TMLT	LHF
GRAPHITE	THC	THC-H451-GRAPH	TF			
	CPS	CPS-H451-GRAPH	TF	1740.0	3866.0	-
	ENH	ENH-H451-GRAPH	TF			
STAINLESS-STEEL-304	-	-	-	-	-	-
ZIRCALOY	THC	THC-H451-GRAPH	TF			
	CPS	CPS-H451-GRAPH	TF	1740.0	3866.0	-
	ENH	ENH-H451-GRAPH	TF			
ZIRCONIUM-OXIDE	-	-	-	-	-	-
STAINLESS-STEEL	THC	THC-2020-GRAPH	TF			
	CPS	CPS-2020-GRAPH	TF	1780.0	3866.0	-
	ENH	ENH-2020-GRAPH	TF			
STAINLESS-STEEL-OXIDE	-	-	-	-	-	-
ALUMINUM	THC	THC-2020-GRAPH	TF			
	CPS	CPS-2020-GRAPH	TF	1780.0	3866.0	-
	ENH	ENH-2020-GRAPH	TF			
ALUMINUM-OXIDE	-	-	-	-	-	-
CARBON-STEEL	-	-	-	-	-	-
BORON-CARBIDE	-	-	-	-	-	-
URANIUM-DIOXIDE	-	-	-	-	-	-
INCONEL	THC	THC-H451-GRAPH	TF			
	CPS	CPS-H451-GRAPH	TF	1000.0	3866.0	-
	ENH	ENH-H451-GRAPH	TF			

Table A.9
TF input for MHTGR model

TF_INPUT	-	-	Signal start of TF input
TF_ID	TFNAME		Tabular function name
	TFSCAL		Tabular function scalar applied to each data point
	TFADCN	Table A.9.1	Tabular function additive constant applied to each data point
TF_TAB	NPAR		Data pair number
	X		Independent variable (e.g. time or temperature)
	Y		Dependent variable

Table A.9.1
TF tabular input for MHTGR model

TFNAME	TF_ID			TF_TAB	
	TFSCAL	TFADCN	NPAR	X	Y
THC-H451-GRAPH	1	0	1	500.0	115.0062
			2	600.0	106.1279
			3	700.0	97.9062
			4	800.0	90.3409
			5	900.0	83.4321
			6	1000.0	77.1798
			7	1100.0	71.5840
			8	1200.0	66.6447
			9	1300.0	62.3619
			10	1400.0	58.7356
			11	1500.0	55.7658
			12	1600.0	53.4525
			13	1700.0	51.7957
			14	1800.0	50.7954
CPS-H451-GRAPH	1	0	1	300.0	712.763
			2	400.0	990.362
			3	500.0	1217.634
			4	600.0	1389.860
			5	700.0	1519.837
			6	800.0	1619.440
			7	900.0	1697.261
			8	1000.0	1759.228
			9	1100.0	1809.429

			10	1200.0	1850.726
			11	1300.0	1885.157
			12	1400.0	1914.205
			13	1500.0	1938.966
			14	1600.0	1960.266
			15	1700.0	1978.737
			16	1800.0	1994.869
			17	1900.0	2009.048
			18	2000.0	2021.582
			19	2100.0	2032.717
			20	2200.0	2042.654
			21	2300.0	2051.559
			22	2400.0	2059.567
			23	2500.0	2066.792
			24	2600.0	2073.331
			25	2700.0	2079.264
			26	2800.0	2084.659
			27	2900.0	2089.576
			28	3000.0	2094.066
ENH-H451-GRAPH	1	0	1	300.0	0.0
			2	773.0	547910.0
			3	1273.0	1414010.0
			4	1773.0	2381110.0
			5	2273.0	3405060.0
			6	2773.0	4464560.0
			7	3866.0	6879871.0
			8	5000.0	9456545.0
THC-2020-GRAPH	1	0	1	295.0	62.4
			2	473.0	67.2
			3	673.0	57.2
			4	873.0	49.8
			5	1073.0	43.9
CPS-2020-GRAPH	1	0	1	300.0	712.763
			2	400.0	990.362
			3	500.0	1217.634
			4	600.0	1389.86
			5	700.0	1519.837
			6	800.0	1619.44
			7	900.0	1697.261
			8	1000.0	1759.228
			9	1100.0	1809.429

				10	1200.0	1850.726
				11	1300.0	1885.157
				12	1400.0	1914.205
				13	1500.0	1938.966
				14	1600.0	1960.266
				15	1700.0	1978.737
				16	1800.0	1994.869
				17	1900.0	2009.048
				18	2000.0	2021.582
				19	2100.0	2032.717
				20	2200.0	2042.654
				21	2300.0	2051.559
				22	2400.0	2059.567
				23	2500.0	2066.792
				24	2600.0	2073.331
				25	2700.0	2079.264
				26	2800.0	2084.659
				27	2900.0	2089.576
				28	3000.0	2094.066
ENH-2020-GRAPH	1		0	1	300.0	0.0
				2	773.0	547910.0
				3	1273.0	1414010.0
				4	1773.0	2381110.0
				5	2273.0	3405060.0
				6	2773.0	4464560.0
				7	3866.0	6879871.0
				8	5000.0	9456545.0

Table A.10
CF input for MHTGR model

CF_INPUT	-	-	Signal start of CF input
CF_ID	CFNAME		Control function name
	CFTYPE		Control function type
CF_SAI	CFSCAL		Control function value scalar
	CFADCN	Table A.10.1	Control function value additive constant
	CFVALR		Control function initial value
CF_ARG	CHARG		Control function argument identifier
	ARSCAL		Control function argument scalar
	ARADCN		Control function argument additive constant

Table A.10.1
CF arguments for MHTGR model

CF_ID		CF_SAI			CF_ARG		
CFNAME	CFTYP	CFSCAL	CFADCB	CFVALR	CHARG	ARSCAL	ARADCN
CORE-POWER	EQUALS	0	3.50E+08	3.50E+08	EXEC-TIME	0	0
SourceP	EQUALS	0	6.40E+06	6.40E+06	EXEC-TIME	0	0
SourceT	EQUALS	0	532.15	532.15	EXEC-TIME	0	0
Humidity	EQUALS	0	0	0	EXEC-TIME	0	0
Source_HE_frac	EQUALS	0	1	1	EXEC-TIME	0	0
SinkP	EQUALS	0	6.35E+06	6.35E+06	EXEC-TIME	0	0
SinkT	EQUALS	0	960.15	960.15	EXEC-TIME	0	0
Sink_HE_frac	EQUALS	0	1	1	EXEC-TIME	0	0
VELOCITY	DIVIDE	1	0	22.52	CVH-RHO('SOURCE',ATM)	1.204	0
					EXEC-TIME	0	157

Table A.11
EXEC MELCOR input for MHTGR model

EXEC_TEND	TEND	0.0	Calculation end time
EXEC_TIME	TIME	-1000.0	Time
	DTMAX	0.5	Maximum time-step
	DTMIN	1.00E-05	Minimum time-step
	DTEDIT	500.0	Frequency of edit printing
	DTPLOT	1.0	Frequency of plot file writing
	DTREST	1000.0	Restart frequency
	DCREST	1.00E+10	Restart frequency with respect to CPU time
EXEC_CPULEFT	CPULEF	30.0	Desired minimum number of CPU seconds left at end of calculation
EXEC_CPULIM	CPULIM	1200.0	Maximum number of CPU seconds for the calculation
EXEC_CYMESF	NCYEDD	100	Number of cycles between messages written to terminal
	NCYEDP	1000	Number of cycles between messages to output file
EXEC_EXACTTIME	N	1	Data string index
	TIME	0	Desired time to land on exactly during calculation

APPENDIX B: HTTF INPUT/CALCULATION NOTEBOOK

Appendix B contains a package-by-package breakdown of HTTF MELCOR input. Tables outlining all input cards, words, and values are included. A brief explanation of each card is also included where appropriate. Hand calculations based on the system design description (the HTTF drawings) were used to compute many of the required input parameters. The input below is a representative example for the HTTF and represents one of several input deck iterations.

Table B.1
Environmental variables input for HTTF model

<i>CARD</i>	<i>WORD</i>	<i>VALUE</i>	<i>BASIS</i>
MEG_DIAGFILE	-	'httfg.dia'	Name of MELGEN diagnostic file
MEL_DIAGFILE	-	'httf.dia'	Name of MELCOR diagnostic file
MEG_OUTPUTFILE	-	'httfg.out'	Name of MELGEN output file
MEL_OUTPUTFILE	-	'httf.out'	Name of MELCOR output file
PLOTFILE	-	'httf.ptf'	Name of plot file
MEG_RESTARTFILE	-	'httf.rst'	Name of MELGEN restart file
MEL_RESTARTFILE	-	httf.rst'	Name of MELCOR restart file
	CYCLE	NCYCLE	Restart based on cycle number
	NREST	-1	Use last available restart dump
MESSAGEFILE	-	'httf.mes'	Name of message file
STATUSFILE	-	'MELSTT_v2-0'	Name of status file
STOPFILE	-	'MELSTP_v2-0'	Name of stop file
WRITENEWINP	-	'httf.txt'	Name of re-written input file

Table B.2
EXEC MELGEN input for HTTF model

<i>CARD</i>	<i>WORD</i>	<i>VALUE</i>	<i>BASIS</i>
EXEC_INPUT	-	-	Signal start of EXEC input
EXEC_TITLE	TITLE	'HTTF'	Title of the calculation
EXEC_JOBID	JOBID	'httf -'	Job identifier
EXEC_TSTART	TSTART	-1000	Time at which to start calculation
EXEC_SS		-1000	Accelerated steady state run at -1000 seconds
		0.0	Run the accelerated steady state case until time 0
		0.01	Take 0.01 s timesteps from -1000 s to 0 s

Table B.3
NCG input for HTTF model

<i>CARD</i>	<i>WORD</i>	<i>VALUE</i>	<i>BASIS</i>
NCG_INPUT	-	-	Signal start of NCG input
NCG_ID	MNAME	'HE'	Activate helium
NCG_ID	MNAME	'H2'	Activate hydrogen
NCG_ID	MNAME	'CO'	Activate carbon monoxide
NCG_ID	MNAME	'O2'	Activate oxygen
NCG_ID	MNAME	'CO2'	Activate carbon dioxide
NCG_ID	MNAME	'CH4'	Activate CH4
NCG_ID	MNAME	'N2'	Activate nitrogen

Table B.4
CVH input for HTTF model

<i>CARD</i>	<i>WORD</i>	<i>VALUE</i>	<i>BASIS</i>
CVH_INPUT	-	-	Signal start of CVH input
CV_ID	CVNAME	Table A.4.1	Unique CV name identifier
	ICVNUM		User-defined CV number
CV_THR	ICVTHR	NONEQUIL	Thermodynamics switch
	IPFSW	FOG	Fog/no fog switch
	ICVACT	ACTIVE	Active/inactive switch
CV_PAS	ITYPTH	SEPARATE	Type of thermodynamic input
	IPIORA	ONLYATM	Pool/atmosphere/both switch
	VAPORSTATE	SUPERHEATED	Thermo. state of CV atmosphere
CV_PTD	PTDID	PVOL	Keyword for CV pressure
	PVOL	8.0E+05	Initial CV pressure
CV_AAD	ATMID	TATM	Keyword for CV atm. temperature
	TATM	532.15	Initial atmosphere temperature
CV_NCG	NMMAT	Table B.4.1	Number of NCG materials
	NCGID		Keyword Identifier, RHUM for all
	VALUE		Value from key, 0.0 = RHUM for all
	NUM		Table row index
	NAMGAS		NCG MELCOR name
CV_VAT	MLFR	Table B.4.2	Mole fraction of NCG in CV
	ICVVZP		Number of volume/altitude data pairs
	NCVZ		Table row index
	CVZ		Altitude of current data pair
	CVVOL		Volume of current data pair

Table B.4.1
CV_NCG for HTTF model

CV_ID		CV_NCG					
CVNAME	ICVNUM	NMMAT	NCGID	VALUE	NUM	NAMGAS	MLFR
CVCR_101	101	1	RHUM	0.0	1	HE	1.0
CVCR_102	102	1	RHUM	0.0	1	HE	1.0
CVCR_103	103	1	RHUM	0.0	1	HE	1.0
CVCR_104	104	1	RHUM	0.0	1	HE	1.0
CVCR_105	105	1	RHUM	0.0	1	HE	1.0
CVCR_106	106	1	RHUM	0.0	1	HE	1.0
CVCR_107	107	1	RHUM	0.0	1	HE	1.0
CVCR_108	108	1	RHUM	0.0	1	HE	1.0
CVCR_109	109	1	RHUM	0.0	1	HE	1.0
CVCore_201	201	1	RHUM	0.0	1	HE	1.0
CCCore_202A	2021	1	RHUM	0.0	1	HE	1.0
CVCore_202B	2022	1	RHUM	0.0	1	HE	1.0
CVCore_203	203	1	RHUM	0.0	1	HE	1.0
CVCore_204	204	1	RHUM	0.0	1	HE	1.0
CVCore_205	205	1	RHUM	0.0	1	HE	1.0
CVCore_206	206	1	RHUM	0.0	1	HE	1.0
CVCore_207	207	1	RHUM	0.0	1	HE	1.0
CVCore_208	208	1	RHUM	0.0	1	HE	1.0
CVCore_209	209	1	RHUM	0.0	1	HE	1.0
CVCore_301	301	1	RHUM	0.0	1	HE	1.0
CCCore_302A	3021	1	RHUM	0.0	1	HE	1.0
CVCore_302B	3022	1	RHUM	0.0	1	HE	1.0
CVCore_303	303	1	RHUM	0.0	1	HE	1.0
CVCore_304	304	1	RHUM	0.0	1	HE	1.0
CVCore_305	305	1	RHUM	0.0	1	HE	1.0
CVCore_306	306	1	RHUM	0.0	1	HE	1.0
CVCore_307	307	1	RHUM	0.0	1	HE	1.0
CVCore_308	308	1	RHUM	0.0	1	HE	1.0
CVCore_309	309	1	RHUM	0.0	1	HE	1.0
CVCore_401	401	1	RHUM	0.0	1	HE	1.0
CCCore_402A	4021	1	RHUM	0.0	1	HE	1.0
CVCore_402B	4022	1	RHUM	0.0	1	HE	1.0
CVCore_403	403	1	RHUM	0.0	1	HE	1.0
CVCore_404	404	1	RHUM	0.0	1	HE	1.0

CVCore_405	405	1	RHUM	0.0	1	HE	1.0
CVCore_406	406	1	RHUM	0.0	1	HE	1.0
CVCore_407	407	1	RHUM	0.0	1	HE	1.0
CVCore_408	408	1	RHUM	0.0	1	HE	1.0
CVCore_409	409	1	RHUM	0.0	1	HE	1.0
CVCore_501	501	1	RHUM	0.0	1	HE	1.0
CCCore_502A	5021	1	RHUM	0.0	1	HE	1.0
CVCore_502B	5022	1	RHUM	0.0	1	HE	1.0
CVCore_503	503	1	RHUM	0.0	1	HE	1.0
CVCore_504	504	1	RHUM	0.0	1	HE	1.0
CVCore_505	505	1	RHUM	0.0	1	HE	1.0
CVCore_506	506	1	RHUM	0.0	1	HE	1.0
CVCore_507	507	1	RHUM	0.0	1	HE	1.0
CVCore_508	508	1	RHUM	0.0	1	HE	1.0
CVCore_509	509	1	RHUM	0.0	1	HE	1.0
CV001-LP	1	1	RHUM	0.0	1	HE	1.0
CV106-LP	16	1	RHUM	0.0	1	HE	1.0
CV107-LP	17	1	RHUM	0.0	1	HE	1.0
CV206-LP	26	1	RHUM	0.0	1	HE	1.0
CV207-LP	27	1	RHUM	0.0	1	HE	1.0
CV306-LP	36	1	RHUM	0.0	1	HE	1.0
CV307-LP	37	1	RHUM	0.0	1	HE	1.0
CV406-LP	46	1	RHUM	0.0	1	HE	1.0
CV407-LP	47	1	RHUM	0.0	1	HE	1.0
CV506-LP	56	1	RHUM	0.0	1	HE	1.0
CV507-LP	57	1	RHUM	0.0	1	HE	1.0
CV606-LP	66	1	RHUM	0.0	1	HE	1.0
CV607-LP	67	1	RHUM	0.0	1	HE	1.0
CV606-Outlet	661	1	RHUM	0.0	1	HE	1.0
CV607-Outlet	671	1	RHUM	0.0	1	HE	1.0
CoolSource	200	1	RHUM	0.0	1	HE	1.0
CoolSink	2011	1	RHUM	0.0	1	HE	1.0
CV160-Gap	160	1	RHUM	0.0	1	HE	1.0
CV161-Gap	161	1	RHUM	0.0	1	HE	1.0
CV162-Gap	162	1	RHUM	0.0	1	HE	1.0
CV163-Gap	163	1	RHUM	0.0	1	HE	1.0
CV164-Gap	164	1	RHUM	0.0	1	HE	1.0
CV165-Gap	165	1	RHUM	0.0	1	HE	1.0
CV166-Gap	166	1	RHUM	0.0	1	HE	1.0

CV167-Gap	167	1	RHUM	0.0	1	HE	1.0
CV168-Gap	168	1	RHUM	0.0	1	HE	1.0
CV108-UP	1081	1	RHUM	0.0	1	HE	1.0
CV301-Cavity	3011	2	RHUM	0.0	1	N2	0.8
					2	O2	0.2
CV302-Cavity	30211	2	RHUM	0.0	1	N2	0.8
					2	O2	0.2
CV303-Cavity	3031	2	RHUM	0.0	1	N2	0.8
					2	O2	0.2
CV304-Cavity	3041	2	RHUM	0.0	1	N2	0.8
					2	O2	0.2
CV305-Cavity	3051	2	RHUM	0.0	1	N2	0.8
					2	O2	0.2
CV306-Cavity	3061	2	RHUM	0.0	1	N2	0.8
					2	O2	0.2
CV307-Cavity	3071	2	RHUM	0.0	1	N2	0.8
					2	O2	0.2
LH_CV	3081	1	RHUM	0.0	1	HE	1.0

Table B.4.2
CV_VAT for HTTF model

CVNAME	CV_VAT				BASIS
	ICVVZP	NCVZ	CVZ	CVVOL	
CVCR_101	3	1	-0.49590	0.000E+00	All CVCR volumes are meant to satisfy COR input requirements and have negligible hydrodynamic volume. No appreciable convection cooling will occur in the solid center reflector
		2	-0.26700	1.000E-03	
		3	-0.24140	2.000E-03	
CVCR_102	4	1	-0.24140	0.000E+00	
		2	-0.10160	1.000E-03	
		3	-0.02540	2.000E-03	
		4	0.00000	3.000E-03	
CVCR_103	3	1	0.00000	0.000E+00	
		2	0.19820	1.000E-03	
		3	0.39640	2.000E-03	
CVCR_104	3	1	0.39640	0.000E+00	
		2	0.59460	1.000E-03	
		3	0.79280	2.000E-03	
CVCR_105	3	1	0.79280	0.000E+00	
		2	0.99100	1.000E-03	
		3	1.18920	2.000E-03	
CVCR_106	3	1	1.18920	0.000E+00	
		2	1.38740	1.000E-03	
		3	1.58560	2.000E-03	
CVCR_107	3	1	1.58560	0.000E+00	
		2	1.78380	1.000E-03	
		3	1.98200	2.000E-03	
CVCR_108	3	1	1.98200	0.000E+00	
		2	2.00740	1.000E-03	
		3	2.08360	2.000E-03	
CVCR_109	4	1	2.08360	0.000E+00	
		2	2.17780	1.000E-03	
		3	2.27940	2.000E-03	
		4	2.37850	3.000E-03	
CVCore_201	3	1	-0.49590	0.000E+00	R2, Z8-9
		2	-0.26700	6.959E-03	
		3	-0.24140	7.737E-03	
CCCCore_202A	2	1	-0.24140	0.000E+00	
		2	-0.15240	2.706E-03	
CVCore_202B	3	1	-0.15240	0.000E+00	

		2	-0.02540	4.544E-03	
		3	0.00000	5.453E-03	R2, Z11-12
CVCore_203	3	1	0.00000	0.000E+00	
		2	0.19820	7.092E-03	
		3	0.39640	1.418E-02	R2, Z12-13
CVCore_204	3	1	0.39640	0.000E+00	
		2	0.59460	7.092E-03	
		3	0.79280	1.418E-02	R2, Z14-15
CVCore_205	3	1	0.79280	0.000E+00	
		2	0.99100	7.092E-03	
		3	1.18920	1.418E-02	R2, Z16-17
CVCore_206	3	1	1.18920	0.000E+00	
		2	1.38740	7.092E-03	
		3	1.58560	1.418E-02	R2, Z18-19
CVCore_207	3	1	1.58560	0.000E+00	
		3	1.78380	7.092E-03	
		3	1.98200	1.418E-02	R2, Z20-21
CVCore_208	3	1	1.98200	0.000E+00	
		2	2.00740	9.089E-04	
		3	2.08360	3.636E-03	R2, Z22-23
CVCore_209	4	1	2.08360	0.000E+00	
		2	2.17780	3.371E-03	
		3	2.27940	7.006E-03	
		4	2.37850	1.055E-02	R2, Z24-25
CVCore_301	3	1	-0.49590	0.000E+00	
		2	-0.26700	6.263E-03	
		3	-0.24140	6.964E-03	R3, Z8-9
CCCCore_302A	2	1	-0.24140	0.000E+00	
		2	-0.15240	2.435E-03	R3, Z10
CVCore_302B	3	1	-0.15240	0.000E+00	
		2	-0.02540	4.542E-03	
		3	0.00000	5.450E-03	R3, Z11-12
CVCore_303	3	1	0.00000	0.000E+00	
		2	0.19820	7.088E-03	
		3	0.39640	1.418E-02	R3, Z12-13
CVCore_304	3	1	0.39640	0.000E+00	
		2	0.59460	7.088E-03	
		3	0.79280	1.418E-02	R3, Z14-15
CVCore_305	3	1	0.79280	0.000E+00	

		2	0.99100	7.088E-03	
		3	1.18920	1.418E-02	R3, Z16-17
CVCore_306	3	1	1.18920	0.000E+00	
		2	1.38740	7.088E-03	
		3	1.58560	1.418E-02	R3, Z18-19
CVCore_307	3	1	1.58560	0.000E+00	
		3	1.78380	7.088E-03	
		3	1.98200	1.418E-02	R3, Z20-21
CVCore_308	3	1	1.98200	0.000E+00	
		2	2.00740	9.080E-04	
		3	2.08360	3.630E-03	R3, Z22-23
CVCore_309	4	1	2.08360	0.000E+00	
		2	2.17780	3.337E-03	
		3	2.27940	7.002E-03	
		4	2.37850	1.055E-02	R3, Z24-25
CVCore_401	3	1	-0.49590	0.000E+00	
		2	-0.26700	7.655E-03	
		3	-0.24140	8.511E-03	R4, Z8-9
CCCore_402A	2	1	-0.24140	0.000E+00	
		2	-0.15240	2.976E-03	R4, Z10
CVCore_402B	3	1	-0.15240	0.000E+00	
		2	-0.02540	3.714E-03	
		3	0.00000	4.456E-03	R4, Z11-12
CVCore_403	3	1	0.00000	0.000E+00	
		2	0.19820	5.795E-03	
		3	0.39640	1.159E-02	R4, Z12-13
CVCore_404	3	1	0.39640	0.000E+00	
		2	0.59460	5.795E-03	
		3	0.79280	1.159E-02	R4, Z14-15
CVCore_405	3	1	0.79280	0.000E+00	
		2	0.99100	5.795E-03	
		3	1.18920	1.159E-02	R4, Z16-17
CVCore_406	3	1	1.18920	0.000E+00	
		2	1.38740	5.795E-03	
		3	1.58560	1.159E-02	R4, Z18-19
CVCore_407	3	1	1.58560	0.000E+00	
		3	1.78380	5.795E-03	
		3	1.98200	1.159E-02	R4, Z20-21
CVCore_408	3	1	1.98200	0.000E+00	

CVCore_409	4	2	2.00740	7.427E-04	R4, Z22-23	
		3	2.08360	2.971E-03		
		1	2.08360	0.000E+00		
		2	2.17780	2.754E-03		
CVCore_501	3	2	2.27940	5.725E-03	R4, Z24-25	
		3	2.37850	8.623E-03		
		1	-0.49590	0.000E+00		
		2	-0.26700	1.390E-03		
CCCore_502A	2	3	-0.24140	1.550E-03	R5, Z8-9	
		1	-0.24140	0.000E+00		
CVCore_502B	3	2	-0.15240	5.411E-04	R5, Z10	
		1	-0.15240	0.000E+00		
CVCore_503	3	2	-0.02540	1.000E-03	R5, Z11-12	
		3	0.00000	2.000E-03		
		1	0.00000	0.000E+00		
CVCore_504	3	2	0.19820	1.000E-03	R5, Z12-13	
		3	0.39640	2.000E-03		
		1	0.39640	0.000E+00		
CVCore_505	3	2	0.59460	1.000E-03	R5, Z14-15	
		3	0.79280	2.000E-03		
		1	0.79280	0.000E+00		
CVCore_506	3	2	0.99100	1.000E-03	R5, Z16-17	
		3	1.18920	2.000E-03		
		1	1.18920	0.000E+00		
CVCore_507	3	2	1.38740	1.000E-03	R5, Z18-19	
		3	1.58560	2.000E-03		
		1	1.58560	0.000E+00		
CVCore_508	3	3	1.78380	1.000E-03	R5, Z20-21	
		3	1.98200	2.000E-03		
		1	1.98200	0.000E+00		
CVCore_509	4	2	2.00740	1.000E-03	R5, Z22-23	
		3	2.08360	2.000E-03		
		1	2.08360	0.000E+00		
		2	2.17780	1.000E-03		
CV001-LP	6	3	2.27940	2.000E-03	R5, Z24-25	
		4	2.37850	3.000E-03		
		1	-1.65420	0.000E+00		Z1
		2	-1.38110	2.000E-03		Z2
		3	-1.10800	3.000E-03	Z3	

		4	-0.83500	4.000E-03	Z4
		5	-0.79590	5.000E-03	Z5
		6	-0.71750	6.000E-03	Bottom of Z6
CV106-LP	2	1	-0.71750	0.000E+00	
		2	-0.60670	1.000E-03	Negligible volume, in center ref. region
CV107-LP	2	1	-0.60670	0.000E+00	
		2	-0.49590	1.000E-03	Negligible volume
CV206-LP	2	1	-0.71750	0.000E+00	
		2	-0.60670	2.227E-02	R2, Z6
CV207-LP	2	1	-0.60670	0.000E+00	
		2	-0.49590	2.270E+00	R2 Z7
CV306-LP	2	1	-0.71750	0.000E+00	
		2	-0.60670	2.270E+00	R3, Z6
CV307-LP	2	1	-0.60670	0.000E+00	
		2	-0.49590	2.270E+00	R3, Z7
CV406-LP	2	1	-0.71750	0.000E+00	
		2	-0.60670	2.270E+00	R4, Z6
CV407-LP	2	1	-0.60670	0.000E+00	
		2	-0.49590	2.270E+00	R4, Z7
CV506-LP	2	1	-0.71750	0.000E+00	
		2	-0.60670	1.550E-01	R5, Z6
CV507-LP	2	1	-0.60670	0.000E+00	
		2	-0.49590	1.550E-01	R5, Z7
CV606-LP	2	1	-0.71750	0.000E+00	
		2	-0.60670	1.070E-01	R6, Z6
CV607-LP	2	1	-0.60670	0.000E+00	
		2	-0.49590	1.070E-01	R6, Z7
CV606-Outlet	2	1	-0.71750	0.000E+00	
		2	-0.60670	1.066E-01	Upper outlet duct
CV607-Outlet	2	1	-0.60670	0.000E+00	
		2	-0.49590	1.066E-01	Lower outlet duct
CoolSource	2	1	-0.87310	0.000E+00	
		2	0.00000	1.000E-01	Arbitrary volume
CoolSink	2	1	-0.71750	0.000E+00	
		2	-0.49590	1.000E-01	Arbitrary volume
CV160-Gap	2	1	-0.87310	0.000E+00	
		2	0.00000	6.600E-02	Gap volumes represent the up-comer region
CV161-Gap	2	1	0.00000	0.000E+00	
		2	0.39640	2.990E-02	

CV162-Gap	2	1	0.39640	0.000E+00	
		2	0.79280	2.990E-02	
CV163-Gap	2	1	0.79280	0.000E+00	
		2	1.18920	2.990E-02	
CV164-Gap	2	1	1.18920	0.000E+00	
		2	1.58560	2.990E-02	
CV165-Gap	2	1	1.58560	0.000E+00	
		2	1.98200	2.990E-02	
CV166-Gap	2	1	1.98200	0.000E+00	
		2	2.08360	7.690E-03	
CV167-Gap	2	1	2.08360	0.000E+00	
		2	2.37850	2.230E-02	
CV168-Gap	2	1	2.37850	0.000E+00	
		2	2.49590	8.880E-03	
CV108-UP	3	1	2.37850	0.000E+00	
		2	2.49590	2.037E-01	
		3	3.14050	2.100E-01	
CV301-Cavity	2	1	-0.87310	0.000E+00	
		2	0.00000	7.484E-01	
CV302-Cavity	2	1	0.00000	0.000E+00	
		2	0.39640	3.398E-01	
CV303-Cavity	2	1	0.39650	0.000E+00	
		2	0.79280	3.398E-01	
CV304-Cavity	2	1	0.79280	0.000E+00	
		2	1.18920	3.398E-01	
CV305-Cavity	2	1	1.18920	0.000E+00	
		2	1.58560	3.398E-01	
CV306-Cavity	2	1	1.58560	0.000E+00	
		2	1.98200	3.398E-01	
CV307-Cavity	3	1	1.98200	0.000E+00	
		2	2.37850	3.398E-01	
		3	3.21050	3.400E-01	

Table B.5
FL input for HTTF model

<i>CARD</i>	<i>WORD</i>	<i>VALUE</i>	<i>BASIS</i>
FL_INPUT	-	-	Signal start of FL input
FL_ID	FPNAME		FL name
	IFPNUM		User-defined FL number
FL_FT	KCVFM	Table B.5.1	Name of "from" control volume
	KCVTO		Name of "to" control volume
	ZFM		Altitude of "from" junction
	ZTO		Altitude of "to" junction
FL_GEO	FLARA		Flow path area
	FLEN		Flow path length
	FLOPO		Flow path open fraction
	FLHGTF		Junction opening height, "from"
	FLHGTT		Junction opening height, "to"
	FL_JSW	KFLGFL	Table B.5.2
FL_SEG	IPNSG		Number of segments
	NSEG		Table row index
	SAREA		Segment flow area
	SLEN		Segment flow length
	SHYD		Segment hydraulic diameter
	FL_VTM	NVOFT	1
NFLT		1	Table row index
FLNAME		FLfromSource	Name of time-dependent flow path
NTFLAG		CF	Flag for CF or TF defining velocity vs. time
NFUN		HeSource	Name of CF or TF

Table B.5. 1
FL_FT for HTTF model

FL_ID		FL_FT			
FPNAME	IFPNUM	KCVFM	KCVTO	ZFM	ZTO
Gap-FL161	161	CV160-Gap	CV161-Gap	0.0000	0.0000
Gap-FL162	162	CV161-Gap	CV162-Gap	0.3964	0.3964
Gap-FL163	163	CV162-Gap	CV163-Gap	0.7928	0.7928
Gap-FL164	164	CV163-Gap	CV164-Gap	1.1892	1.1892
Gap-FL165	165	CV164-Gap	CV165-Gap	1.5856	1.5856
Gap-FL166	166	CV165-Gap	CV166-Gap	1.9820	1.9820
Gap-FL167	167	CV166-Gap	CV167-Gap	2.0836	2.0836
Gap-FL168	168	CV167-Gap	CV168-Gap	2.3785	2.3785
UP-FL108	108	CV168-Gap	CV108-UP	2.4372	2.4372
FL_108to209	209	CV108-UP	CVCore_209	2.3785	2.3785
FL_209to208	208	CVCore_209	CVCore_208	2.0836	2.0836
FL_208to207	207	CVCore_208	CVCore_207	1.9820	1.9820
FL_207to206	206	CVCore_207	CVCore_206	1.5856	1.5856
FL_206to205	205	CVCore_206	CVCore_205	1.1892	1.1892
FL_205to204	204	CVCore_205	CVCore_204	0.7928	0.7928
FL_204to203	203	CVCore_204	CVCore_203	0.3964	0.3964
FL_203to202B	2022	CVCore_203	CVCore_202B	0.0000	0.0000
FL_202Bto202A	2021	CVCore_202B	CVCore_202A	-0.1524	-0.1524
FL_202Ato201	201	CVCore_202A	CVCore_201	-0.2414	-0.2414
FL_108to309	309	CV108-UP	CVCore_309	2.3785	2.3785
FL_309to308	308	CVCore_309	CVCore_308	2.0836	2.0836
FL_308to307	307	CVCore_308	CVCore_307	1.9820	1.9820
FL_307to306	306	CVCore_307	CVCore_306	1.5856	1.5856
FL_306to305	305	CVCore_306	CVCore_305	1.1892	1.1892
FL_305to304	304	CVCore_305	CVCore_304	0.7928	0.7928
FL_304to303	303	CVCore_304	CVCore_303	0.3964	0.3964
FL_303to302B	3022	CVCore_303	CVCore_302B	0.0000	0.0000
FL_302Bto302A	3021	CVCore_302B	CVCore_302A	-0.1524	-0.1524
FL_302Ato301	301	CVCore_302A	CVCore_301	-0.2414	-0.2414
FL_108to409	409	CV108-UP	CVCore_409	2.3785	2.3785
FL_409to408	408	CVCore_409	CVCore_408	2.0836	2.0836
FL_408to407	407	CVCore_408	CVCore_407	1.9820	1.9820
FL_407to406	406	CVCore_407	CVCore_406	1.5856	1.5856
FL_406to405	405	CVCore_406	CVCore_405	1.1892	1.1892
FL_405to404	404	CVCore_405	CVCore_404	0.7928	0.7928
FL_404to403	403	CVCore_404	CVCore_403	0.3964	0.3964
FL_403to402B	4022	CVCore_403	CVCore_402B	0.0000	0.0000

FL_402Bto402A	4021	CVCore_402B	CVCore_402A	-0.1524	-0.1524
FL_402Ato401	401	CVCore_402A	CVCore_401	-0.2414	-0.2414
FL_108to509	509	CV108-UP	CVCore_509	2.3785	2.3785
FL_509to508	508	CVCore_509	CVCore_508	2.0836	2.0836
FL_508to507	507	CVCore_508	CVCore_507	1.9820	1.9820
FL_507to506	506	CVCore_507	CVCore_506	1.5856	1.5856
FL_506to505	505	CVCore_506	CVCore_505	1.1892	1.1892
FL_505to504	504	CVCore_505	CVCore_504	0.7928	0.7928
FL_504to503	503	CVCore_504	CVCore_503	0.3964	0.3964
FL_503to502B	5022	CVCore_503	CVCore_502B	0.0000	0.0000
FL_402Bto502A	5021	CVCore_402B	CVCore_502A	-0.1524	-0.1524
FL_502Ato501	501	CVCore_502A	CVCore_501	-0.2414	-0.2414
FL_201to207LP	2207	CVCore_201	CV207-LP	-0.4959	-0.4959
FL_207LPto206LP	2206	CV207-LP	CV206-LP	-0.6067	-0.6067
FL_301to307LP	2307	CVCore_301	CV307-LP	-0.4959	-0.4959
FL_307LPto306LP	2306	CV307-LP	CV306-LP	-0.6067	-0.6067
FL_401to407LP	2407	CVCore_401	CV407-LP	-0.4959	-0.4959
FL_407LPto406LP	2406	CV407-LP	CV406-LP	-0.6067	-0.6067
FL501to507LP	2507	CVCore_501	CV507-LP	-0.4959	-0.4959
FL_507LPto506LP	2506	CV507-LP	CV506-LP	-0.6067	-0.6067
FL_607LPto606LP	2606	CV607-LP	CV606-LP	-0.6067	-0.6067
FL_207LPto307LP	3307	CV207-LP	CV307-LP	-0.5513	-0.5513
FL_307LPto407LP	3407	CV307-LP	CV407-LP	-0.5513	-0.5513
FL_407LPto507LP	3507	CV407-LP	CV507-LP	-0.5513	-0.5513
FL_507LPto607LP	3607	CV507-LP	CV607-LP	-0.5513	-0.5513
FL_206LPto306LP	3306	CV206-LP	CV306-LP	-0.6621	-0.6621
FL_306LPto406LP	3406	CV306-LP	CV406-LP	-0.6621	-0.6621
FL_406LPto506LP	3506	CV406-LP	CV506-LP	-0.6621	-0.6621
FL_506LPto606LP	3606	CV506-LP	CV606-LP	-0.6621	-0.6621
FL_607LPtoOUT	3707	CV607-LP	CV607-Outlet	-0.5513	-0.5513
FL_606LPtoOUT	3706	CV606-LP	CV606-Outlet	-0.6621	-0.6621
FLtoSinkLow	3806	CV606-Outlet	CoolSink	-0.6621	-0.6621
FLtoSinkHigh	3807	CV607-Outlet	CoolSink	-0.5513	-0.5513
FLfromSource	200	CoolSource	CV160-Gap	-0.4366	-0.4366

Table B.5.2
FL geometric parameters for HTTF model

FPNAME	FLARA	FLEN	KFLGFL	NSEG	SAREA	SLEN	SHYD
Gap-FL161	7.564E-02	1.270	0	1	7.564E-02	1.270	6.214E-02
Gap-FL162	7.564E-02	0.793	0	1	7.564E-02	0.793	6.214E-02
Gap-FL163	7.564E-02	0.793	0	1	7.564E-02	0.793	6.214E-02
Gap-FL164	7.564E-02	0.793	0	1	7.564E-02	0.793	6.214E-02
Gap-FL165	7.564E-02	0.793	0	1	7.564E-02	0.793	6.214E-02
Gap-FL166	7.564E-02	0.498	0	1	7.564E-02	0.498	6.214E-02
Gap-FL167	7.564E-02	0.397	0	1	7.564E-02	0.397	6.214E-02
Gap-FL168	7.564E-02	0.412	0	1	7.564E-02	0.412	6.214E-02
UP-FL108	7.548E-02	0.500	0	1	7.548E-02	0.500	6.191E-02
FL_108to209	3.578E-02	0.412	0	1	3.578E-02	0.412	1.676E-02
FL_209to208	3.578E-02	0.397	0	1	3.578E-02	0.397	1.676E-02
FL_208to207	3.578E-02	0.498	0	1	3.578E-02	0.498	1.676E-02
FL_207to206	3.578E-02	0.793	0	1	3.578E-02	0.793	1.676E-02
FL_206to205	3.578E-02	0.793	0	1	3.578E-02	0.793	1.676E-02
FL_205to204	3.578E-02	0.793	0	1	3.578E-02	0.793	1.676E-02
FL_204to203	3.578E-02	0.793	0	1	3.578E-02	0.793	1.676E-02
FL_203to202B	3.578E-02	0.549	0	1	3.578E-02	0.549	1.676E-02
FL_202Bto202A	3.578E-02	0.241	0	1	3.578E-02	0.152	1.676E-02
				2	3.040E-02	0.109	2.540E-02
FL_202Ato201	3.040E-02	0.344	0	1	3.040E-02	0.344	2.540E-02
FL_108to309	3.576E-02	0.412	0	1	3.576E-02	0.412	1.676E-02
FL_309to308	3.576E-02	0.397	0	1	3.576E-02	0.397	1.676E-02
FL_308to307	3.576E-02	0.498	0	1	3.576E-02	0.498	1.676E-02
FL_307to306	3.576E-02	0.793	0	1	3.576E-02	0.793	1.676E-02
FL_306to305	3.576E-02	0.793	0	1	3.576E-02	0.793	1.676E-02
FL_305to304	3.576E-02	0.793	0	1	3.576E-02	0.793	1.676E-02
FL_304to303	3.576E-02	0.793	0	1	3.576E-02	0.793	1.676E-02
FL_303to302B	3.576E-02	0.498	0	1	3.576E-02	0.498	1.676E-02
FL_302Bto302A	2.736E-02	0.241	0	1	3.576E-02	0.152	1.676E-02
				2	2.736E-02	0.089	2.540E-02
FL_302Ato301	2.736E-02	0.344	0	1	2.736E-02	0.344	2.540E-02
FL_108to409	2.924E-02	0.412	0	1	2.924E-02	0.412	1.676E-02
FL_409to408	2.924E-02	0.397	0	1	2.924E-02	0.397	1.676E-02
FL_408to407	2.924E-02	0.498	0	1	2.924E-02	0.498	1.676E-02
FL_407to406	2.924E-02	0.793	0	1	2.924E-02	0.793	1.676E-02
FL_406to405	2.924E-02	0.793	0	1	2.924E-02	0.793	1.676E-02
FL_405to404	2.924E-02	0.793	0	1	2.924E-02	0.793	1.676E-02
FL_404to403	2.924E-02	0.793	0	1	2.924E-02	0.793	1.676E-02

FL_403to402B	2.924E-02	0.549	0	1	2.924E-02	0.549	1.676E-02
FL_402Bto402A	2.924E-02	0.241	0	1	2.924E-02	0.152	1.676E-02
				2	3.344E-02	0.089	2.540E-02
FL_402Ato401	3.344E-02	0.344	0	1	3.344E-02	0.344	2.540E-02
FL_108to509	1.000E-10	0.412	0	1	1.000E-10	0.412	1.676E-02
FL_509to508	1.000E-10	0.397	0	1	1.000E-10	0.397	1.676E-02
FL_508to507	1.000E-10	0.498	0	1	1.000E-10	0.498	1.676E-02
FL_507to506	1.000E-10	0.793	0	1	1.000E-10	0.793	1.676E-02
FL_506to505	1.000E-10	0.793	0	1	1.000E-10	0.793	1.676E-02
FL_505to504	1.000E-10	0.793	0	1	1.000E-10	0.793	1.676E-02
FL_504to503	1.000E-10	0.793	0	1	1.000E-10	0.793	1.676E-02
FL_503to502B	1.000E-10	0.498	0	1	1.000E-10	0.498	1.676E-02
FL_402Bto502A	2.942E-02	0.241	0	1	2.942E-02	0.152	1.676E-02
				2	6.080E-03	0.089	2.540E-02
FL_502Ato501	6.080E-03	0.345	0	1	6.080E-03	0.345	2.540E-02
FL_201to207LP	3.040E-02	0.365	0	1	3.040E-02	0.365	2.540E-02
FL_207LPto206LP	2.010E-01	0.222	0	1	2.010E-01	0.222	2.604E-01
FL_301to307LP	2.736E-02	0.365	0	1	2.736E-02	0.365	2.540E-02
FL_307LPto306LP	2.010E-01	0.222	0	1	2.010E-01	0.222	1.798E-01
FL_401to407LP	3.344E-02	0.365	0	1	3.344E-02	0.365	2.540E-02
FL_407LPto406LP	2.010E-01	0.222	0	1	2.010E-01	0.222	1.466E-01
FL501to507LP	5.411E-04	0.365	0	1	5.411E-04	0.365	2.540E-02
FL_507LPto506LP	4.340E-01	0.222	0	1	4.340E-01	0.222	2.564E-01
FL_607LPto606LP	9.650E-01	0.222	0	1	9.650E-01	0.222	4.320E-01
FL_207LPto307LP	2.169E-01	0.110	3	1	2.169E-01	0.110	2.216E-01
FL_307LPto407LP	2.795E-01	0.082	3	1	2.795E-01	0.082	2.216E-01
FL_407LPto507LP	3.305E-01	0.101	3	1	3.305E-01	0.101	2.216E-01
FL_507LPto607LP	4.198E-01	0.172	3	1	4.198E-01	0.172	2.216E-01
FL_206LPto306LP	2.169E-01	0.110	3	1	2.169E-01	0.110	2.216E-01
FL_306LPto406LP	2.795E-01	0.082	3	1	2.795E-01	0.082	2.216E-01
FL_406LPto506LP	3.305E-01	0.101	3	1	3.305E-01	0.101	2.216E-01
FL_506LPto606LP	4.198E-01	0.172	3	1	4.198E-01	0.172	2.216E-01
FL_607LPtoOUT	6.996E-02	0.489	3	1	6.996E-02	0.489	3.647E-01
FL_606LPtoOUT	6.996E-02	0.489	3	1	6.996E-02	0.489	3.647E-01
FLtoSinkLow	6.996E-02	0.500	3	1	6.996E-02	0.500	3.647E-01
FLtoSinkHigh	6.996E-02	0.500	3	1	6.996E-02	0.500	3.647E-01
FLfromSource	7.564E-02	0.100	0	1	7.564E-02	0.100	6.214E-02

Table B.6
HS input for HTTF model

<i>CARD</i>	<i>WORD</i>	<i>VALUE</i>	<i>BASIS</i>
HS_INPUT	-	-	Signal start of HS input
HS_ID	HSNAME		HS name
	NUM		User-defined HS number
HS_GD	IGEOM	Table B.6.1	HS geometry
HS_EOD	HSALT		HS bottom elevation
	ALPHA		HS orientation
HS_SRC	ISRC	NO	Internal Power Source Flag
HS_ND	NP		Number of temperature nodes
	N	Table B.6.1	Node index
	XI		Spatial node location
	MATNAM		Material name associated with node N
HS_LB	IBCL	CALCCOEFHS	Boundary condition type
	IBVL	Table B.6.2	Boundary control volume name
	MTEVAL	NO	Switch to evaluate mass transfer at boundary
HS_LBP	IFLOWL	INT	Internal/external flow flag
	CPFPL	0.0	Critical pool fraction
	CPFAL	0.0	Critical pool fraction for atmosphere
HS_LBF	IOPTL		Fluid temperature options for LHS
	NUMAXL	Table B.6.2	Axial level of coupled core cell if necessary
	NUMRAD		Radial ring of coupled core cell if necessary
HS_LBS	ASURFL	1.0	LHS area, calculate internally for cylinders
	CLNL		LHS characteristic length, cylinder height
	BNDZL	Table B.6.2	Heat structure LHS boundary height, cylinder height
HS_LBR	EMISWL	0.8	Surface material emissivity (LHS)
	RMODL	EQUIV-BAND	Radiation model flag (LHS)
	PATHL	0.0508	Radiation path length (LHS)
HS_RB	for RHS , See HS_LB		Same as HS_LB, but for RHS
HS_RBR	for RHS , See HS_LBR		Same as HS_LBR, but for RHS
HS_RBP	for RHS , See HS_LBP	Table B.6.3	Same as HS_LBP, but for RHS
HS_RBS	for RHS , See HS_LBS		Same as HS_LBS, but for RHS
HS_FT	IFTNUM	OFF	Film tracking on/off switch

Table B.6.1
HS geometric parameters for HTTF model

HS_ID		HS_GD	HS_EOD		HS_ND		
HSNAME	IHSNUM	IGEOM	HSALT	ALPHA	N	XI	MATNAM
LPR_MS-04	50004	CYLINDRICAL	-0.8350	1.0	1	0.603	SS304
					2	0.7	SS304
					3	0.743	SS304
					4	0.762	SS304
LPR_MS-05	50005	CYLINDRICAL	-0.7969	1	1	0.603	ALUMINUM
					2	0.7	ALUMINUM
					3	0.743	SS304
					4	0.762	SS304
LPR_MS-06	50006	CYLINDRICAL	-0.7175	1.0	1	0.603	SS304
					2	0.7	SS304
					3	0.743	SS304
					4	0.762	SS304
LPR_MS-07	50007	CYLINDRICAL	-0.6067	1.0	1	0.603	SS304
					2	0.7	SS304
					3	0.743	SS304
					4	0.762	SS304
LPR_MS-08	50008	CYLINDRICAL	-0.4959	1	1	0.603	ALUMINUM
					2	0.7	ALUMINUM
					3	0.743	SS304
					4	0.762	SS304
CB-09	50009	CYLINDRICAL	-0.267	1	1	0.603	SS304
					2	0.7	SS304
					3	0.743	SS304
					4	0.762	SS304
SR_CB-10	50010	CYLINDRICAL	-0.2414	1.0	1	0.603	ALUMINUM
					2	0.7	ALUMINUM
					3	0.743	SS304
					4	0.762	SS304
SR_CB-11	50011	CYLINDRICAL	-0.1524	1	1	0.603	ALUMINUM
					2	0.7	ALUMINUM
					3	0.743	SS304
					4	0.762	SS304
SR_CB-12	50012	CYLINDRICAL	-0.0254	1	1	0.603	ALUMINUM
					2	0.7	ALUMINUM
					3	0.743	SS304
					4	0.762	SS304
SR_CB-13	50013	CYLINDRICAL	0.0000	1.0	1	0.603	ALUMINUM

SR_CB-14	50014	CYLINDRICAL	0.1982	1	2	0.7	ALUMINUM
					3	0.743	SS304
					4	0.762	SS304
					1	0.603	ALUMINUM
SR_CB-15	50015	CYLINDRICAL	0.3964	1	2	0.7	ALUMINUM
					3	0.743	SS304
					4	0.762	SS304
					1	0.603	ALUMINUM
SR_CB-16	50016	CYLINDRICAL	0.5946	1.0	2	0.7	ALUMINUM
					3	0.743	SS304
					4	0.762	SS304
					1	0.603	ALUMINUM
SR_CB-17	50017	CYLINDRICAL	0.7928	1	2	0.7	ALUMINUM
					3	0.743	SS304
					4	0.762	SS304
					1	0.603	ALUMINUM
SR_CB-18	50018	CYLINDRICAL	0.991	1	2	0.7	ALUMINUM
					3	0.743	SS304
					4	0.762	SS304
					1	0.603	ALUMINUM
SR_CB-19	50019	CYLINDRICAL	1.1892	1.0	2	0.7	ALUMINUM
					3	0.743	SS304
					4	0.762	SS304
					1	0.603	ALUMINUM
SR_CB-20	50020	CYLINDRICAL	1.3874	1.0	2	0.7	ALUMINUM
					3	0.743	SS304
					4	0.762	SS304
					1	0.603	ALUMINUM
SR_CB-21	50021	CYLINDRICAL	1.5856	1.0	2	0.7	ALUMINUM
					3	0.743	SS304
					4	0.762	SS304
					1	0.603	ALUMINUM
SR_CB-22	50022	CYLINDRICAL	1.7838	1.0	2	0.7	ALUMINUM
					3	0.743	SS304
					4	0.762	SS304
					1	0.603	ALUMINUM
SR_CB-23	50023	CYLINDRICAL	1.9820	1.0	3	0.743	SS304
					4	0.762	SS304
					1	0.603	ALUMINUM
					2	0.7	ALUMINUM

SR_CB-24	50024	CYLINDRICAL	2.0074	1.0	3	0.743	SS304
					4	0.762	SS304
					1	0.603	ALUMINUM
					2	0.7	ALUMINUM
SR_CB-25	50025	CYLINDRICAL	2.0836	1.0	3	0.743	SS304
					4	0.762	SS304
					1	0.603	ALUMINUM
					2	0.7	ALUMINUM
SR_CB-26	50026	CYLINDRICAL	2.1778	1.0	3	0.743	SS304
					4	0.762	SS304
					1	0.603	ALUMINUM
					2	0.7	ALUMINUM
SR_CB-27	50027	CYLINDRICAL	2.2794	1.0	3	0.743	SS304
					4	0.762	SS304
					1	0.603	SS304
					2	0.7	SS304
CB_TOP	50028	TOPHALFSPHERE	2.3785	1.0000	3	0.743	SS304
					4	0.762	SS304
					1	0.743	SS304
					2	0.819	SS304
RPV-00	60000	CYLINDRICAL	-0.8731	1.0000	1	0.819	SS304
					2	0.832	SS304
RPV-01	60001	CYLINDRICAL	0	1.0000	1	0.819	SS304
					2	0.832	SS304
RPV-02	60002	CYLINDRICAL	0.3964	1.0000	1	0.819	SS304
					2	0.832	SS304
RPV-03	60003	CYLINDRICAL	0.7928	1.0000	1	0.819	SS304
					2	0.832	SS304
RPV-04	60004	CYLINDRICAL	1.1892	1.0000	1	0.819	SS304
					2	0.832	SS304
RPV-05	60005	CYLINDRICAL	1.5856	1.0000	1	0.819	SS304
					2	0.832	SS304
RPV-06	60006	CYLINDRICAL	1.982	1.0000	1	0.819	SS304
					2	0.832	SS304
RPV-07	60007	CYLINDRICAL	2.0836	1.0000	1	0.819	SS304
					2	0.832	SS304
RCCS-00	70000	CYLINDRICAL	-0.8731	1.0000	1	1.022	SS304
					2	1.082	SS304
RCCS-01	70001	CYLINDRICAL	0	1.0000	1	1.022	SS304
					2	1.082	SS304
RCCS-02	70002	CYLINDRICAL	0.3964	1.0000	1	1.022	SS304

RCCS-03	70003	CYLINDRICAL	0.7928	1.0000	2	1.082	SS304
					1	1.022	SS304
RCCS-04	70004	CYLINDRICAL	1.1892	1.0000	2	1.082	SS304
					1	1.022	SS304
RCCS-05	70005	CYLINDRICAL	1.5856	1.0000	2	1.082	SS304
					1	1.022	SS304
RCCS-06	70006	CYLINDRICAL	1.982	1.0000	2	1.082	SS304
					1	1.022	SS304
RCCS-07	70007	CYLINDRICAL	2.0836	1.0000	2	1.082	SS304
					1	1.022	SS304

Table B.6.2
HS LHS boundary conditions for HTTF model

HSNAME	HS_LB	IOPTL	HS_LBF		HS_LBS	
	IBVL		NUMAXL	NUMRAD	CLNL	BNDZL
LPR_MS-04	CV001-LP	DTDZ	4	6	0.03810	0.03810
LPR_MS-05	CV001-LP	DTDZ	5	6	0.07940	0.07940
LPR_MS-06	CV506-LP	DTDZ	6	6	0.11080	0.11080
LPR_MS-07	CV507-LP	DTDZ	7	6	0.11080	0.11080
LPR_MS-08	CVCore_501	DTDZ	8	6	0.22890	0.22890
CB-09	CVCore_501	DTDZ	9	6	0.02560	0.02560
SR_CB-10	CVCore_502A	DTDZ	10	6	0.08900	0.08900
SR_CB-11	CVCore_502B	DTDZ	11	6	0.12700	0.12700
SR_CB-12	CVCore_502B	DTDZ	12	6	0.02540	0.02540
SR_CB-13	CVCore_503	DTDZ	13	6	0.19820	0.19820
SR_CB-14	CVCore_503	DTDZ	14	6	0.19820	0.19820
SR_CB-15	CVCore_504	DTDZ	15	6	0.19820	0.19820
SR_CB-16	CVCore_504	DTDZ	16	6	0.19820	0.19820
SR_CB-17	CVCore_505	DTDZ	17	6	0.19820	0.19820
SR_CB-18	CVCore_505	DTDZ	18	6	0.19820	0.19820
SR_CB-19	CVCore_506	DTDZ	19	6	0.19820	0.19820
SR_CB-20	CVCore_506	DTDZ	20	6	0.19820	0.19820
SR_CB-21	CVCore_507	DTDZ	21	6	0.19820	0.19820
SR_CB-22	CVCore_507	DTDZ	22	6	0.19820	0.19820
SR_CB-23	CVCore_508	DTDZ	23	6	0.02540	0.02540
SR_CB-24	CVCore_508	DTDZ	24	6	0.07620	0.07620

SR_CB-25	CVCore_509	DTDZ	25	6	0.09420	0.09420
SR_CB-26	CVCore_509	DTDZ	26	6	0.10160	0.10160
SR_CB-27	CVCore_509	DTDZ	27	6	0.09910	0.09910
CB_TOP	CV108-UP	-	-	-	0.76200	0.76200
RPV-00	CV160-Gap	-	-	-	0.87310	0.87310
RPV-01	CV161-Gap	-	-	-	0.39640	0.39640
RPV-02	CV162-Gap	-	-	-	0.39640	0.39640
RPV-03	CV163-Gap	-	-	-	0.39640	0.39640
RPV-04	CV164-Gap	-	-	-	0.39640	0.39640
RPV-05	CV165-Gap	-	-	-	0.39640	0.39640
RPV-06	CV166-Gap	-	-	-	0.10160	0.10160
RPV-07	CV167-Gap	-	-	-	0.29490	0.29490
RCCS-00	CV301-Cavity	-	-	-	0.87310	0.87310
RCCS-01	CV302-Cavity	-	-	-	0.39640	0.39640
RCCS-02	CV303-Cavity	-	-	-	0.39640	0.39640
RCCS-03	CV304-Cavity	-	-	-	0.39640	0.39640
RCCS-04	CV305-Cavity	-	-	-	0.39640	0.39640
RCCS-05	CV306-Cavity	-	-	-	0.39640	0.39640
RCCS-06	CV307-Cavity	-	-	-	0.10160	0.10160
RCCS-07	CV307-Cavity	-	-	-	0.29490	0.29490

Table B.6.3
HS RHS boundary conditions for HTTF model

HSNAME	HS_RB		HS_RBP	HS_RBS	
	IBCR	IBVR		IFLOWR	CLNR
LPR_MS-04	CALCCOEFHS	CV160-Gap	INT	0.03810	0.03810
LPR_MS-05	CALCCOEFHS	CV160-Gap	INT	0.07940	0.07940
LPR_MS-06	CALCCOEFHS	CV160-Gap	INT	0.11080	0.11080
LPR_MS-07	CALCCOEFHS	CV160-Gap	INT	0.11080	0.11080
LPR_MS-08	CALCCOEFHS	CV160-Gap	INT	0.22890	0.22890
CB-09	CALCCOEFHS	CV160-Gap	INT	0.02560	0.02560
SR_CB-10	CALCCOEFHS	CV160-Gap	INT	0.08900	0.08900
SR_CB-11	CALCCOEFHS	CV160-Gap	INT	0.12700	0.12700
SR_CB-12	CALCCOEFHS	CV160-Gap	INT	0.02540	0.02540
SR_CB-13	CALCCOEFHS	CV161-Gap	INT	0.19820	0.19820
SR_CB-14	CALCCOEFHS	CV161-Gap	INT	0.19820	0.19820
SR_CB-15	CALCCOEFHS	CV162-Gap	INT	0.19820	0.19820
SR_CB-16	CALCCOEFHS	CV162-Gap	INT	0.19820	0.19820

SR_CB-17	CALCCOEFHS	CV163-Gap	INT	0.19820	0.19820
SR_CB-18	CALCCOEFHS	CV163-Gap	INT	0.19820	0.19820
SR_CB-19	CALCCOEFHS	CV164-Gap	INT	0.19820	0.19820
SR_CB-20	CALCCOEFHS	CV164-Gap	INT	0.19820	0.19820
SR_CB-21	CALCCOEFHS	CV165-Gap	INT	0.19820	0.19820
SR_CB-22	CALCCOEFHS	CV165-Gap	INT	0.19820	0.19820
SR_CB-23	CALCCOEFHS	CV166-Gap	INT	0.02540	0.02540
SR_CB-24	CALCCOEFHS	CV166-Gap	INT	0.07620	0.07620
SR_CB-25	CALCCOEFHS	CV167-Gap	INT	0.09420	0.09420
SR_CB-26	CALCCOEFHS	CV167-Gap	INT	0.10160	0.10160
SR_CB-27	CALCCOEFHS	CV167-Gap	INT	0.09910	0.09910
CB_TOP	SYMMETRY	-	-	0.74300	0.74300
RPV-00	CALCCOEFHS	CV301-Cavity	EXT	0.87310	0.87310
RPV-01	CALCCOEFHS	CV302-Cavity	EXT	0.39640	0.39640
RPV-02	CALCCOEFHS	CV303-Cavity	EXT	0.39640	0.39640
RPV-03	CALCCOEFHS	CV304-Cavity	EXT	0.39640	0.39640
RPV-04	CALCCOEFHS	CV305-Cavity	EXT	0.39640	0.39640
RPV-05	CALCCOEFHS	CV306-Cavity	EXT	0.39640	0.39640
RPV-06	CALCCOEFHS	CV307-Cavity	EXT	0.10160	0.10160
RPV-07	CALCCOEFHS	CV307-Cavity	EXT	0.29490	0.29490
RCCS-00	TempCF	-	-	-	-
RCCS-01	TempCF	-	-	-	-
RCCS-02	TempCF	-	-	-	-
RCCS-03	TempCF	-	-	-	-
RCCS-04	TempCF	-	-	-	-
RCCS-05	TempCF	-	-	-	-
RCCS-06	TempCF	-	-	-	-
RCCS-07	TempCF	-	-	-	-

Table B.7
COR input for HTTF input

COR_INPUT	-	-	Signal start of COR input
COR_RT	IRTYP	PMR	Reactor type flag
	MCRP	B4C	Poison (insignificant for purposes of this calculation)
COR_GP	RFUEL	0.01905	Fuel rod (i.e. fuel compact) outer radius
	RCLAD	0.02631	Clad outer radius, obtained as described in section ?
	DRGAP	0.00E+00	Gap between fuel/clad (i.e. compact and graphite)
	PITCH	0.05207	Fuel rod (i.e. fuel compact) center-to-center distance
COR_VP	RCOR	0.603	Outer radius for active core region
	RVESS	0.819	Inner radius of vessel
	ILHTRN	RVESS	LH transition type (inconsequential in this calculation)
	DZRV	0.01905	Vessel wall thickness
	DZLH	0.01905	LH thickness (inconsequential in this calculation)
	ILHTYP	HEMISPHERE	LH geometry (inconsequential in this calculation)
	RVLH	0.819	For hemispherical lower head, radius of curvature
COR_AVP	HLST	-0.835	Elevation below which the lower head models apply
	HCSP	-0.267	Elevation of core support plate, > HLST
COR_TP	NTPCOR	NO	TP for CAV/FDI (inconsequential)
	RNTPCOR	NO	TP name for radionuclides (inconsequential)
	ICFGAP	NO	Gap conductance CF name (inconsequential)
	ICFFIS	FISPOWALL	CF option, FISPOWALL = whole-core power
	CFNAME	CORE-POWER	CF name giving fission power
COR_MS	IEUMOD	0	Materials interactions switch (inconsequential)
	IHSDT	0	HS boundary condition switch, set to required DT/DZ model usage
	IDTDZ	0	DT/DZ inlet specification option switch
	ICORCV	1	COR/CVH volume consistency switch
COR_BCP	ICBCD	CB	Component Mnemonic for conductor
	MATBCD	HE	Gap material between core and the heat structures
	DXBCD	1.00E-04	Gap thickness
	CDFBCD	8.03E-04	Thermal diffusion constant
COR_CLM	CLMAT	GRAPH	Identifier for cladding material
COR_RFM	RFMAT	GRAPH	Identifier for reflector material
COR_LP	IAXSUP	4	Axial level of support plate (inconsequential)
	HDBH2O	100	HTC from in-vessel falling debris (inconsequential)
	PPFAIL	2.00E+07	Differential pressure for LH failure (inconsequential)
	VFALL	1	Falling debris velocity (inconsequential)
COR_TKE	TKETF	NO	Name of TF for effective conductivity, if TF is used

	PORCHAN	0.0386	Effective porosity used in Tanaka-Chisaka model
	DBLK	1.206	Effective graphite block size for gap model
	BLKGAP	0	Gap width between graphite blocks for gap model
COR_LH	NLH	2	Number of LH nodes in vessel (inconsequential)
	NINSLH	0	Number of insulation layers (inconsequential)
COR_EDV	ITEMP	1	Temperature edit flag
	IMASS	1	Mass edit flag
	IVOL	1	Volume edit flag
	IASUR	1	Surface area edit flag
	IPMV	1	Component masses plot flag
	IPOW	1	Decay heat/fission power edit flag
COR_SS	IA		Axial level number(s)
	IR		Radial Ring number(s)
	ISSMOD	Table B.7.1	Structural model option for SS component
	ISSFAI		Failure model flag
	TSSFAI		Failure temperature (used for ISSFAI = TSFAIL)
	SSMETAL		SS material name
COR_ZP	IA		Axial Level number(s)
	Z		Bottom elevation of axial level
	DZ	Table B.7.2	Axial height of axial level
	PORDP		Particulate debris porosity
	IHSA		Axial boundary heat structure name
	FZPOW		Relative power density
COR_RP	IR		Radial Ring number(s)
	RINGR		Outer ring radius
	ASCELA		Total ring cross-sectional area
	IHSR	Table B.7.3	Radial boundary heat structure name
	UNUSED		Placeholder, use '-'
	ICFCHN		Name of CF to infer positive flow in channel
	ICFBYP		Name of CF to infer positive flow in bypass
	FRPOW		Relative power density
COR_RBV	IA		Axial level number(s)
	IR		Radial Ring number(s)
	IREF	Table B.7.4	Axial level number for reference cell if necessary
	JREF		Radial ring number for reference cell if necessary
	ICVHC		Channel-side control volume name
	ICVHB		Bypass-side control volume name
COR_KFU	IA	Table B.7.5	Axial level number(s)

	IR		Radial Ring number(s)
	XMFUUO		Mass of UO ₂ in FU
	XMFUHT		Mass of electric heater rod material in FU
	XMFXM		Mass of user-defined extra material in FU
	XMFXO		Mass of user-defined extra material oxide in FU
COR_KCL	IA		Axial level number(s)
	IR		Radial Ring number(s)
	XMCLZR	Table B.7.6	Mass of zircaloy in CL
	XMCLZX		Mass of ZrO ₂ in CL
	XMCLIN		Mass of inconel in CL
COR_KSS	IA		Axial level number(s)
	IR		Radial Ring number(s)
	XMSSSS	Table B.7.7	Mass of steel in SS
	XMSSSX		Mass of steel oxide in SS
	XMSSZR		Mass of zircaloy in SS
	XMSSZX		Mass of zircaloy oxide in SS
COR_KRF	IA		Axial level number(s)
	IR	Table B.7.8	Radial Ring number(s)
	XMRF		Mass of graphite in RF
COR_KPD	IA	ALL	Axial level number(s)
	IR	ALL	Radial Ring number(s)
	XMPDZR	0.0	Mass of zircaloy in PD component
	XMPDZX	0.0	Mass of ZrO ₂ in PD component
	XMPDUO	0.0	Mass of UO ₂ in PD component
	XMPDSS	0.0	Mass of steel in PD component
	XMPDSX	0.0	Mass of Steel oxide in PD component
	XMPDCP	0.0	Mass of control poison in PD component
	XMPDIN	0.0	Mass of inconel in PD component
COR_CIT	IA	ALL	Axial level number(s)
	IR	ALL	Radial Ring number(s)
	TFU	763.15	Initial FU temperature
	TCL	763.15	Initial CL temperature
	TCN	763.15	Initial CN temperature
	TCB	763.15	Initial CB temperature
	TPD	763.15	Initial PD temperature
	TSS	763.15	Initial SS temperature
	TNS	763.15	Initial NS temperature
	TPB	763.15	Initial PB temperature
COR_EDR	IA	ALL	Axial level number(s)

	IR	ALL	Radial Ring number(s)
	DHYCL	0.0526	CL equivalent diameter
	DHYPD	0.0168	PD equivalent diameter
	DHYCNC	0.0168	CNC equivalent diameter
	DHYCNB	0.0168	CNB equivalent diameter
	DHYSS	0.0168	SS equivalent diameter
	DHYNS	0.0168	NS equivalent diameter
	DHYPB	0.0168	PB equivalent diameter
COR_RFD	IA		Axial level number(s)
	IR	Table B.7.9	Radial Ring number(s)
	DHYRFC		RF channel side equivalent diameter
	DHYRFB		RF bypass side equivalent diameter
COR_RFG	IA		Axial level number(s)
	IR	Table B.7.10	Radial Ring number(s)
	RADI		Reflector channel-side radius
	THKRF		Reflector thickness
	IGEOMRF		Reflector geometry flag
	FACRF		Factor to split conductance to inner/outer surfaces
COR_BFA	IA		Axial level number(s)
	IR	Table B.7.11	Radial Ring number(s)
	ASCELR		Area of outer radial cell boundary = $2\pi R(DZ)$
	AFLOWC		Channel flow area of cell
	AFLOWB		Bypass flow area of cell
COR_SA	IA		Axial level number(s)
	IR	Table B.7.12	Radial Ring number(s)
	ASFU		FU surface area
	ASCL		CL surface area
	ASCN		CN surface area
	ASSS		SS surface area
	ASNS		NS surface area
COR_RFA	IA		
	IR	Table B.7.13	Radial Ring number(s)
	ASRF		Channel-side reflector surface area
	ASRFB		Bypass-side reflector surface area

Table B.7.1
COR_SS for HTTF model

COR_SS					
IA	IR	ISSMOD	ISSFAI	TSSFAI	SSMETA
9	1-6	PLATEG	TSFAIL	5000.0	STEEL
11	2-4	PLATEG	TSFAIL	5000.0	ZIRC
22	2-4	PLATEG	TSFAIL	5000.0	ZIRC
4	1-6	PLATEG	TSFAIL	5000.0	STEEL
27	1-5	PLATEG	TSFAIL	5000.0	STEEL
25	2-4	PLATEG	TSFAIL	5000.0	ZIRC
23	2-4	PLATEG	TSFAIL	5000.0	ZIRC
12	2-4	PLATEG	TSFAIL	5000.0	ZIRC
8	1-6	PLATEG	TSFAIL	5000.0	ZIRC
6-7	1	PLATEG	TSFAIL	5000.0	ZIRC
5	1-6	PLATEG	TSFAIL	5000.0	ZIRC

Table B.7.2
COR_ZP for HTTF model

COR_ZP					
IA	Z	DZ	PORDP	IHSA	FZPOW
1	-1.6542	0.27310	0.0	NO	0.00
2	-1.3811	0.27310	0.0	NO	0.00
3	-1.1080	0.27300	0.0	NO	0.00
4	-0.8350	0.03810	0.0	LPR_MS-04	0.00
5	-0.7969	0.07940	0.0	LPR_MS-05	0.00
6	-0.7175	0.11080	0.0	LPR_MS-06	0.00
7	-0.6067	0.11080	0.0	LPR_MS-07	0.00
8	-0.4959	0.22890	0.0	LPR_MS-08	0.00
9	-0.2670	0.02560	0.0	CB-09	0.00
10	-0.2414	0.08900	0.0	SR_CB-10	0.00
11	-0.1524	0.12700	0.0	SR_CB-11	0.00
12	-0.0254	0.02540	0.0	SR_CB-12	0.00
13	0.0000	0.19820	0.0	SR_CB-13	0.10
14	0.1982	0.19820	0.0	SR_CB-14	0.10
15	0.3964	0.19820	0.0	SR_CB-15	0.10

16	0.5946	0.19820	0.0	SR_CB-16	0.01
17	0.7928	0.19820	0.0	SR_CB-17	0.01
18	0.9910	0.19820	0.0	SR_CB-18	0.10
19	1.1892	0.19820	0.0	SR_CB-19	0.10
20	1.3874	0.19820	0.0	SR_CB-20	0.10
21	1.5856	0.19820	0.0	SR_CB-21	0.10
22	1.7838	0.19820	0.0	SR_CB-22	0.10
23	1.9820	0.02540	0.0	SR_CB-23	0.00
24	2.0074	0.07620	0.0	SR_CB-24	0.00
25	2.0836	0.09420	0.0	SR_CB-25	0.00
26	2.1778	0.10160	0.0	SR_CB-26	0.00
27	2.2794	0.09910	0.0	SR_CB-27	0.00

Table B.7.3
COR_RP for HTTF model

COR_RP						
IR	RINGR	ASCELA	IHSR	ICFCHN	ICFBYP	FRPOW
1	0.1814	0.1034	CB_TOP	NO	NO	0.00
2	0.3116	0.2010	CB_TOP	FLDIR2	NO	0.33
3	0.4015	0.2010	CB_TOP	FLDIR3	NO	0.33
4	0.4748	0.2010	CB_TOP	FLDIR4	NO	0.33
5	0.6030	0.4340	CB_TOP	NO	NO	0.00
6	0.8190	0.9650	CB_TOP	NO	NO	0.00

Table B.7.4
COR_RBV for HTTF model

COR_RBV					
IA	IR	IREF	JREF	ICVHC	ICVHB
1	1	0	0	CV001-LP	CV001-LP
1	2	1	1	-	-
2	1-3	1	1	-	-
3	1-4	1	1	-	-
1	3-5	1	1	-	-
2	4-5	1	1	-	-

3	5	1	1	-	-
4-5	1-5	1	1	-	-
6	1	0	0	CV106-LP	CV106-LP
7	1	0	0	CV107-LP	CV107-LP
6	2	0	0	CV206-LP	CV206-LP
7	2	0	0	CV207-LP	CV207-LP
6	3	0	0	CV306-LP	CV306-LP
7	3	0	0	CV307-LP	CV307-LP
6	4	0	0	CV406-LP	CV406-LP
7	4	0	0	CV407-LP	CV407-LP
6	5	0	0	CV506-LP	CV506-LP
7	5	0	0	CV507-LP	CV507-LP
8-9	1	0	0	CVCR_101	CVCR_101
10-12	1	0	0	CVCR_102	CVCR_102
13-14	1	0	0	CVCR_103	CVCR_103
15-16	1	0	0	CVCR_104	CVCR_104
17-18	1	0	0	CVCR_105	CVCR_105
19-20	1	0	0	CVCR_106	CVCR_106
21-22	1	0	0	CVCR_107	CVCR_107
23-24	1	0	0	CVCR_108	CVCR_108
25-27	1	0	0	CVCR_109	CVCR_109
8-9	2	0	0	CVCore_201	CVCore_201
10	2	0	0	CVCore_202A	CVCore_202A
11-12	2	0	0	CVCore_202B	CVCore_202B
13-14	2	0	0	CVCore_203	CVCore_203
15-16	2	0	0	CVCore_204	CVCore_204
17-18	2	0	0	CVCore_205	CVCore_205
19-20	2	0	0	CVCore_206	CVCore_206
21-22	2	0	0	CVCore_207	CVCore_207
23-24	2	0	0	CVCore_208	CVCore_208
25-27	2	0	0	CVCore_209	CVCore_209
8-9	3	0	0	CVCore_301	CVCore_301
10	3	0	0	CVCore_302A	CVCore_302A
11-12	3	0	0	CVCore_302B	CVCore_302B
13-14	3	0	0	CVCore_303	CVCore_303
15-16	3	0	0	CVCore_304	CVCore_304
17-18	3	0	0	CVCore_305	CVCore_305
19-20	3	0	0	CVCore_306	CVCore_306
21-22	3	0	0	CVCore_307	CVCore_307
23-24	3	0	0	CVCore_308	CVCore_308
25-27	3	0	0	CVCore_309	CVCore_309

8-9	4	0	0	CVCore_401	CVCore_401
10	4	0	0	CVCore_402A	CVCore_402A
11-12	4	0	0	CVCore_402B	CVCore_402B
13-14	4	0	0	CVCore_403	CVCore_403
15-16	4	0	0	CVCore_404	CVCore_404
17-18	4	0	0	CVCore_405	CVCore_405
19-20	4	0	0	CVCore_406	CVCore_406
21-22	4	0	0	CVCore_407	CVCore_407
23-24	4	0	0	CVCore_408	CVCore_408
25-27	4	0	0	CVCore_409	CVCore_409
8-9	5	0	0	CVCore_501	CVCore_501
10	5	0	0	CVCore_502A	CVCore_502A
11-12	5	0	0	CVCore_502B	CVCore_502B
13-14	5	0	0	CVCore_503	CVCore_503
15-16	5	0	0	CVCore_504	CVCore_504
17-18	5	0	0	CVCore_505	CVCore_505
19-20	5	0	0	CVCore_506	CVCore_506
21-22	5	0	0	CVCore_507	CVCore_507
23-24	5	0	0	CVCore_508	CVCore_508
25-27	5	0	0	CVCore_509	CVCore_509
4-27	6	NULL	NULL	NULL	NULL
1-3	6	1	1	-	-

Table B.7.5
COR_KFU for HTTF model

IA	IR	COR_KFU			
		XMFUUO	XMFUHT	XMFXM	XMFXO
13-22	2	10.98	0.00	0.00	0.00
13-22	3	11.79	0.00	0.00	0.00
13-22	4	10.5742	0.00	0.00	0.00

Table B.7.6
COR_KCL for HTTF model

IA	IR	COR_KCL		
		XMCLZR	XMCLZX	XMCLIN
13-22	2.00	85.01	0.00	0.00
13-22	3.00	82.72	0.00	0.00
13-22	4.00	88.07	0.00	0.00

Table B.7.7
COR_KSS for HTTF model

IA	IR	COR_KSS			
		XMSSSS	XMSSSX	XMSSZR	XMSSZX
25	2	0.000	0.000	7.749	0.000
25	3	0.000	0.000	8.967	0.000
25	4	0.000	0.000	4.649	0.000
23	2	0.000	0.000	12.564	0.000
23	3	0.000	0.000	12.399	0.000
23	4	0.000	0.000	12.889	0.000
12	2	0.000	0.000	12.564	0.000
12	3	0.000	0.000	12.399	0.000
12	4	0.000	0.000	12.889	0.000
8	1	0.000	0.000	69.909	0.000
8	2	0.000	0.000	115.370	0.000
8	3	0.000	0.000	117.420	0.000
8	4	0.000	0.000	113.310	0.000
8	5	0.000	0.000	289.380	0.000
6-7	1	0.000	0.000	33.839	0.000
5	1	0.000	0.000	24.249	0.000
5	2	0.000	0.000	47.149	0.000
5	3	0.000	0.000	47.149	0.000
5	4	0.000	0.000	47.149	0.000
5	5	0.000	0.000	101.810	0.000
27	1	81.240	0.000	0.000	0.000
27	2	131.570	0.000	0.000	0.000
27	3	129.860	0.000	0.000	0.000
27	4	139.180	0.000	0.000	0.000
27	5	341.060	0.000	0.000	0.000

9	1	20.986	0.000	0.000	0.000
9	2	34.633	0.000	0.000	0.000
9	3	35.249	0.000	0.000	0.000
9	4	34.015	0.000	0.000	0.000
9	5	86.871	0.000	0.000	0.000
4	1	31.241	0.000	0.000	0.000
4	2	60.729	0.000	0.000	0.000
4	3	60.729	0.000	0.000	0.000
4	4	60.729	0.000	0.000	0.000
4	5	131.130	0.000	0.000	0.000

Table B.7.8
COR_KRF for HTTF model

COR_KRF		
IA	IR	XMRF
26	1	31.219
26	2	50.548
26	3	49.889
26	4	53.472
26	5	131.030
25	1	28.946
25	5	121.488
24	1	23.414
24	2	37.911
24	3	37.417
24	4	41.104
24	5	98.274
23	1	7.805
23	5	32.758
13-22	1	60.904
13-22	5	255.620
12	1	7.805
12	5	32.758
11	1	23.414
11	2	37.911
11	3	37.417
11	4	40.104
11	5	98.274

10	1	42.956
10	2	70.393
10	3	70.868
10	4	71.051
10	5	178.690

Table B.7.9
COR_RFD for HTTF model

COR_RFD			
IA	IR	DHYRFC	DHYRFB
10-26	1	1.00E-10	1.00E-10
24	2-4	0.0168	1.00E-10
26	2-4	0.0168	1.00E-10
11	2-4	0.0168	1.00E-10
10	2-5	0.0254	1.00E-10
11-26	5	1.00E-10	1.00E-10

Table B.7.10
COR_RFG for HTTF model

COR_RFG				
IA	IR	RADI	THKRF	IGEOMRF
10-26	1	0.1814	-0.18140	1
10	2	0.3116	-0.13020	1
10	3	0.4015	-0.08990	1
10	4	0.4748	-0.07330	1
11	2	0.3116	-0.13020	1
11	3	0.4015	-0.08990	1
11	4	0.4748	-0.07330	1
24	2	0.3116	-0.13020	1
24	3	0.4015	-0.08990	1
24	4	0.4748	-0.07330	1
26	2	0.3116	-0.13020	1
26	3	0.4015	-0.08990	1
26	4	0.4748	-0.07330	1

Table B.7.11
COR_BFA for HTTF model

COR_BFA				
IA	IR	ASCELR	AFLOWC	AFLOWB
27	1	0.1129	0.00000	0.00000
26	1	0.1158	0.00000	0.00000
25	1	0.1074	0.00000	0.00000
24	1	0.0869	0.00000	0.00000
23	1	0.0289	0.00000	0.00000
13-22	1	0.2259	0.00000	0.00000
12	1	0.0289	0.00000	0.00000
11	1	0.0869	0.00000	0.00000
10	1	0.1593	0.00000	0.00000
9	1	0.0292	0.00000	0.00000
8	1	0.2609	0.00000	0.00000
6-7	1	0.1263	0.00000	0.00000
5	1	0.0905	0.00000	0.00000
4	1	0.0434	0.00000	0.00000
3	1	0.3112	0.00000	0.00000
2	1	0.3113	0.00000	0.00000
1	1	0.311	0.00100	0.00000
27	2	0.194	0.03578	0.00000
26	2	0.1989	0.03578	0.00000
25	2	0.1844	0.03578	0.00000
24	2	0.1492	0.03578	0.00000
23	2	0.0497	0.03578	0.00000
13-22	2	0.388	0.03578	0.00000
12	2	0.0497	0.03578	0.00000
11	2	0.1448	0.03578	0.00000
10	2	0.1014	0.03040	0.00000
9	2	0.0501	0.03040	0.00000
8	2	0.4481	0.03040	0.00000
6-7	2	0.2169	0.20100	0.00000
5	2	0.1555	0.00000	0.00000
4	2	0.0746	0.00000	0.00000
3	2	0.5345	0.00000	0.00000
2	2	0.5347	0.00000	0.00000
1	2	0.5347	0.00100	0.00000
27	3	0.2499	0.03576	0.00000
26	3	0.2563	0.03576	0.00000

25	3	0.2376	0.03576	0.00000
24	3	0.1922	0.03576	0.00000
23	3	0.0641	0.03576	0.00000
13-22	3	0.4999	0.03576	0.00000
12	3	0.0641	0.03576	0.00000
11	3	0.1922	0.03576	0.00000
10	3	0.3527	0.02736	0.00000
9	3	0.0646	0.02736	0.00000
8	3	0.5774	0.02736	0.00000
6-7	3	0.2795	0.20100	0.00000
5	3	0.2003	0.00000	0.00000
4	3	0.0961	0.00000	0.00000
3	3	0.6887	0.00000	0.00000
2	3	0.6889	0.00000	0.00000
1	3	0.6889	0.00100	0.00000
27	4	0.2956	0.02924	0.00000
26	4	0.3031	0.02924	0.00000
25	4	0.281	0.02924	0.00000
24	4	0.2273	0.02924	0.00000
23	4	0.0758	0.02924	0.00000
13-22	4	0.5913	0.02924	0.00000
12	4	0.0758	0.02924	0.00000
11	4	0.2273	0.02924	0.00000
10	4	0.4171	0.03344	0.00000
9	4	0.0764	0.03344	0.00000
8	4	0.6829	0.03344	0.00000
6-7	4	0.3305	0.20100	0.00000
5	4	0.2369	0.00000	0.00000
4	4	0.1137	0.00000	0.00000
3	4	0.8144	0.00000	0.00000
2	4	0.8147	0.00000	0.00000
1	4	0.8147	0.00100	0.00000
27	5	0.3755	0.00000	0.00000
26	5	0.3849	0.00000	0.00000
25	5	0.3569	0.00000	0.00000
24	5	0.2887	0.00000	0.00000
23	5	0.0962	0.00000	0.00000
13-22	5	0.7509	0.00000	0.00000
12	5	0.0962	0.00000	0.00000
11	5	0.2887	0.00000	0.00000
10	5	0.5297	0.00608	0.00000

9	5	0.0969	0.00608	0.00000
8	5	0.8672	0.00608	0.00000
6-7	5	0.4198	0.43400	0.00000
5	5	0.3008	0.00000	0.00000
4	5	0.1444	0.00000	0.00000
3	5	1.0343	0.00000	0.00000
2	5	1.0347	0.00000	0.00000
1	5	1.0347	1.00E-03	0.00000
3	6	1.4048	1.00E-03	0.00000
2	6	1.4054	1.00E-03	0.00000
1	6	1.4054	1.00E-03	0.00000

Table B.7.12
COR_SA for HTTF model

IA	IR	COR_SA				
		ASFU	ASCL	ASCN	ASSS	ASNS
1-3	1-2	0.00	0.00	0.00	0.00	0.00
2-3	3	0.00	0.00	0.00	0.00	0.00
3	4	0.00	0.00	0.00	0.00	0.00
4	1	0.00	0.00	0.00	0.04	0.00
4	2-4	0.00	0.00	0.00	0.20	0.00
4	5	0.00	0.00	0.00	4.34E-01	0.00
4	6	0.00	0.00	0.00	0.96	0.00
5	1	0.00	0.00	0.00	0.09	0.00
5	2-4	0.00	0.00	0.00	0.20	0.00
5	5	0.00	0.00	0.00	0.43	0.00
6	1	0.00	0.00	0.00	1.26E-01	0.00
6	2-5	0.00	0.00	0.00	0.00	0.00
7	1	0.00	0.00	0.00	0.13	0.00
7	2-5	0.00	0.00	0.00	0.00	0.00
8	1	0.00	0.00	0.00	0.26	0.00
8	2	0.00	0.00	0.00	1.27	0.00
8	3	0.00	0.00	0.00	1.16	0.00
8	4	0.00	0.00	0.00	1.37	0.00
8	5	0.00	0.00	0.00	0.65	0.00
9	1	0.00	0.00	0.00	2.92E-02	0.00
9	2	0.00	0.00	0.00	0.12	0.00
9	3	0.00	0.00	0.00	0.11	0.00

9	4	0.00	0.00	0.00	0.13	0.00
9	5	0.00	0.00	0.00	0.02	0.00
10	1	0.00	0.00	0.00	0.00	0.00
11	1	0.00	0.00	0.00	0.00	0.00
12	1	0.00	0.00	0.00	0.00	0.00
13-22	1	0.00	0.00	0.00	0.00	0.00
23	1	0.00	0.00	0.00	0.00	0.00
24	1	0.00	0.00	0.00	0.00	0.00
25	1	0.00	0.00	0.00	0.00	0.00
26	1	0.00	0.00	0.00	0.00	0.00
27	1	0.00	0.00	0.00	0.11	0.00
10	2	0.00	0.00	0.00	0.00	0.00
11	2	0.00	0.00	0.00	0.00	0.00
12	2	0.00	0.00	0.00	0.00	0.00
13-22	2	0.96	1.65	0.00	0.00	0.00
23	2	0.00	0.00	0.00	0.00	0.00
24	2	0.00	0.00	0.00	0.00	0.00
25	2	0.00	0.00	0.00	0.00	0.00
26	2	0.00	0.00	0.00	0.00	0.00
27	2	0.00	0.00	0.00	0.00	0.00
10	3	0.00	0.00	0.00	0.00	0.00
11	3	0.00	0.00	0.00	0.00	0.00
12	3	0.00	0.00	0.00	0.00	0.00
13-22	3	1.03	1.69	0.00	0.00	0.00
23	3	0.00	0.00	0.00	0.00	0.00
24	3	0.00	0.00	0.00	0.00	0.00
25	3	0.00	0.00	0.00	0.00	0.00
26	3	0.00	0.00	0.00	0.00	0.00
27	3	0.00	0.00	0.00	0.00	0.00
10	4	0.00	0.00	0.00	0.00	0.00
11	4	0.00	0.00	0.00	0.00	0.00
12	4	0.00	0.00	0.00	0.00	0.00
13-22	4	0.93	1.23	0.00	0.00	0.00
23	4	0.00	0.00	0.00	0.00	0.00
24	4	0.00	0.00	0.00	0.00	0.00
25	4	0.00	0.00	0.00	0.00	0.00
26	4	0.00	0.00	0.00	0.00	0.00
27	4	0.00	0.00	0.00	0.00	0.00
10	5	0.00	0.00	0.00	0.00	0.00
11	5	0.00	0.00	0.00	0.00	0.00
12	5	0.00	0.00	0.00	0.00	0.00

13-22	5	0.00	0.00	0.00	0.00	0.00
23	5	0.00	0.00	0.00	0.00	0.00
24	5	0.00	0.00	0.00	0.00	0.00
25	5	0.00	0.00	0.00	0.00	0.00
26	5	0.00	0.00	0.00	0.00	0.00

Table B.7.13
COR_RFA for HTTF model

COR_RFA			
IA	IR	ASRF	ASRFB
10	1	1.59E-01	0.0000
11	1	8.68E-02	0.0000
12	1	2.90E-02	0.0000
13-22	1	2.26E-01	0.0000
23	1	2.90E-02	0.0000
24	1	8.69E-02	0.0000
25	1	1.07E-01	0.0000
26	1	1.16E-01	0.0000
10	2	4.26E-01	0.0000
11	2	1.00E+00	0.0000
24	2	1.06E+00	0.0000
26	2	1.05E+00	0.0000
10	3	3.84E-01	0.0000
11	3	1.08E+00	0.0000
24	3	0.6501	0.0000
26	3	0.8668	0.0000
10	4	0.4687	0.0000
11	4	0.5618	0.0000
24	4	0.6987	0.0000
26	4	0.7443	0.0000
10	5	0.4171	5.30E-01
11	5	0.2273	2.89E-01
12	5	0.0758	9.62E-02
13-22	5	0.5913	7.51E-01
23	5	0.0758	9.62E-02
24	5	0.2273	2.89E-01
25	5	2.81E-01	0.3569
26	5	3.03E-01	0.3849

Table B.8
MP input for HTTF model

MP_INPUT	-	-	Signal start of MP input
MP_ID	MATNAM		Material name
MP_PRTF	PROP		Property Mnemonic (ENH, CPS, THC, or RHO)
	ITBPRP		Name of TF for property
	CFKEY	Table B.8.1	CF/TF flag
MP_PRC	RHOM		Material density (constant property)
	TMLT		Material melt temperature (constant property)
	LHF		Material latent heat of fusion (constant property)

Table B.8.1
MP properties input for HTTF model

MP_ID	MP_PRTF			MP_PRC		
	PROP	ITBPRP	KEY	RHOM	TMLT	LHF
GRAPHITE	THC	THC-COR_GRAPH	TF			
	CPS	CPS-COR_GRAPH	TF	2971.6	3866.0	-
	ENH	ENH-GRAPH	TF			
STAINLESS-STEEL-304	-	-	-	-	-	-
ZIRCALOY	THC	THC-SRLP_GRAPH	TF			
	CPS	CPS-SRLP_GRAPH	TF	2954.6	3866.0	-
	ENH	ENH-GRAPH	TF			
ZIRCONIUM-OXIDE	-	-	-	-	-	-
STAINLESS-STEEL	-	-	-	-	-	-
ALUMINUM	THC	THC-SRLP_GRAPH	TF			
	CPS	CPS-SRLP_GRAPH	TF	2954.6	3866.0	-
	ENH	ENH-GRAPH	TF			
ALUMINUM-OXIDE	-	-	-	-	-	-
CARBON-STEEL	-	-	-	-	-	-
BORON-CARBIDE	-	-	-	-	-	-
URANIUM-DIOXIDE	THC	THC-SiC	TF			
	CPS	CPS-SiC	TF	2400.0	3003.0	
INCONEL	THC	THC-COR_GRAPH	TF			
	CPS	CPS-COR_GRAPH	TF	2971.6	3866.0	-
	ENH	ENH-GRAPH	TF			

Table B.9
TF input for HTTF model

TF_INPUT	-	-	Signal start of TF input
TF_ID	TFNAME		Tabular function name
	TFSCAL		Tabular function scalar applied to each data point
	TFADCN	Table B.9.1	Tabular function additive constant applied to each data point
TF_TAB	NPAR		Data pair number
	X		Independent variable (e.g. time or temperature)
	Y		Dependent variable

Table B.9.1
TF tabular data for HTTF model

TFNAME	TF_ID			TF_TAB	
	TFSCAL	TFADCN	NPAR	X	Y
THC-COR_GRAPH	1	0	1	25.0	4.1000
			2	400.0	3.9000
			3	985.0	3.4000
			4	1315.0	5.0000
			5	1800.0	6.5000
CPS-COR_GRAPH	1	0	1	25.0	428.000
			2	400.0	849.000
			3	985.0	1078.000
			4	1315.0	1131.000
			5	1800.0	1173.000
ENH-GRAPH	1	0	1	300.0	0.0
			2	773.0	547910.0
			3	1273.0	1414010.0
			4	1773.0	2381110.0
			5	2273.0	3405060.0
			6	2773.0	4464560.0
			7	3866.0	6879781.0
			8	3866.0	8879871.0
			9	5000.0	9456545.0
THC-SRLP_GRAPH	1	0	1	25.0	1.9
			2	370.0	1.8
			3	925.0	1.6
			4	1130.0	2.1

			5	1320.0	3.6
CPS-SRLP_GRAPH	1	0	1	25.0	451.0
			2	370.0	876.0
			3	925.0	1113.0
			4	1130.0	1149.0
			5	1320.0	1175.0
THC-SiC	1	0	1	273.2	340.0
			2	5000.0	340.0
CPS-SiC	1	0	1	273.2	0.16
			2	5000.0	0.35

Table B.10
CF input for HTTF model

CF_INPUT	-	-	Signal start of CF input
CF_ID	CFNAME		Control function name
	CFTYPE		Control function type
CF_SAI	CFSCAL		Control function value scalar
	CFADCN	Table B.10.1	Control function value additive constant
	CFVALR		Control function initial value
CF_ARG	CHARG		Control function argument identifier
	ARSCAL		Control function argument scalar
	ARADCN		Control function argument additive constant

Table B.10.1
CF arguments for HTTF model

CFNAME	CF_ID		CF_SAI			CF_ARG		
	ICFNUM	CFTYP	CFSCAL	CFADCB	CFVALR	CHARG	ARSCAL	ARADCN
RCCS-T-0	700	EQUALS	0.0	300.00	300.00	EXEC-TIME	0.00	0.00
RCCS-T-7	707	EQUALS	0.0	300.00	300.00	EXEC-TIME	0.00	0.00
Trans-T0	1	EQUALS	0.0	0.00	0.00	EXEC-TIME	0.00	0.00
Trans-dt	2	ADD	0.0	0.00	0.00	EXEC-TIME	1.00	0.00
						CF-VALU('Trans-T0')	-1.00	0.00
Trans-Trip-Time	3	EQUALS	0.0	0.00	0.00	EXEC-TIME	0.00	0.00
Trans-Trip	4	L-GT	-	-	-	CF-VALU('Trans-dt')	1.00	0.00
						CF-VALU('Trans-Trip-Time')	1.00	0.00
SS-Mflow	50	EQUALS	0.0	0.96	0.96	EXEC-TIME	0.00	0.00
HeVelocity	51	DIVIDE	1.0	0.00	0.00	CVH-RHO('CV160-Gap',HE)	0.08	0.00
						CF-VALU('SS-Mflow')	1.00	0.00
HeSource	52	L-A-IFTE	1.0	0.00	0.00	CF-VALU('Trans-Trip')	-	-
						EXEC-TIME	0.00	0.00
						CF-VALU('HeVelocity')	1.00	0.00
SS-Pin	53	EQUALS	0.0	8.00E+05	8.00E+05	EXEC-TIME	0.00	0.00
Trans-Pin	54	EQUALS	0.0	1.00E+05	1.00E+05	EXEC-TIME	0.00	0.00
SourceP	55	L-A-IFTE	1.0	0.00	8.00E+05	CF-VALU('Trans-Trip')	-	-
						CF-VALU('Trans-Pin')	1.00	0.00
						CF-VALU('SS-Pin')	1.00	0.00
SS-Pout	56	EQUALS	0.0	8.00E+05	8.00E+05	EXEC-TIME	0.00	0.00
Trans-Pout	57	EQUALS	0.0	1.00E+05	1.00E+05	EXEC-TIME	0.00	0.00

SinkP	58	L-A-IFTE	1.0	0.00	8.00E+05	CF-VALU('Trans-Trip')	-	-
						CF-VALU('Trans-Pout')	1.00	0.00
						CF-VALU('SS-Pout')	1.00	0.00
SS-Tin	59	EQUALS	0.0	532.15	532.15	EXEC-TIME	0.00	0.00
Trans-Tin	60	EQUALS	0.0	300.00	300.00	EXEC-TIME	0.00	0.00
SourceT	61	L-A-IFTE	1.0	0.00	532.15	CF-VALU('Trans-Trip')	-	-
						CF-VALU('Trans-Tin')	1.00	0.00
						CF-VALU('SS-Tin')	1.00	0.00
SS-Tout	62	EQUALS	0.0	960.15	960.15	EXEC-TIME	0.00	0.00
Trans-Tout	63	EQUALS	0.0	300.00	300.00	EXEC-TIME	0.00	0.00
SinkT	64	L-A-IFTE	1.0	0.00	960.15	CF-VALU('Trans-Trip')	-	-
						CF-VALU('Trans-Tout')	1.00	0.00
						CF-VALU('SS-Tout')	1.00	0.00
Humidity	65	EQUALS	0.0	0.00	0.00	EXEC-TIME	0.00	0.00
Src_HeFrac	66	EQUALS	0.0	1.00	1.00	EXEC-TIME	0.00	0.00
Sink_N2-Frac	67	EQUALS	0.0	0.80	0.80	EXEC-TIME	0.00	0.00
Sink_O2-Frac	68	EQUALS	0.0	0.20	0.20	EXEC-TIME	0.00	0.00
InletVlv	69	L-A-IFTE	1.0	0.00	1.00	CF-VALU('Trans-Trip')	-	-
						EXEC-TIME	0.00	0.00
						EXEC-TIME	0.00	1.00
EmisCB	80	EQUALS	0.0	0.21	0.21	EXEC-TIME	0.00	0.00
EmisVes	81	EQUALS	0.0	0.21	0.21	EXEC-TIME	0.00	0.00
EmisRCCS	82	EQUALS	0.0	0.21	0.21	EXEC-TIME	0.00	0.00
CORE-POWER	100	EQUALS	0.0	2.20E+06	2.20E+06	EXEC-TIME	0.00	0.00
FLDIR2	102	EQUALS	1.0	0.0	0.0	FL-VEL('FL_209to208','A')	-1.00	0.00
FLDIR3	103	EQUALS	1.0	0.0	0.0	FL-VEL('FL_309to308','A')	-1.00	0.00
FLDIR4	104	EQUALS	1.0	0.0	0.0	FL-VEL('FL_409to408','A')	-1.00	0.00

Table B.11
EXEC MELCOR input for HTTF model

EXEC_TEND	TEND	0.0	Calculation end time
EXEC_TIME	TIME	-1000.0	Time
	DTMAX	0.5	Maximum time-step
	DTMIN	1.00E-05	Minimum time-step
	DTEDIT	500.0	Frequency of edit printing
	DTPLOT	1.0	Frequency of plot file writing
	DTREST	1000.0	Restart frequency
	DCREST	1.00E+10	Restart frequency with respect to CPU time
EXEC_CPULEFT	CPULEF	30.0	Desired minimum number of CPU seconds left at end of calculation
EXEC_CPULIM	CPULIM	1200.0	Maximum number of CPU seconds for the calculation
EXEC_CYMESF	NCYED	100	Number of cycles between messages written to terminal
	D		
	NCYEDP	1000	Number of cycles between messages to output file
EXEC_EXACTTIME	N	1	Data string index
	TIME	0	Desired time to land on exactly during calculation